

ADVANCED STEEL CONSTRUCTION

An International Journal

Volume 11 Number 3 (Special Issue)

September 2015

CONTENTS

Technical Papers

Fatigue Life Evaluation of In-Service Steel Bridges by using Bi-Linear S-N Curves
Chun-sheng Wang, Ben T. Yen, Hai-ting Li and Lan Duan

Extending the Fatigue Life of Riveted Bridges using Data from Long Term Monitoring
Eugen Brühwiler

Rehabilitation and Improvement of Fatigue Life of Welded Joints by ICR Treatment
Kentaro Yamada, Toshiyuki Ishikawa and Takumi Kakiuchi

Fatigue Service Life Evaluation of Existing Steel and Concrete Bridges
Chun-sheng Wang, Mu-sai Zhai, Lan Duan and Qian Wang

Fatigue Load Model for Highway Bridges in Heavily Loaded Areas of China
Wei-zhen Chen, Jun Xu, Bo-chong Yan and Zhi-ping Wang

Fatigue Reliability Assessment of Orthotropic Steel Bridge Decks Based on Probabilistic Multi-Scale Finite Element Analysis
Tong Guo, Zhong-xiang Liu and Jin-song Zhu

Service Life Evaluation Experience for Existing Railway Steel Bridge in China
Xiao-yan Tao and Yu-ling Zhang

Static and Fatigue Behavior of CFRP-Strengthened RC Bridge Girders Subjected to Vehicle Overloading
Xiao-yan Sun, Jian-guo Dai, Hai-long Wang and Chong Xu

Residual Life Evaluation of Prestressed Reinforced Concrete Highway Bridges under Coupled Corrosion-Fatigue Actions
Jin-song Zhu, Fa-min Huang, Tong Guo and Yun-he Song

Fatigue Life Evaluation for Cracked Long-Span Continuous PC Bridges
Xin Ruan, Hai-ying Ma and Xue-fei Shi

Life-Cycle Cost Based Maintenance and Rehabilitation Strategies for Cable Supported Bridges
Chun-sheng Wang, Mu-sai Zhai, Hai-ting Li, Yi-qing Ni and Tong Guo

Announcement by IJASC :

Announcement for ASCCS 2015

Announcement for SDSS 2016

Announcement for ICMS 2016

Announcement for ICSAS 2016

Copyright © 2015 by :

The Hong Kong Institute of Steel Construction

Website: <http://www.hkisc.org>

ISSN 1816-112X

Science Citation Index Expanded, Materials Science Citation Index and ISI Alerting

Cover: Scene of London with aesthetic steel buildings

e-copy of IJASC is free to download at "www.ascjournal.com" in internet and mobile apps.

ADVANCED STEEL CONSTRUCTION

VOL.11, NO.3 (2015)

ADVANCED STEEL CONSTRUCTION

an International Journal

ISSN 1816-112X

Volume 11 Number 3 (Special Issue)

September 2015



Editors-in-Chief

S.L. Chan, The Hong Kong Polytechnic University, Hong Kong

W.F. Chen, University of Hawaii at Manoa, USA

R. Zandonini, Trento University, Italy

ISSN 1816-112X

Science Citation Index Expanded,
Materials Science Citation Index
and ISI Alerting

EDITORS-IN-CHIEF

Asian Pacific, African and organizing Editor

S.L. Chan
*The Hong Kong Polyt. Univ.,
Hong Kong*

American Editor

W.F. Chen
Univ. of Hawaii at Manoa, USA

European Editor

R. Zandonini
Trento Univ., Italy

INTERNATIONAL EDITORIAL BOARD

F.G. Albermani
The Univ. of Queensland, Australia

I. Burgess
Univ. of Sheffield, UK

F.S.K. Bijlaard
Delft Univ. of Technology, The Netherlands

R. Bjorhovde
The Bjorhovde Group, USA

M.A. Bradford
The Univ. of New South Wales, Australia

D. Camotim
Technical Univ. of Lisbon, Portugal

C.M. Chan
Hong Kong Univ. of Science & Technology, Hong Kong

T.H.T. Chan
Queensland Univ. of Technology, Australia

S.P. Chiew
Nanyang Technological Univ., Singapore

W.K. Chow
The Hong Kong Polyt. Univ., Hong Kong

G.G. Deierlein
Stanford Univ., California, USA

L. Dezi
Univ. of Ancona, Italy

D. Dubina
The Politehnica Univ. of Timisoara, Romania

R. Greiner
Technical Univ. of Graz, Austria

L. Gardner
Imperial College of Science, Technology and Medicine, UK

L.H. Han
Tsinghua Univ. China

S. Herion
University of Karlsruhe, Germany

G.W.M. Ho
Ove Arup & Partners Hong Kong Ltd., Hong Kong

B.A. Izzuddin
*Imperial College of Science, Technology and
Medicine, UK*

J.P. Jaspart
Univ. of Liege, Belgium

S. A. Jayachandran
IIT Madras, Chennai, India

S.E. Kim
Sejong Univ., South Korea

S. Kitipornchai
The Univ., of Queensland, Australia

D. Lam
Univ. of Bradford, UK

L.J. Leu
National Taiwan Univ., Taiwan

G.Q. Li
Tongji Univ., China

J.Y.R. Liew
National Univ. of Singapore, Singapore

E.M. Lui
Syracuse Univ., USA

Y.L. Mo
Univ. of Houston, USA

J.P. Muzeau
CUST, Clermont Ferrand, France

D.A. Nethercot
*Imperial College of Science, Technology and
Medicine, UK*

Y.Q. Ni
The Hong Kong Polyt. Univ., Hong Kong

D.J. Oehlers
The Univ. of Adelaide, Australia

J.L. Peng
Yunlin Uni. of Science & Technology, Taiwan

K. Rasmussen
The Univ. of Sydney, Australia

J.M. Rotter
The Univ. of Edinburgh, UK

C. Scawthorn
Scawthorn Porter Associates, USA

P. Schaumann
Univ. of Hannover, Germany

G.P. Shu
Southeast Univ. China

L. Simões da Silva
*Department of Civil Engineering, University of
Coimbra, Portugal*

J.G. Teng
The Hong Kong Polyt. Univ., Hong Kong

G.S. Tong
Zhejiang Univ., China

K.C. Tsai
National Taiwan Univ., Taiwan

C.M. Uang
Univ. of California, USA

B. Uy
The University of New South Wales, Australia

M. Veljkovic
Univ. of Lulea, Sweden

F. Wald
Czech Technical Univ. in Prague, Czech

Y.C. Wang
The Univ. of Manchester, UK

Y.L. Xu
The Hong Kong Polyt. Univ., Hong Kong

D. White
Georgia Institute of Technology, USA

E. Yamaguchi
Kyushu Institute of Technology, Japan

Y.B. Yang
Chongqing University, China

Y.B. Yang
National Taiwan Univ., Taiwan

Y.Y. Yang
China Academy of Building Research, Beijing, China

B. Young
The Univ. of Hong Kong, Hong Kong

X.L. Zhao
Monash Univ., Australia

X.H. Zhou,
Chongqing University, China

Z.H. Zhou
Alpha Consultant Ltd., Hong Kong

R.D. Ziemian
Bucknell University, USA

Cover: Scene of London with aesthetic steel buildings

e-copy of IJASC is free to download at "www.ascjournal.com" in internet and mobile apps.

General Information

Advanced Steel Construction, an international journal

Aims and scope

The International Journal of Advanced Steel Construction provides a platform for the publication and rapid dissemination of original and up-to-date research and technological developments in steel construction, design and analysis. Scope of research papers published in this journal includes but is not limited to theoretical and experimental research on elements, assemblages, systems, material, design philosophy and codification, standards, fabrication, projects of innovative nature and computer techniques. The journal is specifically tailored to channel the exchange of technological know-how between researchers and practitioners. Contributions from all aspects related to the recent developments of advanced steel construction are welcome.

Instructions to authors

Submission of the manuscript. Authors may submit double-spaced manuscripts preferably in MS Word by emailing to one of the chief editors as follows for arrangement of review. Alternatively papers can be submitted on a diskette to one of the chief editors.

Asian Pacific, African and organizing editor : Professor S.L. Chan, Email: ceslchan@polyu.edu.hk
American editor : Professor W.F. Chen, Email: waifah@hawaii.edu
European editor : Professor R. Zandonini, Email: riccardo_zandonini@ing.unitn.it

All manuscripts submitted to the journal are recommended to accompany with a list of four potential reviewers suggested by the author(s). This list should include the complete name, address, telephone and fax numbers, email address, and at least five keywords that identify the expertise of each reviewer. This scheme will improve the process of review.

Style of manuscript

General. Author(s) should provide full postal and email addresses and fax number for correspondence. The manuscript including abstract, keywords, references, figures and tables should be in English with pages numbered and typed with double line spacing on single side of A4 or letter-sized paper. The front page of the article should contain:

- a) a short title (reflecting the content of the paper);
- b) all the name(s) and postal and email addresses of author(s) specifying the author to whom correspondence and proofs should be sent;
- c) an abstract of 100-200 words; and
- d) 5 to 8 keywords.

The paper must contain an introduction and a conclusion. The length of paper should not exceed 25 journal pages (approximately 15,000 words equivalents).

Tables and figures. Tables and figures including photographs should be typed, numbered consecutively in Arabic numerals and with short titles. They should be referred in the text as Figure 1, Table 2, etc. Originally drawn figures and photographs should be provided in a form suitable for photographic reproduction and reduction in the journal.

Mathematical expressions and units. The Systeme Internationale (SI) should be followed whenever possible. The numbers identifying the displayed mathematical expression should be referred to in the text as Eq. (1), Eq. (2).

References. References to published literature should be referred in the text, in the order of citation with Arabic numerals, by the last name(s) of the author(s) (e.g. Zandonini and Zanon [3]) or if more than three authors (e.g. Zandonini et al. [4]). References should be in English with occasional allowance of 1-2 exceptional references in local languages and reflect the current state-of-technology. Journal titles should be abbreviated in the style of the Word List of Scientific Periodicals. References should be cited in the following style [1, 2, 3].

Journal: [1] Chen, W.F. and Kishi, N., "Semi-rigid Steel Beam-to-column Connections, Data Base and Modelling", Journal of Structural Engineering, ASCE, 1989, Vol. 115, No. 1, pp. 105-119.

Book: [2] Chan, S.L. and Chui, P.P.T., "Non-linear Static and Cyclic Analysis of Semi-rigid Steel Frames", Elsevier Science, 2000.

Proceedings: [3] Zandonini, R. and Zanon, P., "Experimental Analysis of Steel Beams with Semi-rigid Joints", Proceedings of International Conference on Advances in Steel Structures, Hong Kong, 1996, Vol. 1, pp. 356-364.

Proofs. Proof will be sent to the corresponding author to correct any typesetting errors. Alternations to the original manuscript at this stage will not be accepted. Proofs should be returned within 48 hours of receipt by Express Mail, Fax or Email.

Copyright. Submission of an article to "Advanced Steel Construction" implies that it presents the original and unpublished work, and not under consideration for publication nor published elsewhere. On acceptance of a manuscript submitted, the copyright thereof is transferred to the publisher by the Transfer of Copyright Agreement and upon the acceptance of publication for the papers, the corresponding author must sign the form for Transfer of Copyright.

Permission. Quoting from this journal is granted provided that the customary acknowledgement is given to the source.

Page charge and Reprints. There will be no page charges if the length of paper is within the limit of 25 journal pages. A total of 30 free offprints will be supplied free of charge to the corresponding author. Purchasing orders for additional offprints can be made on order forms which will be sent to the authors. These instructions can be obtained at the Hong Kong Institute of Steel Construction, Journal website: <http://www.hkisc.org>

The International Journal of Advanced Steel Construction is published quarterly by learnt society, The Hong Kong Institute of Steel Construction, c/o Department of Civil & Environmental Engineering, The Hong Kong Polytechnic University, Hung Hom, Kowloon, Hong Kong.

Disclaimer. No responsibility is assumed for any injury and / or damage to persons or property as a matter of products liability, negligence or otherwise, or from any use or operation of any methods, products, instructions or ideas contained in the material herein.

Subscription inquiries and change of address. Address all subscription inquiries and correspondence to Member Records, IJASC. Notify an address change as soon as possible. All communications should include both old and new addresses with zip codes and be accompanied by a mailing label from a recent issue. Allow six weeks for all changes to become effective.

The Hong Kong Institute of Steel Construction

HKISC

c/o Department of Civil and Environmental Engineering,

The Hong Kong Polytechnic University,

Hung Hom, Kowloon, Hong Kong, China.

Tel: 852- 2766 6047 Fax: 852- 2334 6389

Email: ceslchan@polyu.edu.hk Website: <http://www.hkisc.org/>

ISSN 1816-112X

Science Citation Index Expanded, Materials Science Citation Index and ISI Alerting

Copyright © 2015 by:

The Hong Kong Institute of Steel Construction.



ISSN 1816-112X

Science Citation Index Expanded,
Materials Science Citation Index and
ISI Alerting

EDITORS-IN-CHIEF

Asian Pacific, African and organizing Editor

S.L. Chan
*The Hong Kong Polytechnic Univ.,
Hong Kong*
Email: ceslchan@polyu.edu.hk

American Editor

W.F. Chen
Univ. of Hawaii at Manoa, USA
Email: waifah@hawaii.edu

European Editor

R. Zandonini
Trento Univ., Italy
Email: riccardo.zandonini@ing.unitn.it

Advanced Steel Construction

an international journal

VOLUME 11 NUMBER 3 SEPTEMBER 2015

Special Issue

Technical Papers

- | | |
|---|-----|
| Fatigue Damage in Steel Bridges and Extending Their Life
<i>John W. Fisher and Sougata Roy</i> | 250 |
| Fatigue Life Evaluation of In-Service Steel Bridges by using
Bi-Linear S-N Curves
<i>Chun-sheng Wang, Ben T. Yen, Hai-ting Li and Lan Duan</i> | 269 |
| Extending the Fatigue Life of Riveted Bridges using Data from
Long Term Monitoring
<i>Eugen Brühwiler</i> | 283 |
| Rehabilitation and Improvement of Fatigue Life of Welded Joints
by ICR Treatment
<i>Kentaro Yamada, Toshiyuki Ishikawa and Takumi Kakiichi</i> | 294 |
| Fatigue Service Life Evaluation of Existing Steel and Concrete
Bridges
<i>Chun-sheng Wang, Mu-sai Zhai, Lan Duan and Qian Wang</i> | 305 |
| Fatigue Load Model for Highway Bridges in Heavily Loaded
Areas of China
<i>Wei-zhen Chen, Jun Xu, Bo-chong Yan and Zhi-ping Wang</i> | 322 |
| Fatigue Reliability Assessment of Orthotropic Steel Bridge Decks
Based on Probabilistic Multi-Scale Finite Element Analysis
<i>Tong Guo, Zhong-xiang Liu and Jin-song Zhu</i> | 334 |
| Service Life Evaluation Experience for Existing Railway Steel
Bridge in China
<i>Xiao-yan Tao and Yu-ling Zhang</i> | 347 |
| Static and Fatigue Behavior of CFRP-Strengthened RC Bridge
Girders Subjected to Vehicle Overloading
<i>Xiao-yan Sun, Jian-guo Dai, Hai-long Wang and Chong Xu</i> | 359 |
| Residual Life Evaluation of Prestressed Reinforced Concrete
Highway Bridges under Coupled Corrosion-Fatigue Actions
<i>Jin-song Zhu, Fa-min Huang, Tong Guo and Yun-he Song</i> | 372 |
| Fatigue Life Evaluation for Cracked Long-Span Continuous PC
Bridges
<i>Xin Ruan, Hai-ying Ma and Xue-fei Shi</i> | 383 |
| Life-Cycle Cost Based Maintenance and Rehabilitation Strategies
for Cable Supported Bridges
<i>Chun-sheng Wang, Mu-sai Zhai, Hai-ting Li, Yi-qing Ni and
Tong Guo</i> | 395 |

Announcement by IJASC :

Announcement for ASCCS 2015
Announcement for SDSS 2016
Announcement for ICMS 2016
Announcement for ICSAS 2016

GUEST EDITORIAL

Special Issue on “Fatigue Performance of Steel and Composites Bridges”

This special issue comprises extended and revised versions of papers selected from those presented at the First International Conference on Performance-based and Life-cycle Structural Engineering (PLSE 2012), which was held on 5-7 December 2012 in Hong Kong, China. PLSE2012 was co-organized by the Faculty of Construction and Environment (FCE) and Research Institute for Sustainable Urban Development (RISUD) of The Hong Kong Polytechnic University (PolyU). It was the first conference of a series to provide an international platform for scientific exchanges and international cooperation in the areas of performance-based structural engineering and life structural engineering for a wide range of structures, such as buildings, bridges and offshore platforms.

The conference program consisted of about 230 presentations, including 9 Keynote Lectures and 34 Invited Lectures. Eleven mini-symposia were also organized as part of the conference. As one of the six special issues that have arisen from PLSE2012, this special issue is focused on “Fatigue Performance of Steel and Composite Bridges”. In addition to 10 papers selected from the mini-symposium “Service Life Evaluation and Extension of Existing Bridges” organized during PLSE 2012, two more papers were invited from Professor John W Fisher at Lehigh University and Professor Eugen Bruhwiler at Swiss Federal Institute of Technology in Lausanne to form this special issue.

As the Guest Editors of this special issue, we would like to acknowledge the contributions of many individuals to the successful compilation of this special issue. In particular, we would like to thank all the authors for their careful preparation of the papers and the reviewers for their high-quality reviews. We also would like to sincerely thank Professor Siu-Lai Chan, Editor-in-Chief of the Journal of Advanced Steel Construction, for his kind support during the development of this special issue.

Guest Editors

Chun-Sheng WANG

Institute of Bridge Engineering, College of Highways, Chang'an University, China

Email: wcs2000@chd.edu.cn

Jian-Guo DAI

Department of Civil and Environmental Engineering,

The Hong Kong Polytechnic University, Hong Kong, China

Email: cejgdai@polyu.edu.hk

FATIGUE DAMAGE IN STEEL BRIDGES AND EXTENDING THEIR LIFE

John W. Fisher* and Sougata Roy

*Center for Advanced Technology for Large Structural Systems, Lehigh University
117 ATLSS Drive, Bethlehem, PA 18015, USA*

**(Corresponding author: E-mail: jwf2@lehigh.edu and sor3@lehigh.edu)*

ABSTRACT: This paper presents an overview of the performance of several welded steel bridges in the USA including fatigue cracking at cover plate and similar attachment details, as well as distortion-induced cracking at web gaps. Also examination methods are studied to improve and retrofit fatigue sensitive details, including modern post-weld enhancement by ultrasonic impact treatment (UIT). Orthotropic steel decks are reviewed based on the results of full-scale prototype laboratory fatigue tests which identified the complex behavior that occurs at fatigue sensitive details and were verified by field measurements on field installations. The orthotropic deck is the only bridge deck system likely to provide a 100 year life when the deck plate thickness equals or exceeds 16 mm.

Keywords: Steel bridges, Orthotropic steel decks, Distortion-induced fatigue, Long-term remote monitoring, Fatigue retrofit, Extending fatigue life, Fatigue damage, Ultrasonic impact treatment

DOI: 10.18057/IJASC.2015.11.3.1

1. INTRODUCTION

Welded and bolted details for bridges have been designed based on the nominal stress range rather than the local “concentrated” stress at the weld detail since 1974. The nominal stress is calculated with mechanics of material equations and does not include the local effect of stress concentrations of welds and attachments. Since fatigue is typically only a serviceability problem, members are designed for fatigue using service loads. It is standard practice in fatigue design of welded structures to separate the weld details into categories having similar fatigue resistance in terms of the nominal stress. Each category of weld details has an associated S-N curve. The S-N curves for steel details in the highway and railway bridge specifications (AASHTO 2012, AREMA 2012 [1-2]) are shown in Figure 1. The S-N curves are presented for seven categories of weld details; A through E', in order of decreasing fatigue strength. (Fisher et al. [3]).

Figure 1 shows the fatigue thresholds or constant amplitude fatigue limits (CAFL) for each category as horizontal dashed lines. When constant amplitude tests are performed at stress ranges below the CAFL, noticeable cracking does not occur. The CAFL occurs at an increasing number of cycles for lower fatigue categories or classes. Sometimes, different details, which share a common S-N curve (or category) in the finite-life regime, have different CAFL. The S-N curve must be based on tests of full size structural components such as girders (Keating & Fisher [4]). Testing on full-scale welded members indicated that the primary effect of constant amplitude loading can be accounted for in the live-load stress range, i.e., the mean stress is not significant. The reason that the dead load has little effect on the lower bound of the results is that, locally, there are very high residual stresses from welding. Mean stress may be important for some details that are not welded, however. In order to be conservative for non-welded details, in which there may be a significant effect of the mean stress, the fatigue test data should be generated under loading with a high tensile mean stress.

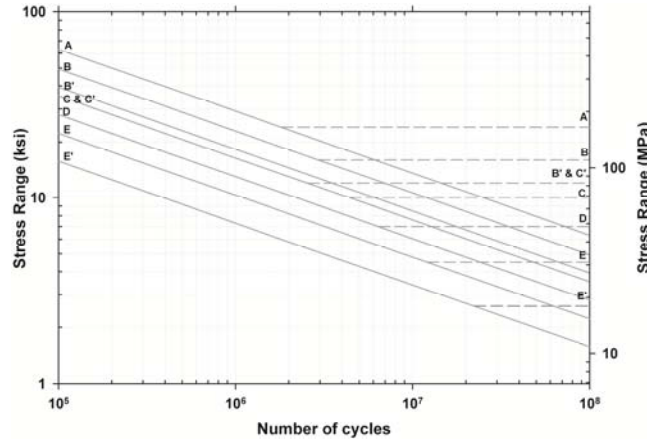


Figure 1. AASHTO Design S-N Curves

2. VARIABLE-AMPLITUDE FATIGUE

Cover plate details and equivalent details such as gusset plates are common on older bridges. Hence it is necessary to examine the service loading that bridges are subjected to. All service load histories for bridges consist of stress range cycles of varying amplitudes, hereafter called variable-amplitude loading. However, the design curves of stress range versus number of cycles, commonly called design S-N curves in the AASHTO LRFD Bridge Design Specifications [1] are based on fatigue tests that were performed under constant-amplitude (CA) loading. Since stress ranges vary in size and numbers, the relationship between CA and VA loading must be understood. A histogram of VA stress ranges can be converted into an equal number of CA stress ranges that produce the same amount of crack growth as is the case for the VA stress ranges. This so-called equivalent CA stress range is based on Miners Rule and given by:

$$S_{re} = \left[\sum_i \varphi_i \cdot S_{ri}^3 \right]^{1/3} \quad (1)$$

where S_{ri} = the i^{th} stress range in the histogram; φ_i = frequency of occurrence of S_{ri} ; and 3 is the slope of the log-log linear S-N line for CA fatigue. This equivalent stress range S_{re} is referred to as the root-mean-cube (RMC) stress range. Schilling, Klippstein, Barsom, & Blake [5] investigated both the RMC and the root-mean-square (RMS) methods of assessing the variable stress range spectrum. In those tests the stress cycles exceeding the CAFL had frequencies that were 10% or greater of the cumulative frequency.

Figure 2 shows the lower part of an S-N curve with variable stress-range distributions added at three different levels. When stress ranges in the variable distribution higher than the CAFL have a frequency of 0.05% or more of the cumulative frequency, the equivalent stress range S_{re} is used with the log-log linear S-N curves the same way as a CA stress range would be used.

Tilly & Nunn [6] tested 14 tensile specimens with category E longitudinal gusset plates under CA cycling and seven specimens under VA cycling with a Rayleigh spectrum. The tests were performed in a resonant fatigue machine at a frequency of 150 Hz. With fatigue lives of up to 415 million cycles, these tests are the longest on record and the only ones carried out into the infinite-life regime of category D, E and E' details. CA and VA stress range data correlated well, and the results confirmed the existence of infinite life if all stress ranges are below the CAFL.

Fisher et al. [7] tested eight beams under VA loading, also with a Rayleigh spectrum. Although the tests were carried out to 150 million cycles, the data fell in a wide band along the sloped S-N line of the finite-life regime. Following up on this study Fisher et al. [8] tested eight more beams. Each beam had two Category E' cover plates, six Category E' web gusset plates and three Category C' transverse stiffeners. As in the earlier study, the VA loading corresponded to a Rayleigh spectrum. All data points for the Category E' cover plates and gusset plates fell in the finite life regime. Two out of 24 stiffeners, with fatigue life of 109 and 120 million cycles respectively, provided some information on the variable amplitude fatigue limits (VAFL). The test data for Category E' details, including all stress cycles greater than 10 MPa from these two studies, are shown in Figure 3 and compared with the fatigue design curves. It is apparent that all test data followed the straight line extension of the resistance curve below the CAFL.

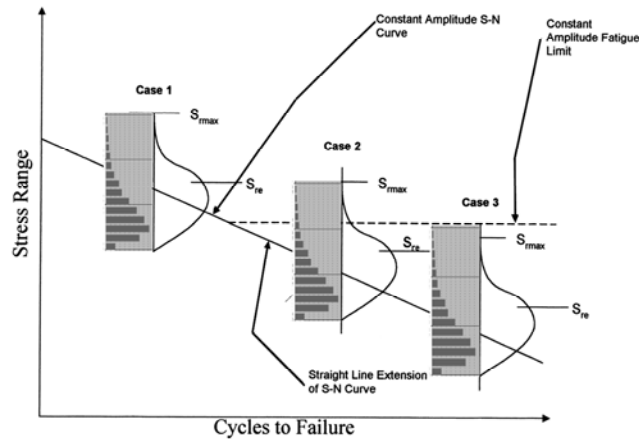


Figure 2. Application of Design S-N Curves under Variable Amplitude Stress Spectrum

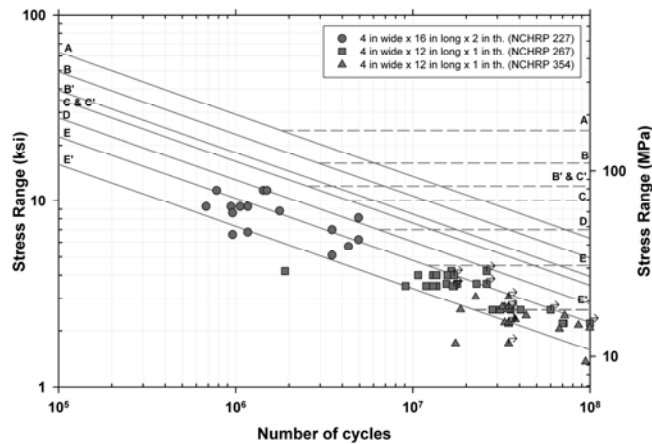


Figure 3. Fatigue Performance of Web Attachments under VA Loading

These studies demonstrated that under long-life variable amplitude loading, the cumulative frequencies of cycles that exceeded the CAFL by more than 0.05% resulted in fatigue cracking of welded web attachments. Damage accumulation was observed to occur from all stress cycles that exceeded 10 to 15 MPa. The tests on stiffeners which were Category C' detail, only developed cracks in two out of 20 details, when 0.01% of the stress cycles exceeded the CAFL. Altogether up to 120 million variable cycles were accumulated in these stiffener details.

3. EXPERIENCE WITH FATIGUE CRACKING

Fatigue cracking in steel bridges in the United States has become more frequent in its occurrence since the 1970's. A large crack was discovered in 1970 at the end of a cover plate in one of the Yellow Mill Pond multi-beam structures located at Bridgeport, Connecticut as shown in Figure 4 (Fisher [9]). Between 1970 and 1981, numerous fatigue cracks were discovered at the ends of cover plates in this bridge. In most cases, fatigue cracking in bridges resulted from an inadequate experimental base and overly optimistic specification provision developed from the experimental data in the 1960's. Subsequent laboratory data has verified the low fatigue strength in the high cycle region. The assumption of a fatigue limit at 2×10^6 cycles proved to be incorrect. As a result of extensive large-scale fatigue testing, it is now possible to clearly identify and avoid details which are expected to have low fatigue strength. The fatigue problems with the older bridges can be avoided in new construction if good detailing practice is followed and each detail is designed such that the stress range due to applied live load is below the design allowable stress range. Fortunately, it is also possible to retrofit or upgrade the fatigue strength of existing steel bridges with poor details. Fatigue crack repair techniques for weld toe surface cracks were developed to repair and extend the life of cracked welded steel bridge details.

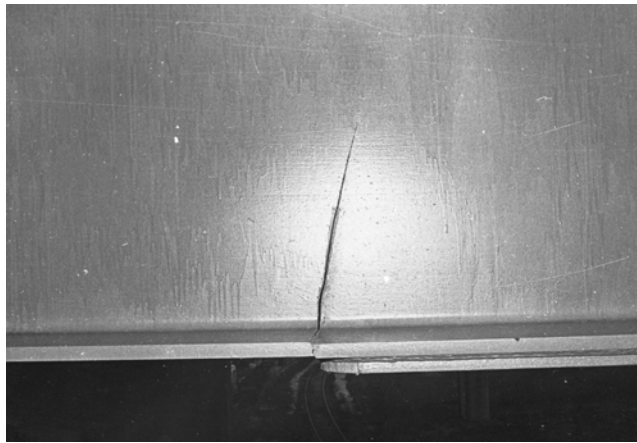


Figure 4. Yellow Mill Pond Bridge: Fatigue Crack at the End of Cover-plate

Peening works primarily by inducing a state of compressive residual stress near the weld toe (Fisher et al. [10]). Because the benefit of peening is derived from lowering the effective tensile stress range, it has been found to be the most effective when conducted under dead load. In this case, the peening only needs to be effective against live load. Air-hammer peening (AHP) can be a successful repair as long as the crack depth does not exceed the zone of compressive stress. The depth of compressive stress can be maximized by using air pressure lower than 290 kPa and up to six passes with a peening tool. Fatigue cracks up to 3 mm deep and 50 mm long at the cover-plate weld toe can be arrested by peening, provided the stress range does not exceed 40 MPa. Peened beams with crack depths larger than 3 mm usually do not show any measurable increase in fatigue life, and may require other repair procedures such as bolted splices.

Figure 5 shows a typical peened weld toe from the Yellow Mill Pond Bridge. The severity of the deformation is indicated by the elongation of the grains, which decreased with the depth below the surface. Fatigue tests of full size cover-plated beams verified their enhanced fatigue resistance. This structure was retrofitted by peening in the 1970's. This prevented subsequent crack growth in this heavily used structure until it was replaced in 1997. Subsequently, several beams removed from the original structure were tested in the laboratory (Takamori & Fisher [11]). These tests were carried out at a stress range of 70 MPa, which exceeded the maximum stress range in the variable

amplitude spectrum that the bridge was subjected to for over 20 years of service after treatment. The tests verified that no fatigue crack growth had occurred in these bridge details after more than 60 million cycles of truck loading. The peened and gas tungsten arc re-melted details had successfully prevented further growth at the retrofitted details. At the higher stress range in the laboratory tests fatigue cracks were found to develop through the weld throat as illustrated in Figure 6, and not at the treated weld toe.

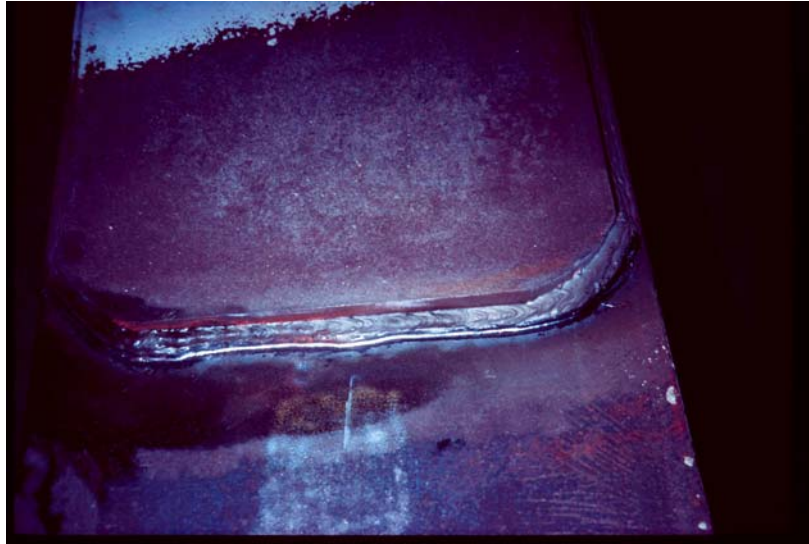
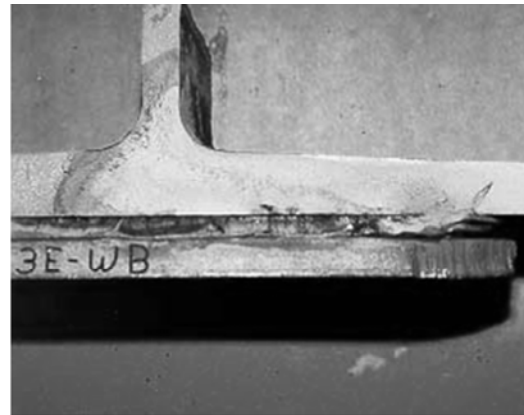


Figure 5. Air Hammer Peened Cover-plate End Weld Toe



(a) Fatigue Crack Progression



(b) Exposed Fracture Surface

Figure 6. Through Throat Cracking at Peened Cover-plate End Weld in Yellow Mill Pond Bridge

4. DISTORTION-INDUCTED FATIGUE

Most cracks found in bridges were caused by distortion of member cross sections and out-of-plane deformations of webs that induced localized bending stresses (Fisher et al. [12]). Out-of-plane distortion occurs mainly at attachment plates for diaphragms, transverse stiffeners and floor beams as illustrated in Figure 7. The solution to this problem lies in proper detailing that eliminates the secondary stresses.

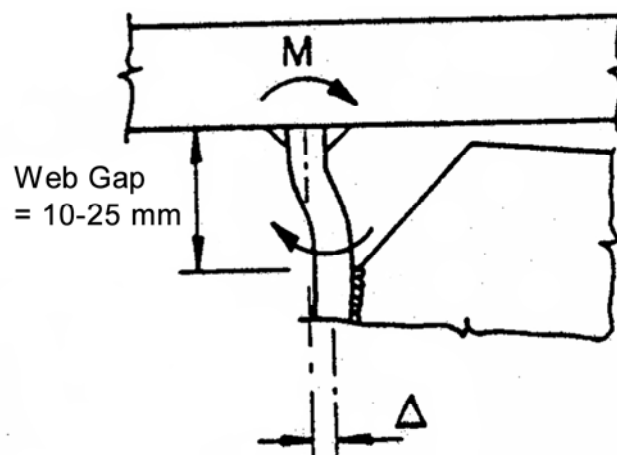


Figure 7. Schematic of Web Gap Distortion

In older bridges, transverse stiffeners and attachment plates used to be not welded to the tension flange of welded I-girders and box girders for the fear that a fatigue crack initiating in the flange would lead to brittle fracture. This well-intended but outdated practice originated in Europe in the 1930's from unexpected brittle fractures in early welded bridges, which was attributed to the welded details, but was primarily due to the poor quality of the steel. This practice has been the main cause of distortion-induced cracking, which can be prevented by welding stiffeners to the web and the flanges. Figure 8 shows a crack that formed along the fillet weld that attaches a diaphragm connection plate to the web of a plate girder. The fatigue cracking in these gaps typically occurs in a longitudinal direction along the fillet weld toe of the longitudinal web-to-flange joint, at the termination of the vertical fillet weld, or at both locations, as shown in Figure 8. In many cases, the displacement causing this distortion is limited and the cracking arrests as the compliance of the gap increases and the stresses are reduced. Because most of the cracks are oriented longitudinally, there is typically no reason to be concerned about fracture of the girder unless the cracks turn downward and propagate across the web. It is typically a mistake to try to weld repair such cracks, as this restores the high stresses which originally caused the cracking and will certainly reinitiate the cracking at the weld repair.

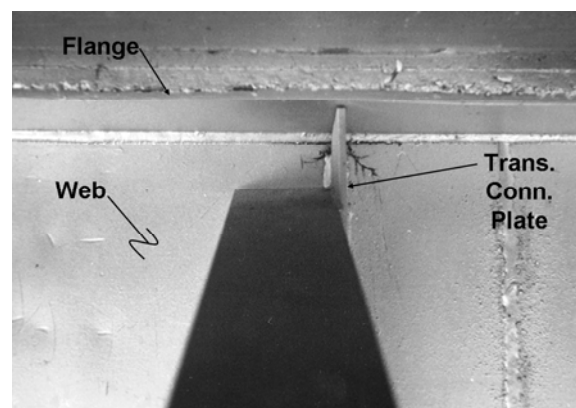


Figure 8. Distortion Induced Fatigue Cracking in the Web Gap

In the case where the distortion is limited, holes may be drilled or cored at the crack tips to temporarily arrest propagation. Figure 9 shows holes used to temporarily arrest crack growth. In this case, the cracks reinitiated because the out-of-plane bending remained excessive. Holes essentially blunt the crack tip. Experimental studies have indicated that the size of the hole must satisfy the relationship in Eq. (2).

$$\frac{K}{\sqrt{\rho}} = \frac{S_r \sqrt{\pi a}}{\sqrt{\rho}} < 10.5 \cdot \sqrt{\sigma_y} \quad (2)$$

where ρ = radius of the hole (mm); $2a$ = assumed crack size (mm), defined between the edges of the hole (Fisher et al. [13]); K = stress intensity factor for a crack size of $2a$; and σ_y = yield strength of the plate (MPa). The validity of this equation has been studied on full-scale welded beams subjected to variable amplitude loading up to 90 million stress cycles.

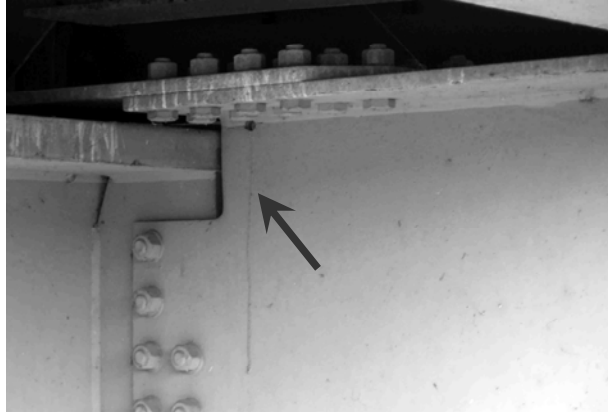


Figure 9. Retrofitting Connection by Drilling Holes

In most cases, problems with web-gap-cracking can be solved by rigidly connecting the attachment plate to the tension flange. To retrofit existing bridges, a rigid tee or angle may be connected to the attachment plate and the tension flange using high-strength bolts. Holes may also be drilled at the ends of short cracks as a temporary means of extending the fatigue life. The cracked detail shown in Figure 9 was retrofitted in this way.

In cases, where the distortion is displacement limited, the stresses can be reduced by increasing the flexibility of the connection. The flexibility may be increased by allowing a small fatigue crack to remain after drilling or coring holes at the crack tips. Another way to increase the flexibility of the joint is to remove part of the stiffener or connection plate and increase the length of the gap, as shown in Figure 10. If the same displacement occurs over a greater length gap, the stresses are significantly reduced. Note also the holes drilled at the crack tips along the web-flange weld.

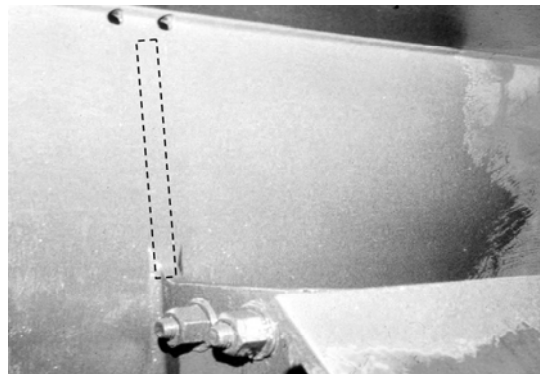


Figure 10. Retrofitting by Connection Softening

In case where the distortion is not displacement limited (i.e. load controlled), drilling holes or increasing the flexibility of a connection will not be successful. In these cases, and in many displacement limited cases, the best solution to distortion induced fatigue cracking is to increase the rigidity of the connection. For new construction, the bridge specifications now recommend that stiffeners and connection plates be rigidly connected to both the flanges and the web in order to “bridge” the web gap.

In view of the distortion induced cracking, considerable care must be exercised when web gusset plates are used for the bottom lateral system. Intersecting welds should not be permitted, and ample copes should be utilized to prevent small web gaps. Positive connections must be provided between horizontal gusset plates and the transverse connection plates. It seems preferable to bolt lateral gusset plates to the bottom flanges, or alternatively avoid the use of bottom lateral systems.

5. HIGH PERFORMANCE STEELS AND ENHANCEMENT

The development of high performance steels such as HPS Grade 485W and HPS Grade 690W has shown that without enhancement of welded details their fatigue resistance is no different than other high strength steels in use during the last four decades (Fisher et al. [3]). Post-weld enhancement of fatigue resistance of welded details such as cover-plates, gussets and stiffeners, which are known to experience crack growth from the weld toe, is essential for an effective use of modern high performance steels. As noted in the previous section, peening and gas tungsten arc re-melting were used in the past to improve the fatigue resistance of welded details that had experienced fatigue damage.

Over the past decade, ultrasonic impact treatment (UIT) has proved to be a consistent and effective means of improving fatigue strength of welded connections. A number of investigators (Wright [14], Statnikov [15], Haagensen et al. [16]) all reported that the fatigue strength of small size welded joints was improved by 50 to 200% at 2 million cycles when treated by UIT. Research at Lehigh University on large scale specimens having stiffener and cover-plate welded details has also demonstrated that substantial increases in fatigue strength of these high strength steel welded details can be achieved by UIT, in particular the elevation of their fatigue limit (Roy & Fisher [17-19]).

UIT involves post-weld deformation treatment of the weld toe by impacts from single or multiple indenting needles excited at ultrasonic frequency, generating force impulses at the weld toe (Statnikov [20]). The treatment introduces beneficial compressive residual stresses at the weld toe and also reduces the stress concentration by enhancing the profile of the weld toe. The UIT equipment consists of a handheld tool consisting of an ultrasonic transducer, a wave guide, and a holder with impact needles; an electronic control box; and a water pump to cool the system. Compared with traditional impact treatment methods such as air hammer peening, shot peening and needle peening, UIT appears to be more efficient and environmentally acceptable. It involves a complex effect of strain hardening, reduction in weld strain, relaxation in residual stress, and reduction in the stress concentration from profiling (Statnikov [20]).

The large scale beam tests showed that although the treated details suppressed crack growth from the weld toe, the failure mode changed to fatigue crack growth from the weld root when an usual end weld size was used. This usually resulted in a longer life, but still led to cracking and failure (Roy & Fisher [17-18]). For enhanced fatigue resistance it was desirable to prevent root cracking, and this could be achieved by increasing the size of the end weld at the cover-plate to the plate thickness, which reduced the stress concentration at the weld root (Takamori & Fisher [11]). This concept was verified by the subsequent fatigue tests. These results showed that the enhancement in fatigue resistance was dependent on both the stress range S_r and the minimum stress S_{min} . A

substantial improvement was realized at the lower minimum stress. This improvement was reduced when subjected to higher minimum stress that was applied after the treatment. This characteristic is also typical of other improvement techniques that introduce compression residual stress through plastic deformation (Fisher et al. [10], Roy & Fisher [19]). Under low levels of minimum stress, the residual compression stress at the treated weld toe is more effective in suppressing crack growth as the discontinuities are not opened until a higher stress range is applied. At higher minimum stress this condition is reached at a lower stress range, causing a reduction in the level of enhancement and a lower fatigue limit. Substantial enhancement results, when the treatment is applied under a high level of minimum stress. The treatment is effective in reducing both the residual tensile stress from welding, as well as the tension from the applied gravity load. This was verified experimentally for weld toes treated by air hammer peening (Fisher et al. [10]).

Design curves for Category E' end welded cover-plates treated by UIT are provided in Figures 11 to 12. As is apparent in Figure 11, treated details under low minimum stress (i.e. the R -ratio of S_{min}/S_{max} is less than 0.1 or, when the detail was treated under dead load) provide a design fatigue limit corresponding to Category B of the AASHTO Specifications. None of the end-welded cover-plate details developed fatigue cracks below 110 MPa, the CAFL for Category B (Roy & Fisher [19]). When the treatment is applied before the dead load stress, and the R -ratio is bracketed by 0.1 and 0.5, the design fatigue limit is decreased to 70 MPa which is the fatigue limit for Category C (Figure 12). Although there is an enhancement in the finite life, it is not as significant as the increase in the fatigue limit for this class of detail.

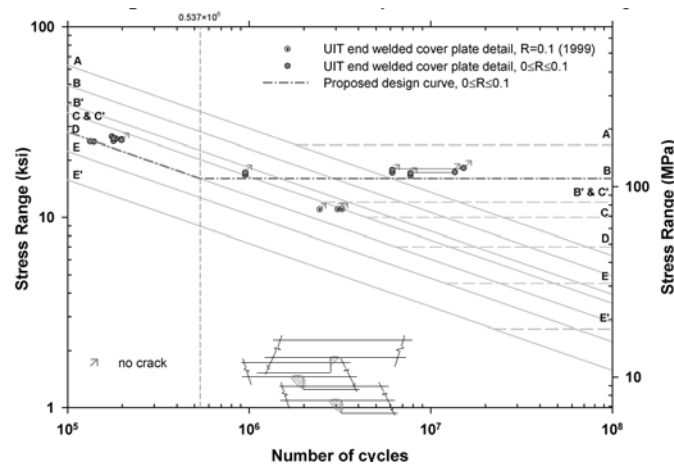


Figure 11. Design Curve for End Welded Cover-plate Details Treated by UIT; $0 \leq R \leq 0.1$

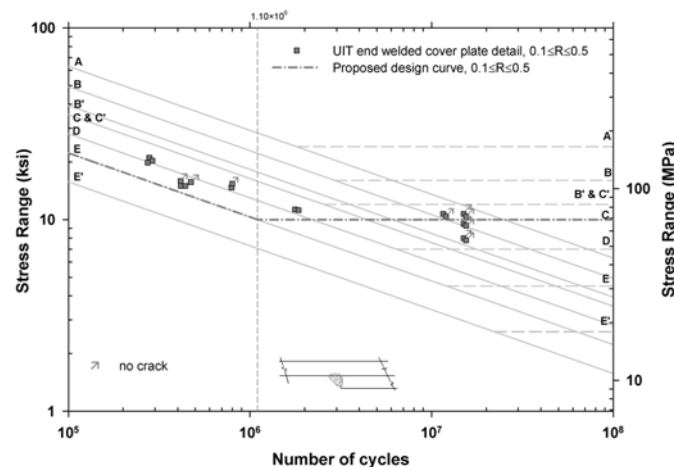


Figure 12. Design Curve for End Welded Cover-plate Details Treated by UIT; $0.1 < R \leq 0.5$

Cover-plate end welds on existing bridges are more likely to be about half the plate thickness. The test results indicated that when the R -ratio was less than 0.1, the enhanced fatigue resistance was applicable to these weld toes. There is a high probability that fatigue crack growth will initiate at the weld root, as was demonstrated in the test girders removed from the Yellow Mill Pond bridge that were treated by air hammer peening and gas tungsten arc re-melting (Takamori & Fisher [11]). This would suggest that inspections should focus on the weld throat to monitor subsequent root cracking. Fortunately, there is a significant increase in life for root cracking to occur and the cycles (time) necessary for the crack to propagate across the cover-plate end to the longitudinal welds, which is the only way the crack can enter into the girder flange. Usual intervals of inspection should identify such throat cracking if it ever occurs.

6. ORTHOTROPIC STEEL DECKS

During the past decade, full-scale laboratory and field testing of portions of several orthotropic bridge decks were conducted (Tsakopoulos & Fisher [21-22], Roy & Fisher [23-24]). These tests were carried out to minimize the possibility of fatigue cracking, as orthotropic deck systems in service in Europe, Australia and Japan have exhibited fatigue cracking in various components of the steel deck system. These included: cracking at rib-to-floor beam (or diaphragm) connections in the rib-wall and in the diaphragm web; and cracking in the deck plate at the rib-to-deck plate, and at the diaphragm-to-deck plate connections, particularly when the deck plate thickness was less than 14 mm, and when fillet welds were used to connect the ribs to the deck plate (Cunningham & Beales [25], Miki et al. [26], Jong [27], Machida et al. [28], Miki [29]).

Particularly sensitive in the orthotropic deck system is the rib-to-diaphragm connection – the welded connection between the transverse (floor beam) diaphragm plate and the continuous longitudinal ribs that are being supported. This connection is subjected to a variable combination of localized in-plane and out-of-plane bending stresses that are complex (Gajer et al. [30]) and make it susceptible to load-induced fatigue cracking.

Concern for the fatigue resistance of rib-to-diaphragm connections on the replacement deck panels resulted in the development of an alternative proposed by the consulting firm Steinman, Boynton, Gronquist, and Birdsall, who performed the engineering work for the rehabilitation of the Williamsburg Bridge that consisted of a complete-penetration groove weld 102 mm along the termination of the diaphragm cutout on the rib, reinforced with back-to-back fillet welds that continued above the groove weld. The combination weld was also continued 25 mm below the edge of the diaphragm cutout onto an extended portion of the diaphragm plate. This small “runoff” tab was subsequently ground off to provide a smooth 13 mm transition radius to the rib wall. Another adjustment was the introduction of an internal bulk-head plate at the diaphragm. This served to minimize the out-of-plane distortion of the rib wall and transmitted forces in the diaphragm across the rib wall as seen in Figure 13(a). (Gajer et al. [30]).

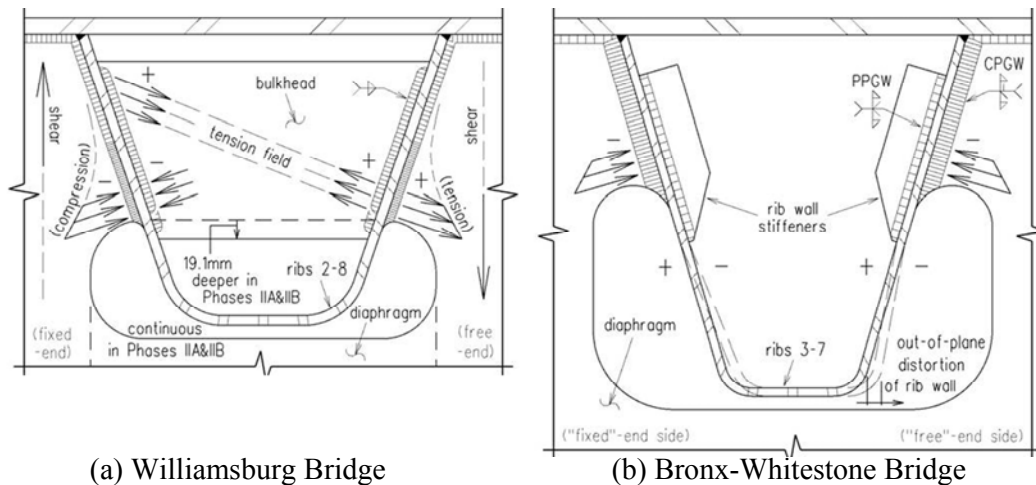


Figure 13. Cross Sections and Schema of Stress Field at Rib to Floor Beam Connection in as-built Orthotropic Decks

The second laboratory and field prototype study was carried out on the Bronx-Whitestone Bridge orthotropic deck. In the concept design, Weidlinger Associates modified the rib-to-diaphragm connection as indicated in Figure 13(b). This modification removed the bulkhead and replaced it with two internal stiffeners. In addition, the groove weld between the diaphragm plate and the rib wall was a complete penetration groove weld over its full length. The internal stiffeners reduced the force transmitted through the rib wall and served to distribute the distortion of the rib wall away from the diaphragm connection. The deeper rib also better accommodated the rib wall distortion (Fanjiang et al. [31]).

Recently, a full-size prototype of the proposed orthotropic deck for the upper level of the Verrazano Narrows Bridge was fatigue tested in the laboratory. In contrast to conventional designs, the diaphragms of replacement deck (designed by Parsons Transportation Group) were integrated with the existing floor framing system, making them load bearing in the transverse direction. The rib-to-diaphragm (called subfloor beam) connection incorporated a similar weld detail as the Williamsburg Bridge; however, to accommodate the high stress concentration a 38 mm transition radius was provided at the cutout terminus on the rib wall. Other variations from the Williamsburg design were a crescent shaped cutout and a full depth internal bulkhead at the subfloor beam, which allowed transmission of shear force in the subfloor beam across the rib wall and around the cutout with minimum stress concentration (Figure 14).

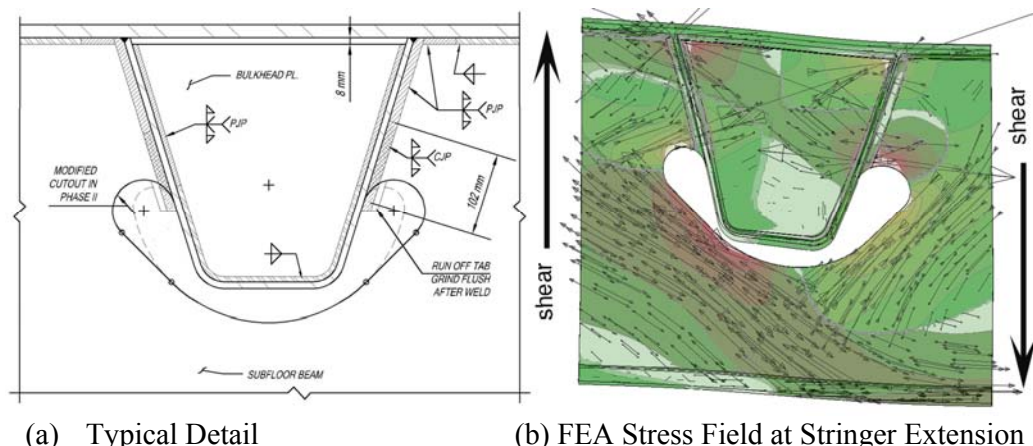


Figure 14. Rib to Floor Beam Connection in Replacement Orthotropic Deck for Verrazano Narrows Bridge

6.1 Prototype Laboratory Tests

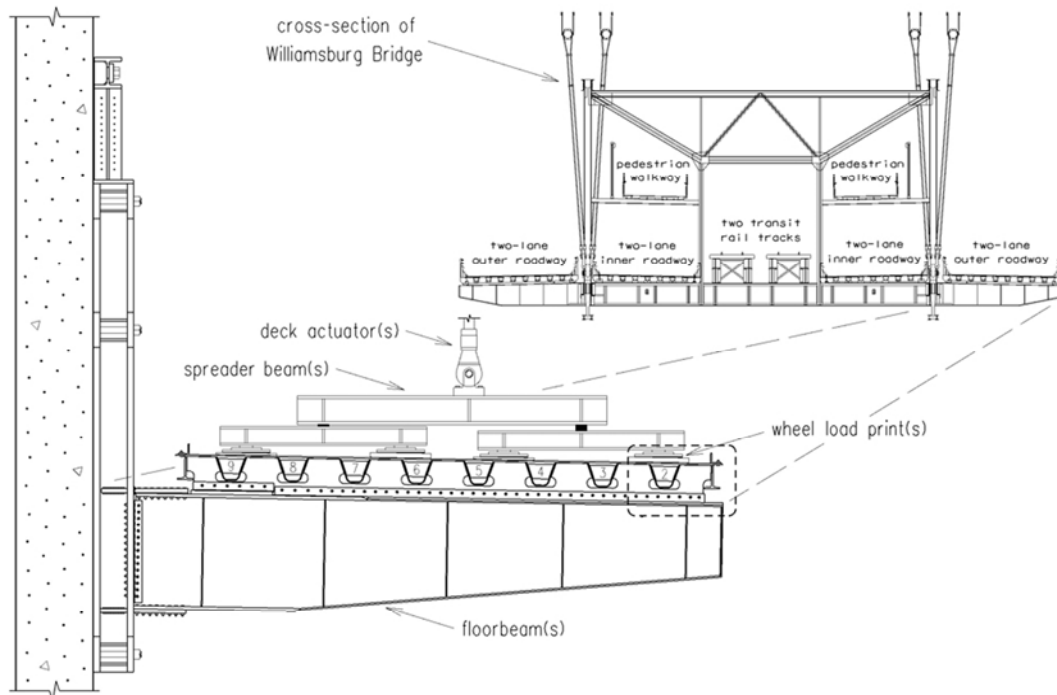
The Williamsburg Bridge test program was carried out between 1995 and 1998 on a prototype and on an as-built deck panel (Tsakopoulos & Fisher [21]). The second test program was carried out between 2001 and 2002 on the prototype deck panel for the Bronx-Whitestone Bridge (Tsakopoulos & Fisher [22]). The testing of the prototype deck for the Verrazano Narrows Bridge (Roy & Fisher [23-24]) was carried out between 2009 and 2011. These independent laboratory fatigue tests on full-size deck panels were conducted in the multidirectional testing facility at the Advanced Technology for Large Structural Systems (ATLSS) Engineering Research Center of Lehigh University.

The replacement orthotropic deck panels were designed to be incorporated onto the suspended portion of the Williamsburg and Bronx-Whitestone Bridge superstructures that consist of a deep longitudinal truss and girder system respectively, and transverse floorbeams located at about 6 m intervals for supporting the roadway decking. The orthotropic deck panels for the Verrazano Narrows Bridge were designed to replace the existing concrete-filled grid deck at the upper level of the suspended structure that consisted of a vertical stiffening truss at each fascia and a transverse twin-cell box at each node of the stiffening truss serving as floor beams to the upper and lower decks. The replacement deck was supported by and integrated with the floor framing that also included eight longitudinal stringers spanning between the floor beams.

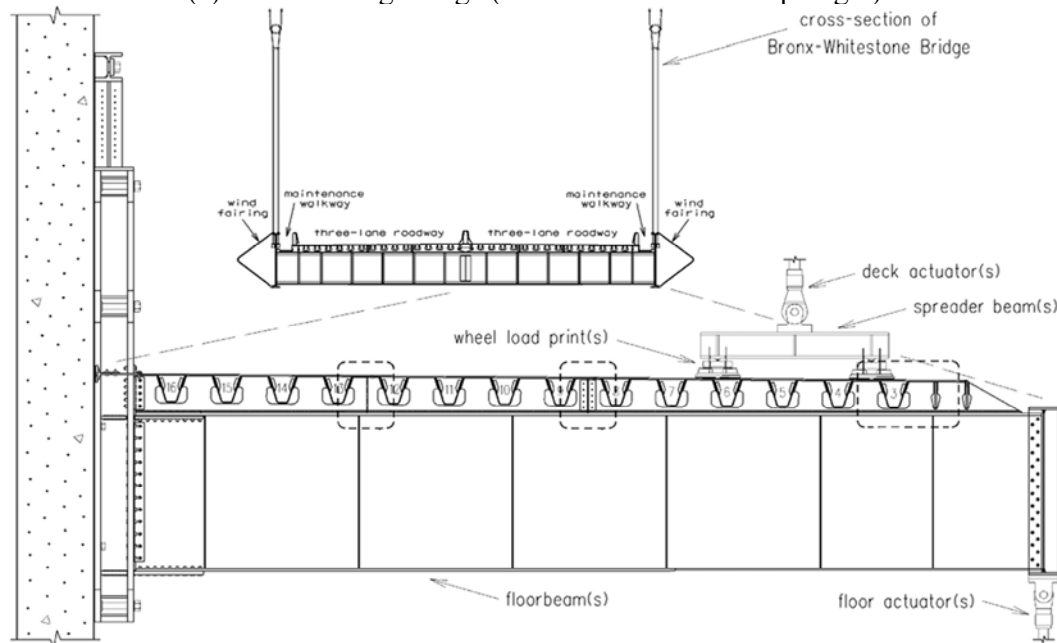
The deck panels were fabricated from structural elements, which included a steel plate deck surface, longitudinal ribs, transverse floorbeam diaphragms or subfloor beams, intermediate diaphragms or subfloor beams, and bracket stiffener plates or stringer extension plates that were welded to the underside of deck plate. The ribs were supported by the floorbeam diaphragms or subfloor beams at the cutouts, and transferred loads from the deck plate to the superstructure. Intermediate diaphragms or the subfloor beams provided additional global torsional stiffness to the deck system by transferring shear and controlling local relative displacement of the deck plate between ribs. For the Verrazano Narrows Bridge deck, where the intermediate subfloor beams were made integral with the stringer extensions, they also transferred load from the deck plate to the floor framing by shear. Figure 15 and 16 show the cross-section of the bridge superstructures upon completion of the rehabilitation, and the full-scale setups of the roadway sections that were simulated in the laboratory.

During the design process of the bridge decks, it was recognized that the welded connection between the transverse floorbeam diaphragm plate or the subfloor beam web and the continuous longitudinal ribs (rib-to-diaphragm or rib-to-subfloor beam) was sensitive to fatigue cracking. Several orthotropic decks in service were known to have developed load-induced fatigue cracks as a result of localized in-plane and out-of-plane bending stresses that are complex and variable at this location (Gajer et al. [30], Fanjiang et al. [31]).

No wearing surface was applied to the 16 mm deck plates, as it was left exposed for the installation of strain gages and inspection of possible fatigue cracking in both test programs. The loading configuration for the Williamsburg Bridge and the Bronx-Whitestone Bridge decks represented a single-axle that was consistent with the characteristics of a HS20 design truck axle and the HS15 fatigue truck. This provided a more severe loading condition on the floorbeam diaphragm(s) than if a tandem-axle was used. For the Verrazano Narrows Bridge deck testing, however, the single axle load was split into a tandem configuration consistent with the AASHTO HL-93 loading and the FHWA Manual for Orthotropic Decks (Connor et al. [32]).



(a) Williamsburg Bridge (as-built Floorbeam Diaphragm)



(b) Bronx Whites Tone Bridge (Prototype Floorbeam Diaphragm)

Figure 15. Cross-section of Full-scale Setup in Laboratory

The test program on the Williamsburg Bridge prototype is described in detail in (Tsakopoulos & Fisher [21]). The axle loads were applied by three to five deck actuators spaced at 3.1 m along the test deck. The dynamic tests had axle loads that varied from (1.33 to 3.07 HS15) 142 kN to 327 kN during the different phases of the test program.

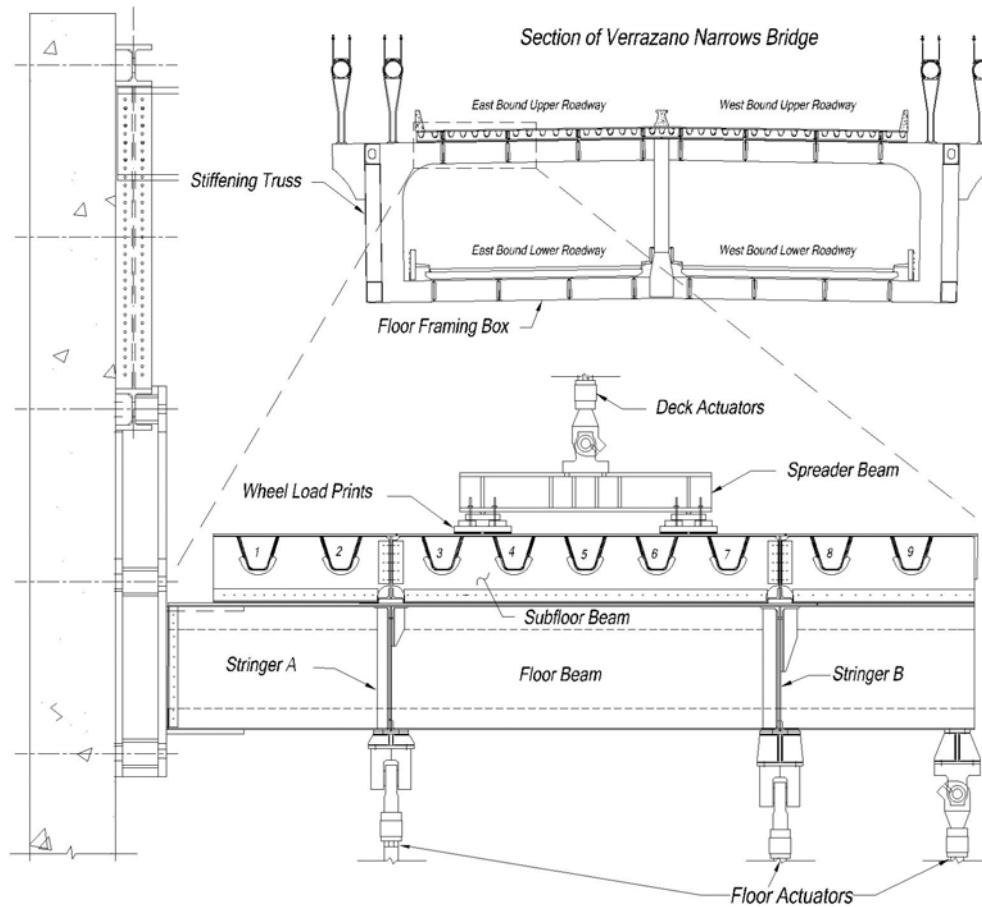


Figure 16. Cross-section of Full-scale Setup in Laboratory for Verrazano Narrows Bridge

The test program for the Bronx-Whitestone Bridge used three deck actuators in the outer lane spaced at 1.5 m along the length of the deck, and two floor actuators spaced at 6.0 m to simulate the curvature of the symmetrically loaded (and deflected) full-width section, shear and moment, and the resulting floorbeam diaphragm effects (Fanjiang et al. [31]). The load level was equivalent to the original load level used for the design of the prototype deck of 3 HS15 fatigue trucks with an additional 15 percent for impact ($3.45 \times \text{HS15} = 369 \text{ kN}$ per single-axle), a load level that corresponded to the (estimated) maximum stress range in the random variable spectrum determined from field measurements by Connor et al. [33]. After application of 4.1 million cycles at a cycling frequency of 0.79 Hz (Tsakopoulos & Fisher [22]), the load level was increased by an additional HS15 fatigue truck with 15 percent impact ($4.60 \times \text{HS15} = 491 \text{ kN}$ per single-axle). Although the load was extreme and unrealistic of actual truck axle loads, it was applied to increase stress range levels that were relatively low at the rib-diaphragm connections. No evidence of fatigue cracking was found after 2.0 million additional cycles.

The deck for the Verrazano Narrows Bridge was tested to the passage of a tandem axle by sequentially loading up to six above deck actuators in pairs; three floor actuators under the stringers and floor beams were used to provide continuity boundary conditions. The above deck actuators were spaced at 1.26 m apart and were loaded to a maximum load range of 184.1 kN equivalent to $3.45 \times \text{HS15}$ loading. The fatigue test was terminated after 5.0 million cycles of simulated passage of AASHTO tandem axle, without any detectable fatigue damage, which translated into more than 75 years' service life without any fatigue cracking (or infinite fatigue life) under site-specific loading.

The laboratory fatigue test programs on full-size steel orthotropic deck panels provided valuable information on the complex behavior and fatigue performance of orthotropic deck systems that were in good agreement with finite element models used for design. The laboratory tests confirmed that loading in Lane 1 (shoulder lane) was the worst-case condition and that the highest stresses were in deck elements and connections directly under the wheel load prints. For transversely load carrying diaphragms or subfloor beams, the rib-to-subfloor beam connection adjacent to the support was the most critical, as it experienced high stress concentrations in the vicinity of the diaphragm cutouts due to shear transfer. Tests revealed how the variation of plate and weld geometry, as well as the in-plane and out-of-plane components of the stress range, influenced fatigue crack development in the rib-to-diaphragm and rib-to-bulkhead plate connections. The general behavior and development of detected cracks appeared to be stable, where the propagation rates of cracks in the rib-to-diaphragm and rib-to-deck plate connections decreased or arrested as cracks extended beyond the local regions of residual tension stress of the weld toe at the termination of the connection. The only cracks that developed in the Bronx-Whitestone Bridge prototype were in the deck plate at the diaphragm connection and extended beyond the wheel load prints on the deck when tested at extreme and unrealistically high load exceeding railway Cooper loading. These observations reflected a capacity inherent to the orthotropic deck system to redistribute stresses induced under elevated truck loadings that were simulated.

The test programs demonstrated the effectiveness of design improvements that have ultimately enhanced the fatigue resistance of the replacement deck panels, and when adequately fabricated they are expected to exceed the required 75-years' design life without any fatigue damage.

6.2 Results of Long Term Remote Monitoring

Long-term monitoring of the Williamsburg Bridge began in August of 1998 and continued for seven months. Immediately after monitoring began, large stress ranges were observed in the diaphragm plate adjacent to the cut-out. These stresses were verified by triggered time histories of selected channels. Figure 17 shows the response of a tandem axle truck at the back-to-back gages on the diaphragm at the cut-out and the response of a transverse deck gage near a rib wall.

It is apparent that the floorbeam, and diaphragm cutout experiences one primary stress cycle during the vehicle passage. The deck gage is showing the local response of each axle. Figure 18 shows the stress range spectrum observed during a 60 day period of measurements at the rib-diaphragm cut-out. The measurements indicated that the variable amplitude stress range spectrum has a wider band width than assumed in the AASHTO-LRFD bridge design specifications (2004) for the rib-diaphragm cut-out. The effective stress range, S_{re} , was about 40 MPa, whereas the maximum stress range was about 140 MPa. Only 0.01% of the cumulative stress cycles in the spectrum exceeded a stress range of about 125 MPa (Connor & Fisher [34]). Similar results were obtained on the Bronx-Whitestone Bridge (Connor et al. [33]).

The field measurement results indicated that the diaphragm-to-rib connection should be designed for a fatigue limit state stress range of 3 S_{re} . Other elements such as the deck plate-to-rib connection and the floorbeam were observed to satisfy the AASHTO LRFD design fatigue limit state stress range of 2 S_{re} as illustrated in Figure 18. The load spectrum assumed in the AASHTO LRFD bridge design specifications for fatigue design was developed for primary bridge members such as main girders, floorbeams, etc. The test data underscores a need for modifications in the fatigue limit state load for the diaphragm details at the cutout. This is similar to observations made on modular joints which are also directly loaded by wheels (Dexter et al. [35]).

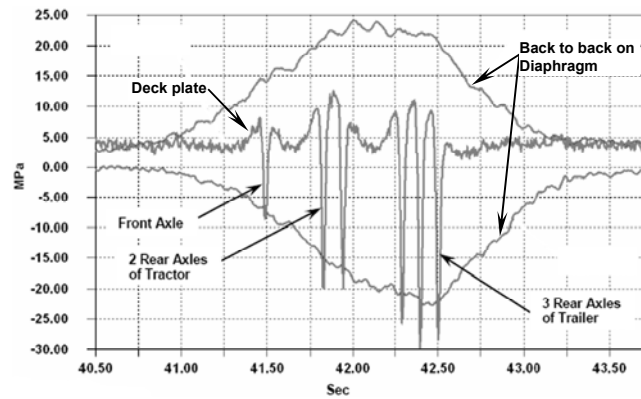


Figure 17. Response of the Deck Plate and the Floorbeam and Diaphragm Cut-out of the Williamsburg Bridge Orthotropic Deck during Passage of a Six Axle Truck

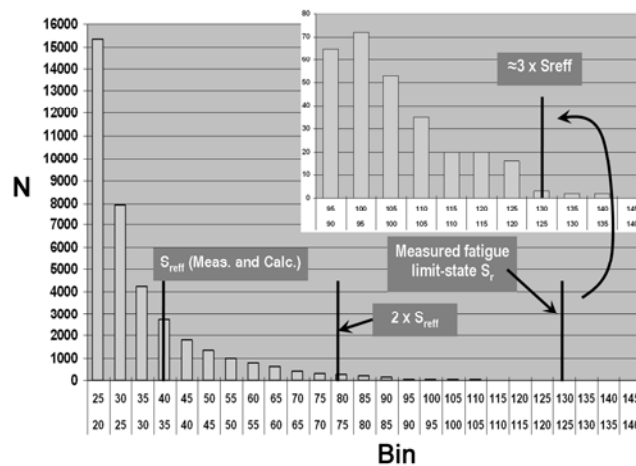


Figure 18. Measured Stress Range Spectrum at a Diaphragm Cutout in an Orthotropic Deck

7. CONCLUSIONS

Fatigue of steel bridges under traffic loading is the most significant issue affecting the service performance of aging transportation infrastructure in the USA and in many other countries around the world. Research and case studies of in-service fatigue cracking of steel bridges over the past 50 years have helped in formulating design guidelines and improved detailing practices, implementation of which have limited fatigue cracking in new construction. However, the risk of fatigue fracture of many steel bridges that were built prior to the implementation of the current practices and the economic impact of replacing the deficient bridges remain high.

Historically most of the fatigue cracking of the welded steel bridges in the USA occurred at cover plate and similar attachment details, as well as at the web gaps from distortion. The attachment details are the most severe of the fatigue critical details, which are characterized by crack growth at the weld toe. While fatigue fracture limit state in new steel bridges can be suppressed by avoiding the fatigue critical Category D, E or E' attachments, the performance of these details in existing bridges may be enhanced by weld toe treatments such as air hammer peening, GTA re-melting, or UIT. Post-weld toe treatments should also be considered in new structures for efficient use of modern HPS, where the attachment details including Category C' connection plates and stiffeners cannot be avoided.

Distortion induced fatigue cracking in the web gaps may be solved by proper detailing that eliminates the secondary stresses driving these cracks. In most cases, the web-gap-cracking can be prevented by rigidly connecting the attachment plates to the tension flange. Where the distortion is displacement controlled, the stresses can be reduced by increasing the flexibility of the connection. If distortion is limited, holes may be drilled or cored at the crack tips to temporarily arrest propagation.

When the cumulative stress ranges in the variable stress spectrum exceeds the CAFL by 0.05% or more of the total stress cycles in the distribution, the fatigue resistance of the attachments is given by the extension of the linear sloped part of the S-N curve below the CAFL. An infinite life may be assumed when the cumulative exceedence of the stress cycles beyond the CAFL is limited to 0.01% of the total. Most structures carry enough truck traffic to justify designing them for an infinite fatigue life, especially the deck elements.

The orthotropic deck is the only bridge deck system likely to provide a 100 year life when the deck plate thickness equals or exceeds 16 mm. Particularly sensitive in this deck system is the rib-to-diaphragm connection, which is subjected to a complex combination of local in-plane and out-of-plane bending stresses rendering it susceptible to load-induced fatigue cracking. Field measurements indicate that the diaphragm-to-rib connection should be designed for a fatigue limit state stress range of three times the effective stress range of the live load stress spectrum. A minimum deck plate thickness is necessary to reduce local stress in the overlay and improve its durability by limiting fatigue cracking.

REFERENCES

- [1] AASHTO 2012, "LRFD Bridge Design Specifications", Washington, D.C.: American Association of State Highway and Transportation Officials (AASHTO).
- [2] AREMA 2012. Manual of railway engineering. Washington, D.C.: American Railway Engineering and Maintenance of Way Association (AREMA).
- [3] Fisher, J.W., Frank, K.H., Hirt, M.A. and McNamee, B.M., "Effect of Weldments on the Fatigue Strength of Steel Beams", NCHRP Report 102, Washington, D.C.: Highway Research Board, 1970.
- [4] Keating, P. and Fisher, J.W., "Evaluation of Fatigue Tests and Design Criteria on Welded Details", NCHRP Report 286. Washington, D.C.: Transportation Research Board, 1986.
- [5] Schilling, C.G., Klippstein, K.H., Barsom, J.M. and Blake, G.T., "Fatigue of Welded Steel Bridge Members under Variable Amplitude Loading", NCHRP Report 188, Washington, D.C.: Transportation Research Board, 1978.
- [6] Tilly, G.P. and Nunn, D.E., "Variable Amplitude Fatigue in Relation to Highway Bridges", Proceedings of the Institution of Mechanical Engineers (London), 1980, Vol. 194, pp. 259-267.

- [7] Fisher, J.W., Mertz, D.R. and Zhong, A., "Steel Bridge Members under Variable Amplitude Long Life Fatigue Loading", NCHRP Report 267. Washington, D.C.: Transportation Research Board, 1983.
- [8] Fisher, J.W., Nussbaumer, A., Keating, P.B. and Yen, B.T., "Resistance of Welded Details under Variable Amplitude Long-life Fatigue Loading", NCHRP Report 354, Washington, D.C.: Transportation Research Board, 1993.
- [9] Fisher, J.W., "Fatigue and Fracture in Steel Bridges: Case Studies", John Wiley, 1984.
- [10] Fisher, J.W., Hausammann, H., Sullivan, M.D. and Pense, A.W., "Detection and Repair of Fatigue Damage in Welded Highway Bridges", NCHRP Report 206. Washington, D.C.: Transportation Research Board, 1979.
- [11] Takamori, H. and Fisher, J.W., "Tests of Large girders Treated to Enhance Fatigue Strength", Transportation Research Record, 2000, Vol. 1696, pp. 93-99.
- [12] Fisher, J.W., Jin, J., Wagner, D.C. and Yen, B.T., "Distortion-induced Fatigue Cracking in Steel Bridges", NCHRP Report 336. Washington, D.C.: Transportation Research Board, 1990.
- [13] Fisher, J.W., Barthelemy, B.M., Mertz, D.R. and Edinger, J.A., "Fatigue Behavior of Full-scale Welded Bridge Attachments", NCHRP Report 227. Washington, D.C.: Transportation Research Board, 1980.
- [14] Wright, W.J., "Post-weld Treatment of a Welded Bridge Girder by Ultrasonic Hammer Peening", FHWA Internal Research Report. McLean, VA: Federal Highway Administration, Turner Fairbank Highway Research Center, 1996.
- [15] Statnikov, E.S., "Comparison of Post-weld Deformation Methods for Increase in Fatigue Strength of Welded Joints", IIW Doc. No. XII-1668-97, Paris: International Institute of Welding, 1997.
- [16] Haagensen, P.J., Statnikov, E.S. and Lopez-Martinez, L., "Introductory Fatigue Tests on Welded Joint in High Strength Steel and Aluminum Improved by Various Methods including Ultrasonic Impact Treatment (UIT) ", IIW Doc. No. XIII-1748-98, Paris: International Institute of Welding, 1998.
- [17] Roy, S., Fisher, J.W. and Yen, B.T., "Fatigue Resistance of Welded Details Enhanced by Ultrasonic Impact Treatment (UIT) ", International Journal of Fatigue, 2003, Vol. 25, No. 9-11, pp. 1239-1247.
- [18] Roy, S. and Fisher, J.W., "Enhancing Fatigue Strength by Ultrasonic Impact Treatment", International Journal of Steel Structures, 2005, Vol. 5, No. 3, pp. 241-252.
- [19] Roy, S. and Fisher, J.W., "Modified AASHTO Design S-N Curves for Post-weld Treated Welded Details", Journal of Bridge Structures - Assessment, Design and Construction, 2006, Vol. 2, No. 4, pp. 207-222.
- [20] Statnikov, E.S., "Applications of Operational Ultrasonic Impact Treatment (UIT) Technologies in Production of Welded Joint", IIW Doc. No. XII-1667-97. Paris: International Institute of Welding, 1997.
- [21] Tsakopoulos, P.A. and Fisher, J.W., "Full-scale Fatigue Tests of Steel Orthotropic Decks for the Williamsburg Bridge", Journal of Bridge Engineering, 2003, Vol. 8, No. 5, pp. 323-333.
- [22] Tsakopoulos, P.A. and Fisher, J.W., "Full-scale Fatigue Tests of Orthotropic Deck Panel for the Bronx-Whitestone Bridge Rehabilitation", Journal of Bridge Structures - Assessment, Design and Construction, 2005, Vol. 1, No. 1, pp. 55-66.
- [23] Roy, S., Fisher, J.W., Manandhar, N.K., Alapati, R.S.D., and Park, Y.C., "Laboratory Fatigue Evaluation of Replacement Orthotropic Deck for a Signature Bridge", Proc. 6th International Conference on Bridge Maintenance, Safety and Management., IABMAS 2012, Jul. 8-12, Lake Como, Italy.
- [24] Roy, S., Fisher, J.W. and Alapati, R.S.D., "Full Scale Laboratory Testing of Replacement Orthotropic Deck for the Verrazano Narrows Bridge", Proc. The Fourth International

- Conference on Bridge Maintenance, Safety and Management, IABMAS 2010, Jul. 11–15, Philadelphia, PA.
- [25] Cuninghame, J.R. and Beales, C., “Strengthening and Refurbishment of Severn Crossing. Part 4. TRRL Research on Severn Crossing”, *Proceedings of the Institution of Civil Engineers, Structures and Buildings*, 1992, Vol. 94, No. 1, pp. 37-49.
 - [26] Miki, C., Tateishi, K., Okukawa, J. and Fujii, Y., “Local Stress and Fatigue Strength of Joint between Longitudinal and Transverse Ribs in Orthotropic Steel Deck Plate”, *Journal of Structural Mechanics and Earthquake Engineering*, 1995, Vol. 519/I-32, No. 7, pp. 127-137.
 - [27] Jong, F.B.P. de, “Overview Fatigue Phenomenon in Orthotropic Bridge Decks in the Netherlands”, 1st Orthotropic Bridge Conference; Proc., Sacramento, CA, August 25-27, 2004.
 - [28] Machida, F., Yuge, T., Miki, C., Yamguchi, E., Shimosato, T. and Masui, T., “Stress Measurements of Fatigue-damaged Structures with Orthotropic Steel Decks in Summer and Winter”, 1st Orthotropic Bridge Conference; Proc., Sacramento, CA, August 25-27, 2004.
 - [29] Miki, C., “Fatigue Damage in Orthotropic Steel Bridge Decks and Retrofit Works”, *International Journal of Steel Structures*, 2006, Vol. 6, No. 4, pp. 255-267.
 - [30] Gajer, R.B., Patel, J. and Khazem, D., “Orthotropic Steel Deck for the Williamsburg Bridge Reconstruction”, 14th Structures Congress; Proc., Vol. 1, Chicago, IL. New York: ASCE, 1996.
 - [31] Fanjiang, G.N., Ye, Q., Fernandez, O.N. and Taylor, L.R., “Fatigue Analysis and Design of Steel Orthotropic Deck for Bronx-Whitestone bridge”, New York City, Transportation Research Record, 2004, Vol. 1892, pp. 69-77.
 - [32] Connor, R., Fisher, J., Gatti, W., Gopalaratnam, V., Kozy, B., Leshko, B., McQuaid, D. L., Medlock, R., Mertz, D., Murphy, T., Paterson, D., Sorensen, O., and Yadlosky, J., “Manual for Design, Construction, and Maintenance of Orthotropic Steel Deck Bridges”, Publication FHWA-IF-12-027. Washington, D.C.: Federal Highway Administration, US Department of Transportation, 2012.
 - [33] Connor, R.J., Richards, S.O. and Fisher, J.W., “Long-term Monitoring of Prototype Orthotropic Deck Panels on the Bronx-Whitestone Bridge for Fatigue Evaluation”, In K.M. Mahmoud (ed.), 2003 New York City Bridge Conference; Proc., New York City, October 20-21. Lisse: Swets & Zeitlinger.
 - [34] Connor, R.J. and Fisher, J.W., “In-service Response of an Orthotropic Steel Deck Compared with Design Assumptions”, *Transportation Research Record*, 2000, Vol. 1696, No. 1, pp 100-108.
 - [35] Dexter, R.J., Connor, R.J. and Kaczinski, M.R., “Fatigue Design of Modular Bridge Expansion Joints”, NCHRP Report 402, Washington, D.C.: Transportation Research Board, 1997.

FATIGUE LIFE EVALUATION OF IN-SERVICE STEEL BRIDGES BY USING BI-LINEAR S-N CURVES

Chun-sheng Wang^{1,*}, Ben T. Yen², Hai-ting Li³ and Lan Duan¹

¹ *Engineering Research Center for Large Highway Structure Safety of Ministry of Education,
College of Highways, Chang'an University, Xi'an, Shaanxi Province, China*

² *Department of Civil and Environmental Engineering, Lehigh University, Bethlehem, PA 18015-4729, USA*

³ *Department of Civil Engineering, The University of Hong Kong, Hong Kong, China*

**(Corresponding author: E-mail: wcs2000wcs@163.com)*

ABSTRACT: The in-service steel bridges are often required to carry increasing volume of traffic and heavier trucks or freight trains. More attention should be paid to possible fatigue damages of such structures. It has been reported that for many structure details with an equivalent stress range below the constant amplitude fatigue limit (CAFL) and free of fatigue cracks, calculations show that the remaining fatigue life has been exhausted. This condition indicates that it could be too conservative to predict the remaining fatigue life of in-service steel bridges by utilizing the equivalent constant amplitude stress ranges with the direct extension of S-N curves of AASHTO specifications with a slope of -3 to below the CAFL. This over-prediction of fatigue damage may lead to unnecessary rehabilitation and maintenance actions. For a better fatigue life evaluation and prediction, a set of bi-linear S-N curves with a break at the CAFL for the AASHTO fatigue strength categories and with a slope of -4 below, has been proposed for fatigue life evaluation of in-service structures. This paper applies the concept of the equivalent constant amplitude stress range for bi-linear curves to AASHTO specifications and Eurocode. Cases of fatigue evaluation of in-service steel bridge components are studied by correlating the field-measured live-load stresses with the bi-linear S-N curves. Comparative results from the bi-linear S-N curve approach, the current AASHTO specifications and Eurocode approach are presented.

Keywords: Steel bridges, Fatigue life evaluation, Bi-linear S-N curve, Constant amplitude fatigue limit, Equivalent stress range

DOI: 10.18057/IJASC.2015.11.3.2

1. INTRODUCTION

For many in-service steel bridges, fatigue is a primary safety concern and each structural detail of a steel bridge has its evaluated fatigue strength according to the current design codes and specifications. The fatigue strength categories (S-N curves) define the relationship between the applied primary stress range (live-load stress range) of constant amplitude and the number of stress cycles when fatigue damage is expected.

The current procedure for predicting the remaining fatigue life of steel bridges by AASHTO specifications [1] utilizes an equivalent constant amplitude stress ranges (S_{re}) with the direct extension of the S-N curves of a single slope of -3 to below the constant amplitude fatigue limit (CAFL) for the different detail categories. In order to calculate the S_{re} , a live load stress range spectrum or histogram for the structural detail should be developed to correlate with the governing S-N curve [2]. The fatigue life evaluated by this approach is generally adequate for bridge safety management [3]. Yet this approach was found to be conservative, often resulting in over-prediction of fatigue damage and may lead to unnecessary rehabilitation or maintenance actions. A number of details have been found to be free of cracks although the calculated remaining fatigue life by the current procedure showed that the details should be suffered from cracks [4]. For this reason, the direct extension of S-N curves from above to below the CAFL was examined analytically [5]. The result is a set of bi-linear S-N curves with a break at the CAFL and a slope of -4 below for the

fatigue strength categories in AASHTO. The utilization of bi-linear S-N curves is being considered by bridge engineers [6].

The fatigue life evaluation of in-service steel bridges should be conducted based on the performance of the bridge structure under actual live loads. This is because the assumptions made on service loads during the design stage usually do not provide sufficiently accurate representation of the actual live load history. Even more importance is the fact that almost all connections and joints of bridge components do not behave exactly in the service state as considered in design according to the strength state. The behavior of a bridge structure under service loads at specific positions of these loads on the bridge can be analyzed using finite element models. However, the positions of the trucks, the size and weight of these truck loads are various. Therefore, direct monitoring of field-measured live-load stresses at fatigue-prone structural details is best suited for the fatigue life evaluation.

2. FATIGUE LIFE EVALUATION BY USING BI-LINEAR S-N CURVES

2.1 The Concept of Bi-linear S-N Curves

The AASHTO S-N curves are typically established based on the results of numerous experimental studies and the values of CAFLs are associated with the stress intensity factor range threshold, ΔK_{th} [7]. The stress intensity factor range can be expressed as Eq. (1).

$$\Delta K = \Delta \sigma \cdot \sqrt{\pi a} \cdot Y \quad (1)$$

And it follows as Eq. (2).

$$\Delta K_{th} = CAFL \cdot \sqrt{\pi a_i} \cdot Y \quad (2)$$

Where $\Delta \sigma$ is the applied stress-range; a is the size of fatigue crack; a_i is the hypothetical initial value of crack size associated with ΔK_{th} ; and Y is a non-dimensional function of the geometry including various factors such as finite width factor, non-uniform stresses factor, free surface effect factor and crack shape factor.

Stress range cycles in a spectrum with amplitudes higher than the CAFL would cause micro-scaled increase of the crack to greater than a_i and, as indicated in Eq. 2, the value of CAFL would decrease as the crack size increases because the value of ΔK_{th} remains constant. It is concluded that this condition would subsequently allow slightly lower magnitude stress-range cycles in a spectrum to contribute to the crack growth [5, 8-9].

By using this concept to examine the repeated cumulative damage of a few stress range histograms, Crudele & Yen [5] analytically examined the extension of S-N curves below the CAFL of four different AASHTO categories (B, C, D, and E). They found that the computed fatigue lives above the CAFL agreed well with the fatigue lives associated with the AASHTO S-N curves for all categories and, however, fatigue lives below the CAFL have to be re-estimated. Results indicated that the average slope of extended lines of the fatigue strength categories is -4 below the CAFL. This slope is recommended for use. Figure 1 shows the derived bi-linear S-N curves for all AASHTO categories [6]. The S-N curve of structural detail Category C' is shown in Figure 2 with some experimental data [10]. The result of Figure 2 provides confidence for the application of bi-linear S-N curves.

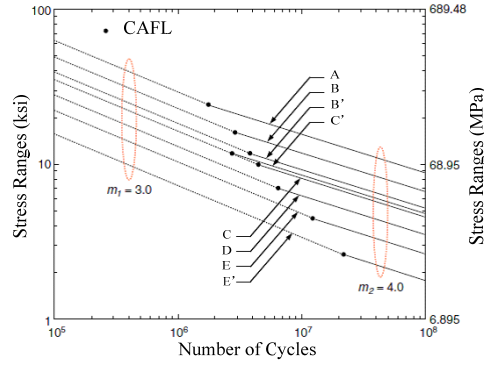


Figure 1. Bi-linear S-N Curves for All Fatigue Categories [6]

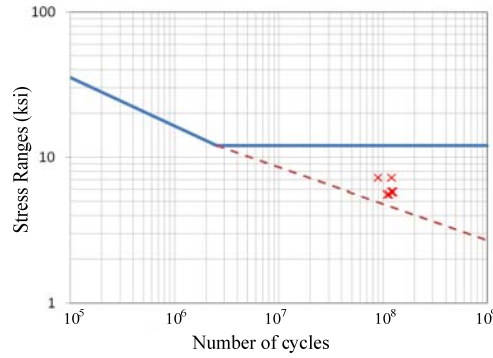


Figure 2. Bi-linear S-N Curves for Category C' [10]

It is worth noticing that Europe has adopted a set of tri-linear S-N curves with a slope of m when stress ranges are above CAFL, and the second slope below CAFL is suggested as $2m-1$ by Haibach [11-12], while $m=3$ is used in Eurocode 3[13] with a horizontal line after the cut-off limit at 100 million cycles, as shown in Figure 3. For other details, the first slope was also found to be $m_1=4$ and the second slope is $m_2 = 2m_1 - 1 = 7$ for riveted and bolted details.

2.2 Evaluation approach

According to Palmgren-Miner linear damage hypothesis, Eq. (3) indicates fatigue failure.

$$D = \sum_i \frac{n_i}{N_i} = 1 \quad (3)$$

Where n_i is number of cycles accumulated at stress range level i , for which damage would occur when the stress is applied N_i cycles; D is the fraction of life consumed by exposure to the cycles at the different stress range levels.

For a bi-linear S-N curve with a break at the magnitude of stress range K and the slopes of m_1 and m_2 above and below K , respectively, the application of Palmgren-Miner linear damage hypothesis shows in Eq. (4).

$$D = \sum_i \frac{n_i}{N_i} + \sum_j \frac{n_j}{N_j} = 1 \quad (4)$$

Where the subscripts i and j mean stress cycles above and below the break at K , respectively. Using the stipulation of equivalent stress range by Schilling et al. [14], Eq. (5) can be acquired.

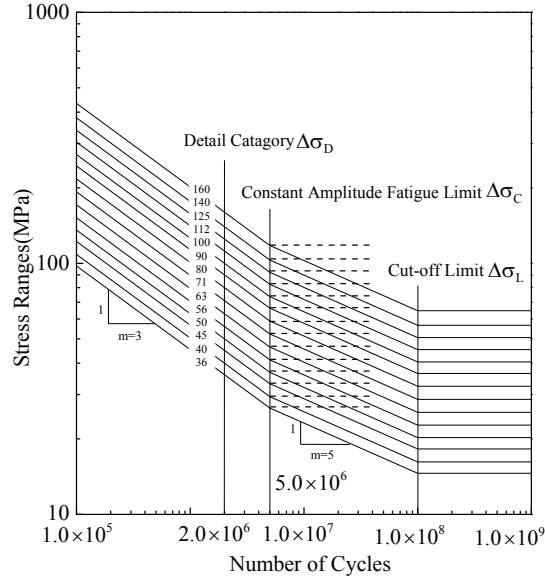


Figure 3. The Tri-linear S-N Curves in Eurocode 3 [13]

$$D = \sum_i \frac{n_i}{N_i} + \sum_j \frac{n_j}{N_j} = \frac{\sum_{i,j} (n_i + n_j)}{N_e} = 1 \quad (5)$$

The symbol N_e is the calculated fatigue life using the equivalent constant amplitude stress range S_{re} . The sum of all stress cycles is $\sum_{i,j} (n_i + n_j) = N$ and the equations for the two segments of the S-N curves are shown in Eq. (6).

$$N_i = A_{m_1} \cdot S_i^{-m_1} \quad \text{and} \quad N_j = A_{m_2} \cdot S_j^{-m_2} \quad (6)$$

Corresponding to N_e for single-slope S-N curves, the equations of the segments of the bi-linear one are shown in Eq. (7).

$$N_e = \begin{cases} A_{m_1} \cdot S_{rem_1 m_2}^{-m_1} & \text{for } S_{rem_1 m_2} \geq K \\ A_{m_2} \cdot S_{rem_1 m_2}^{-m_2} & \text{for } S_{rem_1 m_2} < K \end{cases} \quad (7)$$

$S_{rem_1 m_2}$ with a double subscripts, m_1 and m_2 , is the equivalent constant amplitude stress range for bi-linear S-N curves. By substituting Eq. (6) and Eq. (7) into Eq. (5), and solving for $S_{rem_1 m_2}$, Eq. (8) can be acquired.

$$S_{rem_1 m_2} = \begin{cases} \left(\sum_i \frac{n_i}{N} \cdot S_i^{m_1} + \frac{A_{m_1}}{A_{m_2}} \sum_j \frac{n_j}{N} \cdot S_j^{m_2} \right)^{1/m_1} & \text{for } S_{rem_1 m_2} \geq K \\ \left(\frac{A_{m_1}}{A_{m_2}} \sum_i \frac{n_i}{N} \cdot S_i^{m_1} + \sum_j \frac{n_j}{N} \cdot S_j^{m_2} \right)^{1/m_2} & \text{for } S_{rem_1 m_2} < K \end{cases} \quad (8)$$

By using the stress cycle, the coefficients ratio, N_k , in the Eq. 8 can be determined at the break of the S-N curve, shown in Eq. (9).

$$N_k = A_{m_1} K^{-m_1} = A_{m_2} K^{-m_2} \quad (9)$$

This leads to Eq. (10).

$$\frac{A_{m_1}}{A_{m_2}} = K^{m_1 - m_2}, \quad \frac{A_{m_2}}{A_{m_1}} = K^{m_2 - m_1} \quad (10)$$

In this way, $S_{rem_1 m_2}$ can be determined by Eq. (11).

$$S_{rem_1 m_2} = \begin{cases} \left(\sum_i \frac{n_i}{N} \cdot S_i^{m_1} + K^{m_1 - m_2} \sum_j \frac{n_j}{N} \cdot S_j^{m_2} \right)^{1/m_1} & \text{for } S_{rem_1 m_2} \geq K \\ \left(K^{m_2 - m_1} \sum_i \frac{n_i}{N} \cdot S_i^{m_1} + \sum_j \frac{n_j}{N} \cdot S_j^{m_2} \right)^{1/m_2} & \text{for } S_{rem_1 m_2} < K \end{cases} \quad (11)$$

Specifically, for a bi-linear S-N curve with the break at the CAFL (i.e. $K = CAFL$) and the slopes above and below CAFL of the S-N curve are $m_1 = 3$ and $m_2 = 4$, respectively. The equations for the equivalent constant amplitude stress ranges S_{re34} are expressed by Eq. (12).

$$S_{re34} = \begin{cases} \left(\sum_i \frac{n_i}{N} \cdot S_i^3 + \frac{\sum_j \frac{n_j}{N} \cdot S_j^4}{CAFL} \right)^{1/3} & \text{for } S_{re34} \geq CAFL \\ \left(CAFL \cdot \sum_i \frac{n_i}{N} \cdot S_i^3 + \sum_j \frac{n_j}{N} \cdot S_j^4 \right)^{1/4} & \text{for } S_{re34} < CAFL \end{cases} \quad (12)$$

The corresponding equations for fatigue life estimation are Eq. (13).

$$N_{34} = \begin{cases} A_3 \cdot S_{re34}^{-3} & \text{for } S_{re34} \geq CAFL \\ A_3 \cdot CAFL \cdot S_{re34}^{-4} & \text{for } S_{re34} < CAFL \end{cases} \quad (13)$$

For the categories, the values of A_3 and CAFL can be found in the AASHTO specifications.

In ordinary cases, when evaluating the fatigue life of an in-service steel bridge, only a small percentage of stress ranges in a stress histogram are above the CAFL and the computed S_{re34} would be below the CAFL. Consequently, the segment below of the CAFL with a slope of -4 could conservatively be used from Eq. (14) and Eq. (15) [15].

$$S_{re4} = \left(\sum_i \frac{n_i}{N} \cdot S_i^4 \right)^{1/4} \quad (14)$$

$$N_4 = A_3 \cdot CAFL \cdot S_{re4}^{-4} \quad (15)$$

3. APPLICATIONS

3.1 Wei River Railway Bridge

A railway steel bridge, recorded as No.1 Wei River Railway Bridge and shown in Figure 4, was monitored using field-measurement of live-load stresses at several fatigue-prone structural details. The bridge, built in 1982, is a welded and bolted steel girder bridge with twelve simply supported spans of 26.15m [16]. The monitoring of dynamic stresses under traffic conditions, detailed inspection for crack detection and examination of service traffic were conducted in the years of 2006, 2008 and 2011, for three short time periods.



Figure 4. No.1 Wei River Railway Bridge

3.1.1 Acquisition of stress range spectra

The photographs of two retrofit gusset plates which were studied are shown in Figure 5. These are 10UPU and 10DPU at the bottom flange connection between the end-panel lateral bracing frames and the main girders. The dynamic stresses in 24 hours and the type of trains, locomotives, carriage number and speed were recorded. The rain-flow counting procedure was used to count the different stress ranges. The live load stress range spectra at strain gauges 10UPU-1 and 10DPU-1 are given in Figure 6. As detail of Category B, the maximum stress range at 10UPU-1 is 64MPa and is below

the CAFL of 110 MPa. However, at 10DPU-1 the maximum stress range is 183 MPa and 60 cycles are above the CAFL.

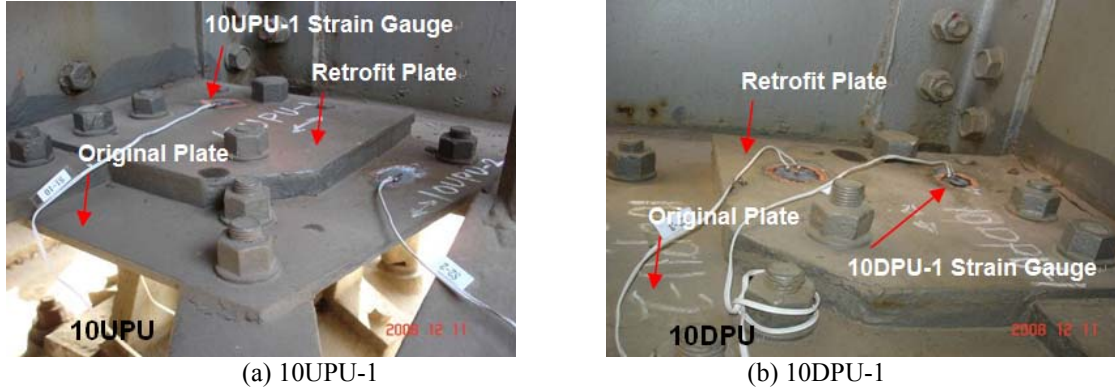


Figure 5. Strain Measure Points of No.1 Wei River Railway Bridge

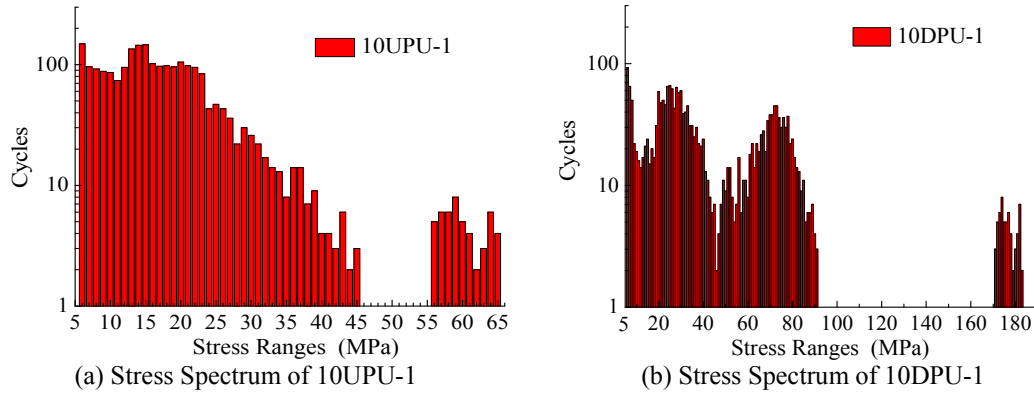


Figure 6. Recorded Stress Spectra of 10UPU-1 and 10DPU-1

3.1.2 Fatigue life evaluation

The equivalent constant amplitude stress ranges, S_{re34} of spectra in Figure 6 are computed using Eq. 12 and Eq. 14 for S_{re34} and S_{re4} , respectively. In addition, the current root-mean-cube (RMC) equivalent stress range in AASHTO specifications for fatigue life evaluation under variable amplitude stress ranges is computed for comparison by using Eq. (16) and Eq. (17).

$$S_{re3} = \left(\sum_i \frac{n_i}{N} \cdot S_i^3 \right)^{1/3} \quad (16)$$

$$N_3 = A_3 \cdot S_{re}^{-3} \quad (17)$$

The corresponding estimated fatigue lives are listed in Table 1.

As indicated earlier, all the stress cycles at gauge 10UPU-1 are below the CAFL of category B, so the expected fatigue life is infinite. At gusset plate measure point 10DPU-1, the increases in estimated fatigue life between using a single-sloped S-N line and the bi-linear line are 4.0 and 4.6 million cycles. The ratio of the increased life is 21.9%, and that of is 38.0%. In addition, as illustrated in Table 1, when the majority of stress range cycles in the spectrum are below the CAFL,

the estimated fatigue life by using a single S-N line of slope -4 below CAFL is very close to that by the bi-linear curve.

Table 1. Comparison of Estimated Fatigue Life

Detail	Category	N_3	N_{34}	N_4	$\frac{N_{34} - N_3}{N_3}$	$\frac{N_{34} - N_4}{N_4}$
		(Mil)	(Mil)	(Mil)		
10UPU-1	B	Infinite	Infinite	Infinite	-	-
10DPU-1	B	13.7	16.7	12.1	21.9%	38.0%

Other retrofitted details of categories C and D in Wei River Railway Bridge have also been evaluated using bi-linear S-N curves. The live load stress range spectra of two other structural details, 10UWI (Category C) and 12CBSD (Category D), are shown in Figure 7. The corresponding fatigue life evaluation results by using the AASHTO S-N curves and the bi-linear S-N curves are listed and compared in Table 2.

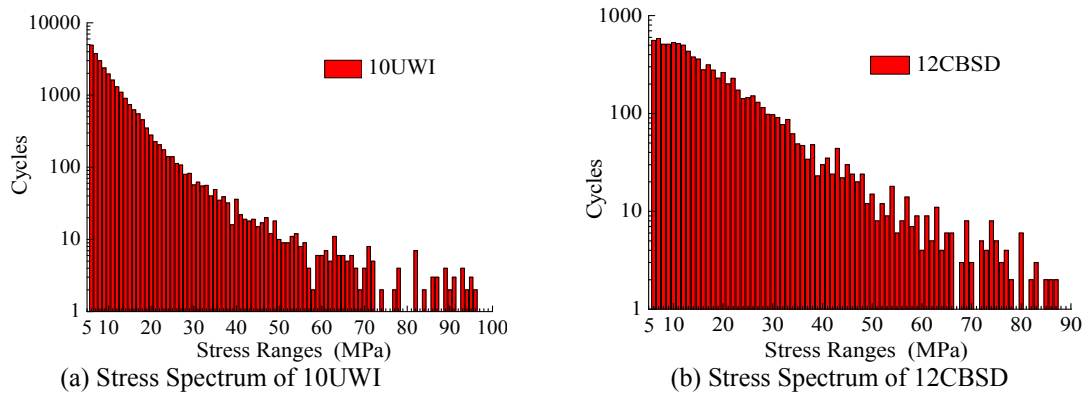


Figure 7. Recorded Stress Spectra of 10UWI and 12CBSD

Table 2. Comparison of Estimated Fatigue Life

Detail	Category	N_3	N_{34}	N_4	$\frac{N_{34} - N_3}{N_3}$	$\frac{N_{34} - N_4}{N_4}$
		(Mil)	(Mil)	(Mil)		
10UWI	C	17.5	22.3	20.1	27.4%	10.9%
12CBSD	D	15.7	18.7	15.2	19.1%	23.0%

From the results listed in Table 2, the evaluation based on bi-linear fatigue S-N curves with different slopes above and below the CAFL always predicts a longer fatigue life compared to that based on the single slope AASHTO S-N curves. The increase of estimated fatigue life can be quite significant. For the category C detail 10UWI, the increase is 4.8 million cycles and the increased life ratio is 27.4%. For the category D detail 12CBSD, the increase is 3.0 million cycles and the increased life ratio is 19.1%. For the 3 details listed in Tables 1 and 2, using bi-linear fatigue S-N curves compared to using the current AASHTO S-N curves results in at least a 19.1% increase of fatigue life. This suggests that it may be unnecessary to take rehabilitation action at some structural details, which could reduce the maintenance fee and life-cycle cost.

To examine the evaluation of fatigue life by the Eurocode S-N curves, the fatigue life of the 3 details are calculated according to the procedure of Eurocode 3. The procedure of using RMC as the equivalent constant amplitude stress range is in essence the extension of slope -3 down to below

the CAFL without considering the portion of the S-N curves with a slope of -5. And ignoring of all stress data below the horizontal cut-off limit means ignoring the contribution of those stress cycles to the growth of the fatigue crack. Consequently, it is expected that the estimated fatigue life by using the suggested procedure for the bi-linear Eurocode S-N curves is longer than that by the suggested bi-linear S-N curves for AASHTO. This is the case for all four details of the Wei River Railway Bridge as listed in Table 3.

It is suggested that a set of equations for the bi-linear S-N curves with the break at the CAFL be used for the Eurocode 3. The slopes above and below CAFL of S-N curves are -3 and -5, respectively. From Eq. (11), the equivalent constant amplitude stress range S_{re35} can be expressed as Eq. (18).

$$S_{re35} = \begin{cases} \left(\sum_i \frac{n_i}{N} \cdot S_i^3 + \frac{\sum_j \frac{n_j}{N} \cdot S_j^5}{(CAFL)^2} \right)^{1/3} & \text{for } S_{re35} \geq CAFL \\ \left[(CAFL)^2 \cdot \sum_i \frac{n_i}{N} \cdot S_i^3 + \sum_j \frac{n_j}{N} \cdot S_j^5 \right]^{1/5} & \text{for } S_{re35} < CAFL \end{cases} \quad (18)$$

The corresponding equations for the estimation of fatigue life is Eq. (19).

$$N_{35} = \begin{cases} A_3 \cdot S_{re35}^{-3} & \text{for } S_{re35} \geq CAFL \\ A_3 \cdot (CAFL)^2 \cdot S_{re35}^{-5} & \text{for } S_{re35} < CAFL \end{cases} \quad (19)$$

In most cases, when evaluating the fatigue life for in-service steel bridges, only a small percentage of stress ranges are above the CAFL and the computed S_{re35} would be below the CAFL. Consequently, the segment below of the CAFL with a slope of -5 could conservatively be used from Eq. 20 and Eq. 21.

$$S_{re5} = \left(\sum_i \frac{n_i}{N} \cdot S_i^5 \right)^{1/5} \quad (20)$$

$$N_5 = A_3 \cdot (CAFL)^2 \cdot S_{re5}^{-5} \quad (21)$$

The procedure of using the bi-linear line with slopes of -3 and -5, and ignoring the damage contribution of stress ranges below the horizontal cut-off limits. Table 3 shows the comparison between the calculated fatigue lives. From Table 3, it is obvious that the estimated fatigue life by using bi-linear line with slopes of -3 and -5 (L_{35}) is close to Eurocode 3 approach (L_{euro}), both of which are slightly longer than by using the suggested bi-linear S-N curves for AASHTO (L_{34}). The suggested procedure of the bi-linear L_{35} is less conservative in fatigue life evaluation compared to using the bi-linear S-N curves with the slopes of -3 and -4 (L_{34}) and the current AASHTO S-N curves.

Table 3. Comparison of Estimated Fatigue Life

Detail	Category	L_{35} (Year)	L_{euro} (Year)	L_{34} (Year)	$\frac{L_{35} - L_{\text{euro}}}{L_{\text{euro}}}$	$\frac{L_{35} - L_{34}}{L_{34}}$
10DPU-1	B	92	88	80	4.5%	15.0%
10UWI	C	211	217	179	-2.8%	17.9%
12CBSD	D	85	93	75	-8.6%	13.3%

3.2 Wei River Freeway Bridge

To further apply and analyze the bi-linear S-N curves for fatigue life evaluation for in-service bridges, a freeway bridge, named as Wei River Freeway Bridge shown in Figure 8, was monitored by field-measurement of live load stress at several fatigue-prone structural details in orthotropic steel bridge deck. Wei River Freeway Bridge, built in 2011, is a continuous concrete bridge as a whole while a 53.68m steel girder is adopted at side span to optimize the overall structural behavior. Since there are many fatigue details in OSDs [17], a twelve-day dynamic stress monitoring under traffic conditions were conducted in 2013 to evaluate the fatigue performance of the structure.

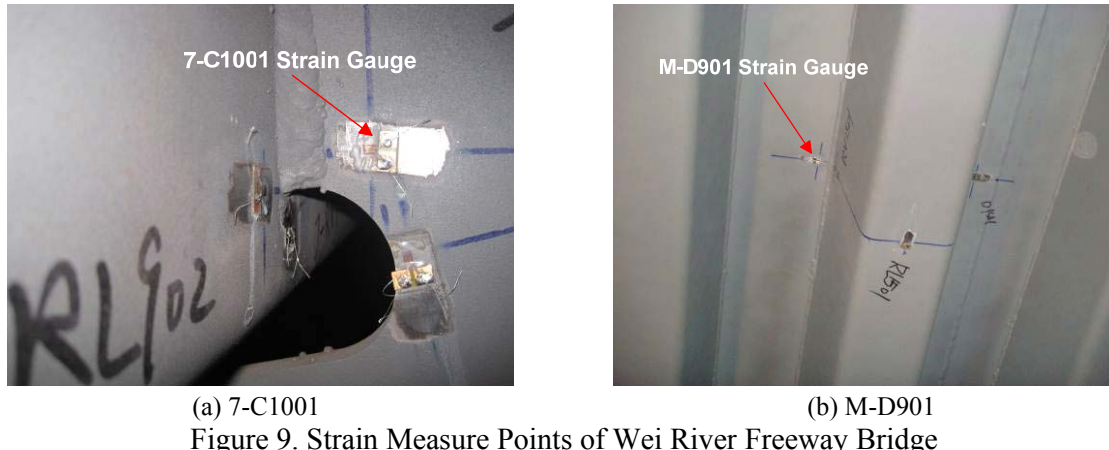


Figure 8. Wei River Freeway Bridge

3.2.1 Acquisition of stress range spectra

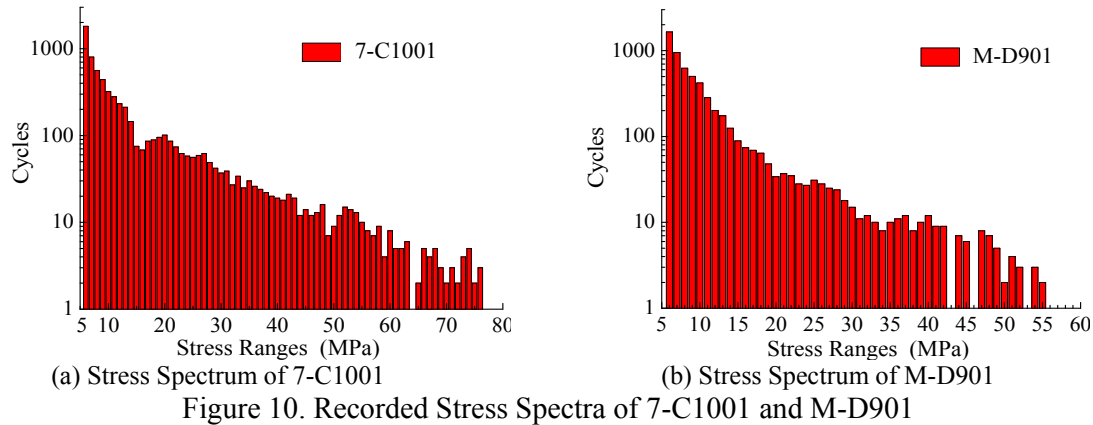
The photographs of two fatigue details which were studied at the case of Wei River Freeway Bridge are shown in Figure 9. The strain gauge 7-C1001 is at the end of rib-to-diaphragm in a diaphragm. The strain gauge M-D901 is at the weld joint of rib-to-deck in a deck plate. The dynamic stresses, the number and type of trucks were recorded. The rain-flow counting procedure was used to count the different stress ranges.

However, Wei River Freeway Bridge is a part of a new freeway open to traffic since December, 2011. This newly built freeway is planned to have more branches, but at this stage it just connect Xi'an city and Tongchuan city. Meanwhile, there is an old in-service freeway nearby, and the old one has more branches and cheaper tolls. Thus, the traffic volume of the new freeway is relatively small at present, and the average daily truck volume is about 500.



(a) 7-C1001 (b) M-D901
Figure 9. Strain Measure Points of Wei River Freeway Bridge

The resulting live load stress range spectra at strain measure points 7-C1001 and M-D901 are given in Figure 10. The maximum stress ranges at 7-C1001 and M-D901 are 78 MPa and 57 MPa, respectively.



(a) Stress Spectrum of 7-C1001 (b) Stress Spectrum of M-D901
Figure 10. Recorded Stress Spectra of 7-C1001 and M-D901

3.2.2 Fatigue life evaluation

The estimated fatigue lives for the details in Figure 9 are calculated using Eq. 13, Eq. 15 and Eq. 17 for N_3 , N_{34} and N_4 , and, respectively. The corresponding life L_3 , L_{34} and L_4 are listed and compared in Table 4.

Table 4. Comparison of Estimated Fatigue Life

Detail	Category	N_3	L_3	N_{34}	L_{34}	N_4	L_4	$\frac{L_{34} - L_3}{L_3}$	$\frac{L_4 - L_{34}}{L_{34}}$
		(Mil)	(Year)	(Mil)	(Year)	(Mil)	(Year)		
7-C1001	C	21.0	93	29.7	131	29.3	129	40.9%	-1.5%
M-D901	D	22.6	118	29.5	154	28.8	151	30.5%	-1.9%

At 7-C1001, the increase in estimated fatigue life between using a single-slope S-N curve and the bi-linear curve is $131 - 93 = 38$ years. The ratio of the increased life $(L_{34} - L_3) / L_3$ is 40.9%. At M-D901, the ratio of $(L_{34} - L_3) / L_3$ is 30.5%. It is also proved that the evaluation based on bi-linear fatigue S-N curves with different slopes above and below the CAFL will predict a longer fatigue life compared to that based on the single slope AASHTO S-N curves. In addition, compared

to single slope of -4, the decreased life ratio of the bi-linear S-N curve approach $(L_4 - L_{34}) / L_{34}$ is -1.5% and -1.9%.

To examine the proposed bi-linear S-N curves for Eurocode 3, the estimated fatigue lives for 7-C1001 and M-D901 are calculated using Eq. 19 for N_{35} . The corresponding L_{35} is compared with L_{euro} and L_{34} in Table 5. From Table 5, it is obvious that the estimated fatigue life by using bi-linear curves with slopes of -3 and -5 (L_{35}) is longer than by using the suggested bi-linear S-N curves for AASHTO (L_{34}).

Table 5. Comparison of Estimated Fatigue Life

Detail	Category	L_{35} (Year)	L_{euro} (Year)	L_{34} (Year)	$\frac{L_{35} - L_{\text{euro}}}{L_{\text{euro}}}$	$\frac{L_{35} - L_{34}}{L_{34}}$
7-C1001	C	170	162	131	4.9%	29.8%
M-D901	D	189	201	154	-6.0%	22.7%

4. SUMMARY AND CONCLUSIONS

This paper provides information for fatigue life evaluation of in-service steel bridges by integrating field-measured live-load stresses into the bi-linear S-N curves with a break at the constant amplitude fatigue limit (CAFL). The current procedure of AASHTO specifications, with a direct extension of S-N curves to below the CAFL, appears to be too conservative. The slopes of suggested bi-linear S-N curves for the AASHTO specifications are -3 and -4, while for the Eurocode are -3 and -5. Equations for the calculation of the equivalent constant amplitude stress range are presented and applied.

From this study, the following conclusions can be drawn:

- (1) Compared to the estimated fatigue life using the current single-slope AASHTO S-N curves, applying the bi-linear S-N curves always results in a longer fatigue life for the structural details in a bridge.
- (2) When the majority of stress range cycles in a stress spectrum are below the CAFL, the calculated fatigue life by using only the portion of S-N curves below the CAFL can be close to that by using bi-linear curves.
- (3) The estimated fatigue life by using the suggested procedure for the bi-linear Eurocode S-N curves is always longer than that by using the suggested bi-linear S-N curves for AASHTO. This is due to the difference in slope below the CAFL.
- (4) There are only limited data of long time or high cycle fatigue damage due to variable stresses. Development of such data is recommended.

ACKNOWLEDGMENTS

The writer gratefully acknowledges the financial support provided by National Natural Science Foundation of China (Grant No.51078039), the Major State Basic Research Development program of China (973 Program) Sub-program (2015CB057703, 2015CB057706), the Special Fund for Basic Scientific Research of Central Colleges of the P.R. China, Chang'an University

(10821153501, 310821153401, 310821153314 and 2013G3212002), the Applied Basic Research Program of the Ministry of Transport of the P.R. China (2014319812080) and the technical support provided by Xi'an Railway Bureau for the field measurements.

REFERENCES

- [1] AASHTO, "AASHTO LRFD Bridge Design Specifications 5th Ed.", AASHTO, Washington, DC., USA, 2010.
- [2] AASHTO, "AASHTO Manual for Bridge Evaluation", AASHTO, Washington, DC., USA, 2008.
- [3] Yen, B.T., Hodgson, I.C., Zhou, Y. E. and Crudele, B.B., "Estimation of Fatigue Life Below CAFL", Proceeding of the 2nd International Conference on Fatigue and Fracture in the Infrastructure, ATLSS Engineering Research Center, Lehigh University, Bethlehem, USA, 2009.
- [4] Connor, R.J., Hodgson, I.C., Mahmoud, H.N. and Bowman, C.A., "Field Testing and Fatigue Evaluation of the I-79 Neville Island Bridge over the Ohio River", Center for Advanced Technology for Large Structural Systems (ATLSS), Lehigh University, Bethlehem, USA, 2005.
- [5] Crudele, B.B. and Yen, B.T., "Analytical Examination of S-N Curves Below Constant Amplitude Fatigue Limit", Proceeding of the 1st International Conference on Fatigue and Fracture in the Infrastructure, ATLSS Engineering Research Center, Lehigh University, Bethlehem, PA, USA, 2006.
- [6] Kwon, K., Frangopol, D.M. and Soliman, M., "Probabilistic Fatigue Life Estimation of Steel Bridges by Using a Bilinear S-N Approach", Journal of Bridge Engineering, ASCE, 2012, Vol.17, No.1, pp. 58–70.
- [7] Barsom, J.M. and Rolfe, S.T., "Fracture and Fatigue Control in Structures: Applications of Fracture Mechanics, Third Edition", American Society for Testing and Materials, West Conshohocken, USA, 1999.
- [8] Xiang, Y.B., Lu, Z.Z. and Liu, Y.M., "Crack Growth-based Fatigue Life Prediction Using an Equivalent Initial Flaw Model. Part I: Uniaxial Loading", International Journal of Fatigue. 2010, Vol.32, No.2, pp. 341-349.
- [9] Lu, Z.Z., Xiang, Y.B. and Liu, Y.M., "Crack Growth-based Fatigue Life Prediction Using an Equivalent Initial Flaw Model. Part II: Multiaxial Loading", International Journal of Fatigue. 2010, Vol.32, No.2, pp. 376-381.
- [10] Fisher, J.W., Nussbaumer, A., Keating, P.B. and Yen, B.T., "Resistance of Welded Details under Variable Amplitude Long-life Fatigue Loading", National Cooperative Highway Research Program (NCHRP), Rep. No. 354, Transportation Research Board, National Research Council, Washington, DC., USA, 1993.
- [11] Haibach, E., "Modified Linear Damage Accumulation Hypothesis Accounting for a Decreasing Fatigue Strength During Increasing Fatigue Damage", Laboratorium für Betriebsfestigkeit, Darmstadt, 1970.
- [12] Haibach, E., "Questions Concerning the Fatigue Strength of Welded Joints Considered from a Conventional and a Fracture Mechanical Point of View", Schw. Schn., 1977, No.4, pp. 140-142.
- [13] EN 1993-2, "Eurocode 3: Design of Steel Structures: Part 2: Steel Bridges", European Committee for Standardization, Brussels, 2006.
- [14] Schilling, C.G., Klippstein, K.H., Barsom, J.M., et al., "Fatigue of Welded Steel Bridge Members under Variable Amplitude Loading", National Cooperative Highway Research Program (NCHRP), Rep. No. 188, Transportation Research Board, National Research Council, Washington, DC., USA, 1978.

- [15] Yen, B.T., Hodgson, I.C., Zhou, Y.E. and Crudele, B.B., "Bi-linear S-N Curves and Equivalent Stress Ranges for Fatigue Life Estimation", *Journal of Bridge Engineering*, ASCE, 2013, Vol. 18, No.1, pp.26-30.
- [16] Wang, C.S. Yan, S.L. and Hao, L., "Fatigue Safety Assessment of Existing Railway Steel Bridges Based on In-situ Monitoring Data", *Proceeding of the 6th International Conference on Maintenance, Safety and Management*, Italy, 2012, pp. 812-817.
- [17] Partov, D., and Dinev, D., "Structure, Design and Construction of a Steel Orthotropic Bridge in Sofia ", *Advanced Steel Construction*, 2007, Vol. 3, No. 4, pp. 752-764.

EXTENDING THE FATIGUE LIFE OF RIVETED BRIDGES USING DATA FROM LONG TERM MONITORING

Eugen Brühwiler

*Civil Engineering Institute, Swiss Federal Institute of Technology (EPFL),
Station 18, CH-1015 Lausanne, Switzerland
(Email: eugen.bruehwiler@epfl.ch)*

ABSTRACT: A methodology inherent to existing structures is presented for the fatigue safety verification of riveted bridges. The suggested approach allows for the determination of updated action effects explicitly considering data from long term monitoring. Data from monitoring allow for accurate determination of fatigue relevant stresses in fatigue prone bridge elements, and uncertainties in the determination of updated action effects are reduced. By means of the presented approach, the fatigue safety of a riveted railway bridge of high cultural heritage value was verified after 115 years of service duration. Data from monitoring were exploited by Rainflow analysis and served as the basis for the fatigue safety verification. As the locations of measurements are generally not identical with the cross sections of verification, measured strains were translated to the relevant verification cross section by means of factors that were determined by structural analysis. Sufficient fatigue safety was finally verified for the entire riveted structure and additional service duration of at least 50 years was validated.

Keywords: Fatigue safety, Service life, Riveted steel bridge, Fatigue damage accumulation, Structural health monitoring, Examination

DOI: 10.18057/IJASC.2015.11.3.3

1. INTRODUCTION

In many countries, civil structures have been in service already for several generations. As part of the transportation infrastructure, bridges add value to the public economy. Therefore, there is high interest in economic performance while providing unrestricted utilisation (e.g. without limits on traffic loads) and responding to increasing traffic demands. Obviously, there is a need to extend the service life of civil structures even further, i.e., significantly beyond 100 years, which often is the arbitrarily presumed service life of structures.

In this context, structural engineers have to devise novel ways to examine the structural safety of existing structures, in particular when high cultural values are involved. The contemporary approach is based on an inherent methodology that essentially includes collecting detailed in situ information about the structure, for example, by long term monitoring of structural behaviour. Parameters controlling structural safety are determined more precisely and, for example, the structural safety of an existing bridge can be proved using so-called updated values for actions (loads) and resistance. In this way, it can often be shown that an existing structure may be subjected to higher load effects while meeting the safety requirements, thereby avoiding intervention.

Regarding existing bridges, a greater source of uncertainty lies on the traffic loading or more specifically the action effects arriving in the structural elements. In recent years, increasingly sophisticated approaches have emerged for load effect estimation using traffic simulations incorporating Weigh-in-Motion (WIM) data which form the basis of load models in design and “assessment” codes. While vital for design, these codes are based on generic heavy vehicle data from a range of locations and therefore may not always represent the site conditions at the existing bridge under investigation. In addition, codes include provisions for illegally overloaded vehicles

which can be reduced substantially through adequate policing (on roads and also on railways) which varies hugely between countries.

An important distinction between existing bridge safety verification and fatigue design of a new bridge is that an existing bridge structure can be monitored to determine the real ‘action effects’ experienced. The advent of cheap and high storage capacity hardware in recent years means that direct measurement of elemental action effects via structural monitoring is now a viable option. Monitoring can overcome limitations of accurately modelling in-service behaviour at an elemental level. For example, material properties may change over time and secondary elements may reduce the stress levels in the structural parts which can provide uncertainty in modelling but these effects are inherent in the measured data. In addition, reliable local WIM data is not always available.

This paper introduces a novel approach to verify and predict the future service duration and the fatigue safety of bridges using data from monitoring. The approach is illustrated by means of an application case in Switzerland related to a larger riveted railway bridge of high cultural value and in service for more than 115 years. It will be shown that there are no ‘old’ bridges, but bridges that provide adequate performance (or not). Extending the service life of bridges by following the approach presented in this paper may allow continuous utilisation of existing structures rather than their replacement. This approach is clearly in agreement with the principles of sustainable development.

2. PROPOSED APPROACH

2.1 Introduction

Examination (also called “assessment”) of an existing structure may be performed following the principles such as the ones defined in the Swiss Standards for existing structures enforced by the Swiss Society of Engineers and Architects (SIA) (Brühwiler et al. [1], SIA 269 [2]). In Switzerland, these standards provide the regulative basis the structural engineer can rely on to deal professionally with existing structures.

These principles lead to a methodology inherent to existing structures which has already been successfully applied over the last 25 years. Yet, many structural engineers nowadays still apply codes for the design of new structures to assess existing structures. This is fundamentally wrong and this over-conservative approach often leads to unnecessary and costly interventions. A change of paradigm is urgently needed aiming the structural engineering community to clearly distinguish between codes for new structures and codes for existing structures.

The contemporary approach to existing structures is based on updating, which means collecting and exploiting detailed in-situ information from the existing structure while reducing uncertainties in structural parameters. The controlling parameters are determined as precisely as needed following a stepwise procedure with increasing focus on details. The general examination comprises the whole structure with the objective to identify aspects that need to be examined in more detail. One or more detailed examinations follow with the focus on the identified aspects.

2.2 Structural Safety Verification Format

The structural safety verifications are performed using updated values, called examination values, with the objective to verify for the existing structure that the relevant limit states are not exceeded. Usually, deterministic verification is conducted, and the notion of degree of compliance n is introduced in the deterministic verification of structural safety:

$$n = \frac{R_{d,updated}}{E_{d,updated}} \quad (1)$$

where $R_{d,updated}$ and $E_{d,updated}$ are the examination values of resistance and action effect, respectively. The degree of compliance is a numerical statement showing the extent to which an existing structure fulfils the structural safety requirements. This formulation not only gives the information whether the structural safety is fulfilled, i.e. $n \geq 1,0$, it also indicates by how much the verification is fulfilled (or not). The latter is necessary for the evaluation of results and in view of the planning of interventions.

In this context, monitoring of structural behaviour has thereby the general objective to determine more accurately effective action effects in terms of measured strains (stresses), displacement or accelerations, arriving in structural elements such as relevant parts of steel structures, steel reinforcing bars and concrete in reinforced concrete or other structures.

2.3 Determination of Updated Action Effect

In the first step of verification on Level 1 (general examination), the examination value of action effect $E_{d,updated}$ is determined using updated load models (for permanent and live loads) (SIA 269/1 [3]) which are applied to a structural model to obtain sectional forces, stresses and strains, i.e. action effects, through structural analysis (Figure 1). This approach is analogous to the one generally applied for the design of new structures. While this simple approach may lead in many cases to suitable results (i.e. showing that structural safety is fulfilled), it only takes partly advantage of the fact that the existing structure exists and thereby information may be gained.

If safety verification is not conclusive on Level 1, further updating may be performed on Level 2 in a detailed examination, by performing monitoring of action effects due to live loads (Figure 1). In this way, action effects are directly measured by monitoring reducing thus sources of uncertainty.

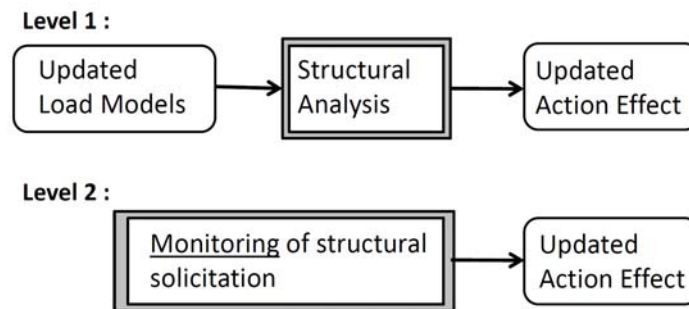


Figure 1. Determination of Updated Action Effect

However, it may not always be possible to obtain data from monitoring directly in the cross sections determinant for the safety verification. Also, action effect due to permanent load (dead load) obviously cannot be recorded by monitoring. Structural analysis is thus needed to “translate” data from monitoring to sections determinant for the structural safety verification (Figure 2) and to determine the solicitation of the existing structure due to permanent loads.

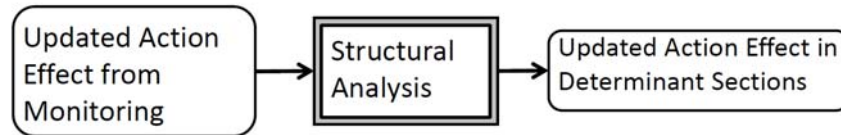


Figure 2. Translation of Data from Monitoring to Sections Determinant for Structural Safety

Consequently, the use of structural models changes its importance when compared to structural analyses for the design of new structures. Also, data from monitoring are used to calibrate the structural model with the objective to obtain sectional forces as accurate as possible thereby reducing uncertainty usually implied in structural analysis.

Such a calibrated structural model may then be used to determine, for example, fatigue action effects of future traffic scenarios. Note that following the approach on Level 2, no more load model is actually needed as solicitation of structural elements is directly recorded which obviously is the most reliable data to verify structural safety.

2.4 Safety Requirements

The structural safety requirements imposed on an existing structure need to be clearly defined as they may have a major influence on the extent of interventions. Monitoring of action effects on structural elements reduces uncertainties. Yet, some safety margin needs to be respected, either by considering a partial safety factor or, in the case of fatigue safety verification, by some criterion of target level of acceptable fatigue damage.

3. CASE STUDY OF A RIVETED RAILWAY BRIDGE

The approach presented in Chapter 2 has been applied for the verification of fatigue safety of a riveted steel railway bridge as shown in the following. More detailed information on this case study is given in Brühwiler et al. [4].

3.1 Description of the Bridge

The railway bridge across the River Rhine at Eglisau in Switzerland was built from 1895 to 1897 for single lane railway traffic. The central part of the 457 m long bridge is a riveted steel truss structure made of early mild steel. The truss has a span of 90m and a height of 9m. Multiple arch approach viaducts in natural stone masonry with piers up to 50m in height follow in the north and south of the steel structure (Figure 3).

In 1982/83, the original carriageway (that consisted of a ballasted track on Zores iron profiles) was replaced by a steel trough with ballast. This led to the situation that structural parts of the carriageway (which are usually of most fatigue relevance) are no longer determinant. In the following, only the main girder is discussed.



Figure 3. Railway Bridge across the River Rhine at Eglisau, Switzerland

3.2 Model for Structural Analysis

In the first phase of this case study, the truss structure was modelled by means of a three-dimensional bar model in order to determine sectional forces necessary for structural safety verification. A three-dimensional model was necessary because the carriageway (consisting of the trough, cross girders and floor beams) is located approximately 1.5 m below the top chord of the main truss and thus contributes to the global structural behaviour by carrying significant compression forces in addition to the top chord. The nodes of the main truss were modelled with fixed connections and eccentricity was taken into account. However, the bars of the upper and lower wind bracing as well as of the transverse bracings were modelled with pinned connections. Comparison of the results from the load tests and structural analysis confirmed the adequacy of the structural model allowing calculating the structural behaviour with sufficient precision.

3.3 Monitoring

Strain gauges relevant for the verification of the fatigue safety were mounted on structural elements and zones that are essentially subjected to tensile stresses in (Figure 4):

- Field 1 on the two tensile diagonals and posts of the main truss and on the trough, floor beams and cross girders of the carriageway, and
- Field 10 on the lower chord at mid-span.

In addition to the criterion of having good accessibility, strain gauges were placed such that strain distribution in the measured cross section corresponds most likely to gross section stresses (Figure 4 right). This means, that the measuring locations lie as far away as possible from rivet holes or other “hot spots”, to avoid measuring any stress concentration close to rivets. Figure 5 (left) shows some cross sections with the arrangement of strain gauges.

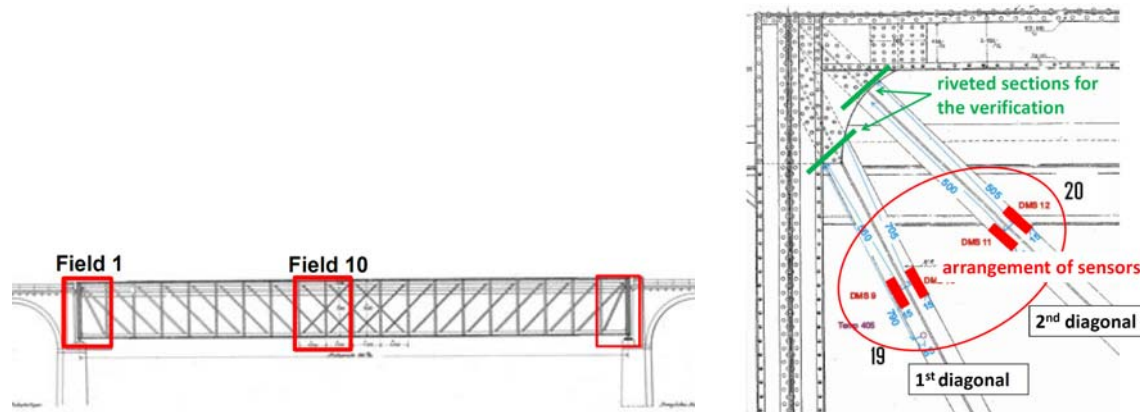


Figure 4. Left: Localisation of the Strain Gauges Relevant for the Fatigue Safety Verification; Right: Location of Sensors and Verification Sections of Diagonals in Field 1

The strain readings of all sensors due to the passage of every train, including passenger and freight trains, were recorded over a period of 12 months. As an example, Figure 5 (right) shows the structural response (as a function of time) of various elements due to the passage of a freight train. As expected, the results depict the small influence of single axle loads on diagonals and lower chord of the truss girder, while the strain readings for the cross girder show first a continuous increase (due to the global load bearing behaviour) followed by the distinct effect of the passage of each axle with rather large strain variations (local load bearing behaviour). Analysis of recorded data confirmed that the fully automatic monitoring system allowed for reliable long term readings that could subsequently be exploited as a basis for the verification of fatigue safety.

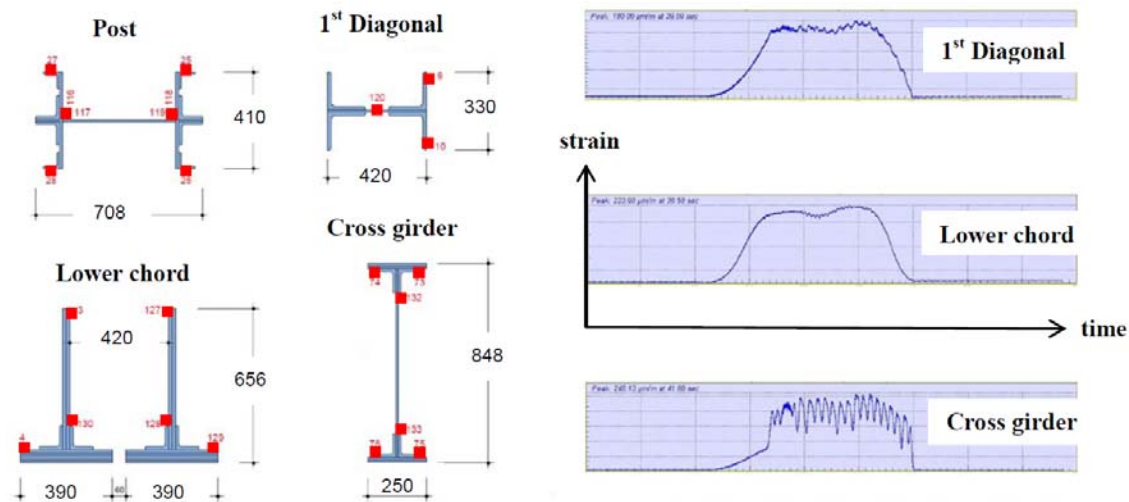


Figure 5. Left: Arrangement of Strain Gauges in Cross Sections; Right: Recorded Data of One Gauge on the 1st Diagonal and Lower Chord of the Truss Girder as well as on a Cross Girder

Monitored raw data from every train passage were analysed by means of Rainflow analysis, i.e. stress ranges were assigned to selected strain (stress) range groups and the number of strain ranges per group was counted. All monitored values were added over one calendar month, stored on Excel tables. Finally, the results from all 12 months of monitoring were summed up. Figure 6 shows graphically presented histograms for the two analysed diagonals (which turned out to be the most fatigue relevant elements).

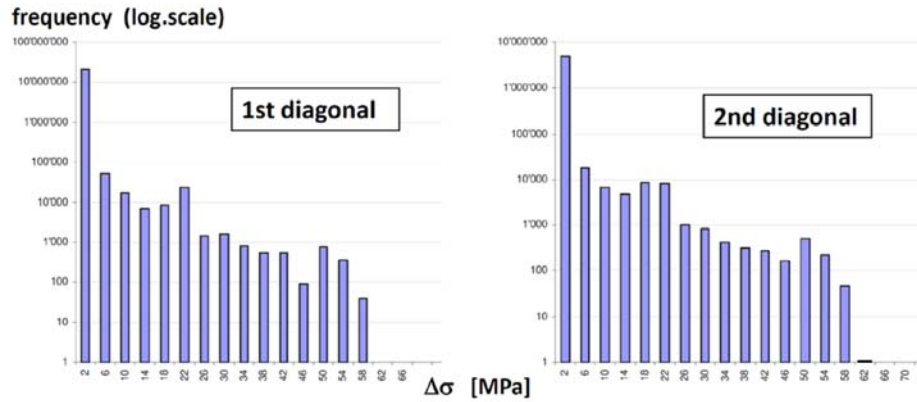


Figure 6. Histograms of a Compilation of Stress Ranges over the Whole Monitoring Period of the Two Diagonals of the Main Truss

3.4 Fatigue Safety Verification

Fatigue safety is verified for determinant cross sections (details) with rivets. Since the location of the strain sensors were intentionally chosen to avoid measuring any stress concentration near rivets, monitored strain (stress) values need to be translated to the determinant rivet positions of the cross sections relevant for verification (Figure 4 right). Consequently, conversion factors were determined for each verified cross section using the calibrated model for structural analysis. For this, a specific loading configuration was chosen to determine the sectional forces. Moreover, as tensile stresses obtained from monitored values are valid for gross sections, the conversion factor also considers net sectional areas in the relevant sections with rivet holes. These conversion factors were then applied to the monitored values to obtain stress range values for the fatigue safety verification.

Fatigue safety was verified with respect to fatigue resistance for riveted details as given in SIA 269/3 [5] and Taras & Greiner [6] (Figure 7). Fatigue category of 71 MPa (with a constant amplitude fatigue limit of 51 MPa) was taken into account for the diagonals and the lower chord of the main truss girder. This fatigue resistance is to be compared with stress ranges calculated using net-section stresses.

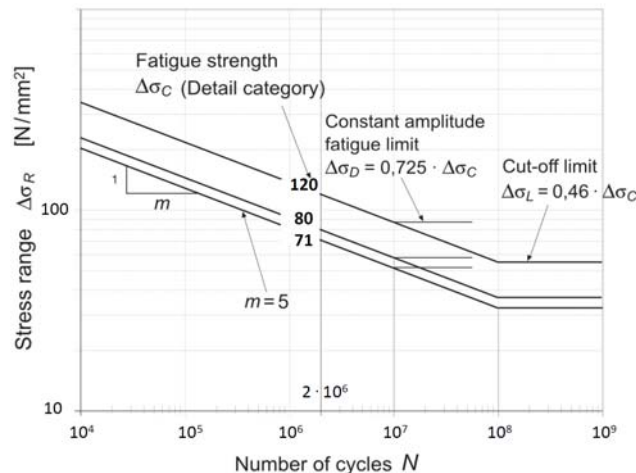


Figure 7. Fatigue Strength for Riveted Structural Details, According to SIA 269/3 [5]

The fatigue resistance given in Figure 7 is considered to be rather conservative in particular in the domain of low stress ranges and high numbers of cycles which is the relevant domain in the present case. Indeed, constant-amplitude fatigue limit of riveted members was estimated to be at a stress range level of 70 MPa based on fatigue tests up to 20 million cycles (Brühwiler et al. [7]); more research is needed to explore more in detail the fatigue behaviour of riveted details at high numbers of cycles.

Verification of fatigue safety followed a stepwise procedure:

– *Step 1: Fatigue safety verification with respect to the fatigue limit :*

For every fatigue relevant verification section, the maximum monitored value of stress range over the whole monitoring period was translated into maximum stress range for the verification using the corresponding conversion factor. The results for the two diagonals are given in Table 1. The fatigue safety is verified if the degree of conformity n , i.e., the ratio of fatigue limit to maximum fatigue stress range, is equal to or larger than 1.0.

Table 1. Results of the Verification with Respect to the Fatigue Limit for the Two Main Diagonals

Structural element	max. stress range from monitoring [MPa]	Conversion factor	max. stress range (verific. section) $\Delta\sigma_{\max}$ [MPa]	Fatigue limit $\Delta\sigma_D$ [MPa]	Degree of conformity $n = \frac{\Delta\sigma_D}{\Delta\sigma_{\max}}$
<i>Main truss:</i>					
1 st diagonal	58	1.71	99	51	0.52
2 nd diagonal	62	1.33	82	51	0.62

The two main diagonals do not pass the fatigue safety check with respect to the fatigue limit. Consequently, they are verified on the next verification level according to Step 2.

– *Step 2: Fatigue damage accumulation calculation and fatigue safety verification*

The first and second diagonals were investigated by means of Palmgren-Miner damage accumulation method using the S-N curves for riveted details (Figure 6). Stress ranges below the cut off limit were neglected.

In a first step, fatigue damage over the 12 months of monitoring (April 2011 – March 2012, average of 159 trains per day) was determined. Histograms of stress range as obtained from Rainflow analysis were translated to the verification sections by applying the conversion factors. Then, for each stress range $\Delta\sigma_i^m$, the maximum number of cycles N_i was determined as follows:

$$N_i = \frac{\Delta\sigma_c \cdot 2 \cdot 10^6}{\Delta\sigma_i^m} \quad (2)$$

with $\Delta\sigma_c$ being the fatigue strength at 2 million cycles. The measured number of cycles n_i for each stress range was then used to determine the theoretical fatigue damage d_i per stress range:

$$d_i = \frac{n_i}{N_i} \quad (3)$$

And by summing up over all k stress ranges, the total damage D is obtained:

$$D = \sum_{i=1}^k d_i \quad (4)$$

Fatigue failure is supposed to occur if the total damage reaches a value of $D = 1.0$.

Past traffic was modelled using the load models valid for the respective allowable Line Classes as defined by the European Railways (UIC Code 700 [8]). During the initial phase of railway service, traffic similar to Line Class B2 was allowed. With the electrification in 1928, traffic loads were increased to Line Class C3. With the modification of the carriageway in 1982, the Line Class was again increased to D4. In addition, reliable data was available regarding train numbers and gross register tonnage (GRT) per year from the statistical yearbooks of the Swiss Federal Railways. With this data, fatigue solicitation of the bridge during the past service period from 1897 to 2011 could be estimated with good precision. For the future railway traffic, a scenario for the expected traffic in terms of number of trains and GRT was developed in accordance with the Swiss Federal Railways and considered to forecast cumulated fatigue damage for the future. This led to the results shown in Table 2.

Table 2. Total Projected Fatigue Damage for the Diagonals

Structural element	Cumulated fatigue damage until year		
	2012	2035	2065
1 st diagonal	0.133	0.247	0.420
2 nd diagonal	0.025	0.045	0.075

A maximum value of theoretical fatigue damage of 0.42 in the year 2065 was obtained for the 1st diagonal of the main truss while for the 2nd diagonal and the lower chord at mid-span much smaller accumulated fatigue damage was calculated. The rather large difference between the two diagonals is due to the fact that the 1st diagonal gets higher stress values after considering the conversion factor of 1.71 (which is rather high because of significant moments due to high fixity of the 1st diagonal) (Table 1). These higher stresses contribute over-proportionally to damage accumulation as there is a more significant number of stress range values higher than the assumed fatigue limit when compared to the 2nd diagonal. This shows again the importance of precise stress determination and more precise knowledge of the fatigue limit. However, as all cumulated fatigue damage values are significantly lower than the theoretical value of $D = 1.0$ for fatigue failure, no further detailed examination of the 1st diagonal was performed.

No partial safety factors have hitherto been applied on the fatigue action effect and fatigue resistance values. The project team decided to accept a safety criterion given by a fatigue damage value of 0.50 as being acceptable and providing a sufficient safety margin with respect to theoretical fatigue failure of the element. The reasoning for this safety criterion comprises the good accessibility for inspection of the fatigue relevant details, the rather conservative approach in the determination of the conversion factor and the considered rather conservative fatigue category which is a 5% fractile value established based on mean test data and which probably underestimates the fatigue endurance or high cycle domain. As the highest forecasted maximum cumulated damage value of 0.42 for a further service duration of 50 years is smaller than 0.50, the fatigue safety verification is fulfilled for the entire riveted structure.

3.5 Discussion and Recommendation

The fatigue safety verifications based on the monitored values show sufficient fatigue safety for the diagonals of the main truss and thus for the entire riveted structure for at least the next 50 years of service duration. Also, the structural elements having priority during inspections were identified.

As the determinant structural element, i.e. the 1st tension diagonal of the main truss, showed the by far highest theoretical fatigue damage value, it is recommended to strengthen this structural element in the near future. By performing this intervention which has a preventive character and is not costly, very long future service duration (going well beyond 50 years) could be expected and attributed to the entire riveted structure, while taking into account the significantly more intense fatigue solicitation due to increasing traffic demand in the future.

Moreover, information and data regarding the railway traffic and the calculated fatigue damage (Table 2) actually indicate that the riveted structure was exposed to a relatively low fatigue solicitation during its past service duration of 115 years. In fact, the structure is today virtually still in an undamaged condition in terms of fatigue, and only the future higher railway traffic loading may produce some fatigue damage in certain structural elements.

A 115 year old bridge is commonly considered to be “old” and a thus often condemned to be a candidate for replacement. The present example shows however again, that a change in paradigm is needed when considering the notion of service duration: there is no “old” bridge, and solely the structural performance (and not the age of a structure) is the relevant and adequate criterion.

4. CONCLUSIONS

A methodology inherent to existing structures is presented for the fatigue safety verification leading to the following conclusions:

- (1) The suggested approach to determine updated action effects allows for explicit consideration of data from long term monitoring.
- (2) Data from monitoring allow for accurate determination of fatigue relevant stresses in fatigue prone bridge structures. Hence, uncertainties (due to load models and structural analysis) in the determination of updated action effects are reduced.
- (3) By means of the presented approach, the fatigue safety of a riveted railway bridge of high cultural heritage value was verified after 115 years of service duration. Long future service duration may be expected taking into account higher future traffic loading.

The present approach is economic as the cost for the long term monitoring and accompanying theoretical studies is only a small fraction of the cost of a hypothetical major strengthening or bridge replacement project which could thus be avoided by this study.

5. OUTLOOK

Obviously, this approach may also be applied for the structural safety verification at ultimate limit state. For example, in an accompanying monitoring project of a 50 year old post-tensioned concrete highway bridge subjected to heavy traffic, over 350 days of element level continuous

measurements have been performed to provide a unique insight into the behaviour in the monitored deck slab at an elemental level [9]. Bridge action effect estimation was approached from two separate directions, namely monitoring and simulation. The work represents a development towards improved methodologies for safety assessment based on data from monitoring. Direct measurement of strain in steel reinforcing bars has considerable potential as a means to determine the characteristic behaviour of extreme traffic action effects in bridge deck slabs. It was found that the measurement duration required to capture the extreme behaviour in reinforced concrete bridge elements is highly dependent on element location and orientation. The tested extrapolation techniques show high instability of extreme predictions for low measurement periods. Data from monitoring showed that the ULS strain and hence stress predictions are far too low to provide any fatigue or ULS concerns in this case. Hence the lifetime of many such bridge details could be extended well into the future. In some cases this new level of information could potentially be used to justify increases in legal loading without any safety risk to the users.

ACKNOWLEDGMENTS

The author wishes to thank Max Bosshard and Pirmin Steck (Flückiger + Bosshard Consulting Engineers Zurich), Christian Meyer (Terra Monitoring Zurich), Dr Marcel Tschumi and Dr Senta Haldimann (SBB Berne), all from the Eglisau Bridge project team, for their contributions to the case study and the Swiss Federal Railways (SBB) for funding.

REFERENCES

- [1] Brühwiler, E., Vogel, T., Lang, T., Lüchinger, P., “Swiss Standards for Existing Structures”, Structural Engineering International, IABSE Zurich, 2012, Vol. 22, No. 2, pp. 275-280.
- [2] SIA 269, “Existing Structures – Bases for Examination and Interventions”, Swiss Society of Engineers and Architects (SIA), Zurich, 2011.
- [3] SIA 269/1, “Existing Structures – Actions”, Swiss Society of Engineers and Architects (SIA), Zurich, 2011.
- [4] Brühwiler, E., Bosshard, M., Steck, P., Meyer, C., Tschumi, M. and Haldimann, S., “Fatigue Safety Examination of a Riveted Railway Bridge using Data from Long Term Monitoring”, Proceedings, IABSE Conference on Assessment, Upgrading and Refurbishment of Infrastructures, Rotterdam, The Netherlands, May 6 - 8, 2013.
- [5] SIA 269/3, “Existing Structures – Steel Structures”, Swiss Society of Engineers and Architects (SIA), Zurich, 2011.
- [6] Taras, A. and Greiner, R., “Development and Application of a Fatigue Class Catalogue for Riveted Bridge Components”, Structural Engineering International, IABSE Zurich, 2010, Vol. 20, No. 1, pp. 91- 103.
- [7] Brühwiler, E., Smith, I. and Hirt, M., “Fatigue and Fracture of Riveted Bridge Members” , ASCE J. Struct. Eng., 1990, Vol. 116, No. 1, pp. 198–214.
- [8] UIC Code 700, “Classification of Lines and Resulting Load Limits for Wagons”, International Union of Railways, 2004.
- [9] Treacy, M. and Brühwiler, E., “Extreme Action Effects in Reinforced Concrete Bridges from Monitoring”, Proceedings, IABSE Conference on Assessment, Upgrading and Refurbishment of Infrastructures, Rotterdam, The Netherlands, May 6 - 8, 2013.

REHABILITATION AND IMPROVEMENT OF FATIGUE LIFE OF WELDED JOINTS BY ICR TREATMENT

Kentaro Yamada ^{1,*}, Toshiyuki Ishikawa ² and Takumi Kakiichi ³

¹ Professor Emeritus, Nagoya University, Japan

Advisor, Central Nippon Highway Engineering Nagoya, Co. Ltd., Japan

² Dept. of Urban Management, Kyoto University, Japan

³ JFE Engineering Corporation, Japan

*(Corresponding author: E-mail: k.yamada.e@c-nexco-hen.jp)

ABSTRACT: Over 150,000 highway bridges exist in Japan and about 47 percent of the bridges will be over 50 years old in 2026. The Ministry of Land, Infrastructure, Transport and Tourism (MLIT) launched nation-wide projects to inspect and to establish maintenance plans. About one half of the highway bridges were steel bridges with concrete slabs. Due to heavy truck traffics being operated in or between industrial cities, some of which were illegally overloaded, severe deteriorations to concrete slabs and fatigue cracks in steel girders have been observed. Fatigue cracks in orthotropic steel decks were also found. It is urgent to tackle such fatigue cracks observed in welded joints of steel bridges. Various attempts have been made in Japan to repair and rehabilitate such fatigue cracked members. One is to improve fatigue strength of welded joints in existing bridges, and the other is to repair and rehabilitate cracked members. The latter were, for example, re-welding cracked joints, strengthening by using high strength bolted splices, adding glue to cracks, rehabilitating by gluing CFRP. The authors developed a technique, so-called ICR Treatment, or Impact Crack Closure Retrofit treatment, where fatigue cracks was closed by giving plastic yielding at plate surface near fatigue cracks. Since fatigue cracks do not open due to applied stress ranges, the cracks either do not propagate, or propagate much slower, to prolong remaining fatigue life of the bridges. Fatigue tests were carried out on various welded joints to show how fatigue life was improved by applying the ICR treatment to the cracked welded joints.

Keywords: Fatigue test, Welded joint, Crack, Rehabilitation, Improvement

DOI: 10.18057/IJASC.2015.11.3.4

1. INTRODUCTION

Various types of fatigue cracks have been observed in steel highway bridges in Japan. At first, they were due to inappropriate welded joints associated with insufficient knowledge about fatigue. Then, increase in number and weight of trucks caused larger stress ranges and their number of cycles, and caused fatigue cracks to welded joints. In order to prevent such fatigue cracks, fatigue design was adapted to the design specification of highway bridges by Japan Road Association in 2002. It was enhanced further in 2012 Specifications.

Three main factors are normally considered in fatigue of welded structures. They are structural details, applied stress ranges and their number of cycles. When the structures or the welded joints to be considered are subjected to certain levels of stress ranges and their number of cycles, structural detail with higher fatigue strength is to be used to prevent fatigue crack. Alternative is to improve fatigue strength of the welded joints.

Various fatigue strength improvement techniques are developed in the past, such as grinding weld toe to reduce stress concentration, peening technique to round the weld toe and to introduce

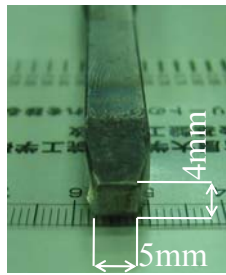
compression residual stress (Haagensen et al. [1], Anami et al. [2], Branco et al. [3]). More advanced techniques are UIT (Ryo et al. [4], Tominaga et al. [5]) or HFP (Pedersen et al. [6]), which is the similar technique to the peening, but with less noise, was now widely used in fabrication process. High compressive residual stress is the main contributor to the improvement of fatigue strength.

When fatigue cracks are found in existing highway bridges in Japan, they are often leave as they are, and monitored until the cracks grow to rather larger crack sizes. However, larger fatigue cracks often caused expensive repair and retrofiting works. Therefore, simple and inexpensive repair technique is requested from the field.

We have developed a technique called ICR treatment, or Impact Crack Closure technique, to repair fatigue cracks (Yamada et al. [7]). It used small pneumatic tool to hit surface of steel plate to introduce plastic yielding. It will help to create high compressive residual stress at weld toe, or to close fatigue crack at its surface. Various fatigue tests were carried out at Nagoya University, where the authors belonged until 2010 (Yamada et al. [8]). Some of the fatigue test results of ICR treated specimens were described hereafter.

2. ICR TREATMENT

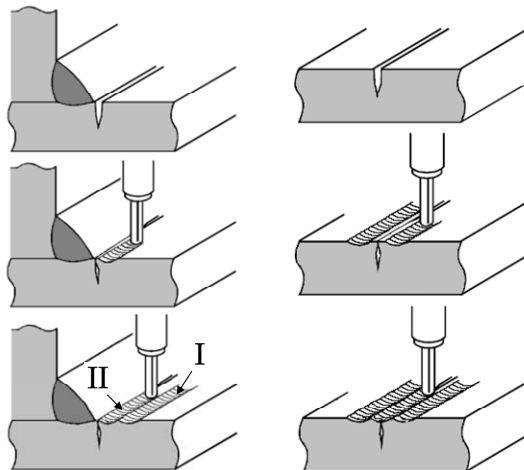
The ICR treatment, or Impact Crack Closure technique, is a technique to introduce plastic yielding of steel plate near fillet weld toe or near fatigue cracks. It uses a pneumatic tool to hit steel surface and an air compressor, as shown in Figure 1.



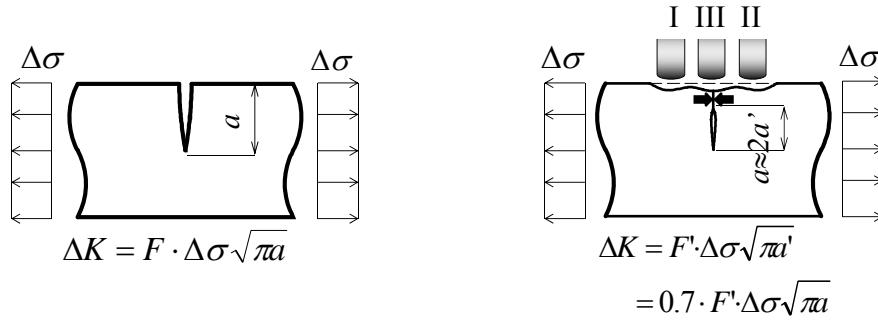
(a) Pneumatic Tool and Tip

(b) Air Compressor

Figure 1. Tools Used for ICR Treatment



(a) Small Crack at Weld Toe (b) Crack Propagating in Plate
Figure 2. Schematic View of ICR Treatment for Fatigue Crack



(a) Edge Crack (b) Crack When Crack Remain Closed Due to Applied Load
Figure 3. Schematic View of Repair of Fatigue Crack Using ICR Treatment

The basic concept of the ICR treatment is based on fracture mechanics consideration, as described in Figures 2 and 3. If a crack is found at weld toe, the ICR treatment is carried out at plate near the crack to cause plastic yielding. The surface of the crack is then closed at the surface. If one can create enough plastic yielding, then the crack do not open due to applied stresses. Two steps can be carried out, I and II as shown in Figure 2, to create even larger compressive plastic yielding at the weld toe, if one needs. When the crack propagates to plate, then the ICR treatments are carried out from both sides and on the top of the crack.

The mechanism of the repair of fatigue crack by ICR treatment is briefly described in Figure 3, where a plate with an edge crack is subjected to tension stresses. When the crack is closed and do not open due to the applied stress, the crack can be considered as an internal crack. Then the crack size can be considered as a half of that of the edge crack. Stress intensity factor range, ΔK , which expresses severity of crack tip according to fracture mechanics, becomes about 70 percent of the edge crack. Fatigue crack growth rate, da/dN , of steel is a function of ΔK and is proportional to the power of three of ΔK . Therefore, da/dN slows down to 0.34 times of the one for the edge crack. It implies that the fatigue crack propagation life becomes about three times longer. If the ΔK becomes less than threshold value of stress intensity factor range, ΔK_{th} , below which crack do not propagate, the fatigue life after the ICR treatment becomes infinite.

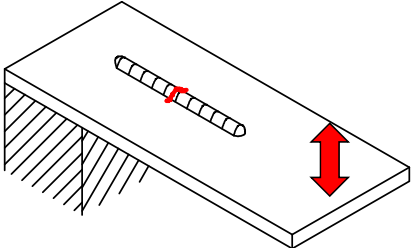
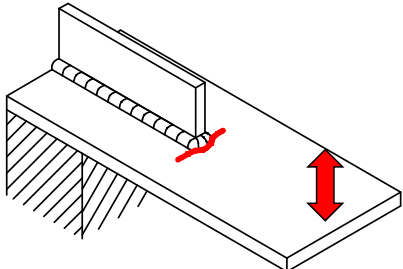
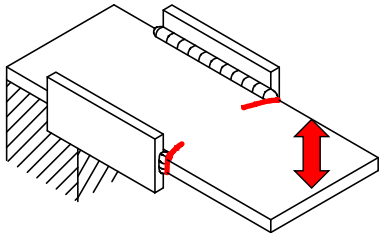
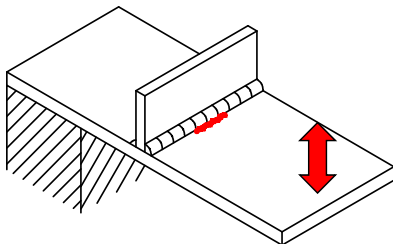
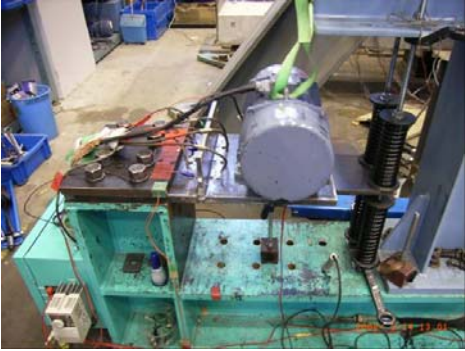
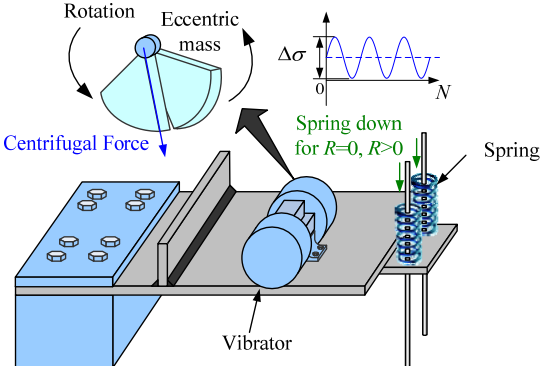
The technique can be also used to improve fatigue strength of weld toes, since large compressive residual stress can be introduced to the weld toe in the same way as the peeing technique and the UIT, although weld toe profiles are not rounded.

3. FATIGUE TESTS OF VARIOUS WELDED DETAILS WITH SMALL CRACKS

Fatigue tests of various welded joints were carried out to verify the effectiveness of the ICR treatment, as shown in Table 1. They were a) bead-on plates with a notch, b) out-of-plane gusset specimens, c) plate edge gusset welded joints (T joints), and d) fillet-welded joints. All these tests were carried out in plate-bending type of loading, with plate bending fatigue testing machines developed at Nagoya University (Yamada et al. [9, 10]). A photo and a schematic illustration of the plate bending fatigue testing machine are shown in Table 1, where a vibrator, a motor with two

eccentric mass on both side gives repeated loading to specimens. Springs are to give initial static loading in order to obtain desired stress ratio. Strain gages were monitored during fatigue tests to obtain stress ranges to be used for S-N curves. Also attached to the specimens were thin copper wires of 0.04 mm diameter at designated points. The copper wires were connected to the fatigue testing machine. When fatigue crack cut the copper wires, the fatigue testing machine stopped. For example, the copper wires were glued to weld toe, 10 mm from weld toe, and 30 mm of the specimens with out-of-plane gusset. These copper wires helped us to stop the fatigue testing machine automatically at designated crack sizes.

Table 1. Fatigue Test Specimens with and Without Fatigue Crack

a) Bead on Plate	b) Out-of-plane Gusset Welded Joints
 <p>Width and thickness of base plate: 300x12mm ICR treated crack length: 12mm</p>	 <p>Width and thickness of base plate: 300x12mm Thickness and height of gusset plate : 12x100mm ICR treated crack lengths: N_{10}, N_{20}</p>
c) Plate Edge Gusset Welded Joints (T Joint)	d) Fillet Welded Joints
 <p>Width and thickness of base plate: 310x12mm Thickness and height of gusset plate: 12x100mm ICR treated crack lengths: N_{10}, N_{20}</p>	 <p>Width and thickness of base plate: 300x12mm Thickness and height of rib plate: 12x100mm ICR treated crack lengths: 12, 24mm</p>
<div style="display: flex; align-items: center;">  <div style="margin-left: 20px;">  <p>Rotation Eccentric mass Centrifugal Force Spring down for $R=0$, $R>0$ Spring Vibrator</p> </div> </div> <p>Plate-bending Fatigue Testing Machine Used</p>	

3.1 Fatigue Test Results of Bead-on Plate

The first test on verification of ICR treatment was carried out on bead-on plate, which had a notch at a weld bead at center of the plate. Fatigue crack of a semi-elliptical shape was first developed at the notch, and then the ICR treatment was carried out to close the crack opening. Then, the fatigue test was continued. The fatigue test data of ICR treated specimens showed much longer fatigue life, compared with the data without the ICR treatment, as shown in Figure 4.

After the fatigue tests, the section of the test specimen with ICR treatment was cut-out to see how the crack was closed with the ICR treatment. The section is shown in Figure 4. The ICR treatment was found to close the fatigue crack up to about 1 mm from the surface.

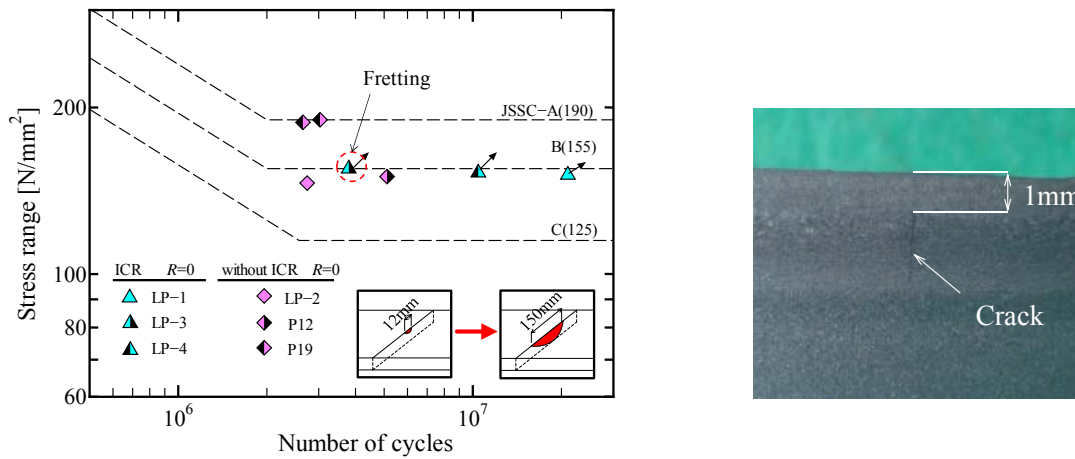


Figure 4. Fatigue Test Results of Bead-on Plate with or without ICR Treatment and Internal Crack

3.2 Fatigue Test Results of Out-of-Plane Gusset

Fatigue tests were carried out for out-of-plane gusset welded joints in bending. First, fatigue cracks were developed at weld toe, and propagated around the turn-around weld of the gusset end, as shown in Figure 5. The crack at this stage was defined as N_b . Then, fatigue crack separated from the weld toe, and propagated to main plate. When the crack became about 10 mm long from weld toe, the crack was defined as N_{10} . The crack was detected by copper wire of 0.04 mm diameter glued at designated location. When the fatigue crack reached and cut the copper wire, it stopped the fatigue testing machine.

The ICR treatment was carried out around fillet weld of the turn-around weld of gusset end for N_b crack, as shown in Figure 5. For N_{10} crack, the ICR treatment was first applied to both sides of the crack in base plate, on top of the crack, and then along the turn-around weld, as shown by I, II, III, and IV in Figure 5.

Fatigue test results showed the significant improvement of fatigue life due to the ICR treatment, as shown in Figure 6. For example, when the ICR was applied to N_b crack, all test data showed lives over 10 million cycles, while the specimens failed at less than 3 million cycles without the ICR treatment. In order to see the fracture surface, a specimen was re-tested with higher stress range,

and it failed at around Stress Category C of Fatigue Design Recommendations by the Japanese Society of Steel Construction (JSSC [11]).

The same results were observed for the N_{10} cracks. When the N_{10} crack was retrofitted by the ICR treatment, the fatigue life became longer than 10 million cycles.

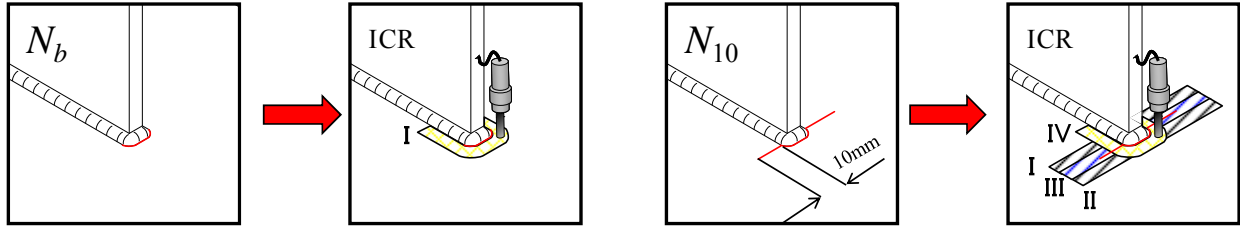


Figure 5. Definition of Crack Sizes and ICR Treatments at N_b and N_{10}

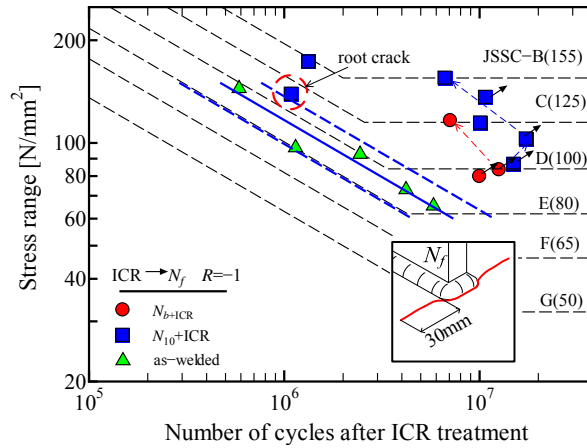


Figure 6. Fatigue Test Results of Out-of Plane Gusset with ICR Treatment at N_b and N_{10}

3.3 Fatigue Test Results of Plate Edge Gusset Welded Joints (T joints)

Fatigue cracks are normally initiated and propagated from fillet weld toes at the end of gussets welded perpendicular to the plate edge. Normally four fatigue cracks were observed at both sides and surface and back surface of the main plate. These cracks were ICR treated when they were 10 mm long (N_{10} crack) and when they were 20 mm long (N_{20} crack). Fatigue test results are shown in Figure 7. Base data for T joints in as-welded condition are shown with scatter band of S-N curves.

When all four cracks were ICR treated, regardless of the crack sizes, i.e. N_{10} or N_{20} , the test data showed the life more than 10 million cycles. It implies that the beneficial effect of the ICR treatment is significant. However, when the ICR treatment was applied only surface of the plate, fatigue cracks in back surface propagated and the specimen failed, although it was tested in tension-tension stress condition, or stress ratio $R > 0$. Yet, it showed life corresponding to the upper bound of the specimens tested in as-welded condition.

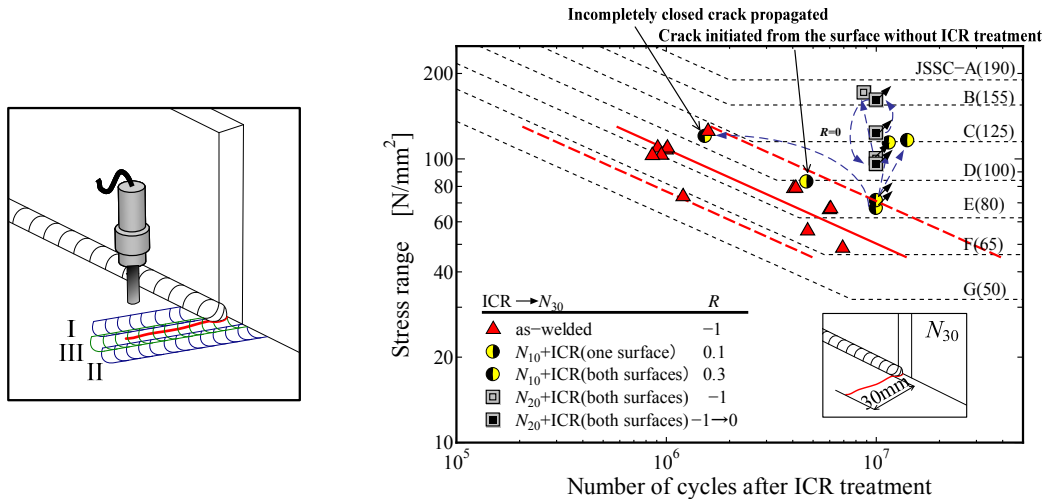


Figure 7. Fatigue Test Results of T joints with ICR Treatment

3.4 Fatigue Test Results of Fillet Welded Joints

Fillet welded specimens often showed fatigue cracks along the fillet weld toe. In order to control the size of the semi-elliptical cracks at the fillet weld toe, the ICR treatment was carried out first along the fillet weld toe, but leaving untreated zones at the center of the main plate by 12mm or 24 mm, as shown in Figure 8. After the preliminary fatigue tests, fatigue cracks of $2b=12$ mm or 24 mm were observed along the fillet weld toe.

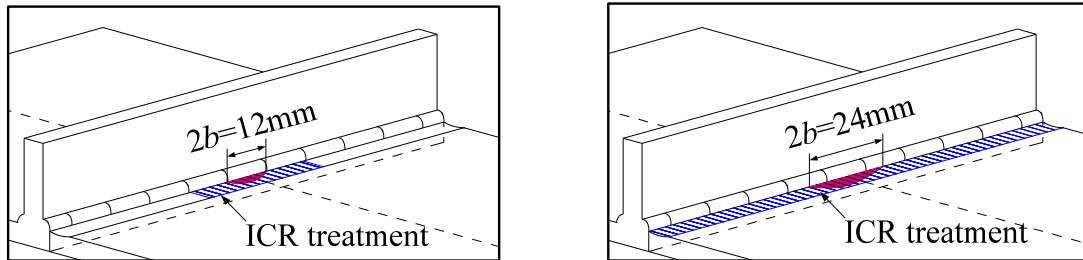


Figure 8. ICR Treatment for Fillet Welded Joints

Then, the ICR treatments were carried out. For the 12 mm crack, the ICR treatment was carried out along the crack and 20 mm more on both sides. The fatigue life after retrofitting was longer than the upper bound of the as-welded specimens, and retrofitting work was proved to be effective, as shown in Figure 9. By observation of fatigue fracture surface, the 12 mm crack, which initially introduced and ICR-treated, did not propagate. A new fatigue crack initiated and propagated from the weld toe at the point where the ICR treatment was terminated. We found that the beneficial compressive residual stress was diminished by the second application of the ICR treatment.

For the 24 mm crack, we applied the ICR treatment along the whole length of fillet weld toe. Then, no fatigue crack propagation was observed even over 10 million cycles of loading. The applied stress range was increased, but again no fatigue crack propagation was observed over 10 million cycles. Some specimens failed at the support due to fretting fatigue.

The test result shows that ICR treatment is effective to retrofit cracks at fillet weld toe. If the ICR treatment is applied along whole length of the fillet weld, not only at the crack location, the beneficial effect is more significant.

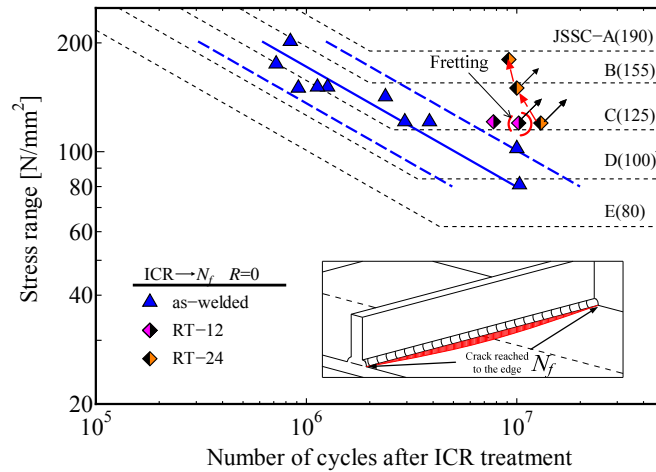


Figure 9. Fatigue Test Results of Fillet Welded Joints with ICR Treatment

4. PRACTICAL APPLICATION OF ICR TREATMENT IN EXISTING BRIDGES

During the process of developing the ICR treatment, we have carried out fatigue tests of specimens in as-welded conditions. All test data showed significant increase in fatigue strength, and the technique is proved to be applicable to fatigue strength improvement of existing bridges. We have applied the ICR treatment to fatigue prone details in several highway bridges with orthotropic steel decks.



(a) Fatigue Crack at End of Vertical Stiffener



(b) Demonstration of ICR Treatment



(c) ICR Treated Crack

Figure 10. Fatigue Cracks in Orthotropic Steel Decks Retrofitted by ICR Treatment

The ICR treatments were also used to repair and retrofit fatigue cracks observed at upper ends of vertical stiffeners, which were often observed in Japanese orthotropic steel decks (Yamada & Ya [12]), as shown in Figure 10. The details were once retrofitted by drilling circular holes near the cracks. The circular holes were expected to reduce stress concentration at the end of the vertical stiffeners, and hence reduced fatigue crack growth rates. Therefore, the fatigue cracks were left as they were. We applied the ICR treatment to seven locations of these cracks on March 2009.

The ICR treatments for these cracks took several minutes each, not counting preparation stages. The time needed for ICR treatment was much less than other retrofitting measures. Other retrofitting measure, for example adding high strength bolted splice plates, needed normally several hours with closure of traffic lane.

Stress measurements were carried out in order to prove that the ICR treated cracks remained closed under service loading. The strain curves due to three axle trucks are shown in Figure 11(a). They were measured in deck plate at 12mm off from the turn-around weld.

Four strain waves were measured at the locations where a) as-welded (no crack) one, b) with N_{10} crack, c) with ICR treated N_b crack, and d) with ICR treated N_{10} crack. The strain curve for the as-welded one showed compressive strain due to rear wheel, while that for N_{10} crack showed tensile strain due to the rear wheel. When the ICR treatment were carried out for the N_b and N_{10} cracks, the strain waves due to rear wheel became compressive strain, in the same manner as the as-welded one. It implies that the ICR treated details behaved in the same manner as the as-welded condition. Periodic monitoring of the strain was carried out after six month and 1.5 years. As shown in Figures 11(b) and 11(c), the strain measured waves showed the same tendency as the strain measured after ICR treatment shown Figure 11(a).

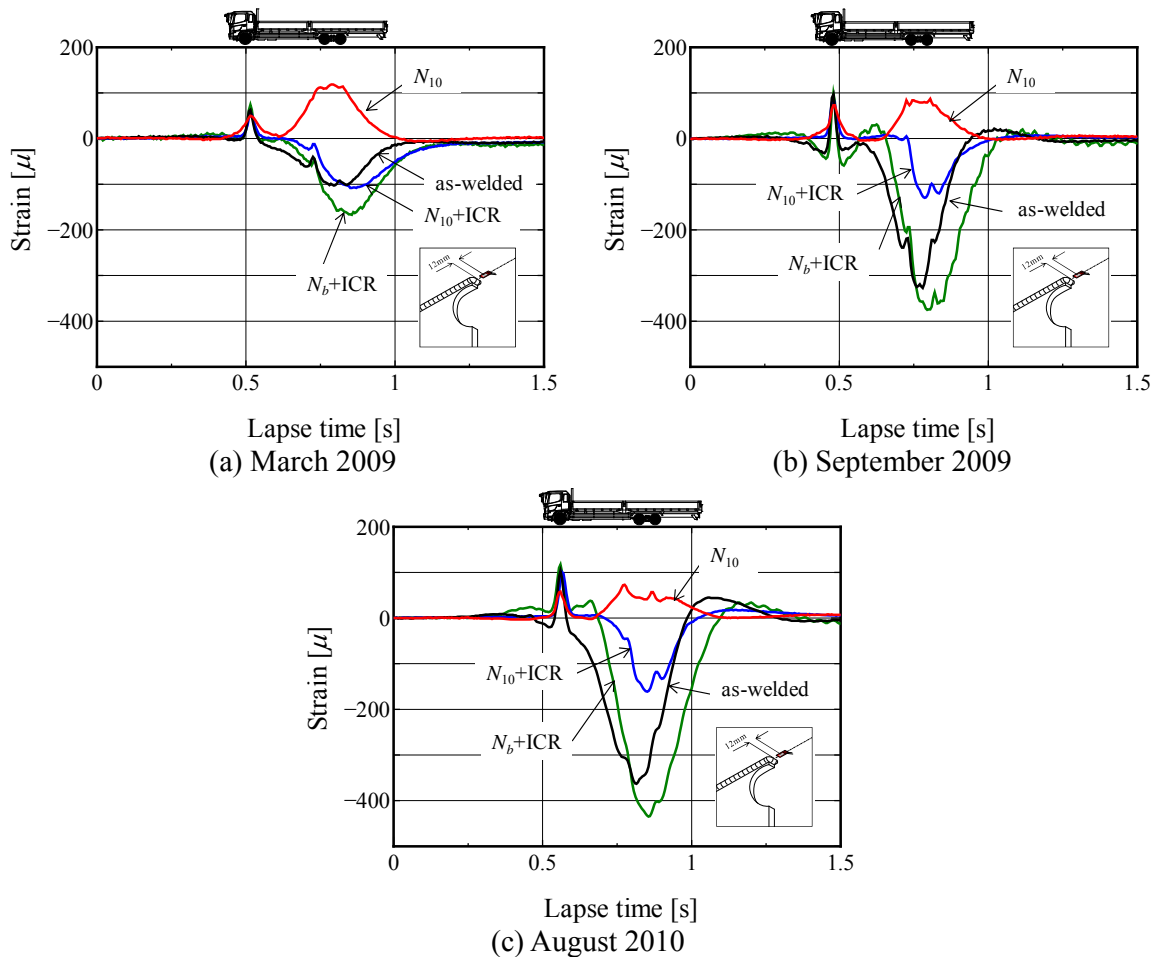


Figure 11. Strains Measured under Service Loading

5. CONCLUSIONS

Fatigue cracks were observed in Japanese highway bridges, especially in orthotropic steel decks, in the past two decades. Increase in truck weight and their numbers, including over loaded trucks, were one cause of those fatigue cracking. Efficient and economical retrofitting measures were urgently requested by bridge owners. Various fatigue strength improvement techniques, such as grinding weld toe, peening technique and UIT, can be used to improve fatigue resistance of the existing bridges. Repair methods, such as adding splice plates with high strength friction type bolts, were often used for retrofitting fatigue cracked members.

We have developed a technique called ICR treatment, or Impact Crack Closure Retrofit treatment, which enabled us to retrofit fatigue cracks when they are small. When fatigue cracks are detected, the opening of the crack is closed by giving plastic yielding near the crack. If the crack is not open due to applied stress ranges, the crack growth rates decreases, which yields to increase in fatigue crack propagation life. If the situation meets, such as the stress intensity factor range becomes less than its threshold value, the fatigue cracks do not propagate. Fatigue tests of various details showed significant increase in fatigue life after the ICR treatment. Fracture mechanics consideration also proves the mechanism of the phenomena.

In order to apply plastic yielding near the crack surface, commercially available pneumatic tools can be used. The ICR treatment takes a few minutes to retrofit one crack, and it is economical way to retrofit fatigue cracks. The ICR treatment was applied to fatigue cracks developed at the upper ends of vertical stiffeners of orthotropic steel decks. Monitoring the ICR treated cracks also proved that the technique can be applied to fatigue cracks in existing members.

ACKNOWLEDGMENTS

The authors acknowledge all former graduate students of Nagoya University to contribute the fatigue tests of welded joints. Fatigue testing machines used in this experiment were developed by the first author with Drs. Satoshi Yamada and Tatsuya Ojio, and their contribution is also greatly acknowledged. The fatigue testing machine enabled us to carry out fatigue tests very fast. Without them the fatigue tests would have taken several years. The experimental works were financially supported by Nagoya Expressway Authority.

REFERENCES

- [1] Haagensen, P. J. and Maddox, S. J., "IIW Recommendations on Post Weld Improvement of Steel and Aluminum Structures", 2007, XIII-2200r-07.
- [2] Anami, K., Miki, C., Tani, H. and Yamamoto H., "Improving Fatigue Strength of Welded Joints by Hammer Peening and TIG-dressing", St. Eng./Earthquake Eng., 2000, JSCE, Vol. 17, No. 1, pp.67-78.
- [3] Branco, C.M., Infante, V. and Baptista, R., "Fatigue Behaviour of Welded Joints with Cracks, Repaired by Hammer Peening", Fatigue Fract. Engng. Mater. Struct., 2004, Vol. 27, pp. 785-798.

- [4] Roy, S., Fisher, J. W. and Yen, B. T., "Fatigue Resistance of Welded Details Enhanced by Ultrasonic Impact Treatment (UIT)", *International Journal of Fatigue*, 2003, Vol. 25, No. 9-11, pp. 1239-1247.
- [5] Tominaga, T., Matsuoka, K. and Satoh, Y., "Fatigue Improvement Method for Weld Repaired Crane Runway Girder by Ultrasonic Impact Treatment", *Steel Construction Engineering*, 2007, Vol. 14, No. 55, pp. 47-58. (in Japanese)
- [6] Pedersen, M.M., Mouritsen, O.Ø., Hansen, M.R., Andersen, J.G. and Wenderby, J., "Comparison of Post Weld Treatment of High Strength Steel Welded Joints in Medium Cycle Fatigue", *International Institute of Welding*, 2009, IIW Document XIII-2272-09.
- [7] Yamada, K., Ishikawa, T., Kakiichi, T. and Li, H., "Extending Fatigue Life by Closing Crack Opening with ICR Treatment", *Fatigue Design 2009*, 2009, November 25-26, Cetim, Senlis, France.
- [8] Yamada, K., Kakiichi, T. and Ishikawa, T., "Extending Fatigue Life of Cracked Welded Joint by Impact Crack Closure Retrofit Treatment", *International Institute of Welding*, 2009, IIW Document XIII-2289 r1-09.
- [9] Yamada, K., Ya, S., Baik B. and Torii, A., "Development of a New Fatigue Testing Machine and Some Fatigue Tests for Plate Bending", *International Institute of Welding*, 2007, IIW Document XIII-2161-07.
- [10] Yamada, K., Osonoe, T. and Ojio, T., "Bending Fatigue Test on Welded Joint between Vertical Stiffener and Deck Plate, *Steel Construction Engineering*", 2007, Vol. 14, No. 55, pp. 1-8.
- [11] Japan Society of Steel Constructions (JSSC), "Fatigue Design Recommendations for Steel Structures", 1993. (in Japanese), 1995. (in English)
- [12] Yamada, K. and Ya, S., "Review of Orthotropic Steel Deck Bridge and Some Fatigue Cracks and Retrofitting Measures in Japan", *Orthotropic Bridge Conference*, Sacramento, 2008, USA, pp. 531-542.

FATIGUE SERVICE LIFE EVALUATION OF EXISTING STEEL AND CONCRETE BRIDGES

Chun-sheng Wang^{1,*}, Mu-sai Zhai¹, Lan Duan¹ and Qian Wang¹

¹ Key Laboratory for Bridge and Tunnel of Shaanxi Province,
Chang'an University, Xi'an, Shaanxi Province, China
*(Corresponding author: E-mail: wcs2000wcs@163.com)

ABSTRACT: In recent years, traffic loads and vehicle speeds on both existing steel and concrete bridges have increased to provide fast and sufficient transportation service in China. Chinese government and bridge engineers are paying more attention to the structural fatigue life, service safety, maintenance intervals and the ability to improve capacity of such infrastructure. To study evaluation methods using modern technologies to achieve economical maintenance and extend the sustainable service life, a deterministic evaluation approach was proposed in this paper based on investigation of linear fatigue-damage accumulation theory and fracture mechanics, in which the fatigue failure behaviour of existing steel and concrete bridges was reflected. According to the stochastic fatigue failure mechanism of existing bridges, the member fatigue reliability assessment models were proposed using probabilistic fracture mechanics. Furthermore, based on a Monte-Carlo method, a fatigue reliability analysis program was developed to calculate member fatigue failure probability of existing bridges. The deterministic and probabilistic assessment methods proposed in this paper were applied to evaluate typical existing steel and concrete bridges. According to assessment results, the deterministic and probabilistic remaining fatigue life, safe inspection intervals and maintenance strategies were determined, which can avoid fatigue failure accidents and reduce the life-cycle cost of these bridge structures.

Keywords: Existing steel and concrete bridges, Fracture mechanics, Probabilistic fracture mechanics, Fatigue life evaluation, Maintenance strategy

DOI: 10.18057/IJASC.2015.11.3.5

1. INTRODUCTION

Existing steel and concrete bridges are aging and experiencing increased levels of fatigue deterioration due to increased demands in traffic volume, vehicular weights and environmental corrosion. As a result, the service safety of existing steel and concrete bridges is declining. In recent years, bridge engineers are paying more attention to the actual fatigue life, service safety, maintenance intervals and load carrying capacity of such infrastructure. Researchers devoted to develop effective evaluation methods, and then provide structural behavior prediction for existing steel and concrete bridges, which can make reasonable maintenance and management decisions to ensure the structural safety [1-5].

To acquire reliable fatigue life evaluation technique, this paper proposed deterministic and probabilistic evaluation approaches, which reflect fatigue failure behavior of existing steel and concrete bridges. According to the stochastic fatigue failure mechanism of existing bridges, the fatigue reliability assessment models for member were proposed using probabilistic fracture mechanics. Furthermore, based on a Monte-Carlo method, a fatigue reliability analysis program was developed to calculate member fatigue failure probability of existing bridges. To verify the effectiveness of proposed evaluation approaches, five typical existing steel bridges and concrete bridges were selected as case studies. Continuous dynamic monitoring technique was adopted to acquire real fatigue stress spectrum, in order to evaluate the real fatigue life of existing bridges. Based on evaluation results, the deterministic and probabilistic remaining fatigue life, safe

inspection intervals and maintenance strategies were determined, which can avoid fatigue failure accidents and reduce the life-cycle cost of these bridge structures.

2. OVERVIEW OF THE EVALUATION AND CASE STUDY BRIDGES

The general evaluation procedure is conducted by the following eight steps. Firstly, investigation of the existing archives is conducted to collect the original design documents, each repairing record, and the results of each in-situ test. Secondly, three-dimensional finite element models (3D-FEM) of existing bridges are established. Thirdly, derivation of traffic load spectrum is conducted. Fourthly, it is to calculate the stress spectrum by means of both the 3D-FEM and the traffic load spectrum as well as by in-situ measured stress histogram. Fifthly, it is to estimate of the service fatigue life and inspection priority using conventional fatigue method on the basis of stress spectrum. Sixthly, the remaining fatigue life is evaluated using fracture mechanics method. Seventhly, the probable remaining fatigue life is assessed by probabilistic fracture mechanics method. Eighthly, decision of the maintenance strategy is proposed based on the fatigue safety evaluation results of existing steel bridges. The fifth to eighth steps mentioned above are introduced in details in the following sections.

The frame of deterministic and probabilistic assessment approaches of existing steel bridges is demonstrated by Ganjiang River Bridge, which is a typical old riveted bridge. The case study structure, Ganjiang River Bridge, is a combined railway and highway riveted steel through-truss bridge with nine simple supported spans of 64m. The two main trusses are spaced 9.7m apart and loaded through a floor system consisting of transverse floor beams and longitudinal stringers. Each side of the main trusses is one 4.5m-width traffic lane. The bridge is part of the Chinese Jingjiu Rail mainline system, built in 1962, and carried only one track before 1995. In 1995, the service status changed greatly and the bridge began to carry double tracks. In recent years, the volume of train and truck has been increased. Therefore, Jiangxi Railway Management Bureau and the bridge owner paid attention to the service safety of this bridge, and decided to evaluate the remaining fatigue life and the service safety.

Houdingxiang No.1 Bridge shown in Figure 1 is selected as the typical modern steel box girder bridge with orthotropic steel bridge (OSD) to evaluate the fatigue life of OSD. The steel box girder is composed of three small box chambers with 3.75-meter wide and 3-meter high. The distance between two diaphragms is 3 meters. The thickness of top plate and diaphragm is 16mm and 10mm, respectively. The thickness of U-shaped ribs is 8mm. The structural steel used in the bridge is weathering steel Q345qENH. Weld among deck plate, diaphragm and stiffeners is fillet-weld joint. In-situ deck-to-deck joints are single-surface weld with two-side shaped and field rib-to-rib joints are high-strength bolted connections.

Two typical prestressed concrete (PC) T-girder bridges, i.e., a simple-supported PC girder bridge and a continuous PC girder bridge are chosen to evaluate the fatigue life using different methods. The simple-supported PC girder bridge shown in Figure 2(a) is a freeway bridge built in 1992, which contains two separate parts composed of 12 T-girders with the total width of 26.2m. The continuous one was open to traffic in 2013, which is parallelling to the old simple-supported PC girder bridge. As shown in Figure 2(b), the cross-section contains 8 T-girders with the total width of 19.75m. The every span length of both bridges is all 30m. These two bridges are in the same district, the traffic volume and vehicle kinds are similar.

The Qilangwo Yellow River Bridge is taken as a case study of existing concrete bridges, which is built in 1971. After having been used for 35 years, the serious fatigue cracks and damages were found in the reinforced concrete deck T-beams. For ensuring the bridge service safety, the old deck T-beams were replaced by the new reinforced concrete deck Π -beams in 2006. In order to

evaluate the fatigue safety of the retrofit bridge decks, the 24-hour in-situ dynamic strains of the bottom concrete surface were monitored at mid-span sections of new concrete deck beams in 2008. According to the monitoring data, the characters and effect of overloading and oversize trucks can be analyzed for the further research. The stress history of reinforced bars could be gained by further calculation, and the stress spectrums of rebar could also be obtained using the rain-flow counting method.



(a) Steel Box Girder with OSD



(b) Heavy Truck Crossing the Bridge

Figure 1. Houdingxiang No.1 Bridge with OSD



(a) Simple-supported PC T-girder Bridge



(b) Continuous PC T-girder Bridge

Figure 2. The Two PC T-girder Bridges

3. FATIGUE LIFE EVALUATION BY USING S-N CURVE

The procedure of fatigue life evaluation for all the tension members in existing steel bridges or the tension steel bar in existing concrete bridges based on S-N curves includes three steps. Firstly, the fatigue strength and parameters for S-N curves should be confirmed. Secondly, the load history and stress spectrum should be developed. Finally, the used life and the remaining fatigue life can be evaluated by using the Miner's cumulative damage rule as shown in Figure 3. If using the recent traffic load spectrum to evaluate fatigue life, the result is more conservative, because the traffic load in the past is not heavier than present. Nevertheless the inspection priority can be ranked according to the assessment results. Figure 4 shows the S-N curves in Eurocode 3 [6].

4. FRACTURE MECHANICS EVALUATION MODEL

In remaining fatigue life prediction results of the tension members or steel bar in the existing bridges based on S-N curve method are very conservative due to the over-estimated load history. In this section the fracture mechanics to be applied for the calculation of fatigue crack growth from the visualized or detected initial crack in structural members or the assumption, that the crack size is just the limit of visualization or detection. If the traffic load through the existing bridges will not change in future service condition remarkably, the recent traffic load spectrum can be used for the

calculation of remaining fatigue life. The general procedure to determine the remaining fatigue life of existing bridges based on fracture mechanics can be divided into the following four steps: (1) identification of the vital elements or steel bar to be analyzed from bridge system; (2) calculation of the critical crack size; (3) simulation of crack growth from the initial crack size to the critical crack size; (4) determination of the remaining fatigue life and economical inspection intervals as shown in Figure 5.

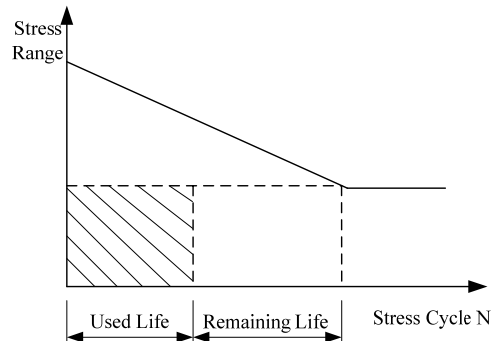


Figure 3. Fatigue Life Evaluation Based on S-N Curve

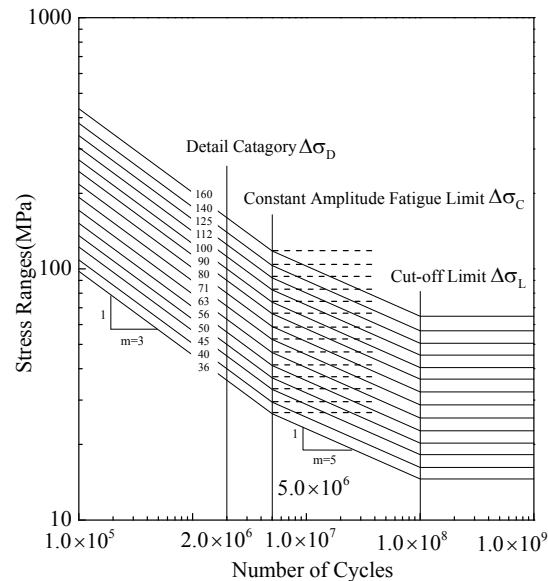


Figure 4. S-N Curves in Eurocode 3[6]

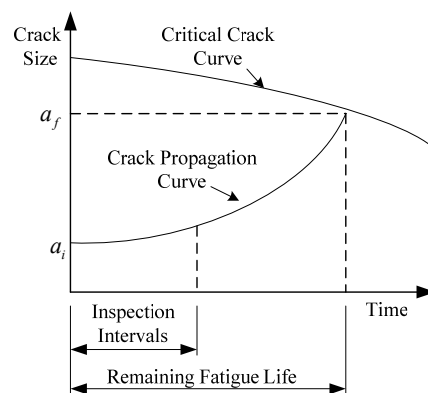


Figure 5. Remaining Fatigue Life Evaluation Based on Fracture Mechanics

4.1 Evaluation Approach Based on Fracture Mechanics for the Existing Steel Bridges

In the old riveted steel bridges all members are built up by rivet with plates and angles, so the main crack configurations can be simplified into two types of fracture mechanics models: CCT-Centric Crack Tension and DECT-Double Edge Crack Tension. According to the chemical component analysis and the material test results for bridge steel using in the riveted construction time, the material strength and toughness values can be determined as $R_{el} = 240\text{MPa}$, $K_{IC} = 50\text{MPa} \cdot \text{m}^{\frac{1}{2}}$. In this paper ultrasonic detection is applied to determine the initial crack size. If the fracture occurs before net section yielding with only local yielding at the crack tips, this failure mode commonly is called “brittle” failure. The critical crack size a_{cr} can be defined as Eq. (1).

$$a_{cr} = \frac{1}{\pi} \left(\frac{K_{IC}}{Y\sigma_{\max}} \right)^2 \quad (1)$$

Where Y is geometry function for CCT or DECT models; σ_{\max} is the max-stress of dead and live load. If the fracture failure occurs after net-section yielding, the failure mode is ductile. In this case, $a_{cr} = a_N$, the practical values of a_N for CCT or DECT can be calculated using Eq. (2) and Eq. (3).

$$a_N = W(1 - \sigma_{\max} / R_{el}) \quad (2)$$

$$a_N = W \sqrt{2.25 + 4(1 - \sigma_{\max} / R_{el})} - 1.5W \quad (3)$$

Where W is half width of specimen. Based on investigation of riveted members fatigue test results, the fatigue crack propagation cannot exceed the width of angle leg. Though the critical crack size can be proposed as Eq. (4).

$$a_f = \min(a_N, a_{cr}, a_{\max}) \quad (4)$$

Where a_{\max} is the width of angle leg.

The fatigue crack growth rate in structural steel may be proposed to follow a power law as Eq. (5).

$$\frac{da}{dN} = \begin{cases} 0 & \Delta K \leq \Delta K_{th} \\ C(\Delta K^m - \Delta K_{th}^m) & \Delta K > \Delta K_{th} \end{cases} \quad (5)$$

Where da/dN is fatigue crack growth rate; C and m are crack growth coefficients; ΔK_{th} is the threshold stress intensity factor range; $\Delta K = Y\Delta\sigma\sqrt{\pi a}$. The crack growth coefficients can be taken as $C = 6.889 \times 10^{-12}$, $m = 3$ according to the experiment results of old riveted steel [7]. The threshold stress intensity factor range can be determined according to the empirical relation in BSI PD 6493 [8], as shown in Eq. (6).

$$\Delta K_{th}(R) = \begin{cases} 170 - 214R & R \leq 0.5 \\ 63 & R > 0.5 \end{cases} \quad (6)$$

Where R is the stress ratio.

According to linear elastic fracture mechanics theory and fatigue crack initiates and propagates regularly in modern steel bridges, the stress intensity factor range ΔK , for a surface semi-elliptical crack in welded joints (indicated in Figure 6) subjected to tension and bending loads, can be expressed by Eq. (7) [9-10].

$$\Delta K = K_{\max} - K_{\min} = M_k Y (\sigma_m + H \sigma_b) \sqrt{\pi \frac{a}{Q}}. \quad (7)$$

For $0 < a/c \leq 1.0$, $0 \leq a/t < 1.0$, $c/b < 0.5$, and $0 \leq \phi \leq \pi$.

Where σ_m is membrane stress range; σ_b is shell bending stress range; M_k is stress concentration correction factor considering geometry effect of welded joints; $Q = 1 + 1.464 \left(\frac{a}{c}\right)^{1.65}$;

$$H = H_1 + (H_2 - H_1) \sin^p \phi; \quad p = 0.2 + \frac{a}{c} + 0.6 \frac{a}{t}; \quad H_1 = 1 - 0.34 \frac{a}{t} - 0.11 \frac{a}{t} \left(\frac{a}{c}\right); \quad H_2 = 1 + G_1 \left(\frac{a}{t}\right) + G_2 \left(\frac{a}{t}\right)^2;$$

$G_1 = -1.22 - 0.12 \left(\frac{a}{c}\right)$; $G_2 = 0.55 - 1.05 \left(\frac{a}{c}\right)^{0.75} + 0.47 \left(\frac{a}{c}\right)^{1.5}$; a is the crack depth; c is the crack half-length; t is plate thickness; b is plate half-width; The geometry function Y can be calculated by Eq. (8).

$$Y = [M_1 + M_2 \left(\frac{a}{t}\right)^2 + M_3 \left(\frac{a}{t}\right)^4] g f_\phi f_w \quad (8)$$

Where $M_1 = 1.13 - 0.09 \left(\frac{a}{c}\right)$; $M_2 = -0.54 + 0.89 / (0.2 + \frac{a}{c})$; $M_3 = 0.5 - \frac{1}{0.65 + a/c} + 14(1 - \frac{a}{c})^{24}$;

$$g = 1 + \left[0.1 + 0.35 \left(\frac{a}{t}\right)^2\right] (1 - \sin^2 \phi)^2; \quad f_\phi = \left[\left(\frac{a}{c}\right)^2 \cos^2 \phi + \sin^2 \phi\right]^{1/4}; \quad f_w = \sqrt{\sec\left(\frac{\pi c \sqrt{a/t}}{2b}\right)}.$$

In modern welded steel bridges the other fatigue crack type is the end corner crack subjected to tension and bending loads (indicated in Figure 7). Its stress intensity factor range ΔK can be expressed by Eq. (9) [9, 11].

$$\Delta K = (\sigma_m + \sigma_b H) \frac{\sqrt{\pi a}}{E(k)} F_1 \left(\frac{a}{c}, \frac{a}{t}, \frac{c}{w}, \phi\right) \quad (9)$$

For $0.2 \leq a/c \leq 2$, $a/t < 1$, $0 \leq \phi \leq \frac{\pi}{2}$, $c/w < 0.5$.

Where c is the crack length; w = plate width; and F_1 and H can be calculated by Eq. (10) and Eq. (11).

$$F_1 = [M_1 + M_2 (a/t)^2 + M_3 (a/t)^4] g_1 g_2 f_\phi f_w \quad (10)$$

$$H = H_1 + (H_2 - H_1) \sin^p \phi. \quad (11)$$

For $a/c \leq 1$:

$$M_1 = 1.08 - 0.03(a/c); M_2 = -0.44 + \frac{1.06}{0.3 + a/c}; M_3 = -0.5 + 0.25(a/c) + 14.8(1 - a/c)^{1.5};$$

$$g_1 = 1 + [0.08 + 0.4(a/t)^2](1 - \sin \phi)^3; g_2 = 1 + [0.08 + 0.15(a/t)^2](1 - \cos \phi)^3;$$

$$f_\phi = [(a/c)^2 \cos^2 \phi + \sin^2 \phi]^{1/4}; f_w = 1 - 0.2\lambda + 9.4\lambda^2 - 19.4\lambda^3 + 27\lambda^4;$$

$$\lambda = (c/w)(a/t)^{1/2}; p = 0.2 + a/c + 0.6(a/t); H_1 = 1 - 0.34(a/t) - 0.11(a/c)(a/t);$$

$$H_2 = 1 + G_{21}(a/t) + G_{22}(a/t)^2; G_{21} = -1.22 - 0.12(a/c);$$

$$G_{22} = 0.64 - 1.05(a/c)^{0.75} + 0.47(a/c)^{1.5}; E(k) = [1 + 1.464(a/c)^{1.65}]^{1/2}.$$

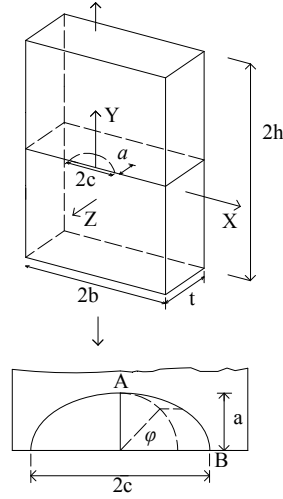


Figure 6. Surface Semi-elliptical Crack Model

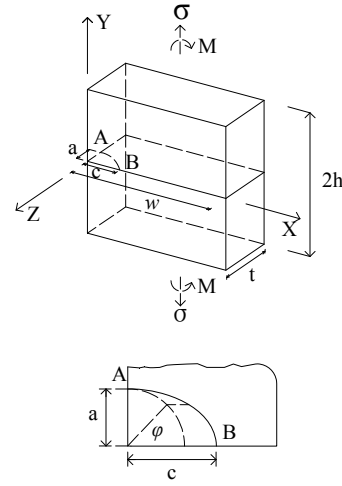


Figure 7. End Corner Crack Model

4.2 Evaluation Approach Based on Fracture Mechanics for the Existing Concrete Bridges

The remaining service life of reinforced concrete bridges or bridge elements is controlled by the reinforcement when inspection shows that concrete is in good condition. In this section, the fatigue life of reinforced concrete bridges is evaluated based on the steel bar fatigue failure using Paris Law. Fracture of rebar occurs, when the depth of crack reaches $a = a_{cr}$ or the applied stress is equal to the resistance of the remaining cross section. The brittle fracture and fracture by yielding are two existing fracture modes. Usually, the depth of critical brittle fracture crack size a_{cr} can be calculated by Eq. (1). If the remaining cross section is yielding, the crack depth $a = a_y$ is determined by calculating the necessary area-reduction, and a_y can be calculated by Eq. (12) [12].

$$A(a_y) = A_0 \left(1 - \frac{\sigma_{sup}}{f_y} \right) \quad (12)$$

Where A_0 is the cross section area of the undamaged rebar; $A(a_y)$ is the cross section area of yielding state for the damaged rebar. Then the failure crack size is proposed as Eq. (13).

$$a_f = \min(a_{cr}, a_y, 2r) \quad (13)$$

Where r is the radius of the rebar.

Parameters of rebar are not well known in fracture mechanics. In order to calculate the crack propagation, the initial flaw on a cylindrical steel bar is assumed as a semi-circular crack (Figure 8), which has a depth of $a = a_i$. The plane, in which the semi-circular crack lies, is perpendicular to the steel axis. The stable crack growth from initial crack is calculated using Paris law.

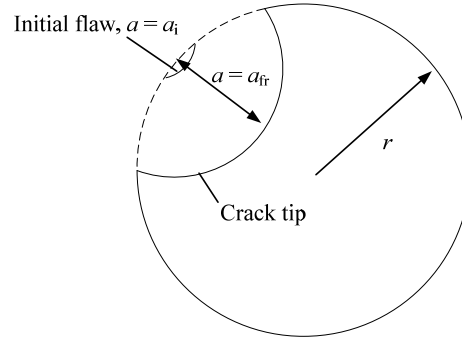


Figure 8. The Cross Section of Rebar with Initial Flaw and Crack Propagation [12]

The number of cycles N_{ij} from the crack depth $a = a_i$ to a_j can be obtained by integrating Eq. (5) without considering the effect of threshold stress intensity factor range, shown in Eq. (14). Y is assumed to be constant when ranging from a_i to a_j .

$$N_{ij} = \int_{a_i}^{a_j} \frac{1}{C \Delta K^m} da = \int_{a_i}^{a_j} \frac{1}{C Y^m \Delta \sigma^m \pi^{m/2} a^{m/2}} da = \frac{1}{C \alpha \pi^{m/2} Y^m \Delta \sigma^m} \frac{1}{a_i^\alpha} \left[1 - \left(\frac{a_i}{a_j} \right)^\alpha \right] \quad (14)$$

Where α is integration constant, and can be expressed as $\alpha = m/2 - 1$; Y is correction factor depends on radius r of the rebar and the depth of the crack. BS 7910 [13] gives formulas for Y , shown as Eq. (15).

$$Y = \frac{1.84 \left\{ \tan \left(\frac{\pi a}{4r} \right) / \frac{\pi a}{4r} \right\}^{0.5}}{\cos \left(\frac{\pi a}{4r} \right)} \left[0.752 + 2.02 \left(\frac{a}{2r} \right) + 0.37 \left\{ 1 - \sin \left(\frac{\pi a}{4r} \right) \right\}^3 \right] \quad (15)$$

The remaining fatigue life of steel reinforcement N_f , shown in Eq. (16), can be estimated by Eq. (14) from the initial crack size a_i to the critical crack size a_f .

$$N_f = \frac{1}{C \alpha \pi^{m/2} Y^m \Delta \sigma^m} \frac{1}{a_i^\alpha} \left[1 - \left(\frac{a_i}{a_f} \right)^\alpha \right] \quad (16)$$

Furthermore, an analysis program based on the linear elastic fracture mechanics evaluation method is developed to calculate the fatigue life of reinforced concrete bridges using monitoring stress data.

4.3 Evaluation Approach Based on Probabilistic Fracture Mechanics for Existing Steel Bridges

Uncertainties in the fatigue loading, material fatigue properties, geometry effects, and fatigue crack non-destructive inspection (NDI) are significant and must be considered explicitly in any comprehensive fatigue assessment procedure [14-15], so the probabilistic fracture mechanics model using the Paris equation and the Monte-Carlo simulation technique is developed for determining the fatigue failure probability of existing steel bridges in this study (Figure 9).

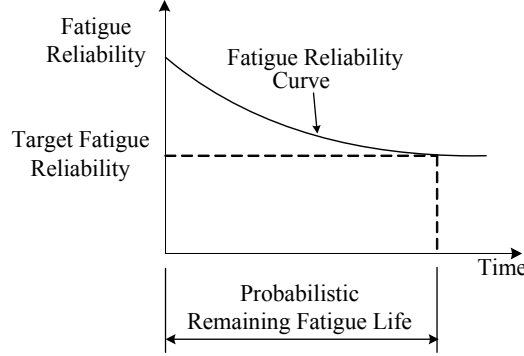


Figure 9. Probabilistic Remaining Fatigue Life Evaluation

At first a deterministic fracture mechanics calculation of crack growth with stochastic inputs for crack growth rate, fracture toughness, initial and critical crack size, and load history is proposed. According to the stochastic fatigue failure mechanism of existing steel bridges, the limit-state functions of two probabilistic fatigue failure models – brittle and ductile are defined as Eq. (17) and Eq. (18).

For brittle failure:

$$Z_B = a_f - a_t = a_{cr} - \left\{ a_i + \int_0^{N_t} CS^m B_Y^m Y^m(a) (\pi a)^{m/2} dn \right\} \quad (17)$$

For ductile failure:

$$Z_D = a_f - a_t = a_N - \left\{ a_i + \int_0^{N_t} CS^m B_Y^m Y^m(a) (\pi a)^{m/2} dn \right\} \quad (18)$$

Where a_{cr} is the critical crack size of brittle failure (random variable); a_N is the critical crack size of ductile failure (random variable); a_i is the initial crack size (random variable); a is crack size; C is Paris coefficient (random variable); m is Paris exponent (constant); S is the stochastic simulation stress range; B_Y is a random variable defining the random character of geometry function; N_t is the number of cumulative stress cycles. For the reliability analysis, the uncertainties associated with all the basic variables must be quantified. According to the research results [14-17], the statistical characteristics of the random variables are given in Table 1.

According to the fatigue failure mechanism of riveted members, a double-angle probabilistic fatigue failure model (DAPFFM) for riveted bridge members is proposed as shown in Figure 10. For the riveted member fatigue failure models including brittle and ductile, the riveted member must be investigated as parallel systems. Therefore, the fatigue failure probability and fatigue reliability of DAPFFM can be calculated as Eq. (19) and Eq. (20).

Table 1. Statistical Characteristics of the Random Variables

Variables	Type	Mean Value	Coefficient
a_i	Lognormal	$\overline{a_i}$	0.1
a_N	Lognormal	$\overline{a_N}$	0.1
a_{cr}	Lognormal	$\overline{a_{cr}}$	0.5
C	Lognormal	4.7423×10^{-12}	0.6
m	Constant	3	0
B_Y	Lognormal	1	0.1
S	Stochastic Simulation		

$$P_f = P(F) = P\left(\bigcap_{i=1}^2 F_i\right) = \bigcap_{i=1}^2 P_{f,i} \quad (19)$$

$$P_r = P(\bar{F}) = P\left(\bigcup_{i=1}^2 \bar{F}_i\right) = 1 - \bigcap_{i=1}^2 (1 - P_{r,i}) \quad (20)$$

Furthermore, a reliability analysis program DAPFFM, based on Monte-Carlo method, is developed to compute the fatigue failure probability of DAPFFM for riveted steel bridges [18].

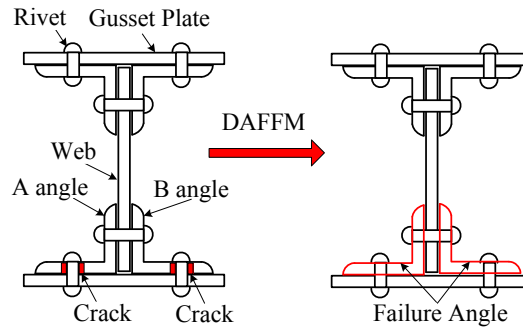


Figure 10. DAPFFM of Riveted Member

5. CASE STUDIES

5.1 Fatigue Life and Service Safety Evaluation of the Existing Steel Bridges

5.1.1 Main Truss Girder of Ganjiang River Bridge

According to the analysis of full-scale fatigue experiments [19], the Eurocode Detail Category 71 is adopted to evaluate the fatigue damage of Ganjiang River Bridge, and the cut-off limit is 29 MPa [6]. Fatigue life of all the vital members in Ganjiang River Bridge is evaluated by using the Miner's cumulative damage rule. The fatigue life of downstream suspender U1L1 of Ganjiang River Bridge (61 years) is the shortest. Therefore, the inspection priority of downriver suspender U1L1 is much higher than others in Ganjiang River Bridge.

The remaining fatigue life and safe inspection intervals of members in Ganjiang River Bridge are evaluated using fracture mechanics model and the safety factor is taken as 2.0. The calculation results show that the upriver suspender U1L1 are critical for this riveted truss bridges. It is suggested that the ultrasonic detection intervals of main truss is 3 years for Ganjiang River Bridge. The inspection should be arranged before the coming cold winter.

Based on the sensitivity and detection results of ultrasonic instrument and steel mechanical property for Ganjiang River Bridge, the mean values of initial crack size and critical crack size for brittle and ductile failure model shown in Table 2 and Table 3 can be calculated using Eq. (1), Eq. (2) and Eq. (3), where $R_{ei} = 280\text{MPa}$ and $K_{IC} = 95\text{MPa} \cdot \text{m}^{\frac{1}{2}}$ [17].

Table 2. Mean Value of a_i , a_N , a_{cr} for Members at Integrity State (mm)

Members	Mean Value of a_i	Mean Value of a_N	Mean Value of a_{cr}
Upriver U1L1	16.5	64.681	82.201
Downriver U1L1	14.5	63.342	80.960

Table 3. Mean Value of a_i , a_N , a_{cr} for A or B Angle at Fatigue Failure State (mm)

Members	After A or B Angle Brittle Failure		After A or B Angle Ductile Failure	
	a_N	a_{cr}	a_N	a_{cr}
Upriver U1L1	55.885	74.034	59.635	77.514
Downriver U1L1	54.297	72.567	58.047	76.038

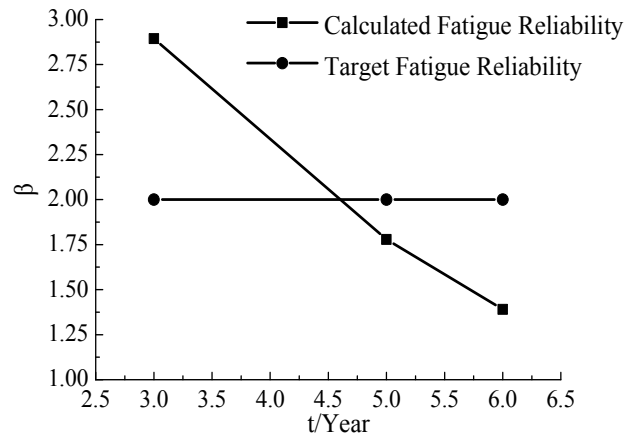


Figure 11. The β -t Curve of Downriver Suspender U1L1

In this paper, the target fatigue reliability index plotted in Figure 11 is assumed to be 2.0 [16]. From Figure 11 the safe inspection intervals can be determined according to the probabilistic remaining fatigue life of downriver suspender U1L1. The safe inspection intervals of upriver and downriver suspender U1L1 are all about 4.5 years.

5.1.2 Orthotropic Steel Decks of Houdingxiang No.1 Bridge

In order to acquire real stress histogram, continuous monitoring technique was adopted and different methods were used to calculate the fatigue life of fatigue-sensitive details. Figure 12 shows the 20-day continuous recorded dynamic stress spectrum of four fatigue-sensitive details in OSDs of Houdingxiang No.1 Bridge. S-N curve used in fatigue life evaluation of orthotropic steel bridge deck is suggested in Eurocode 3[6]. For free edges of diaphragm cutouts and bolted splice plate, the initial crack model used in LEFM evaluation is assumed as end corner crack (shown in

Figure 7), when fatigue crack propagates through the diaphragm or bolted splice plate, the model changes into single-edge crack. For rib-to-deck joint and rib-to-diaphragm joint, the initial crack model is assumed as surface semi-elliptical crack (shown in Figure 6), and fatigue failure occurs when the crack propagate through the deck plate or the rib web.

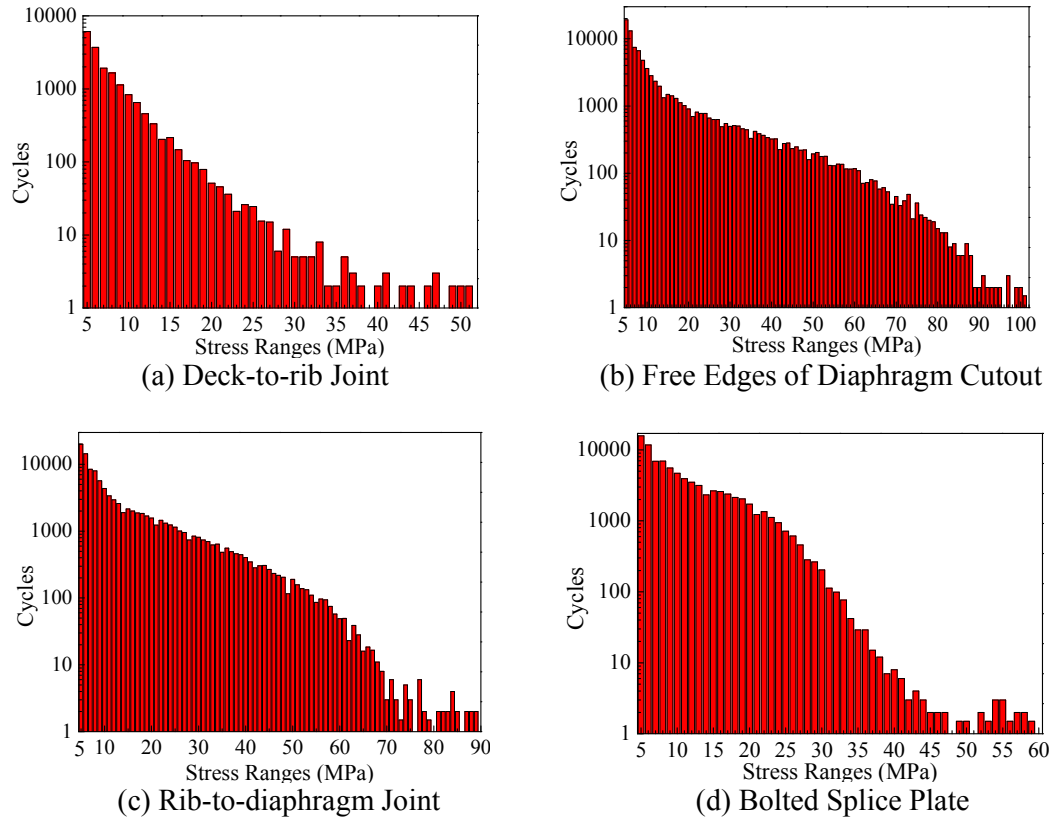


Figure 12. Recorded Dynamic Stress Spectra for Fatigue Details in OSDs

Recorded dynamic stresses of deck-to-rib joint are smaller than the constant amplitude fatigue limit (CAFL), so the fatigue life is infinity; fatigue life of free edges of diaphragm cutout is 46 years; fatigue life of rib-to-diaphragm joint is 204 years, and bolted splice plate is 3420 years. The steel used in OSDs of Houdingxiang No.1 Bridge is Q345qENH, based on previous research, C can be taken as $C = 4 \times 10^{-12}$ and $C = 8 \times 10^{-12}$ for base metal and weld metal, respectively, and m has the same value of $m = 3$. Based on LEFM models for the typical details in OSDs, the depth of initial cracks is assumed as 0.5mm and 1.0 mm, and fatigue lives evaluation results are shown in Table 4. As monitoring recorded stress spectrum of deck-to-rib joint is relatively low, fatigue life of this detail is 1746 years and 868 years; fatigue life of free edges of diaphragm cutout is 299 years and 109 years; fatigue life of rib-to-diaphragm joint is 186 years and 67 years; and bolted splice plate is infinity and 1820 years.

Fatigue life of free edges of diaphragm cutout is far short than design service life based on S-N curves. For LEFM approach, with the depth of initial cracks increase, fatigue life of sensitive details in OSD decrease sharply, so fabrication quality of OSD should be controlled strictly. Actually, fabrication errors, low welding quality and high residual stress are always existed in OSD. If these factors are considered with the increasing traffic volume and overloading together, the fatigue life of sensitive details will be shortened sharply. Therefore, in the future management, regular inspection and continuous monitoring are needed to ensure the service safety of OSD.

Table 4. Fatigue Life Evaluation Results of OSDs

Detail	Fatigue life (Year)		
	S-N Curve	LEFM	
		Depth of initial crack(mm)	
		0.5	1.0
Deck-to-rib joint	Infinity	1746	868
Free edges of diaphragm cutout	46	299	109
Rib-to-diaphragm joint	204	186	67
Splice plate	3420	Infinity	1820

5.2 Fatigue Life and Service Safety Evaluation of the Existing Concrete Bridges

5.2.1 Main Girder of PC Bridges

To evaluate the fatigue life of the PC T-girder bridges, in-situ dynamic strain monitoring was conducted continuously over one month, and traffic volume was recorded manually. Figure 13(a) is the cross section of simple supported PC T-girder bridge, which is built in 1992. Carbon steel wires are used in prestressing steel tendons, and every tendon contains 24 wires with 5mm in diameter. Longitudinal steel bar in the bottom part of T-girder is 20mm in diameter. Figure 13(b) is the cross section of continuous PC T-girder bridge, prestressing steel strands (9-7 Φ 5) and 20-diameter steel bars are used in T-girders. Since the steel bars and prestressing steel tendons or strands in the lower position are subject to more fatigue damage, the lowest longitudinal steel bar and the lowest prestressing steel wires or strands are selected to evaluate the fatigue life. S-N curve for longitudinal steel bar used in this paper is from European Convention for Constructional Steelwork (ECCS) [20], S-N curve for prestressing steel wires is proposed by Song [21], and S-N curve for prestressing steel strand is suggested by Ma [22].

In order to considering contributions of corrosion and low stress ranges, fatigue categories of steel bars and prestressing steel wires or strands are lowered to the 65% [23]. Considering contributions of low stress ranges, fatigue life of the lowest steel bar in simple supported PC girder bridge is 4421 and 9380 years for girders under the heavy lane and light lane, respectively; and fatigue life of lowest prestressing steel wire is 1390 and 1616 years. Fatigue life of lowest steel bar in continuous PC girder bridge is 145389 and 333211 years for girders under the heavy lane and light lane, respectively; and fatigue life of lowest prestressing steel wire is 32100 and 46751 years. Based on LEFM and the depth of initial cracks are assumed as 1.0mm considering the corrosion pit flaws, fatigue life of the lowest steel bar in simple supported PC girder bridge is 1094 and 1287 years for girders under the heavy lane and light lane, respectively; and fatigue life of lowest prestressing steel wire is 1734 and 2326 years. Fatigue life of lowest steel bar in continuous PC girder bridge is 29186 and 39763 years for girders under the heavy lane and light lane, respectively; and fatigue life of lowest prestressing steel wire is 24773 and 26661 years, as indicated in Table 5.

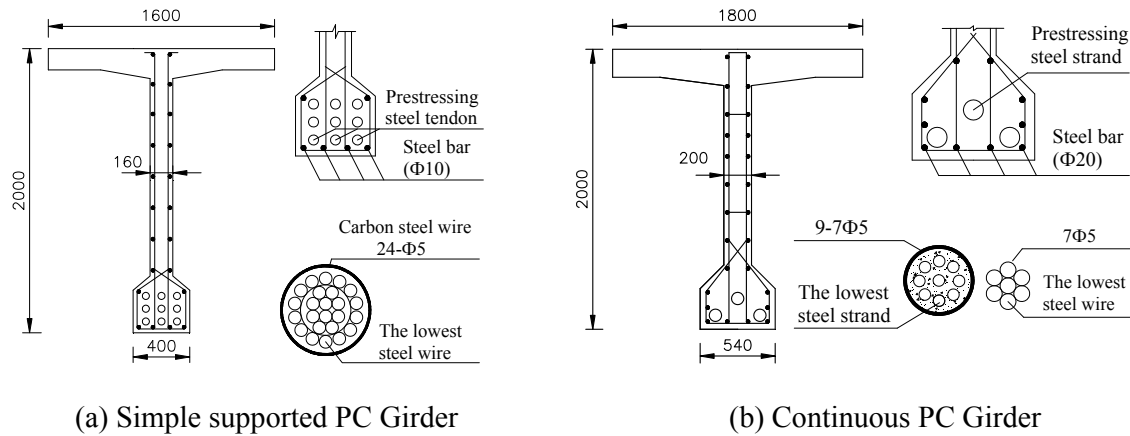


Figure 13. Critical Steel Bar and Steel Wire in PC Girder Bridges

Table 5. Fatigue Life Evaluation Results of PC Bridges

Bridge	Position	Object	Fatigue life (Year)	
			S-N Curve	LEFM
Simple supported PC bridge	Heavy Lane	Prestressing steel wire	1390	1734
		Steel bar	4421	1094
	Light Lane	Prestressing steel wire	1616	2326
		Steel bar	9380	1287
Continuous PC bridge	Heavy Lane	Prestressing steel wire	32100	24773
		Steel bar	145389	29186
	Light Lane	Prestressing steel wire	46751	26661
		Steel bar	333211	39763

From the two PC bridges evaluation results, it can be concluded that under the similar traffic load, the fatigue life of continuous PC girder bridge is longer than simple supported PC girder bridge. For PC girder bridges, fatigue life of steel bar and wire calculated by LEFM method or S-N Curve method is more large than the bridge design service life (100 years), but the fatigue life should be shortened sharply considering the overloading, concrete crack, corrosion fatigue and durability damage.

5.2.2 RC Deck Beams

Conservative S-N curve of ECCS [20] is applied to evaluate the fatigue life of Qilangwo Yellow River Bridge. On the basis of monitoring data and considering traffic volume increase prediction, the evaluation result showed that the fatigue life of RC deck beams for Qilangwo Yellow River Bridge is 418 years. Due to reinforced concrete structure is permitted cracking in service life, corrosion of steel reinforcement can cause the reduction of fatigue strength. According to previous research [23], a reduction factor for fatigue strength, which defined as stress range, was 1.35 (pitting causing loss of cross section up to 25 percent). By corrosion fatigue re-evaluation, the fatigue life was reduced to 93 years. Through the calculation above, corrosion of rebar would greatly reduce the fatigue life of RC bridges.

Then the LEFM evaluation method is applied to calculate the fatigue life of RC deck beams for Qilangwo Yellow River Bridge. The crack growth coefficients C and m for rebar of RC deck beams can be taken as $C = 2 \times 10^{-10}$, $m = 4$ according to the suggestions in the reference [12], and the initial crack size is assumed as 1mm considering the weld defects in the steel bars. The fatigue crack propagation curve of rebar was calculated using the LEFM model based on monitoring strain data. Figure 14 shows that the fatigue life of RC deck was about 102232 days (280 years).

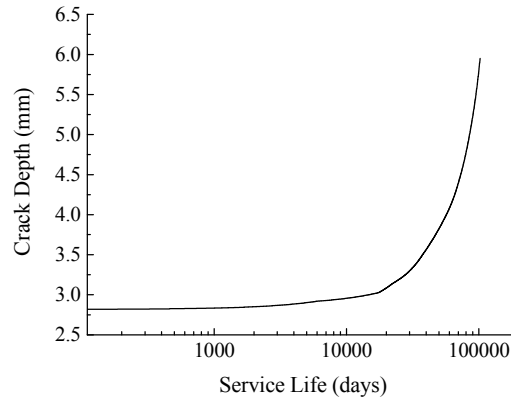


Figure 14. The Fatigue Crack Growth Curve of Steel Bar

6. CONCLUSIONS

Based on investigation of linear fatigue-damage accumulation theory and fracture mechanics, a deterministic evaluation approach was proposed in which the fatigue failure behavior of existing steel and concrete bridges was reflected. Following conclusions can be obtained:

- (1) According to the stochastic fatigue failure mechanism of existing steel bridges, the member fatigue reliability assessment models were proposed using probabilistic fracture mechanics. Furthermore, based on a Monte-Carlo method, a fatigue reliability analysis program was developed to calculate member fatigue failure probability of existing steel bridges.
- (2) From the case study of Ganjiang River Bridge for an existing steel bridge, it is concluded that: the inspection priority of downriver suspender U1L1 is much higher than others in Ganjiang River Bridge; The analytical results according to the fracture mechanic based concept show that the upriver suspender U1L1 has the shortest remaining fatigue life of 5.1 years, and ultrasonic detection intervals of main truss is 3 years; Based on fatigue reliability assessment of main truss members, the safe inspection intervals of Ganjiang River Bridge is about 4.5 years.
- (3) For orthotropic steel bridge decks, based on S-N curves and LEFM, fatigue lives of sensitive details in OSDs are calculated. Fatigue life by S-N curves of deck-to-rib joint, free edges of diaphragm cutout, rib-to-diaphragm joint and bolted splice plate is infinity, 46 years, 204 years and 3420 years, respectively. Based on LEFM approach, the depth of initial cracks is assumed as 0.5mm and 1.0 mm, fatigue lives of deck-to-rib joint, free edges of diaphragm cutout, rib-to-diaphragm joint, bolted splice plate are: 1746 years and 868 years, 299 years and 109 years, 186 years and 67 years, infinity and 1820 years. If considering fabrication errors, low welding quality, high residual stress, the increasing traffic volume and overloading together, the fatigue life should be shortened sharply.

- (4) S-N curves and LEFM approaches are verified by fatigue life evaluation of two PC girder bridges. The simple supported PC bridge fatigue life by S-N curves of is at least 1390 years, and continuous PC girder bridge is 32100 years. Fatigue life by LEFM approach of simple supported PC girder bridge is more than 1094 years, and continuous PC girder bridge is 24773 years. Fatigue life by S-N curves of RC deck beams for Qilangwo Yellow River Bridge is 418 years, which will decrease to 93 years when taking corrosion into consideration; fatigue life by LEFM approach is about 280 years. Based on the fatigue safety evaluation of existing concrete bridges, the following conclusions could be gained: (a) The S-N curve and LEFM approaches could be effectively applied to evaluate the fatigue safety of actual PC girders and RC deck beams. (b) Combined with other factors of deterioration such as corrosion, corrosion fatigue could cause the remarkable reduction of fatigue life for concrete bridges. (c) Furthermore, the effect of overloading and oversize trucks should be investigated in-depth.
- (5) The deterministic and probabilistic assessment methods proposed in this paper were verified by fatigue life evaluation of typical existing steel and concrete bridges. According to assessment results, the deterministic and probabilistic remaining fatigue life, safe inspection intervals and maintenance strategies were determined, which can avoid fatigue failure accidents and reduce the life-cycle cost of these transportation structures.

ACKNOWLEDGMENTS

The writer gratefully acknowledges the financial support provided by the Major State Basic Research Development program of China (973 Program) Sub-program (2015CB057703), the Special Fund for Basic Scientific Research of Central Colleges of the P.R. China, Chang'an University (10821153501, 310821153401 and 310821153314), the Transportation Science and Technology Project of Transport Ministry of P. R. China (2013318223040), Science and Technology Research Project of China Communications Construction Company Limited (Grant No.2012-ZJKJ-3), the Shaanxi Province Transportation Technology Research Project (Grant No.07-04k) and the Doctoral Postgraduate Technical Project of Chang'an University (2014G5290008).

REFERENCES

- [1] Wang, C.S., Chen, A.R., Chen, W.Z. and Xu, Y. "Application of Probabilistic Fracture Mechanics in Evaluation of Existing Riveted Bridges", *Journal of Bridge Structures*, 2006, Vol.2, No.4, pp. 223-232.
- [2] Wang, C.S., Chen, W.Z. and Chen, A.R., "Fatigue Safety Assessment of Existing Steel Bridges in China", *Structural Engineering International*, 2009, Vol. 19, No. 2, pp. 174-179.
- [3] Wang, C.S., Li G., Dong X.H., Hao L. and Wang J.H., "Fatigue Life Evaluation of Existing Highway Reinforced Concrete Bridges", *Proceeding of the 5th International Conference on Maintenance, Safety and Management*, CRC Press, Taylor & Francis Group, 2010, pp.685.
- [4] Wang, C.S., Zhou J., Wu Q.Y., Wang Y.J. and Dong X.H., "Fatigue Life and Service Safety Assessment for Existing Concrete Bridges", *China Journal of Highway and Transport*, 2012, Vol. 25, No. 6, pp. 101-107. (in Chinese)
- [5] Pijpers, R.J.M., Kolstein, M.H., Romeijn, A. and Bijlaard, F.S.K. "Fatigue Experiments on Very High Strength Steel Base Material and Transverse Butt Welds", *Advanced Steel Construction*, 2009, Vol. 5, No. 1, pp. 14-32.
- [6] EN 1993-2, "Eurocode 3: Design of Steel Structures: Part 2: Steel Bridges", European Committee for Standardization, Brussels, 2006.

- [7] Barsom, J.M. and Rolfe, S.T., "Fracture and Fatigue Control in Structures: Applications of Fracture Mechanics, Third Edition", American Society for Testing and Materials, West Conshohocken, USA, 1999.
- [8] British Standards Institution, "Guidance on Methods for Assessing the Acceptability of Flaws in Fusion Welded Structures", BSI PD 6493, London, UK, 1991.
- [9] Newman, J.C. and Raju, I.S., "An Empirical Stress-intensity Factor Equation for the Surface Crack", Engineering Fracture Mechanics, 1981, Vol. 15, No.1-2, pp. 185-192.
- [10] Hobbacher, A., "Stress Intensity Factors of Welded Joints", Engineering Fracture Mechanics, 1993, Vol. 46, No. 2, pp. 173-182.
- [11] China Aerospace Research Institute, "Handbook of Stress Intensity Factor", Science Press, Beijing, China, 1993. (in Chinese)
- [12] Herwig, A., "Reinforced Concrete Bridges under Increased Railway Traffic Loads", Ph.D. Thesis, École Polytechnique Fédérale de Lausanne, Lausanne, 2008.
- [13] British Standard Institute, "Guide on Methods for Assessing the Acceptability of Flaws in Metallic Structures", BS7910, London, UK, 2007.
- [14] Zhao, Z.W., Haldar, A. and Breen, JR. F.L., "Fatigue Reliability Evaluation of Steel Bridges", J. Struct. Eng., ASCE, 1994, Vol. 120, No. 5, pp. 1608-1623.
- [15] Zhang, R.X. and Mahadevan, S., "Fatigue Reliability Analysis Using Nondestructive Inspection", J. Struct. Eng., ASCE, 2001, Vol.127, No.8, pp. 957-965.
- [16] Yazdani, N. and Albrecht, P., "Risk Analysis of Fatigue Failure of Highway Steel Bridges", J. Struct. Eng., ASCE, 1987, Vol. 113, No. 3, pp. 483-500.
- [17] Geißler, K., "Beitrag zur Probabilistischen Berechnung der Restnutzungsdauer Stahlerner Brucken", Ph.D. Thesis, Technische Universitaet Dresden, Dresden, 1995.
- [18] Wang, C.S., "Assessment of Remaining Fatigue Life and Service Safety for Riveted Steel Bridges", Tongji University Press, Shanghai, China, 2007. (in Chinese)
- [19] Dibattista, J.D., Adamson D.E.J. and Kulak, G.L., "Fatigue Strength of Riveted Connections", J. Struct. Eng., ASCE, 1998, Vol. 124, No. 7, pp. 792-797.
- [20] ECCS, "Recommendations for the Fatigue Design of Steel Structures". European Convention for Constructional Steelwork, Brussels, Belgium, 1985.
- [21] Song, Y.P., "Fatigue Behavior and Design Principle of Concrete Structures", China Machine Press, Beijing, China, 2006. (in Chinese)
- [22] Ma, L., "Fatigue Performance Study of 1860 MPa Low Relaxation Prestressing Steel Wires", Railway Standard Design, 2000, Vol. 20, No.5, pp. 21-23. (in Chinese)
- [23] Walker, E.F., Harrison, I.M. and Morley, J., "Fatigue and Corrosion Fatigue of Reinforcement Bars", Proc. Conf. Underwater Construction Technology, Department of Civil and Structural Engineering Report, University College, Cardiff, 1975.

FATIGUE LOAD MODEL FOR HIGHWAY BRIDGES IN HEAVILY LOADED AREAS OF CHINA

Wei-zhen Chen¹, Jun Xu^{1,*}, Bo-chong Yan² and Zhi-ping Wang¹

¹*Department of Bridge Engineering, Tongji University, Shanghai, China*

²*Shanghai Donghua Local Railway Development Co., Ltd, Shanghai, China*

**(Corresponding Author: E-mail: jxuun@tongji.edu.cn)*

ABSTRACT: Fatigue is one of the main factors that cause the collapse of steel bridges. Anti-fatigue design therefore draws close attention all over the world. The design must have a fatigue load model based upon native traffic load conditions. But the Chinese steel bridge design specification does not include any fatigue load model for anti-fatigue design. So it is imperative to develop the model. This paper proposes a single vehicle fatigue load model and a 5-vehicle fatigue load spectrum model, which are based upon the latest weigh-in-motion data collected from heavily loaded area of China. Taking the effects of multi-vehicle presence into account on the basis of queuing theory, the proposed fatigue load models could be easily adapted to real traffic, thus providing substantial support to the bridge structural fatigue evaluation in the heavily loaded areas of China.

Keywords: Load model, Fatigue, Highway bridge, Heavily loaded areas

DOI: 10.18057/IJASC.2015.11.3.6

1. INTRODUCTION

The development of fatigue damage is closely related to the safety and durability of highway bridges which are dependent primarily on traffic loads the structure has experienced. The fatigue behavior and bearing capacity are greatly influenced by the coupled actions of material degradation, vehicle load and environment [1]. Thus, it is necessary to find a method for fatigue analysis that considers real traffic load history. But the research of vehicle fatigue loads is tedious, time-consuming, cost-ineffective, and, in particular, place-sensitive, making the research result for one place inapplicable to another place and therefore impracticable for construction of new bridges. Consequently, different countries have to make different vehicle fatigue load models according to their own national conditions.

The fatigue load model in BS5400 [2] is established according to the representative vehicle inflecting the worst fatigue damage to the bridges. The fatigue load model in AASHTO [3] is evolved from the load model for strength checking. Eurocode [4-6] provides 5 fatigue load models as reference. The Japanese fatigue design guideline uses the axle loads in the specifications for highway bridges to make the fatigue load model [7-8]. The parameters of these fatigue load models are all different, reflecting different characteristics of traffic in different countries. In China, however, the traffic load model for fatigue check is still a blank in the current steel bridge design code [9]. So it is high time to fill in the blank.

It is a fundamental principle that the simulated loads of a vehicle fatigue model must cause structural fatigue damage that is the closest to that caused by the actual traffic loads. Among relevant researches, Prat [10] introduced the origin of the fatigue load model adopted by Eurocode, compared precisions of various fatigue models and analyzed the impact of longitudinal and transverse multi-vehicle presence upon the fatigue calculation using the queuing theory.

Moses [11] studied the fatigue design methods adopted by AASHTO, and exhibited the procedures of fatigue evaluation for bridge structure design and assessment. Calgaro [12] analyzed the characteristics of traffic loads on highway bridges. Laman [13] proposed a fatigue load model in accordance with the analytic results of 5 girder bridges based on traffic load investigation. He also compared the fatigue load model with standard fatigue truck adopted by AASHTO. Chotickai [14] provided the recommended fatigue load model after his study of reliability-based fatigue design method according to mass traffic survey data.

Tong et al. [15] calculated the fatigue load spectrum for urban roads in Shanghai, China. Wang et al. [16] studied the fatigue load model for elevated roads in Guangzhou, China. Man et al. [17] analyzed the load value determination for test of cable-girder anchorage zone fatigue model, and researched corresponding fatigue truck in accordance with traffic status in China and bridge design specifications in other countries. Ren et al. [18] made a preliminary study on the selection of standard fatigue load models for highway bridges in China. Chen [19] discussed the seasonal and month variation of traffic flow and proposed a 3-axle fatigue load model in line with traffic load data collected from several measuring sites in Shandong, China. Zhang et al. [20] investigated the vehicle data of Jiangyin, Humen, Nanjing No.2 and No.3 bridges in China. He then studied the load model designed for analysis of structural with short influence line as well as the simulation method of stochastic fatigue loads for analysis of structural with long influence line. Ren [21] developed a 3-axle and a 4-axle fatigue truck, on the basis of traffic on Jiangyin Yangtze River highway, Huning, Zhenluo, Jinan Yellow River No.2 bridges and Sichuan Chengnan expressway. By means of probabilistic method and the principle of equivalent fatigue damage, Zhou et al. [22, 23] developed fatigue representative trucks for various areas of Shanxi, Fujian, Nanjing, Guangdong, Hubei, Henan, Liaoning and Chongqing, where traffic investigations were carried out. At the end, adjustments are made considering the length of influence line and longitudinal and transverse multi-vehicle presence.

Yan et al. [24] conducted a comprehensive analysis of current traffic load level in China in terms of structural ultimate bearing capacity, using huge amounts of traffic data gathered from typical road sections scattered across 23 provinces, municipalities and autonomous regions of China during the time period of 2007-2011. His study indicates that the traffic load level in Guangdong province is higher than other areas. Considering all this, the weigh-in-motion traffic data measured on 3 representative roads of Guangdong in 2008 are selected as the analytic bases in this paper. Hence, the fatigue load model proposed in this paper is applicable to heavily loaded areas.

2. STATISTICAL ANALYSIS OF TRAFFIC LOADS

The weigh-in-motion traffic load data are collected from 3 typical highway roads in Guangdong province of China. Table 1 lists the basic information of the traffic load.

Table 1. Measuring Sites of Traffic Load

Sites (ABBR)	Measuring duration	Classification	Vehicle amounts	Notes
National Road No. 107 (107)	20/Dec/2008-26/ Dec /2008	First class	237,187	2-way 6 lanes
Guangshen (GE)	20/ Dec /2008-26/ Dec /2008	Express way	541,778	2-way 6 lanes
Humen (HE)	28/Aug/2008-03/Sept/2008	Express way	326,949	2-way 6 lanes

The current researches [25-31] show that the probability density distribution curve of gross vehicle weight usually presents an unimodal form or a multimodal form (as seen in Figure 1). According to

the fitting analysis of various sets of function (normal, lognormal, inverse Gaussian, Weibull, Gamma, and multimodal Gaussian distribution), the stochastic characteristics of vehicle weight can be described by the function shown in Table 2.

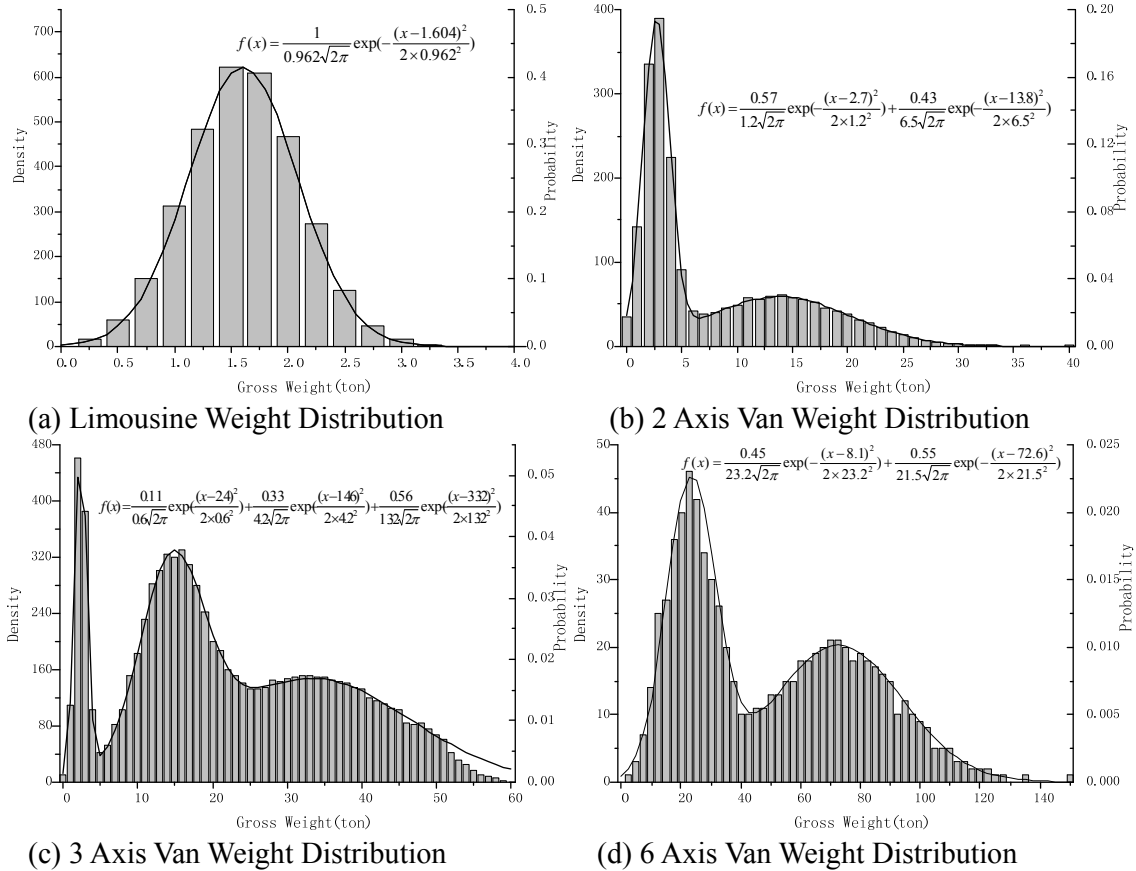


Figure 1. The Probability Density Distribution of Gross Vehicle Weight at Guangshen Expressway

Table 2. Vehicle Gross Weight Density Distribution Function

Number of axle	Vehicle type	Vehicle weight function
2	Passenger car	Lognormal, Inverse Gaussian
	Truck	Lognormal, Bimodal Gaussian
3-6	Truck	Multimodal Gaussian

(Note: as vehicle weight distribution of different places complies with different functions, specific mean values and standard deviation data are not provided in this table.)

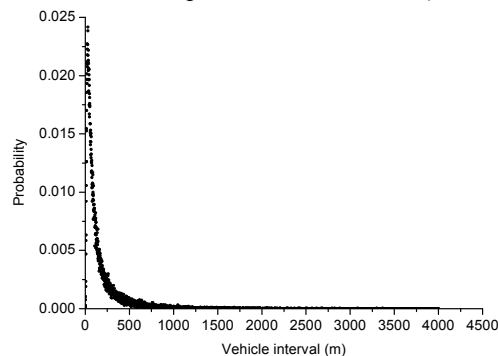


Figure 2. Statistical Histogram of Interval Between Sequent Vehicles on National Road No. 107

As far as moderate and large span bridges are concerned, the cumulative fatigue damage depends not only on gross vehicle weight and traffic volume, but also on the interval between adjacent vehicles. Therefore, key parameters affecting traffic density have been analyzed, such as traffic flow, time headway, vehicle interval (Figure 2 shows the statistical histogram of vehicle interval at National Road No. 107), vehicle speed and so on.

Shown in

Table 3 are the analytic results [26] of stochastic characteristics of traffic parameters which are basically consistent with the relevant research results from other places [12,27,29,32-34].

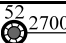
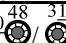
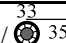
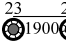
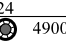
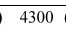
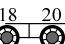
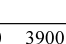
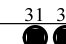
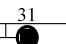
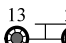
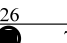
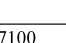
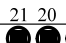
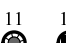
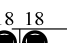
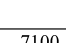
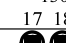
Table 3. Characteristics of Traffic Parameters



Item (ABBR)	Density function type [Density distribution curve] (Correlation)
Lane speed	Normal
Lane headway	[3 curves: skew line, level line and exponential function curve]
Interval	Lognormal
Headway divided by average headway within each hour (H/A)	Exponential
Traffic flow per hour and average headway within each hour (T-A)	(Exponential function)
Traffic flow per hour divided by average traffic flow per hour (T/A)	Uniform

3. SIMULATION OF VIRTUAL TRAFFIC

Due to the disadvantages of traffic measuring method as described before, the amount of data is small, as a result of the short duration of records listed in Table 1. Sample size enlargement is of great importance for the reliability enhancement of analytic results. The numerical technology is adopted to simulate virtual traffic stream of enough-long duration so as to reflect the stochastic variation characteristics of real traffic (as detailed in the section of statistical analysis of traffic loads).

Table 4. Vehicle Classifications

Vehicle type	Parameters (wheel base/mm, axle weight/%)	Equivalent weight (t)
car/coach/2-axle truck	 2700  5300  3500	8/18/20.2
3-axle truck	 1900  4900  4300	29.2/36.6
4-axle truck	 2000  3900  1400  3600 7000 1300	42.3/44.9
5-axle truck	 3600  7100  1300  3100 1400 7000 1300	62.1/59.0
6-axle truck	 3100  1400  7100  1300 1300 1300	76.8/63.3

Notes:  denotes 2-wheel set;  denotes 4-wheel set.

The simulation process is described as follows:

1) Both the ratio of vehicle type per hour and traffic volume per hour from every lane is acquired via traffic survey (WIM).

- 2) Data from various lanes are sampled to obtain simulated group of vehicles, using Monte Carlo method.
- 3) To simulate space headway of vehicle group, the average headway for each lane of that hour is calculated via T-A. Then, through H/A, the headway distribution for each roadway within that hour is obtained. Finally, each space headway during that hour is computed as the product of sampled headway and speed.
- 4) The load space of various axles in vehicle group is determined according to space headway and the vehicle models listed in Table 4.
- 5) The gross vehicle weight in the vehicle group is simulated by Monte Carlo method according to the probability distribution function of vehicle weight. Axle load of various axles is then determined according to Table 4.

The vehicle type classification is shown in Table 4, which is drawn out on the basis of more than 20,000 types of on-road vehicles in China and the investigation of vehicle data collected across China [24]. The classification includes most Chinese vehicle types on highway bridges and for each type the space between axles as well as the axle weight is acquired, according to Eq. 1 and Eq. 2, respectively.

$$W_{ej} = \left[\sum (f_i W_{ij}^m) \right]^{\frac{1}{m}} \quad (1)$$

Where W_{ej} denotes the j^{th} equivalent axle weight of vehicle type e ; W_{ij} denotes the j^{th} axle weight of i^{th} vehicle of type e ; f_i denotes the occurrence frequency of i^{th} vehicle of type e ; m denotes the slope of fatigue $S-N$ curve.

$$A_{ej} = \sum f_i A_{ij} \quad (2)$$

Where A_{ej} denotes the j^{th} equivalent axle spacing of vehicle type e ; A_{ij} denotes the j^{th} axle spacing of i^{th} vehicle of type e .

4. SINGLE VEHICLE FATIGUE LOAD MODEL

In this paper, the rain-flow counting method proposed by Matsuishi and Endo is employed to count stress spectrum. The fatigue damage of structural component can be quantified by Palmgren-Miner linear cumulative damage rule. The total damage D is defined as the summation of damages generated by load cycles of various amplitudes, as shown in Eq. 3.

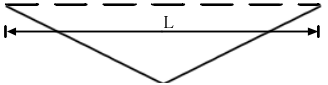
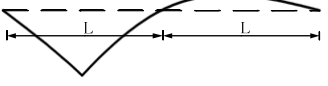
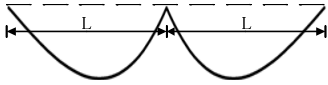
$$D = \sum_{i=1}^k \Delta D_i = \sum_{i=1}^k \frac{n_i}{N_i} \quad (3)$$

Where N_i denotes the fatigue lifetime of the i^{th} load stress amplitude; n_i denotes the actually occurring cycle times of the i^{th} load stress amplitude; k denotes the number of all possible amplitude value classes.

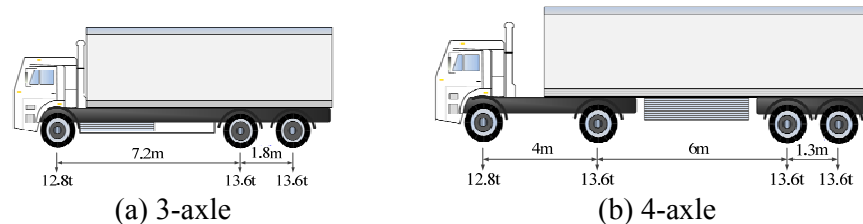
By loading the virtual traffic flow on the structural influence line, the load effect history can be acquired. Then the corresponding fatigue damage can be calculated via Eq. 3. All the considered theoretical influence lines are listed in Table 5. The span length in the third column of Table 5, which is denoted by ' L ' in the schematic diagram of the second column, is used in the calculation.

The cumulative fatigue damage of each vehicle in the simulated vehicle group can be calculated when the vehicle pass the influence line in the way of one vehicle load one time within the influence line. In the same way, the calculation of the same number of single vehicle model loading on the influence line can thus simulate cumulative damage of fatigue. The ratio of the two kinds of damage is used as analytic parameter, with ratio 1 indicating that the model can represent the real traffic flow. The parameters corresponding to typical influence lines listed in Table 5 are calculated, respectively. Then 1 is taken as the target value of the parameter, and the parameters (axle load and wheel base) of single vehicle model are modified to render the least sum of squares of differences between 1 and various parameters of influence line.

Table 5. Theoretical Influence Line for Calculation

Type (Num)	Schematic diagram	Span- L (m)
Simply support midspan moment (A)		1.25
		2.5
		5
2-span continuous midspan moment (B)		10
		20
		30
2-span continuous intermediate support moment (C)		50
		75
		100

According to the calculation, when the influence line is long, wheel base and distribution of axle loads have less effect on fatigue damage, with various damage ratios calculated by equivalent vehicle weight all close to 1; and when the influence line is short, the wheel base and the axial ratio have more effect on fatigue damage. Also according to the calculation result, various measuring points find big differences in the vehicle load model based on the method of the least-square fatigue damage variance: different measuring points and influence lines lead to different better vehicle types, and even in the case of the same count of vehicle axles, the axle load ratio still displays big differences. But generally speaking, a single truck with 3 or 4 axles will be better. The final fatigue load models are shown in Figure 3.



(a) 3-axle (b) 4-axle

Figure 3. Single Vehicle Fatigue Load Model

5. VEHICLE SPECTRUM FATIGUE LOAD MODEL



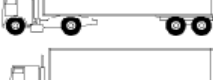
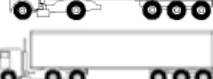
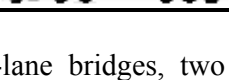
The single truck fatigue model is easy to apply, but the model is short of flexibility. Therefore, the vehicle spectrum fatigue load model is also applied. As the types of vehicle, as shown in Table 4, are too many to be directly applied in calculation, this paper chooses 5 truck types in light of axle

numbers for vehicle spectrum. The development of vehicle spectrum fatigue load model works on the principle that the fatigue damage caused by fatigue load model is equal to that caused by real vehicle group. The 5-truck spectrum fatigue load model is shown in Table 6.

6. ANALYSIS OF MULTI-VEHICLE PRESENCE

When structural influence surface is large while space headway is small, multiple vehicles tend to simultaneously appear within the same influence range and structural load effects caused by individual vehicle tend to joint together. In this case, the load effect is very difference from that caused by vehicles passing one after another.

Table 6. Vehicle Spectrum Fatigue Load Model

Vehicle type	Vehicle configuration		Type proportion (%)		
	Wheel base (m)	Axle weight (t)	107	GE	HE
	5.0	7-13	66	63	57
	5.0-1.6	8-12-12	14	12	7
	3.2-6.8-1.3	7-13-11-11	8	7	23
	3.4-6.8-1.3-1.3	9-15-12-12-12	6	9	9
	2.6-1.4-6.8-1.3-1.3	8-14-14-12-12-12	6	10	4

For multi-lane bridges, two aspects of multi-vehicle presence should be considered: multiple vehicles present simultaneously on the same roadway or on multiple roadways. Multi-lane bridges should be therefore designated as longitudinal and transverse multi-vehicle effects, respectively. In this paper, the queuing theory is adopted to analyze the multi-vehicle effects on fatigue damage.

Longitudinal multi-vehicle effects: passing bridge could be regarded as a service for vehicles [33], with the vehicular arrivals supposedly obeying Poisson process, with the rate parameter designated as λ (i.e. the average traffic density-veh/s), and the stochastic duration τ of vehicular passing bridge supposedly complying with exponential distribution. The multi-vehicle presence on the same lane can then be managed by the queuing theory of $M/M/k/0$ service system, whose number of service window is designated as k , that is, the roadway capacity of vehicle, which is defined here as the rounded ratio between the mean value of τ and the least value of headway T_s . For n ($n \leq k$) vehicles simultaneously present on the same lane, the mean service (passing bridge) time of each vehicle is computed according to $T_i = T - i \cdot T_s$ ($i=1, 2, 3 \dots n$), thus generating various service rates for each vehicle. Shown in Figure 4 is the system state transition.

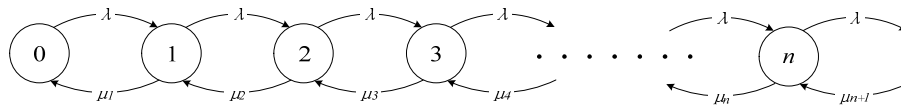


Figure 4. The Schematic Diagram of State Transition of Single Lane Service System

In Figure 4, $\mu_n = \alpha + \sum_{i=1}^n \psi_i$, $\alpha = \frac{1}{T}$ and $\psi_i = \frac{1}{T_i}$. According to the queuing theory, the probability of n vehicles loading at any time on the same lane of a bridge can be described by Eq. 4.

$$\begin{aligned}
P_n &= \left(\frac{\lambda}{\alpha} \right)^n \left\{ 1 + \frac{\lambda}{\alpha} + \sum_{i=2}^k [\lambda^i (\alpha \prod_{s=1}^{i-1} (\alpha + \sum_{j=1}^s \psi_j))^{-1}] \right\}^{-1} \quad (n=0,1) \\
P_n &= \left\{ \frac{\lambda^n}{\alpha} [\prod_{s=1}^{n-1} (\alpha + \sum_{j=1}^s \psi_j)]^{-1} \right\} \left\{ 1 + \frac{\lambda}{\alpha} + \sum_{i=2}^k [\lambda^i (\alpha \prod_{s=1}^{i-1} (\alpha + \sum_{j=1}^s \psi_j))^{-1}] \right\}^{-1} \quad (2 \leq n \leq k)
\end{aligned} \tag{4}$$

For simplification of the analysis, only one kind of vehicle type and the rectangular influence line are considered. Then, the mean occurrence number of n -vehicle presence on the same lane is as follows.

$$N_n = \frac{P_n}{1 - P_0} \frac{N}{n} \tag{5}$$

Where N denotes the total number of vehicles that have passed the same lane.

The adjustment factor of longitudinal multi-vehicle effect is defined as the ratio of cumulative fatigue damage between real group configuration passing and single vehicle passing along the same lane (see Eq. 6).

$$\gamma_k = \sqrt[m]{\frac{P_1}{1-P_0} + \frac{P_2}{1-P_0} 2^{m-1} + \frac{P_3}{1-P_0} 3^{m-1} + \dots + \frac{P_k}{1-P_0} k^{m-1}} \tag{6}$$

Where m denotes the slope of fatigue S-N curve.

Transverse multi-vehicle effects: Similarly, M/M/k'/0 service system of queuing theory is adopted here to analyze transverse multi-vehicle effects, where k' denotes the total number of roadways. Shown in Figure 5 is the corresponding system state transition.

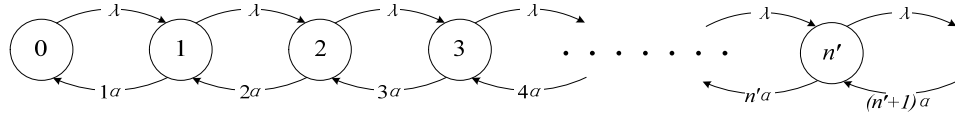


Figure 5. The Schematic Diagram of State Transition of Multi-lane Service System

In Figure 5, $\alpha = \frac{1}{T}$. The probability of n' ($n' \leq k'$) lanes occupied at the same time by a single vehicle is as follows (see Eq. 7):

$$P_{n'} = \frac{\lambda^{n'}}{\alpha^{n'} n'!} \left(\sum_{i=0}^{k'} \frac{\lambda^i}{\alpha^i i!} \right)^{-1} \quad (0 \leq n' \leq k') \tag{7}$$

Similarly, when only one kind of vehicle type and the rectangular influence line are considered, the mean occurrence number of n' -vehicle present on the n' lanes is as follows (see Eq. 8):

$$N_{n'} = \frac{P_{n'}}{1 - P_0} \frac{N'}{n'} \tag{8}$$

Where N' denotes the total number of vehicles that have passed the n' lanes.

The adjustment factor of transverse multi-vehicle effect is defined as the caused cumulative fatigue damage ratio between multiple vehicles passing side by side and single vehicle passing one after another along multiple lanes (see Eq. 9).

$$\gamma_k' = \sqrt[m]{\frac{P_1}{1-P_0} + \frac{P_2}{1-P_0} 2^{m-1} + \frac{P_3}{1-P_0} 3^{m-1} + \dots + \frac{P_{k'}}{1-P_0} k'^{m-1}} \quad (9)$$

Take 2-vehicle presence, the mean passing speed is 15m/s, the least headway T_s is 1s, the slope of S-N curve is 3, and one year consists of 280 days. The following equations can then be acquired: $\lambda = N/280/24/3600 = N/24192000$ (veh/s), $\alpha = 1/T = 15/L$ and $\psi = 1/T_1 = 1/(L/15 - 1)$. Thus, an approximately linear relationship between γ_2 and $N \cdot L$ can be obtained as shown by Eq. 10.

$$\gamma_2 = 1.004 + 0.0001 \cdot \frac{8.85 \cdot N \cdot L}{10^6} \quad (10)$$

Where L denotes the length of influence line (m); N denotes the yearly traffic volume for a single lane (veh).

Then, an approximately linear relationship between γ_2' and $N \cdot L$ can be obtained (see Eq. 11).

$$\gamma_2' = 1.009 + 0.0001 \cdot \frac{9.41 \cdot N \cdot L}{10^6} \quad (11)$$

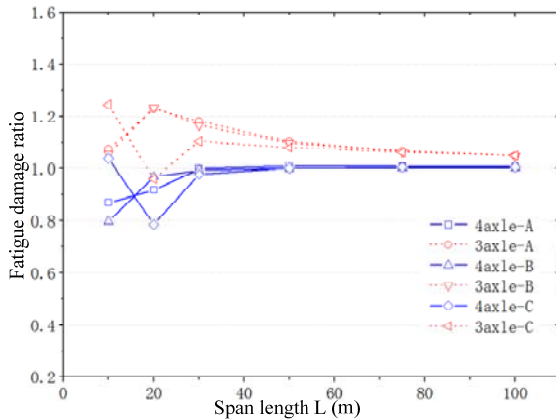
Where N denotes the yearly traffic volume for a single lane (veh), and here it can be taken as the mean value of the volume on all lanes.

The above analysis is simplified, and much more complicated situations will have to be considered in future researches which may include numerical simulation of multi-vehicle effects.

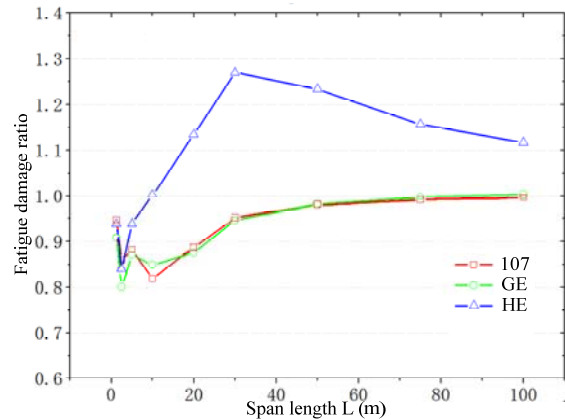
7. APPLICABILITY ANALYSIS OF FATIGUE LOAD MODEL

In order to verify the applicability of the proposed fatigue load models, a comparison of caused fatigue damages between load model (truck model plus multi-vehicle adjustments) and virtual traffic group is conducted for various influence lines (Table 5). And the variation tendencies of ratio curves are provided in Figure 6 and Figure 7.

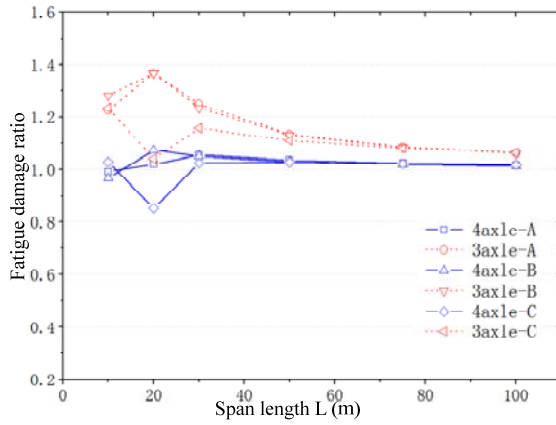
The fatigue damage ratio curves demonstrate that the developed load models, with influence lines longer than 40m, are good in applicability and conservative in nature. When influence lines are shorter than 40m, the curve tendencies are not so clear and an adjustment factor of 1.25 should be multiplied to consider the length effects of influence line.



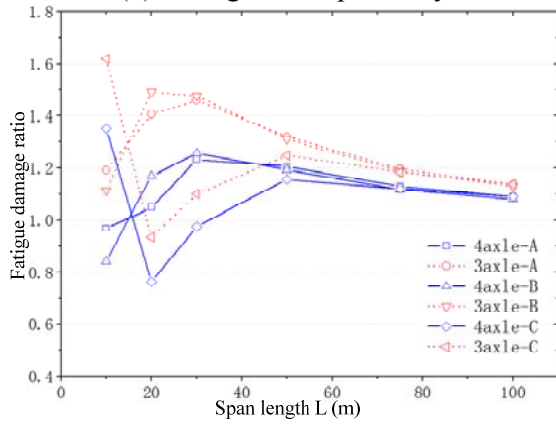
(a) National Road No. 107



(a) Influence Line A

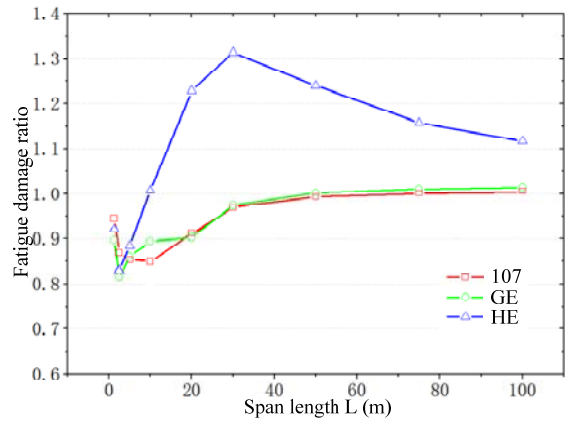


(b) Guangshen Expressway

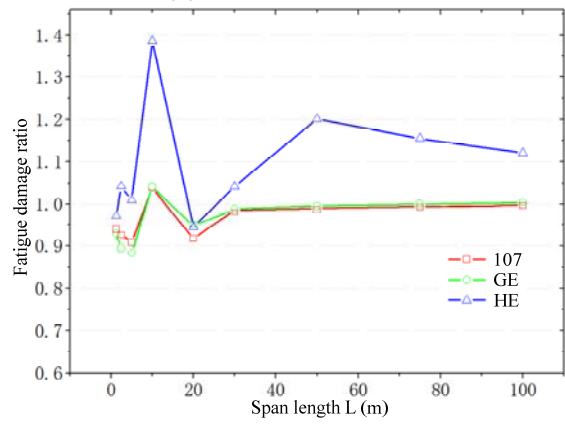


(c) Humen Expressway

Figure 6. The Damage Comparison Between Single Truck Model and Real Traffic



(b) Influence Line B



(c) Influence Line C

Figure 7. The Damage Comparison Between 5-Truck Model and Real Traffic

8. CONCLUSIONS

- (1) This paper develops a single truck fatigue load model (3 or 4 axles) and a 5-truck spectrum fatigue load model which are based on weigh-in-motion traffic load data, virtual vehicle simulation, linear fatigue cumulative damage rule, rain-flow counting method, and typical structural influence lines.
- (2) This paper has deduced computational equations for multi-vehicles according to the queuing theory and the linear fatigue damage criterion. It also proposes a multi-vehicle coefficient factor to cooperate with the fatigue load model.
- (3) The traffic load data adopted in this paper is collected from the primary highway roads in Guangdong province of China, where the level of traffic loads is higher than other areas of China. Therefore, the fatigue load model provided in this paper can be well applied to other areas of China to obtain conservative calculation results.
- (4) The proposed load models can generate good results in terms of fatigue damage relative to real traffic loads with influence lines longer than 40m. An adjustment factor of 1.25 should be multiplied for influence lines shorter than 40m.

- (5) The stochastic characteristics of vehicle gross weight and traffic parameters in Guangdong, China is basically similar to the relevant research findings from other studies, respecting the universal law of variation in traffic loads.

REFERENCES

- [1] Sharifi, Y., "Uniform Corrosion Wastage Effects on the Load-carrying Capacity of Damaged Steel Beams", *Advanced Steel Construction*, 2012, Vol. 8, No. 2, pp. 153-167.
- [2] British Standard, BS5400 Steel, Concrete and Composite Bridges Part 10: Code of Practice for Fatigue, 1980.
- [3] American Association of State Highway and Transportation Officials, AASHTO LRFD Bridge Design Specifications (SI Units), 2007.
- [4] CEN. Eurocode 1, Actions on Structures, Part 2-Traffic Loads on Bridges, BS EN 1991-2, Brussels, 2003.
- [5] CEN. Eurocode 3, Design of Steel Structures, Part 2-Steel Bridges, BS EN 1993-2, Brussels, 2006.
- [6] CEN. Eurocode 3, Design of Steel Structures, Part 1-9-Fatigue, BS EN 1993-1-9, Brussels, 2005.
- [7] Japan Road Society. Fatigue Design Guidelines for Steel Bridges, 2002.
- [8] Japan Road Society. Specifications for Highway Bridges, 2002.
- [9] Ministry of Communications of PRC. Specifications for Design of Steel Structure and Timber Structure Highway Bridges and Culverts (JTJ 025-86), 1987.
- [10] Prat, M., "Traffic Load Models for Bridge Design Recent Developments and Research", *Progress in Structural Engineering and Materials*, 2001, Vol.3, pp. 326-334.
- [11] Moses, F., Schilling, C.G. and Raju, K.S., "Fatigue Evaluation Procedures for Steel Bridges", NCHRP Report 299, 1987.
- [42] Calgaro, J.A., "Loads on Bridges", *Progress in Structural Engineering and Materials*, 1998, Vol.4, pp. 452-461.
- [13] Laman, J.A., "Fatigue Load Models for Girder Bridges", *Journal of Structural Engineering ASCE*, 1996, Vol. 7, pp. 726-733.
- [14] Chotickai, P., *Fatigue Reliability Based Analysis Methods for the Evaluation of Steel Bridge Structure*, Ph.D. Thesis, Purdue University, 2004.
- [15] Tong, L.W., Shen, Z.Y. and Chen, Z.Y., "Fatigue Load Spectrum for Urban Road Bridges", *China Civil Engineering Journal*, 1997, Vol.30, No.5, pp. 20-27. (in Chinese)
- [16] Wang, R.H., Chi, C. and Chen, Q.Z., et al., "Study on the Model of the Fatigue-loaded Vehicles in Guangzhou Trestle Bridges". *Journal of South China University of Technology (Natural Science Edition)*, 2004, Vol. 32, No.12, pp. 94-96. (in Chinese)
- [17] Man, H.G., Li, Q. and Tang, L., "Determination of Fatigue Load for Cable and Girder Anchorage Structure of Highway Steel Cable-Stayed Bridge", *Bridge Construction*, 2007, No. 3, pp. 13-16. (in Chinese)
- [18] Ren, J., Zhao, R.D. and Mao, X.M., "Study of Fatigue Load Spectrum for Highway Bridge". *Sichuan Building Science*, 2007, Vol.33, No.1, pp. 34-37. (in Chinese)
- [19] Chen, M. "Research on Highway Bridge Fatigue Truck Model, Ph.D. Thesis, Tongji University, China, 2009. (in Chinese)
- [20] Zhang, L., *Investigation and Study of Highway Bridge Loads for Fatigue Design*, Ph.D. Thesis, Tongji University, China, 2009. (in Chinese)
- [21] Ren, W.P., *Fatigue Behavior and Fatigue Life Evaluation of Structural Details in Welded Steel Girder Bridges*, Ph.D.Thesis, Southwest Jiaotong University, China, 2008. (in Chinese)

- [22] Zhou, Y.T., Zhai, H. and Bao, W.G., et al., "Research on Standard Fatigue Vehicular Load for Highway Bridges". Highway, 2009, Vol. 12, pp. 21-25. (in Chinese)
- [23] Zhou, Y.T., Bao, W.G. and Zhai, H., et al., "Study of Standard Fatigue Design Load for Steel Highway Bridges", China Civil Engineering Journal, 2010, Vol. 43, No. 11, pp. 79-85. (in Chinese)
- [24] Yan, B.C., Chen, W.Z. and Xu, J., "Analysis of the Current Situation of Highway Traffic Load in China", Proceedings of the First International Conference on Performance-based and Life-cycle Structural Engineering, Hong Kong, China, 2012, pp. 1278-1286.
- [25] CCCC Highway Consultants Co., Ltd., "Research on Bridge Design Load and Safety Verification Load", Research Report, 2012. (in Chinese)
- [26] Tongji University, "Research on Fatigue Load Model of Highway Steel Bridge and its Technical Parameters", Volume Report of Western Transportation Construction Projects (2008 318 494 04) of Chinese Ministry of Transport, 2012. (in Chinese)
- [27] Bailey, S.F. and Bez, R., "Site Specific Probability Distribution of Extreme Traffic Action Effects", Probabilistic Engineering Mechanics, 1999, Vol. 14, pp. 19-26.
- [28] Vu, K.A.T. and Stewart, M.G., "Structural Reliability of Concrete Bridges Including Improved Chloride-induced Corrosion Models", Structural Safety, 2000, Vol. 22, pp. 313-333.
- [29] Miao, T.J., "Bridge Live Load Models With Special Reference to Hong Kong", Ph.D.Thesis, Hong Kong Polytechnic University, Hong Kong, 2001.
- [30] Gindy M., "Development of A Reliability Based Deflection Limit State for Steel Girder Bridges", Ph.D. Thesis, State University of New Jersey, New Brunswick, New Jersey, 2004.
- [31] Caprani, C.C., O'Brien, E.J. and McLachlan, G.J., "Characteristic Traffic Load Effects from A Mixture of Loading Events on Short to Medium Span Bridges", Structural Safety, 2008, Vol. 30, pp. 394-404.
- [32] Crespo-Minguillón, C. and Casas, J.R., "A Comprehensive Traffic Load Model for Bridge Safety Checking", Structural Safety, 1997, Vol. 19, No. 4, pp. 339-359.
- [33] Croce, P. and Salvatore, W., "Stochastic Model for Multilane Traffic Effects on Bridges", Journal of Bridge Engineering, 2001, Vol. 6, No. 2, pp. 136-142.
- [34] Miao, T.J. and Chan, T.H.T., "Bridge Live Load Models from WIM Data", Engineering Structures, 2002, Vol. 24, pp. 1071-1084.

FATIGUE RELIABILITY ASSESSMENT OF ORTHOTROPIC STEEL BRIDGE DECKS BASED ON PROBABILISTIC MULTI-SCALE FINITE ELEMENT ANALYSIS

Tong Guo ^{1,2,*}, Zhong-xiang Liu ² and Jin-song Zhu ³

¹ Key Laboratory of Concrete and Prestressed Concrete Structures of the Ministry of Education, Southeast University, Nanjing, China

² School of Civil Engineering, Southeast University, Nanjing, China

³ School of Civil Engineering, Tianjin University, Tianjin, China.

*(Corresponding author: E-mail: guotong@seu.edu.cn)

ABSTRACT: The orthotropic steel deck (OSD) has been utilized successfully for thousands of bridges worldwide; however, fatigue cracking of the OSD has been observed frequently due to the complicated welded details combined with stresses that can be difficult to quantify, and the uncertainties in fatigue damage accumulation. In this paper, a fatigue reliability assessment method is proposed based on a comprehensive vehicle load model and probabilistic multi-scale finite element (FE) analysis. The vehicle load model, obtained from statistical data of toll stations, consists of probability distribution functions regarding the number of axles, axle weights, and transversal positions of vehicles, etc. The multi-scale finite element model not only captures the main features of the entire bridge but also gives an accurate description on local stress responses of the OSD in a relatively efficient way. Based on the probabilistic FE analysis combined with the developed vehicle load model, the fatigue reliabilities of the OSD could be obtained. Application of the proposed method is made in the fatigue reliability assessment of the OSD of the Runyang Cable-stayed Bridge for demonstration.

Keywords: Fatigue reliability; Orthotropic steel deck; Vehicle load; Multi-scale; Finite element analysis

DOI: 10.18057/IJASC.2015.11.3.7

1. INTRODUCTION

The orthotropic steel deck (OSD) has been utilized successfully for thousands of bridges worldwide due to its notable advantages [1], i.e., increased rigidity, material savings, low maintenance, suitability for standardization and prefabrication, etc. However, fatigue cracking of the OSD is frequently observed in practice [2-5], resulting in considerable maintenance or rehabilitation costs. During the past decades, design specifications and approaches to predict the remaining fatigue life of the OSD have been developed and applied actively [6-10]. However, the challenge for extending the fatigue life of the OSD still exists, resulting from the complicated welded details in which stresses can be difficult to quantify. Besides, with the increase of span lengths, bridges are becoming more flexible, which makes them more vulnerable to the vehicle loads, wind-induced vibration and/or fluctuations of ambient temperatures [11]. Therefore, the accurate prediction of fatigue life of the OSD requires that all influencing factors should be taken into account, which includes not only the configuration of fatigue details and vehicle loads but also the global structural behavior and/or environmental effect, etc.

In fatigue analyses, one important step is to obtain the fatigue stress spectra, and in general there are two types of approaches, namely the model-based approaches and monitoring-based approaches. The traditional way of obtaining the fatigue stress spectra on bridges is based upon the stress analysis with a traffic load model and a structural model [12-13]. Therefore, the accuracy of model-based approaches depends upon the rationality of traffic load models as well as the structural models. The monitoring-based approaches, however, provide authentic fatigue stress spectra. Especially, the recent development of structural health monitoring (SHM) systems enables long-term measurements on structural responses of bridges subjected to various loads and their

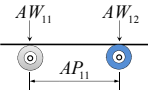
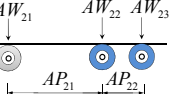

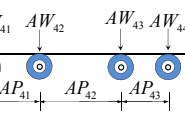
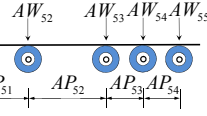
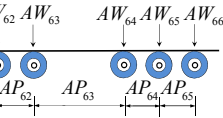
combined action [14-18]. However, the long-term SHM is often costly and not all concerned details could be covered due to limited budget.

In addition, fatigue analyses also abound with uncertainties, coming from external loads, material properties, corrosion actions and/or the measured data themselves, etc [19-23]. In order to study the fatigue reliability of the OSD under the combined action of vehicle loads and environmental factors, a probabilistic FE approach is proposed in this paper, which consists of a comprehensive vehicle model, obtained from statistical data of toll stations, and a multi-scale FE model that simulates the global responses of the whole bridge as well as the local stresses of fatigue-prone details in the OSD. Combined with a certain ambient temperature model, the coupling effect due to ambient temperature and vehicle loads is taken into account.

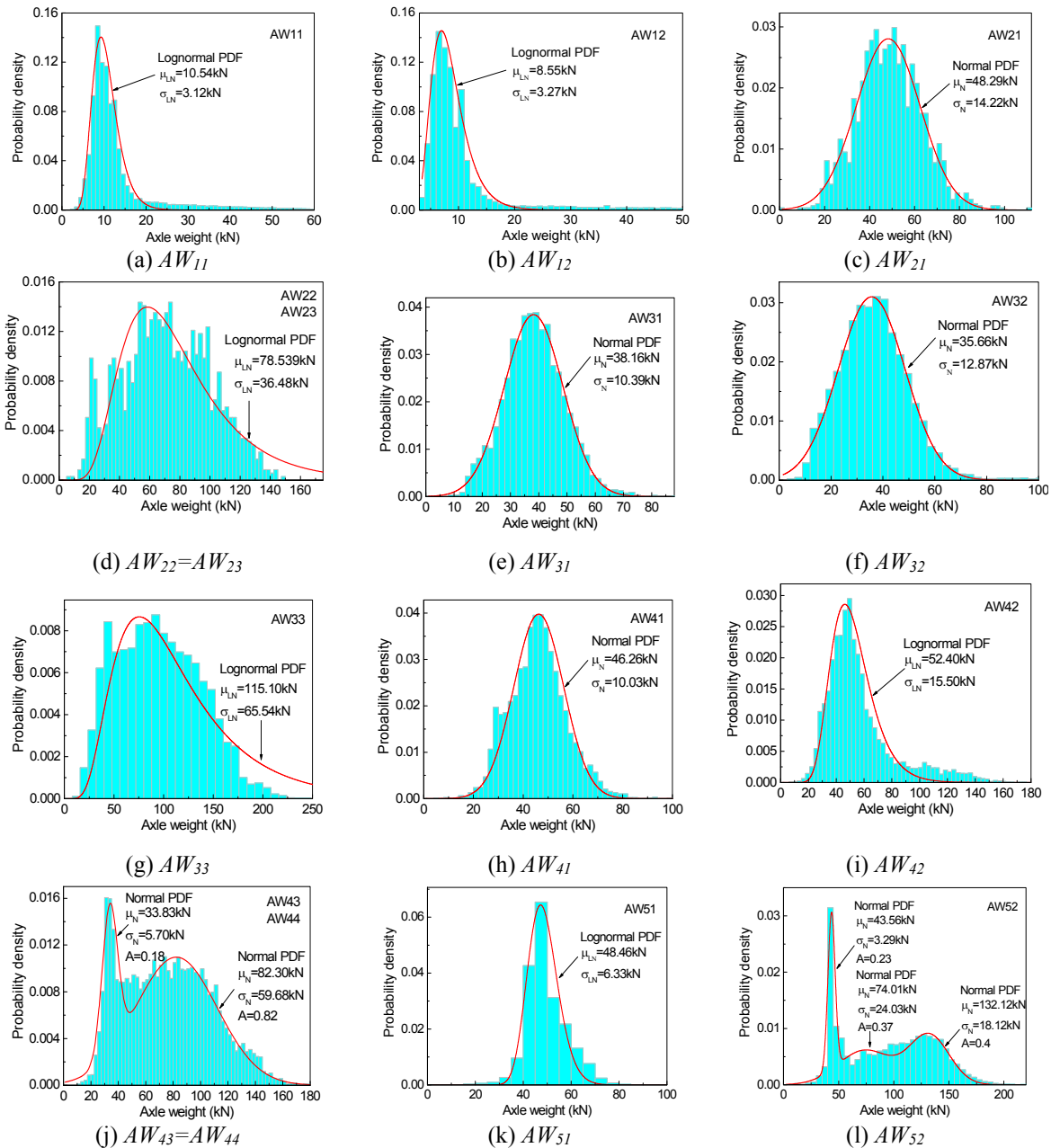
2. VEHICLE LOAD MODELS

According to the records from toll stations of the Runyang Bridge (consisting of a cable-stayed bridge and a suspension bridge), there were a total of 371,167 vehicles passing through the bridge during July 28, 2011 to August 31, 2011. Information including the types of vehicles, number of vehicles in each type, number of axles, and axle weights, etc., is obtained and analyzed. Using the video camera, the transversal positions (i.e., outer lane, middle lane or inner lane) are also identified.

Table 1. Probabilistic Properties of Axle Weights (dimensions in kN)

Vehicle type	Graphic illustration	Variable designation	Distribution type	Mean value	Standard deviation
1		AW_{11}	Lognormal	10.54	3.12
		AW_{12}	Lognormal	8.55	3.27
2		AW_{21}	Normal	48.29	14.22
		$AW_{22}=AW_{23}$	Normal	78.54	36.48
3		AW_{31}	Normal	38.16	10.39
		AW_{32}	Normal	35.66	12.87
		AW_{33}	Lognormal	115.10	65.54
4		AW_{41}	Normal	46.26	10.03
		AW_{42}	Lognormal	52.40	15.50
		$AW_{43}=AW_{44}$	Normal (0.18)	33.83	5.70
			Normal (0.82)	82.30	29.84
		AW_{51}	Lognormal	48.46	6.33
5		AW_{52}	Normal (0.23)	43.56	3.29
			Normal (0.37)	74.01	24.03
			Normal (0.4)	132.12	18.12
		$AW_{53}=AW_{54}=AW_{55}$	Normal (0.27)	22.96	1.71
			Normal (0.30)	52.23	13.92
6			Normal (0.43)	83.35	9.51
		AW_{61}	Lognormal	53.86	5.95
		$AW_{62}=AW_{63}$	Normal (0.13)	35.35	4.79
			Normal (0.87)	82.17	15.62
			Normal (0.07)	22.68	3.20
		$AW_{64}=AW_{65}=AW_{66}$	Normal (0.16)	38.11	13.95
			Normal (0.77)	80.94	13.11

As summarized in Table 1, there are mainly six types of vehicles crossing the bridge, and the axle weights of most types of vehicles can be described by a single-peak probability density function (PDF), as shown in Figure 1. However, for the last three types, multi-peaks exist in the PDFs, and therefore, a weighted sum of PDFs are used to describe such distributions. For example, the normal PDF is a non-skewed one and suitable for negative as well as positive variables; while the lognormal PDF is suitable for skewed distribution but only suitable for positive variables. For the multi-peaks distribution, the optimal number of PDFs, weights, and parameters of these PDFs can be determined through existing literature [24]. In this study, normal, lognormal PDFs and their combination are used. It is observed from Table 1 that the vehicle type 1 with two axles takes a large portion of the traffic volume (i.e., 76.7 percent), followed by the vehicle type 6 with six axles (taking about 16.94 percent), indicating that there is a considerable portion of heavy trucks in the total traffic volume. However, the portion of vehicle type 2 with three axles is very small, i.e., 0.65 percent, and vehicle types 3, 4 and 5 are all within 5% of the traffic volume.



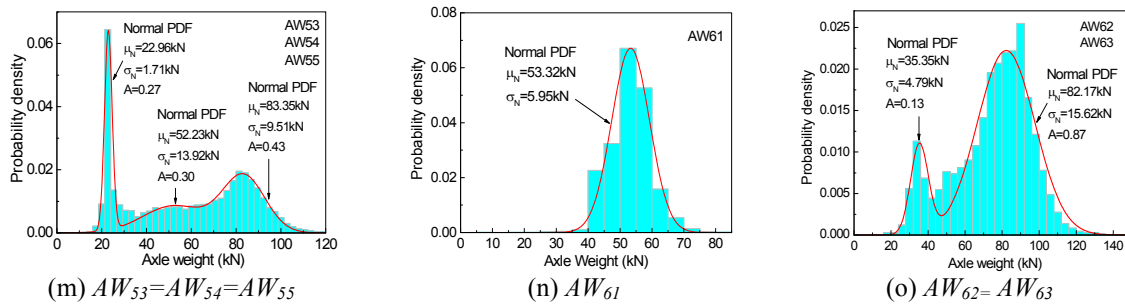


Figure 1. PDFs of Axle Weights

In addition, 36.65 percent and 42.03 percent vehicles ran in the middle lane and inner lane (i.e., the fast lane), respectively; whereas 21.32 percent vehicles ran in the outer lane (i.e., the slow lane). For the vehicle type 1 with light weight, most of them (i.e., 41.23 percent) were in the fast lane, and only 9.7 percent were in the slow lane. However, for the vehicle type 6 with heavy weight, their lane occupation was just opposite to that of vehicle type 1. Most heavy trucks were in the middle lane and the slow lane while only a small portion of them were in the fast lane.

Table 2. Constitution of Vehicles

Vehicle type	Percentage in traffic volume (%)	Percentage in each lane (%)		
		Outer lane	Middle lane	Inner lane
1	76.66	9.70	25.74	41.23
2	0.65	0.36	0.26	0.03
3	1.57	0.60	0.87	0.10
4	1.64	0.92	0.67	0.04
5	2.54	1.31	1.17	0.06
6	16.94	8.43	7.94	0.57

3. MULTI-SCALE FE MODELING OF RUNYANG CABLE-STAYED BRIDGE

3.1 Bridge Description

In this paper, the proposed method is demonstrated through the fatigue reliability assessment of the Runyang Cable-stayed Bridge (RCB). The RCB, connecting Yangzhou and Zhenjiang, has a total length of 756.8 m, consisting of a main span of 406 m and two side spans of 175.4 m, respectively. The two vase-shaped concrete towers are 146.9 m high, and each of them has two reinforced concrete legs and three prestressed concrete cross-beams, supporting the bridge girder through stay cables. The girder is an aerodynamically shaped closed steel box one with a width of 37.4 m and a height of 3.0 m, as shown in Figure 2(a), carrying two carriageways and each has three lanes. Two steel trusses, as shown in Figure 2(b), are placed longitudinally along the girder, so as to provide additional bending stiffness.

3.2 Finite Element Modeling

A multi-scale FE model of the RCB is developed using the FE program ANSYS, as shown in Figure 3. As demonstrated in previous study integrating multi-scale FE modeling [17], a tradeoff should be made elaborately between accuracy and computational efficiency. In this study, the

towers are modeled using the 3D iso-parametric beam elements (i.e., the Beam 4 element in ANSYS) having six DOFs at each node.

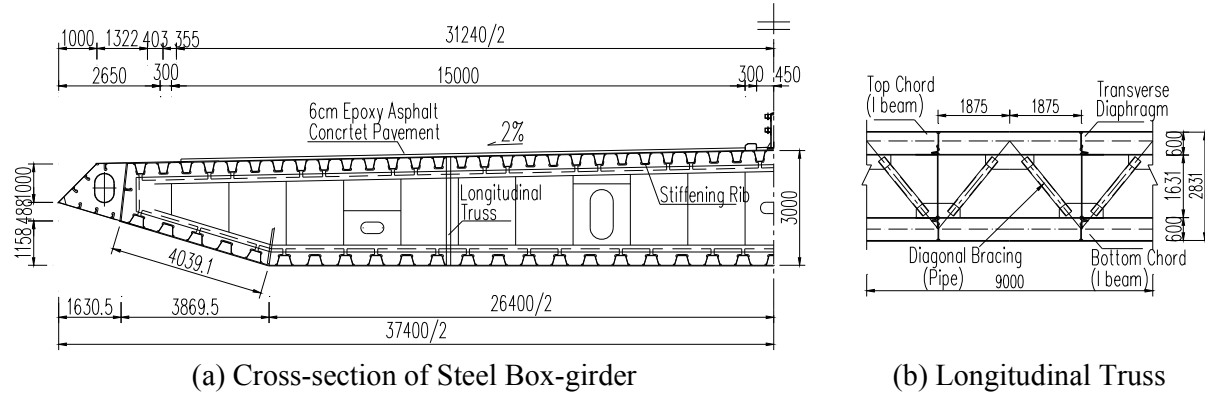


Figure 2. Box-girder of the RCB and Its Longitudinal Truss (dimension unit in mm)

The stayed-cables are modeled using the 3D linear elastic link elements (i.e., the Link 10 element) with three degrees of freedom (DOF) for each node. This link element is defined to bear tension only. The cable stresses in the equilibrium configuration are input in terms of initial strains. The material properties and real constants (i.e., areas of cross-section, moments of inertia, etc.) are strictly calculated and assigned to the corresponding elements. The box girders are modeled using shell elements (i.e., the shell 63 element). To reduce the number of elements, the orthotropic decks and bottom plates of the girder are modeled respectively using a layer of plates without U-ribs, and these plates are assigned with orthotropic material properties. The element dimension of such deck plates is 0.3 m (transversal) \times 1.5 m (longitudinal) for most parts. However, to have a precise observation on the deck details, the decks near the mid-span are refined twice. The first refinement is conducted for decks with a distance no larger than 50.5 m to the mid-span, and U-ribs are modeled with an element dimension of 0.3 m (transversal) \times 0.35 m (longitudinal). The second refinement is conducted for decks with a distance within 1.75 m to the mid-span, and the element dimension is 0.033 m (transversal) \times 0.039 m (longitudinal). In addition, the layered element (i.e., Shell 181 element) is used for the top plate, which simulates the 14mm thick steel plates as well as the 60 mm thick epoxy asphalt concrete pavements. Different elastic moduli and thicknesses are assigned to the elements. The concrete and steel blocks, placed inside the box-girders at two side spans to adjust the configuration of the bridge, are modeled using the Mass 21 element. To simulate the influence of ambient temperature on the structural responses, temperatures are applied as a form of load in the FE analysis. The coefficients of the thermal expansion of concrete and steel are set as $1.0 \times 10^{-5}/^{\circ}\text{C}$ and $1.2 \times 10^{-5}/^{\circ}\text{C}$ respectively. In addition, past investigation revealed that temperature fluctuation may soften or stiffen the epoxy asphalt concrete pavements, as shown in Table 3, and thus influences the stresses of the decks under a moving vehicle [11]. Therefore, in this study, the elastic modulus of the pavements (i.e., the top layer of the Shell 181 element) is updated with different temperature value.

Table 3. Changes in the Elastic Modulus of Pavements with Different Temperatures [11]

Temperature ($^{\circ}\text{C}$)	60	55	50	45	40	35	30	25	20	15	10	5	0	-5
Elastic modulus (MPa)	300	337	374	411	448	485	522	559	596	633	670	707	744	781

The displacements of the girders at two ends are coupled with those of tower cross-beams, except that the longitudinal displacement is free. This is to simulate the connection of the slide bearing between girders and towers. In total, there are 584,784 shell elements, 3,752 beam elements, 104 link elements, and 3,174 mass elements in the FE model.

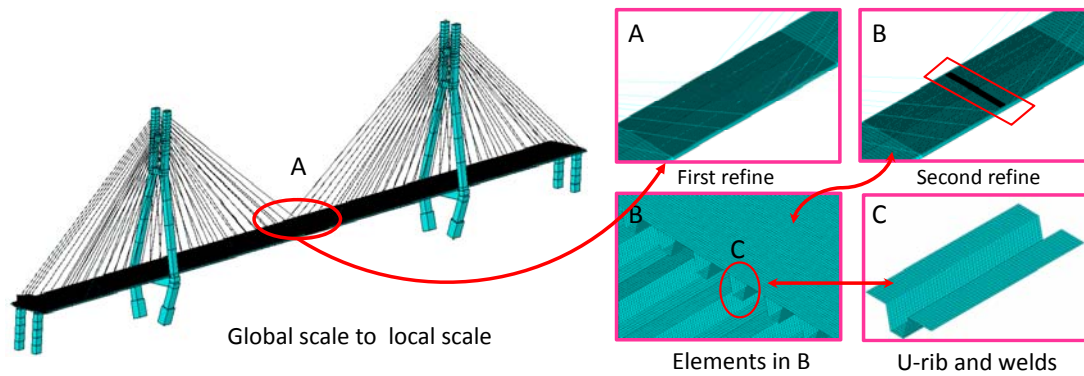


Figure 3. Multi-scale FE Model of the RCB

3.3 Validation of FE Model

Field measured data in the controlled load tests of the RCB are used to calibrate the above FE model, and two typical load cases, as shown in Table 4 are selected for illustration purpose. Dump trucks, as shown in Table 5, were used in the field tests, and each truck had a weight of 300 kN. Strain gauges installed at the mid-span cross-section of the girder were used to measure the normal stresses during the tests, as shown in Figure 4. Note that the prefixes “T” and “U” in Figure 4 denote that the gauges are on top plates and U-ribs, respectively.

Table 4. Description of Load Cases

Load test	Truck positions	Illustration
Case 1	Eight trucks, symmetrically loaded at the mid-span in 4 lines and 2 rows,	
Case 2	All the trucks in Case 1 move 1.75 m forward	

Table 5. Trucks Used in the Controlled Load Tests

Load case	Wheel loads (kN)	Wheel prints (mm)		Distance between (mm)	
		Width	Length	Wheels	Axles
Single tyre (front axle)	30	299.9	375	1700	3500
Double tyre (rear axle)	60	598.8	375	2000	1300

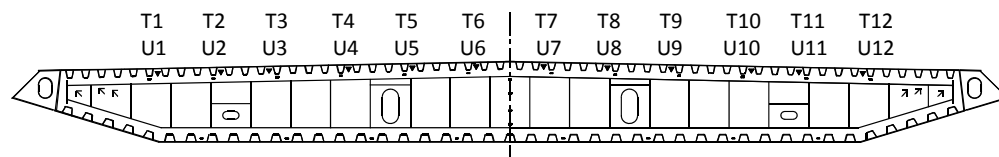


Figure 4. Layout of Strain Gauges at Mid-span Cross-section of the Girder

According to the vehicle parameters in the controlled load tests such as axle weight, axle spacing, etc., tyre loads are applied to selected deck elements and static elastic analyses are performed. Figure 5 illustrates the comparison between the calculated and measured stresses, where good

agreement is observed, showing the effectiveness of the FE model. It is worth noting that the difference in the stresses of top plates between two cases are in general not large, and similar stress distributions on the cross-section of girder between two cases are observed; however, significant differences exist in the stresses of U-ribs between the two cases, both in stress magnitudes and distribution patterns, which may be attributed by the longitudinal trusses.

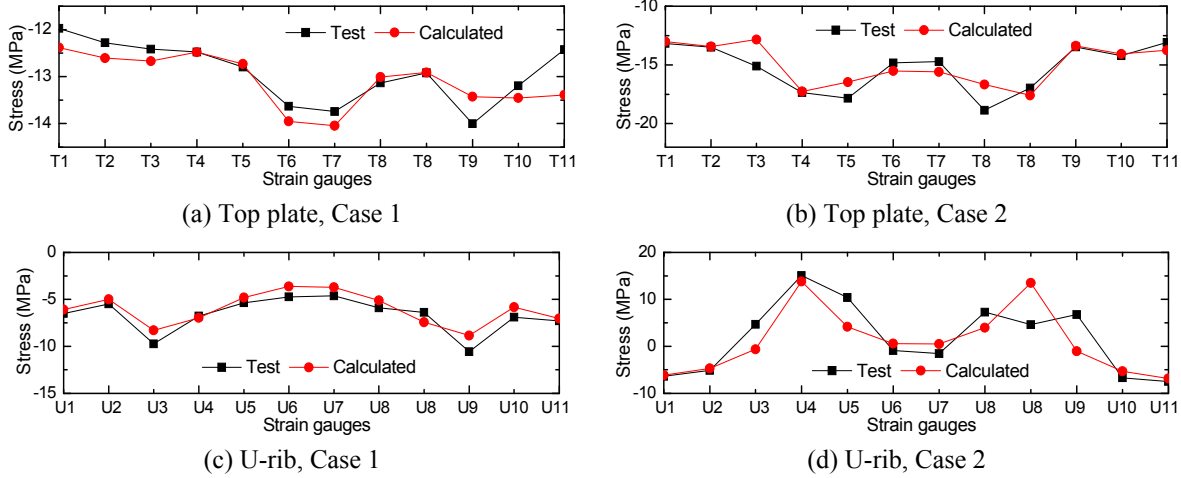


Figure 5. Comparison between Calculated and Measured Stresses

4. FATIGUE RELIABILITY ASSESSMENT USING PROBABILISTIC FE ANALYSIS

4.1 Fatigue Analysis Using AASHTO Approach

The AASHTO approach to fatigue assessment is based on the S-N curves in the AASHTO design specification [6] and the Miner's rule. The AASHTO specification defines a number of S-N curves to account for the metallic fatigue life. Each curve is defined on the basis of nominal stress range vs life in cycles, and corresponds to one of the Category detail (A, B, C, etc.). The curves have a constant slope between 10^5 and 10^7 cycles, defined from experimental test data, and the curves are extended for longer lives using theoretical calculation, when N is greater than 10^7 . The stress-life relationship is thus defined by:

$$N = \frac{A \cdot \Delta}{S^m} \quad (1)$$

where N is the actual fatigue life in cycles of a detail; A is the detail category constant; Δ is the Miner's critical damage accumulation index. S is the constant stress range. When stress ranges are random variables, an equivalent stress range S_{re} , which represents the same fatigue damage caused by a stress range histogram, should be used instead of S :

$$S_{re} = \left[\sum \frac{n_i}{N} \cdot S_i^m \right]^{1/m} \quad (2)$$

where m is the slope of S-N curves on log-log axes, and in most cases; m has a value of 3.0. n_i is the number of stress ranges corresponding to stress range S_i .

4.2 Fatigue Reliability

The design of any structure requires that its resistance R is greater than the load effect S . This requirement (i.e. $R > S$) is expressed as

$$G(\mathbf{X}) = R - S > 0 \quad (3)$$

where $\mathbf{X} = \{X_1, X_1, \dots, X_n\}^T$ denotes the vector of random variables; $G(\mathbf{X})=0$ represents the limit state.

In the context of fatigue assessment based on monitored data, according to Eq. (1), the limit state function in Eq. (3), can be written into

$$G(\mathbf{X}) = \Delta - e \cdot N \cdot (S_{re})^m / A = 0 \quad (4)$$

where e is an error factor of a typical measurement in SHM.

To consider the uncertainties that abound in the SHM as well as in the material resistance (S-N curves), parameters in Eq. (4) are treated as random variables. Frangopol *et al.* assumed that e followed a lognormal distribution with the mean value of 1.0 and the COV of 0.3[22]. A and Δ are also lognormally distributed variables. For Category details B and E in this study, the mean values of A are $14.4 \times 10^{11} (\text{MPa}^3)$ and $39.3 \times 10^{11} (\text{MPa}^3)$ respectively and the COV is 0.45[21]; the mean values of Δ is 1.0 and the COV is 0.3[25].

Assuming all the variables in Eq. (4) are independent, the fatigue reliability index β can be written as [23]

$$\beta = \frac{\sum \mu_{\ln X_{i,R}} - \sum \mu_{\ln X_{i,S}}}{\sqrt{\sum \sigma_{\ln X_{i,R}}^2 + \sum \sigma_{\ln X_{i,S}}^2}} = \frac{\mu_{\ln \Delta} - [\mu_{\ln e} + \ln(N) - \mu_{\ln A} + m \cdot \mu_{\ln S_{re}}]}{\sqrt{\ln[(1 + \delta_{\Delta}^2) \cdot (1 + \delta_A^2) \cdot (1 + \delta_e^2)] + m^2 \ln(1 + \delta_{\ln S_{re}}^2)}} \quad (5)$$

where the accumulated number of cycles N in the year t can be estimated by the following equation:

$$N(t) = 365 \cdot ADT \cdot \int_0^t (1 + \alpha)^t dt \quad (6)$$

where ADT represents the average daily vehicles and α is the traffic increase rate per year. Since S_{re} is obtained from the static FEA in which the dynamic amplification is not taken into account, a dynamic load amplification (DLA), with a mean value of 1.10 and a standard deviation of 0.08 [26], is multiplied to the calculated S_{re} . Considering that the variables in Eq. (5) should be lognormally distributed, the normal PDF of DLA is replaced by a lognormal PDF, which is the best fit of the normal PDF, with a mean value of 0.097 and a standard deviation of 0.073. To this end, the limit state function in Eq. (4) can be established as

$$G(\mathbf{X}) = \Delta - e \cdot N(t) \cdot (DLA \cdot S_{re})^m / A = 0 \quad (7)$$

Accordingly, Eq. (5) can be rewritten into

$$\beta = \frac{\mu_{\ln \Delta} + \mu_{\ln A} - [\mu_{\ln e} + m \cdot \mu_{\ln S_{re}} + m \cdot \mu_{\ln DLA} + \ln N(t)]}{\sqrt{\sigma_{\ln \Delta}^2 + \sigma_{\ln A}^2 + \sigma_{\ln e}^2 + (m \cdot \sigma_{\ln DLA})^2 + (m \cdot \sigma_{\ln S_{re}})^2}} \quad (8)$$

4.3 Finite Element Analysis under Uncertainty

To obtain the probabilistic distributions of S_{re} , a probabilistic FEA code is developed in the MATLAB environment, and this probabilistic finite element analysis is performed according to the following procedure:

1) A uniformly distributed variable VT is defined regarding the vehicle type, and m numbers are generated in the value domain of $[0, 1]$, which are used in m times of finite element analyses to simulate m vehicles crossing the bridge in a day (i.e., $m=1000$). In each FEA, the vehicle type is determined by the value of $VT(i)$, ($i=1, \dots, m$), as shown in Table 1. For instance, if $VT(i) \leq 0.7666$, loads of vehicle type 1 will be applied; if $0.7666 < VT(i) \leq 0.7731$, loads of vehicle type 2 are applied, etc.

2) A uniformly distributed variable NL is defined to determine the lane in which the vehicle travels. Similar to VT , m numbers are generated in the value domain of $[0, 1]$, and the value of $NL(i)$, ($i=1, \dots, m$), determines the transversal position of the vehicle loads. For instance, if loads of vehicle type 1 are to be applied and $NL(i) < 0.0970$, loads should be applied in the outer lane; if $0.0970 < NL(i) \leq 0.4123$, loads should be applied in the middle lane; otherwise, loads are in the inner lane.

3) A uniformly distributed variable T is defined, and m numbers are generated in the value domain of $[1, 365]$. Previously, daily ambient temperatures are measured and form an uniform distribution with a volume of 365. Therefore, the value of $T(i)$, ($i=1, \dots, m$), determines the ambient temperature used in the FE analysis.

4) m random numbers are generated for each variable in Table 1 (i.e., axle weights and axle spacing), according to normal or lognormal PDFs by using the truncated Latin Hypercube sampling (LHS) [27], and the correlations between axle weights and axle spacing are neglected to simplify the analysis.

5) According to the vehicle type, the transversal position of vehicle loads, axle loads and the axle spacing of the vehicle determined in the above three steps, loads of a vehicle are applied on the finite element model in ANSYS in k load steps (i.e., $k=24$). Each load step corresponds to a static FEA, and after each load step, the loads move forward to simulate the movement of the vehicle. Note that in each FE analysis, temperature loads are applied simultaneously and the corresponding changes are made to the elastic modulus of pavements, so that the influence of ambient temperatures on the fatigue stress spectra can be taken into account.

6) After each FEA, stresses at studied details under the moving loads are calculated, and the stress time-histories are obtained and output into a text file.

7) According to the simulated stress time-histories, rain-flow counting is made in the MATLAB environment to calculate $S_{re}(i)$, ($i=1, \dots, m$).

8) The probabilistic distributions of S_{re} are fitted according to $S_{re}(i)$, ($i=1, \dots, m$).

4.4 Results and Discussion

According to the above analysis procedure, fatigue reliability assessment is made for the RCB. First, the daily averaged temperature of the RCB in 2011 is obtained from the temperature gauge

installed underneath the deck plates at the mid-span of the bridge, as shown in Figure 6, where seasonal fluctuations are clearly observed.

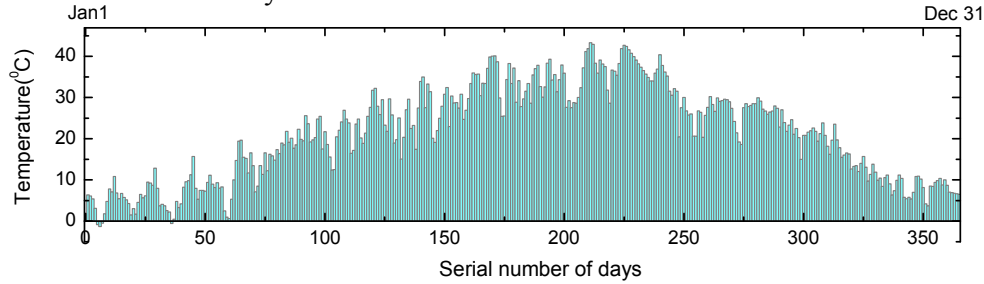


Figure 6. Daily Averaged Temperature from the SHM

Based on the procedure depicted in Section 4.2, probabilistic FE analyses are conducted, and three welded details in bridge decks are selected for evaluation, as shown in Figure 7. Weld A is the single-fillet weld at the rib-to-deck joint, whereas the Welds B and C are the butt welds at the U-rib and the top plate, respectively. According to the classification in AASHTO, Category detail C is assumed for Weld A and Category detail B is assumed for Welds B and C. In the following analyses, six positions on the bridge decks (i.e., Positions 1, 2,...,6) are selected for comparison, corresponding to the positions of stress gauges in Figure 4 (i.e., U1, U2,..., U6). For example, position A4, B4 and C4 represents the welds A, B and C near stress gauges U4, respectively.

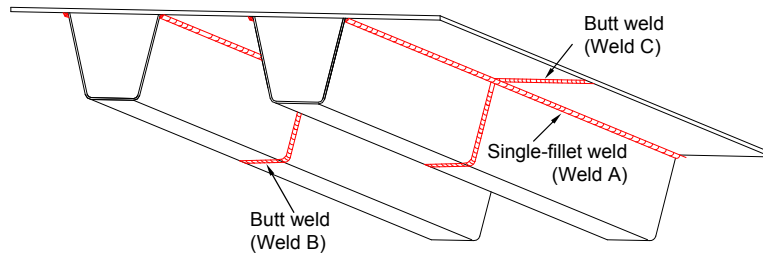


Figure 7. Welded Details in the OSD

Based on the FE analysis, Figure 8 shows stress time-histories of the three details under a moving truck (i.e., vehicle type 6) with mean axle weights as shown in Table 1. It is observed that welds A4 and C4 have similar responses while weld B4 shows a quite different pattern. Influence of six axles on stress time-histories can be clearly identified from the peaks or valleys of the stress time-histories.

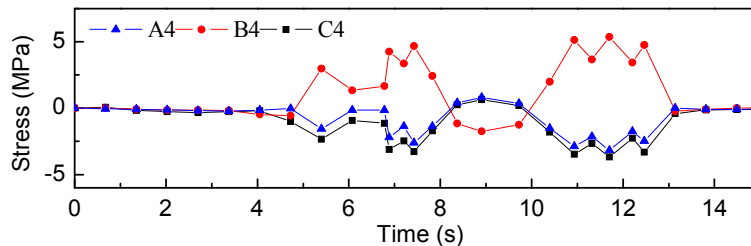


Figure 8. Stress Time-histories under A Moving Truck

According to the results of probabilistic analyses, PDFs of S_{re} of the three welded details are obtained, as shown in Figure 9, which in general can be described using lognormal PDFs. Taking A3 in Figure 9(a) for example, the mean value and the standard deviation of $\ln S_{re}$ are 8.125MPa and 2.844MPa, while if the temperature effect is not considered, the values are 7.442MPa and 2.687MPa, respectively. Therefore, the temperature effect has a significant influence on the mean

value of the S_{re} . Based on the fitted PDFs of S_{re} and Eq. (8), fatigue reliabilities at each specific time can be calculated and to this end, time-variant reliabilities are obtained as shown in Figure 10. It is observed that the fatigue reliabilities decrease rapidly during the first ten to twenty years of service, and Weld A seems to have lowest reliabilities among the three details, though the mean values and standard deviations of $\ln S_{re}$ of the three welds are in general close to each other. Note that Weld A corresponds to the detail category C with a smaller value of the fatigue parameter A , as compared with Welds B and C. However, for the same welded detail (i.e., Weld A), the reliabilities at different positions are not the same, which is due to different S_{re} in these details and existence of longitudinal trusses. In general, details in outer lane with more heavy trucks and details in middle lane with highest vehicle occupation have lower reliabilities. Assuming the target reliability index β_{target} is 1.5, reliabilities of welds A may fall below β_{target} prior to the designed life (i.e., 100 years).

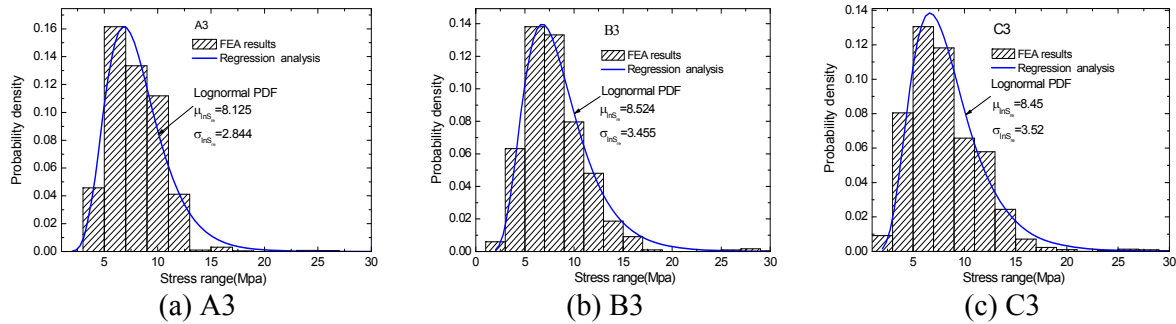


Figure 9. PDFs of S_{re} of Various Details

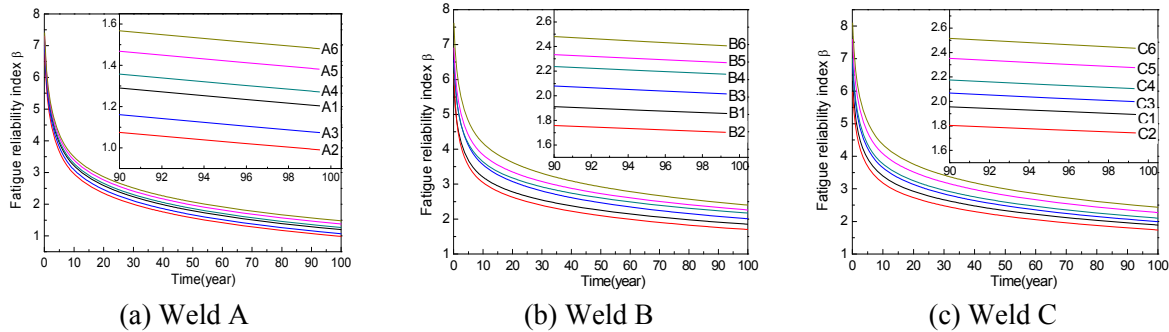


Figure 10. Time-variant Reliabilities of Various Details

5. CONCLUSIONS

This paper presents an approach to evaluate the time-variant reliabilities of the OSD of long-span bridges. Both measured vehicle loads and multi-scale finite element analysis are used in conjunction with the AASHTO fatigue evaluation methodology. Field measured responses are also adopted to calibrate the multi-scale FE model. The following conclusions can be drawn from this study.

- (1) The proposed method provides a tool to evaluate the fatigue performance of the OSD with relatively lower costs and fewer limitations on the locations of details, as compared with the SHM. In addition, the coupling effect of vehicle loads and ambient temperature could be taken into account, which is the superiority over previous studies. The effectiveness of the proposed method, however, relies on the accuracy of the vehicle load models and the FE model of the bridge.

- (2) The multi-scale FE model enables an accurate description on the stresses in complex details; however, it is important to mesh the FE model in a most efficient way so that the computational cost is minimized.
- (3) It is observed that fatigue reliabilities decrease rapidly during the first ten to twenty years of service, and Weld A seems to be the most vulnerable one among the three details. However, for the same welded detail (i.e., Weld A), the reliabilities at different positions are not the same. In general, details in middle lane and outer lane have relatively lower reliabilities.
- (4) According to the presented analyses, reliabilities of some welded details may fall below β_{target} prior to the designed life. The future work of this ongoing study includes using monitored data and/or field inspection results to calibrate the proposed model.

ACKNOWLEDGMENTS

The financial support from 1) the Jiangsu Transportation Department under grants No. 2011Y09-2 and No. 2011Y03; 2) the Natural Science Foundation of Jiangsu under grants No. BK2011611 and No. BK20130023 and 3) the National Science Fund of China under grant No. 51178305 and the Key Projects in the Science & Technology Pillar Program of Tianjin under grant No. 11ZCKFSF00300 are gratefully acknowledged.

REFERENCES

- [1] Partov, D. and Dinev, D., "Structure, Design and Construction of a Steel Orthotropic Bridge in Sofia", *Advanced Steel Construction*, 2007, Vol. 3, No. 4, pp. 752-764.
- [2] Jong, F.B.P.de. "Overview Fatigue Phenomenon in Orthotropic Bridge Decks in the Netherlands," 2004 Orthotropic Bridge Conference, Sacramento, California, USA, August 25-27, 2004.
- [3] Wolchuk, R. "Lessons from Weld Cracks in Orthotropic Decks on Three European Bridges", *Journal of Structural Engineering*, 1990, Vol. 116, No.1, pp.75-84.
- [4] Xiao, Z.G., Yamada, K., Inoue, J. and Yamaguchi, K. "Fatigue Cracks in Longitudinal Ribs of Steel Orthotropic Deck", *International Journal of Fatigue*, 2006, Vol.28, No.4, pp.409-416.
- [5] Fisher, J.W., "Fatigue and Fracture in Steel Bridges", 1984, New York: John Wiley & Sons.
- [6] AASHTO. "Guide Specifications for Fatigue Evaluation of Existing Steel Bridges", Washington, DC: American Association of State Highway and Transportation Officials, 1990.
- [7] BS5400. "Steel, Concrete and Composite Bridges, Part 10. Code of Practice for Fatigue", London: British Institute, 1982.
- [8] Eurocode 3. "Design of Steel Structures – Part 1-9: Fatigue", London: British Institute, 2005.
- [9] FHWA. "Manual for Design, Construction, and Maintenance of Orthotropic Steel Deck Bridges (FHWA-IF-12-027)", February 2012.
- [10] Kozy, B. M., Connor, R. J., Paterson, D. and Mertz, D. R. "Proposed Revisions to AASHTO-LRFD Bridge Design Specifications for Orthotropic Steel Deck Bridges", *Journal of Bridge Engineering*, 2011, Vol. 16, No. 6, pp.759-767.
- [11] Guo, T., Li, A.Q. and Li, J.H. "Fatigue Life Prediction of Welded Joints in Orthotropic Steel Decks Considering Temperature Effect and Increasing Traffic Flow", *Structural Health Monitoring-An International Journal*, 2008, Vol. 7, No. 3, pp. 189-202.

- [12] Frýba, L., "Estimation of Fatigue Life of Railway Bridges Under Traffic Loads", *Journal of Sound and Vibration*, 2008, Vol. 70, No. 4, pp. 527-541.
- [13] Szerszen, M.M., Nowak, A.S. and Laman, J.A., "Fatigue Reliability of Steel Bridges", *Journal of Constructional Steel Research*, 1999, Vol. 52, No. 1, 83-92.
- [14] Freitas, S. T. D., Kolstein, H. and Bijlaard, F. "Structural Monitoring of a Strengthened Orthotropic Steel Bridge Deck Using Strain Data", *Structural Health Monitoring*, 2012, Vol.11, No.5, pp. 558-576.
- [15] Li, Z.X., Chan, T.H.T. and Zheng, R., "Statistical Analysis of Online Strain Response and Its Application in Fatigue Assessment of a Long-span Steel Bridge", *Engineering Structures*, 2003, Vol. 25, No.14, pp.1731-1741.
- [16] Leander, J., Anderson, A. and Karoumi, R. "Monitoring and Enhanced Fatigue Evaluation of a Steel Railway Bridge", *Engineering Structures*, 2010, Vol. 32, No.3, pp. 854-863.
- [17] Wang, Y., Li, Z.X. and Li, A.Q. "Combined Use of SHMS and Finite Element Strain Data for Assessing the Fatigue Reliability Index of Girder Components in Long-span cable-stayed bridge", *Theoretical and Applied Fracture Mechanics*, 2010, Vol. 54, No. 3, pp.127-136.
- [18] Zhou, Y.E. "Assessment of Bridge Remaining Fatigue Life Through Field Strain Measurement", *Journal of Bridge Engineering*, 2006, Vol. 11, No. 6, pp.737-744.
- [19] Zhang, W. and Cai, C.S. "Fatigue Reliability Assessment for Existing Bridges Considering Vehicle Speed and Road Surface Conditions", 2012, Vol. 17, No. 3, pp. 443-453.
- [20] Ni, Y.Q., Ye, X.W. and Ko, J.M. "Monitoring-based Fatigue Reliability Assessment of Steel Bridges: Analytical Model and Application", *Journal of Structural Engineering*, 2010, Vol.136, No.2, pp.1563-1573.
- [21] Liu, M., Frangopol, D.M. and Kwon, K. "Fatigue Reliability Assessment of Retrofitted Steel Bridges Integrating Monitored data", *Structural Safety*, 2010, Vol. 32, No.1, pp.77-89.
- [22] Frangopol, D. M., Strauss, A. and Kim, S., "Bridge Reliability Assessment Based on Monitoring", *Journal of Bridge Engineering*, 2008, Vol. 13, No. 3, pp. 258-70.
- [23] Guo, T., Frangopol, D.M. and Chen, Y.W., "Fatigue Reliability Assessment of Steel Bridge Details Integrating Weigh-in-motion Data and Probabilistic Finite Element Analysis", *Computers & Structures*, 2012, Vol. 112-113, pp. 245-257.
- [24] Ni, Y.Q., Ye, X.W. and Ko, J.M., "Modeling of Stress Spectrum Using Long-term Monitoring Data and Finite Mixture Distributions", *Journal of Engineering Mechanics (ASCE)*, 2012, Vol.138, No.2, 175-183.
- [25] Wirsching, P. H. "Fatigue Reliability for Offshore Structures", *Journal of Structural Engineering*, 1984, Vol. 110, No.10, pp. 2340-2356.
- [26] Kulicki, J.M., Prucz, A., Clancy, C.M., Mertz, D.R. and Nowak, A.S., , "Updating the Calibration Report for AASHTO LRFD code", NCHRP 20-07/186, Transportation Research Board, National Research Council, Washington, DC, 2007.
- [27] Stein, M., "Large Sample Properties of Simulations Using Latin Hypercube Sampling", *Technometrics*. 1987, Vol. 29, No. 2, pp. 143-151.

SERVICE LIFE EVALUATION EXPERIENCE FOR EXISTING RAILWAY STEEL BRIDGE IN CHINA

Xiao-yan Tao* and Yu-ling Zhang

Bridge Section, China Academy of Railway Sciences, No. 2 Daliushu Road, Xiwai, Beijing, 100081, China

**(Corresponding author: E-mail: taoxy1994@163.com)*

ABSTRACT: It is well-known that the stress range spectrum is the key factor to the service life evaluation of existing railway steel bridge based on the damage accumulation theory. Taking two typical existing railway steel bridges in China as examples, two technical methods were introduced to determine the operation stress range spectra during the service condition in this paper, and then the service life was evaluated. One is named as Test Method and another is named as Load Simulation Method. Comparing the process and the workload, pros and cons of two technical methods were studied. The actual load effects can be considered in Test Method, such as dynamic effect, acceleration effect, etc. But potential limitation of Test Method is too dependent on the test data, and the deviation of selecting the test position will affect the assessment result. Load Simulation Method can be used to calculate the fatigue stress history of any position, thus avoiding potential limitation of Test Method, but it must be based on adequate statistical information and large amount of calculation. In order to improve the accuracy of assessment results by these two methods in the future, some new research works are proposed at the end of the paper.

Keywords: Railway steel bridge, Damage accumulation, Fatigue life evaluation, Stress range spectrum, Stress history

DOI: 10.18057/IJASC.2015.11.3.8

1. INTRODUCTION

Steel bridges are widely used in railway infrastructure in China, which includes 6550 steel girder bridges by the end of 2010. Most of the steel railway bridges are steel plate girder bridges or steel truss girder bridges, and box girder bridges have begun to be used in railway bridges in recent years. There are 4547 steel girder bridges that have serviced for more than 50 years under railway traffic, including 3884 steel plate girder bridges and 484 steel truss girder bridges. More data can be found in statistical information [1, 2].

Along with the growth of the traffic volume and the traffic flow rate coupled with environment actions [3], it is the matter of concern for the bridge engineers how to evaluate the safety and the fatigue remaining life of the existing steel bridges, and it is also an important research topic in current railway bridge professions.

There are generally two following steps to analyze the fatigue life of railway steel bridges based on damage accumulation theory in China. First, determine the operation stress range spectrum in detail during the bridge service condition by simulating the stress range spectrum in various historical periods and predict the stress range spectrum in future, which are shown in Figure 1. Next, calculate the damage in each operation period based on the Palmgren-Miner rule and S-N curve, which is shown in Figure 2, and then the remaining life of the bridge is determined by the following criteria (see Eq.(1)). More information can be found in the researches of Pan [4, 5] and Shi [6, 7].

$$D = \sum \frac{n_i}{N_i} = \frac{n_1}{N_1} + \frac{n_2}{N_2} + \dots + \frac{n_n}{N_n} \leq 1 \quad (1)$$

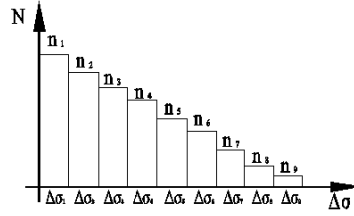


Figure 1. The Operation Stress Range Spectrum

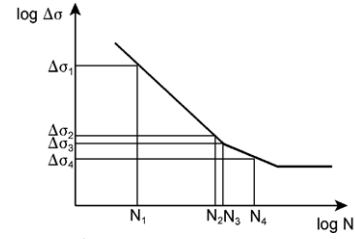


Figure 2. S-N Curve

Railway steel bridge researchers always calculate the damage by the same research method mentioned above in China. But to determine the operation stress range spectrum, there are two technical methods at present. One is named as Test Method, the other is named as Load Simulation Method. Taking two typical existing railway steel bridges in China as examples, two technical methods are introduced as below, and the service life is evaluated.

2. TWO METHODS FOR DETERMINING THE OPERATION STRESS RANGE SPECTRUM

How to determine the operation stress range spectrum during the service condition is an important step during the course of the bridge fatigue assessment. Stress range spectrum can be determined by the following two methods.

2.1 Test Method

The stress history can be recorded by installing the strain gauges to the position of the bridge where the fatigue failure is more prone to happen. Then, simulate the stress range spectrum in various historical operation periods and forecast the stress range spectrum in future through the short-term stress spectrum in test period together with the traffic volume. Because actual test period is extremely shorter than the bridge service life and many influencing factors are impossible to be included, the stress range and their numbers of cycles which are determined by rainflow method in each operation period need to be corrected.

The stress range can be corrected as follows (see Eq.(2)).

$$[\sigma_f] = k_1 k_2 k_3 k_4 k_5 \begin{bmatrix} \sigma_1 \\ \sigma_2 \\ \vdots \\ \sigma_n \end{bmatrix} \quad (2)$$

Where $\begin{bmatrix} \sigma_1 \\ \sigma_2 \\ \vdots \\ \sigma_n \end{bmatrix}$ is stress range related to a stress spectrum in a short test period; k_1 is the adjustment

factor considering eccentricity of vertical load; k_2 is the adjustment factor of considering some special heavy train which do not operate in short-term test period; k_3 is the stress conversion factor between the evaluated detail and the actual test detail; k_4 is the adjustment factor of considering the difference of locomotive and vehicle types between the test period and the service period (If the stress history is directly corrected by referencing to pervious similar test or simulating calculation, k_4 is taken as 1.0.); k_5 is the adjustment factor of considering secondary stress.

Their numbers of cycles can be corrected as Eq. (3)

$$[n_f] = \alpha_1 \alpha_2 \alpha_3 \alpha_4 \begin{bmatrix} n_1 \\ n_2 \\ \vdots \\ n_n \end{bmatrix} \quad (3)$$

Where $\begin{bmatrix} n_1 \\ n_2 \\ \vdots \\ n_n \end{bmatrix}$ is the number of stress cycle related to a stress spectrum in a short test period; α_1 is

the adjustment factor of considering the different daily traffic volume within one month; α_2 is the adjustment factor of considering the different monthly traffic volume within one year; α_3 is the adjustment factor of considering the different yearly traffic volume during entire service period; α_4 is the adjustment factor corresponding to vehicles gross weight change in every train, which closely linked to the locomotive traction gross weight, and is given in Table 1.

Table 1. The Locomotive Traction Gross Weight and α_4

Locomotive	Steam locomotive	Diesel locomotive	Electric locomotive
Gross Weight (t)	2000	3500	5000
α_4	0.57	1.00	1.43

After correcting the stress range and their numbers of cycles in each operation period, the operation stress range spectrum during bridge service condition can be determined.

2.2 Load Simulation Method

Firstly, analyze the vehicles marshalling in a train and the train formation within one day. Secondly, simulate the typical operation train in every operation period on the basis of the statistics data. Thirdly, adjust the various factors of the typical operation train by matching its action effect to the actual train effect. Finally, calculate the stress history induced by the typical operation train and determine the operation stress range spectrum.

2.2.1 Typical operation train Determination

In every operation period, the typical operation train for fatigue research is determined by average weight of different type locomotives and vehicles, the vehicle numbers, and the vehicle carrying capacities. The types of the locomotives or the vehicles are decided by the P values, which can be calculated as Eq. (4).

$$P = \frac{p_i}{\sum p_i} \quad (4)$$

Where p_i is the number of specific type of locomotives or vehicles; $\sum p_i$ is the total number of locomotives or vehicles.

Vehicle number of every train shall be determined according to Eq. (5)

$$N = \frac{\sum n_i k_i}{\sum k_i} \quad (5)$$

Where n_i is the vehicle number of a train; $\sum k_i$ is the number of trains passing through.

Since the vehicle carrying capacities are stochastic and complex, they are divided into several grades for simplification. Carrying capacities in each grade can be calculated by Eq. (6).

$$W = \frac{\sum p_i w_i}{\sum p_i} \quad (6)$$

Where p_i is vehicle number of specific carrying capacity in one grade; w_i is the average value of vehicle carrying capacity; $\sum p_i$ is the total vehicle number in one grade.

The typical operation train can be obtained on the basis of the above calculation. Then the train operation frequency can be determined according to the traffic volume.

2.2.2 Theoretical load effect Correction for fatigue research

Stress history of the typical operation train can be calculated by theoretical simulation. Stress ranges and their numbers of cycles can be determined by rainflow method. In order to match theoretical effects to the actual train effects, stress range shall be adjusted by Eq. (7).

$$[\sigma_f] = \delta_1 \delta_2 \begin{bmatrix} \sigma_1 \\ \sigma_2 \\ \vdots \\ \sigma_n \end{bmatrix} \quad (7)$$

Where δ_1 is the adjustment factor considering dynamic effect, and can be referenced according to Eq. (8).

$$\delta_1 = 1 + \frac{14}{40 + L} \quad (8)$$

Where L is the span length (m). More information about dynamic effect can be found in [8]; δ_2 is the adjustment factor considering the random arrangement of the vehicles of a train; $\delta_1 \delta_2$ can also be experientially obtained by analyzing the theoretical load effect and the tested train load effect. Same to Test Method, after correcting the stress range in every operation period, the operation stress range spectrum during bridge service condition can be determined.

There are two examples below to illustrate and compare these two technical methods further.

3. EXAMPLE ONE: EVALUATION OF A STEEL PLATE GIRDER BRIDGE

The first example is a riveted steel plate girder bridge with 32m span, which is under a single track railway. This bridge was built in 1911, and located in a branch railway. The steel plate girder is mainly composed of main beams, floor beams and stringers. The main beams and floor beams were riveted by the angle steel and the steel plate and the stringers were hot rolled I-shape section. Webs of two main beams were riveted by ten steel plates, and the stiffeners were arranged on the both

sides of main beam webs.

Before 1994, the traction engines were steam locomotives, but now they are DF4 diesel locomotives. About ten trains pass through the bridge every day, and the trains are primarily coal trains and a few of passenger trains. After 2011, the traction engines are SS4 electric locomotives. The bridge operation state is good, and its scenery can be seen in Figure 3.



Figure 3. Steel Plate Girder Bridge

Main beams, floor beams and stringers are the critical members of the bridge to bear the train load. The strain gauges were placed in their mid-span sections. According to the results of structural stress analysis, the control details of main beams and floor beams are the cross sections which were weakened by rivet holes. Because the stringer is the hot rolled I-shaped steel, the control detail is the base metal section in mid-span. According to “Railway Bridge Examination Standard (2004)” [9], the S-N curve of the main beam and the floor beam is $\lg N = 13.14 - 3.5 \lg \Delta \sigma$, and the S-N curve of the stringer is $\lg N = 13.30 - 3.5 \lg \Delta \sigma$. The fatigue damage and the fatigue remaining life of this bridge were evaluated by the two technical methods mentioned above.

The main adjustment factors of Test Method are listed in Table 2, and the operation stress range spectrums determined by Test Method are shown in Figure 4. According to the test result of eccentricity, k_1 is taken as 1.02. k_2 can be determined by train formation during the service period. The strain gauges of the main beams were placed in the gross section, so k_3 for the main beam is the area ratio of gross and net section. The strain gauges of the floor beams were placed in the net section, so k_3 for the floor beam is taken as 1.0. The stringers were the hot rolled I-shaped steel, so k_3 for the stringer is also taken as 1.0. The influence of the locomotive and vehicle types is considered by directly correcting the stress history according to pervious test before 1994 and by simulating calculation after 2011, so k_4 is taken as 1.0. The influence of secondary stress can be ignored in the bridge, so k_5 is taken as 1.0. The daily traffic volume in one month is almost the same, so α_1 is taken as 1.0. The value of α_2 is the traffic volume ratio of the testing month and the annual monthly average, so α_2 can be easily determined. The value of α_3 can be determined by the forecasted traffic volume in future and listed in Table 2. The value of α_4 is given in Table 1 and also listed in Table 2 below.

Table 2. Values of Adjustment Factor in Test Method

Time	Members	Adjustment factors					
		k_1	k_2	k_3	α_2	α_3	α_4
1911-1994	Main beam	1.020	1.005	1.110	0.912	1.000	0.570
	Floor beam	1.000	1.005	1.000	0.912	1.000	0.570
	Stringer	1.020	1.005	1.000	0.912	1.000	0.570
1995-2011	Main beam	1.020	1.005	1.110	0.912	1.000	1.000
	Floor beam	1.000	1.005	1.000	0.912	1.000	1.000
	Stringer	1.020	1.005	1.000	0.912	1.000	1.000
2012-2020	Main beam	1.020	1.005	1.110	0.912	1.590	1.430
	Floor beam	1.000	1.005	1.000	0.912	1.590	1.430
	Stringer	1.020	1.005	1.000	0.912	1.590	1.430
2021-	Main beam	1.020	1.005	1.110	0.912	2.260	1.430
	Floor beam	1.000	1.005	1.000	0.912	2.260	1.430
	Stringer	1.020	1.005	1.000	0.912	2.260	1.430

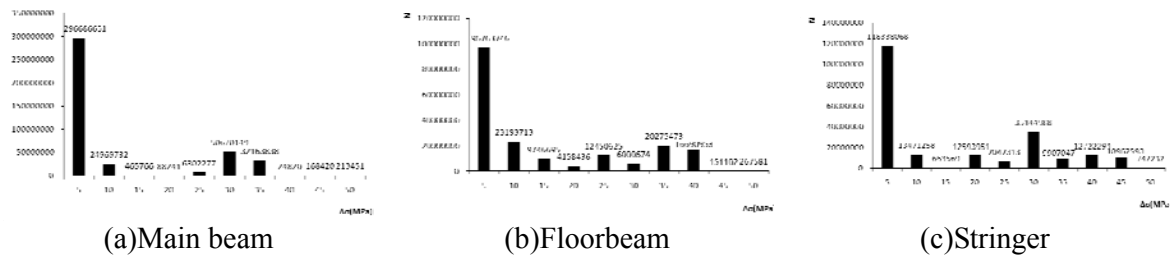


Figure 4. The Operation Stress Range Spectrums Determined by Test Method

The typical operation trains of Load Simulation Method are listed in Table 3.

Table 3. Typical Operation Trains of Load Simulation Method

Year	Vehicle number	The vehicles carrying capacity (t)								Operation times	Passenger train	Locomotive
		30	35	45	50	55	60	65				
		0	~	~	~	~	~	~	~			
		35	40	50	55	60	65	70				
1911-1994	50	8	4	5	2	3	8	12	8	9	-	QJ
1995-2011	50	8	4	5	2	3	8	12	8	9	-	DF4
2012-2020	50	8	4	5	2	3	8	12	8	13	1	SS4/SS7E
2021-	50	8	4	5	2	3	8	12	8	20	2	SS4/SS7E

The value of δ_1 can be calculated according the formula given above. The random arrangement of the vehicles in a train can be ignored in the bridge, so δ_2 is taken as 1.0. Values of δ_1 and δ_2 are given in Table 4.

Table 4. Values of δ_1 and δ_2

Values	Main beam	Floor beam	Stringer
δ_1	1.194	1.302	1.324
δ_2	1.000	1.000	1.000

Figure 10 consists of three bar charts (a, b, and c) showing the effect of ΔT on the residual stress of the substrate. The y-axis for all charts is 'Residual stress (MPa)' ranging from 0 to 140,000,000. The x-axis is ' ΔT (MPa)' with values 5, 10, 15, 20, 25, 30, 35, 40, 45, 50.

(a) Residual stress (MPa) vs ΔT (MPa) for the substrate. The chart shows a single bar at $\Delta T = 5$ with a value of 130811871.

(b) Residual stress (MPa) vs ΔT (MPa) for the substrate. The chart shows bars for $\Delta T = 5, 10, 15, 20, 25, 30, 35, 40, 45, 50$. The values are: 130811871, 54202014, 17400000, 110985, 14724232, 11300, 1059202, 17700000, 17700000, 17700000.

(c) Residual stress (MPa) vs ΔT (MPa) for the substrate. The chart shows bars for $\Delta T = 5, 10, 15, 20, 25, 30, 35, 40, 45, 50$. The values are: 130811871, 8769882, 4076816, 8040730, 17700000, 11475871, 17700000, 11810410, 17700000.

Figure 5. The Operation Stress Range Spectrums Determined by Load Simulation Method

The results of the fatigue accumulation damage and the remaining life of the bridge until 2011 are all listed in Table 5.

Table 5. Evaluation Results of Steel Plate Girder Bridge

Members	Test Method		Load Simulation Method	
	Damage	Remaining life (Year)	Damage	Remaining life (Year)
Main beam	0.051	452	0.026	2220
Floor beam	0.133	147	0.295	116
Stringer	0.171	102	0.394	64

From the results of two technical methods, the main beams and the floor beams are generally no fatigue problems. The remaining life of stringer in mid-span is about 64-102 years.

4. EXAMPLE TWO: EVALUATION OF A STEEL TRUSS BRIDGE

The second example is a riveted steel truss bridge which is on a single track railway. The bridge is 165m long and composed of three simply supported steel girders with 55m span. It was built in 1953, and located in a railway trunk line. This length of the truss member was 5.5m, and the truss height was 8.5m. All members of the bridge were made up of angle steels and the steel plates.

The operation state of this bridge is good, whose scenery can be seen in Figure 6. Before 1994, the traction engines were the steam locomotives, and from 1995 to 2009 the traction engines were the DF4 diesel locomotives. After completing the electrification improvement in 2010, the traction engines are SS3 or SS4 electric locomotives.



Figure 6. Steel Truss Girder Bridge

Bottom chords, diagonals, hangers, floor beams and stringers are the critical members of this bridge for bearing the train load, so the strain gauges were placed at their sections. Their control details are all cross sections which were weakened by rivet holes. Same to the first example, the fatigue damage and the fatigue remaining life of this bridge will be evaluated by the two technical methods mentioned above. According to “Railway Bridge Examination Standard (2004)” [9], the S-N curves is $\lg N = 13.14 - 3.5 \lg \Delta \sigma$.

The main adjustment factors of Test Method are given in Table 6. The value of k_1 is taken as 1.02 according to the test result of eccentricity. The value of k_2 can be determined by train formation during the service period. The strain gauges of the members were all placed in the gross section, so k_3 is the area ratio of gross and net section. Same to the first example, the influence of the locomotive and vehicle types is considered by directly correcting the stress history through referencing to pervious test before 1994 and by simulating calculation after 2010, so k_4 is taken as 1.0. Secondary stress needs to be considered in the truss members, and the values of k_5 are conservatively taken as 1.2 in bottom chords, diagonals and hangers. The influence of secondary stress can be ignored in floor beams and stringers, so their values of k_5 are taken as 1.0. The daily traffic volume in a month and the monthly traffic volume in a year are basically the same, so α_1 and α_2 are all taken as 1.0. The value of α_3 can be determined by the past and the future traffic volume. The value of α_4 is given in Table1.

Table 6. Values of Adjustment Factors in Test Method

Year	Members	Adjustment factors						
		k_1	k_2	k_3	k_5	α_2	α_3	α_4
1953-1971	Bottom chord	1.02	1.005	1.306	1.200	1.000	0.280	0.570
	Diagonal	1.02	1.005	1.243	1.200	1.000	0.280	0.570
	Hanger	1.02	1.005	1.235	1.200	1.000	0.280	0.570
	Floor beam	1.02	1.005	1.197	1.000	1.000	0.280	0.570
	Stringer	1.02	1.005	1.236	1.000	1.000	0.280	0.570
1972-1994	Bottom chord	1.02	1.005	1.306	1.200	1.000	0.590	0.570
	Diagonal	1.02	1.005	1.243	1.200	1.000	0.590	0.570
	Hanger	1.02	1.005	1.235	1.200	1.000	0.590	0.570
	Floor beam	1.02	1.005	1.197	1.000	1.000	0.590	0.570
	Stringer	1.02	1.005	1.236	1.000	1.000	0.590	0.570
1995-2009	Bottom chord	1.02	1.005	1.306	1.200	1.000	1.000	1.000
	Diagonal	1.02	1.005	1.243	1.200	1.000	1.000	1.000
	Hanger	1.02	1.005	1.235	1.200	1.000	1.000	1.000
	Floor beam	1.02	1.005	1.197	1.000	1.000	1.000	1.000
	Stringer	1.02	1.005	1.236	1.000	1.000	1.000	1.000
2010-	Bottom chord	1.02	1.005	1.306	1.200	1.000	1.450	1.430
	Diagonal	1.02	1.005	1.243	1.200	1.000	1.450	1.430
	Hanger	1.02	1.005	1.235	1.200	1.000	1.450	1.430
	Floor beam	1.02	1.005	1.197	1.000	1.000	1.450	1.430
	Stringer	1.02	1.005	1.236	1.000	1.000	1.450	1.430

The operation stress range spectrums determined by Test Method are shown in Figure 7.

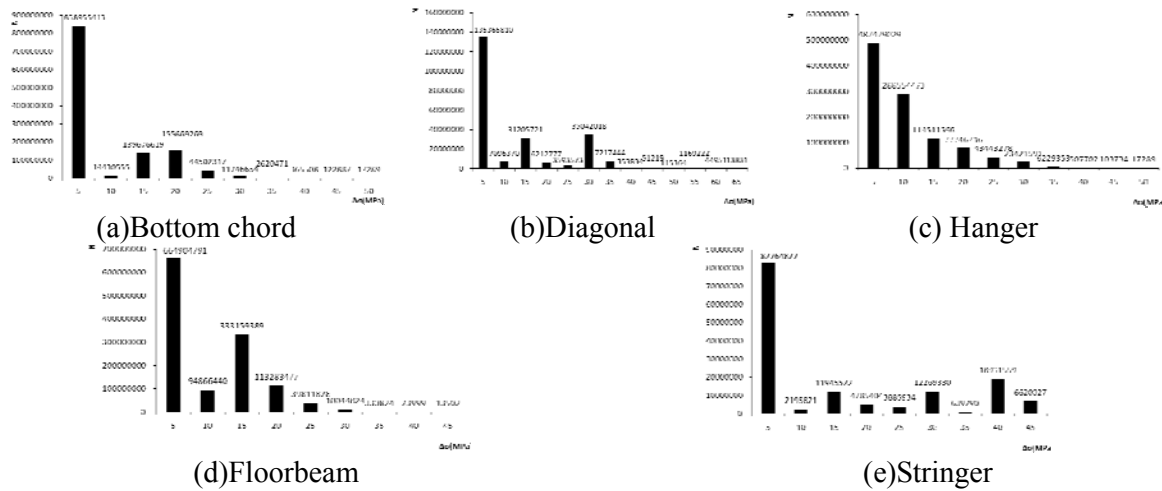


Figure 7. The Operation Stress Range Spectrums Determined by Test Method

The typical operation trains of Load Simulation Method are listed in Table 7. Values of δ_1 and δ_2 are given in Table 8. Same to the steel plate girder bridge, the value of δ_1 can be calculated according the formula given. The random arrangement of the vehicles in a train can be ignored in the bridge, so δ_2 also is taken as 1.0.

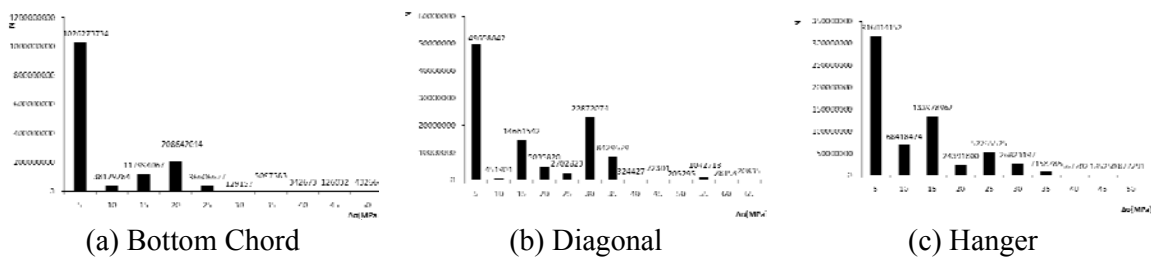
Table 7. Typical Operation Trains of Load Simulation Method

Year	Vehicle number	The vehicles carrying capacity (t)									Operation times	Passenger train	Locomotive
		0	30	35	40	45	50	55	60	65			
		35	40	45	50	55	60	65	70	70			
1953-1971	40	15	1	5	3	4	2	3	4	3	23	3	JF/SL
1972-1993	47	10	8	3	6	3	2	4	4	7	35	5	QJ/SL
1994-2009	50	1	2	1	1	4	1	2	4	34	36	7	DF4
2010-	65	1	3	2	3	3	1	2	2	48	40	8	SS3/SS4

Table 8 Values of δ_1 and δ_2

Values	Bottom chord	Diagonal	Hanger	Floor beam	Stringer
δ_1	1.147	1.147	1.274	1.274	1.307
δ_2	1.000	1.000	1.000	1.000	1.000

The operation stress range spectrums determined by Load Simulation Method are shown in Figure 8.



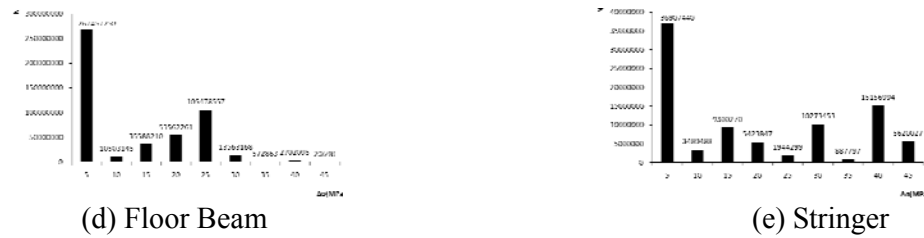


Figure 8. The operation stress range spectrums determined by Load Simulation Method

The results of the fatigue accumulation damage and the remaining life of this bridge are listed in Table 9.

Table 9. Evaluation Result of Steel Truss Bridge

Members	Test Method		Load Simulation Method	
	Damage	Remaining life(Year)	Damage	Remaining life(Year)
Bottom chord	0.205	125	0.160	197
Diagonal	0.115	378	0.127	241
Hanger	0.182	167	0.175	196
Floor beam	0.077	445	0.102	210
Stringer	0.593	33	0.413	37

From the results of two technical methods, it is generally no fatigue problem in the bottom chord, the diagonal, the hanger, and the floor beam. The remaining life of stringer in mid-span is about 30 years.

5. COMPARISON OF THE TWO TECHNICAL METHODS

Through the fatigue life evaluation processes of two examples, the specifically differences of the two technical methods for determining the operation stress range spectrum are listed below.

(1) In Test Method, the eccentricity of vertical load and the special heavy train influence have been considered with k_1 and k_2 , but in Load Simulation Method, these two influences have not been considered.

(2) The specific structural influence is considered with k_3 and k_5 in Test Method, however, it is directly considered in the bridge model in Load Simulation Method.

(3) The change of locomotive and vehicle types in Test Method is considered with k_4 , but in Load Simulation Method, it is directly reflected in the stress history by the change of the locomotives and the vehicles of the typical train. Since it is quite cursory to only using k_4 in Test Method, it is often directly reflected in the stress history by referencing to pervious test or simulating calculation.

(4) The traffic volume change is reflected in two technical ways. It is corrected by α_1 , α_2 and α_3 in Test Method, and is adjusted by the typical train carrying capacity and the vehicle numbers in Load Simulation Method.

(5) Regarding the quantity change of hauling vehicles, Test Method is corrected by α_4 which

change with the locomotive traction gross weight. But in the actual operation, locomotive traction gross weight may not truly reflect the quantity change of hauling vehicles. Load Simulation Method is adjusted by the vehicle number of the typical train, which is obtained by the weighting average of vehicle numbers of actual trains, so it is closer to reality.

6. CONCLUSIONS

Through the analysis above, it can be concluded that two technical methods for estimating the operation stress range spectrum in the bridge service condition have characteristics as follows:

(1) From the point view of present analysis data, the main advantage of Test Method is the direct use of test data. The actual load effects can be considered in Test Method, such as dynamic effect, acceleration effect, etc. But Load Simulation Method is difficult to consider actual load effects by numerical simulation analysis. From this point of view, Test Method is closer to reality.

(2) From the point view of entire structure fatigue evaluation, Test Method is to calculate the fatigue performance of the detail based on the test data of the measurement position. The deviation of selecting the test position will affect the overall assessment of the fatigue life of the structure. But Load Simulation Method can be used to calculate the fatigue stress history of any position of the structure, thus avoiding potential limitation of Test Method.

(3) From the point view of working condition, statistics workloads of Test Method are relatively small, but this method needs on-site test, so it is applicable to the bridge with better test conditions. Load Simulation Method avoids the site test tasks, but is based on adequate statistical information and large amount of calculation. The calculation steps are also relatively complex.

7. RECOMMENDATIONS

Through the above assessment practices and the characteristics analysis of the two technical methods, in order to improve the assessment accuracy, the following works need to be carried out in future.

- (1) The operation stress spectrum is the key factor to the entire evaluation. Regardless of Test Method or Load Simulation Method, both need the complete material or data are needed to obtain more accurate result. Therefore, the existing bridge material database needs to be established, including design material, general vehicles, all previous years traffic volume and so on.
- (2) The S-N curve for carrying out the evaluation often uses the experiment of the new material, which cannot consider the material quality of the old bridge and the characteristic deterioration along with the time. Their influence on the fatigue requires to be studied.
- (3) Two technical methods are both based on the Palmgren-Miner rule. For this rule itself, there are also many questions need to be studied, such as whether the load order affects the fatigue damage or not, if the stress which is lower than the fatigue cut-off limit induces the fatigue damage, as well as the criteria of cut off limit, and so on.

REFERENCES

- [1] The Statistics Centre of China Railway Ministry, "National Railway Statistics Abstract in 2010", China Railway Publishing House, Beijing, 2012. (in Chinese)
- [2] Liu, X.G, Zhang, Y.L. and Zhao, X.X., "Key Technologies of Existing Railway Steel Bridge of Adapting Heavy Transport", Research Report TY- 3225, China Academy Of Railway Sciences, Beijing, 2011. (in Chinese)
- [3] Sharifi, Y., "Uniform Corrosion Wastage Effects on the Load-carrying Capacity of Damaged Steel Beams", Advanced Steel Construction, 2012, Vol. 8, No. 2, pp. 153-167.
- [4] Pan, J.Y., "Reliability Theory of Fatigue in Design of Railway Steel Bridges", Steel Construction, 1995, Vol. 10, No. 27, pp. 1-8. (in Chinese)
- [5] Pan, J.Y., "Railway Steel Bridge Design", Railway Construction Technology, 2009, Vol. 10, No. 27, pp. 1-9. (in Chinese)
- [6] Shi, Y.G, Yang, Y.M., Li, Z.R., Shi, Z.Q. and Hou, W.W., "Remaining Life Evaluation of Old Riveted Steel Railway Bridge", China Academy of Railway Science, 1994, Vol. 15, No. 1, pp. 66-81. (in Chinese)
- [7] Shi, Y.J., "Remaining Life Evaluation of 'Old Riveted' Steel Railway Bridge", Railway Engineering, 1995, Vol. 12, No. 2, pp. 44-76. (in Chinese)
- [8] China Railway Ministry, "Code for Design on Steel Structure of Railway Bridge" TB10002.2-2005, China Railway Publishing House, Beijing, 2005. (in Chinese)
- [9] China Railway Ministry, "Railway Bridge Examination Standard (2004)", China Railway Publishing House, Beijing, 2004. (in Chinese)

STATIC AND FATIGUE BEHAVIOR OF CFRP-STRENGTHENED RC BRIDGE GIRDERS SUBJECTED TO VEHICLE OVERLOADING

Xiao-Yan Sun¹, Jian-Guo Dai², Hai-Long Wang^{1,*} and Chong Xu³

¹ Department of Civil Engineering, Zhejiang University, Hangzhou, China.

² Department of Civil and Environmental Engineering, The Hong Kong Polytechnic University, Hong Kong, China.

³ Hanjia Design Group of China, Hangzhou 310005, China

*(Corresponding author: Email: hlwang@zju.edu.cn)

ABSTRACT: This paper presents an experimental study into the static and fatigue behavior of three pairs of small-scaled reinforced concrete (RC) bridge girders, in order to investigate the influences of overloading on the fatigue strengthening effects of externally bonded carbon fiber reinforced polymer (CFRP) laminates and understand the mechanisms of fatigue damage accumulation in CFRP-strengthened RC bridge girders under vehicle overloading. Two pairs were strengthened with CFRP laminates and the remained one pair was un-strengthened as references. Two types of overloading were implemented in this test program: one was overloading both prior to and after FRP strengthening and the other was cyclic overloading only after FRP strengthening. At the end of the cyclic overloading all the girders were tested under monotonic loading until failure. Through the evaluation of the pre-fatigue static strength, the development of deflection and cracks during the fatigue loading and the post-fatigue strength of both un-strengthened and CFRP-strengthened RC girders, the effects of the above two different types of overloading on their static and fatigue behaviors are extensively discussed.

Keywords: RC girders, CFRP, Strengthening, Overloading, Fatigue

DOI: 10.18057/IJASC.2015.11.3.9

1. INTRODUCTION

Reinforced concrete (RC) bridge structures designed for public traffic service usually need to experience millions of loading cycles over their service life. To guarantee the fatigue safety of an RC bridge structure, the load level under a service condition needs to be well controlled so that the working stress in steel reinforcement is lower than a threshold value (e.g., 60% of the yield strength of steel reinforcement) according to AASHTO [1]. However, Karabinis and Kioussis [2] found that the high stress amplitude in steel reinforcement may often exceed the recommended service load level because of the ever-increasing vehicle transportation demand. Sun et al. [3] monitored the structural behavior of a 25 m span simply-supported RC girder bridge in China on basis of the in-situ traffic survey data and found that the maximum stress in the longitudinal reinforcement may reach up to about 85% of its yield strength. Usually the vehicle overloading does not cause an RC bridge to collapse instantly, but the high stress amplitude caused by overloading will definitely accelerate the damage accumulation and the structural performance degradation in critical details [4]. In both USA and China, Hersi [5], Ji and Fu [6] found that vehicle overloading has become a major factor leading to the failure of bridge structures (Figure1 and Figure 2).

Use of externally bonded fiber reinforced polymer (FRP) composites has proven to be a cost-effective method for the flexural strengthening of RC bridge structures for both static (Grace et al.[7], Pham and Al-Mahaidi[8], Esfahania et al.[9], Wang et al.[10,11]) and fatigue enhancement purposes (Xie et al.[12], Dong et al.[13], Ferrier et al.[14]). It has been recognized that the FRP strengthening can improve the strength of existing RC members, decrease the stress level in steel

reinforcement under service load and thus improve their fatigue performance. However, very little has been explored on the fatigue performance of FRP-strengthened RC beams subjected to cyclic overloading. Breña et al. [15] compared the fatigue life of no pre-damaged carbon FRP(CFRP)-strengthened beams under a high stress level (i.e., 90% of the rebar yield strength) with that under a normal service load level (i.e., below 60% of the rebar yield strength), found that the fatigue life of CFRP-strengthened beam was decreased sharply in the former case. Al-Hammoud et al.[16] investigated the fatigue flexural behavior of CFRP-strengthened beams pre-damaged with rebar corrosion and found that, while the pre-corrosion damage the same, the higher stress amplitude (e.g., 80% of the rebar yield strength) led to a reduction of the fatigue life down to 13%-19% of that under a normal service load level (e.g., 60% of the rebar yield strength). Al-Rousan and Issa [17] conducted an experimental program to investigate the static response of non-pre-damaged CFRP-strengthened beams after cyclic loading of different stress amplitude. They found that the high stress range had a significant effect on the permanent deflection at mid-span, especially for the stress range of 45-90% of the rebar yield strength.

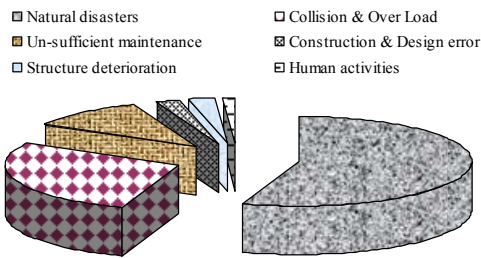


Figure 1. Statistics of Bridge Failures in USA (2000-2008) (Hersi [5])

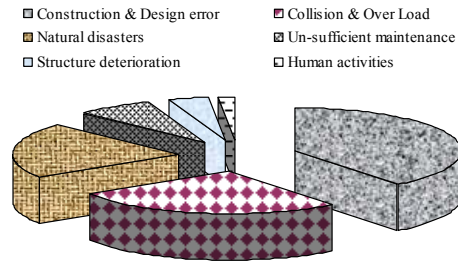


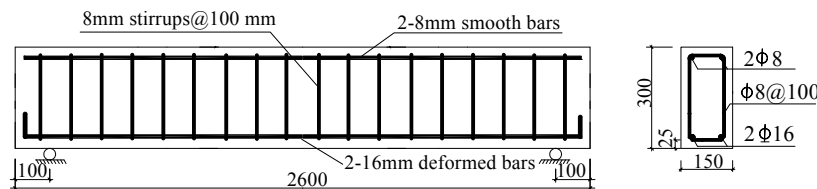
Figure 2. Statistics of Bridge Failures in China (2000-2010) (Ji and Fu [6])

This paper aims to conduct an experimental study to investigate: (1) the fatigue behavior of un-strengthened and CFRP flexurally strengthened RC beams subjected to cyclic overloading; and (2) the static and fatigue behavior of CFRP flexurally strengthened RC beams with initial overloading damage prior to the CFRP strengthening.

2. EXPERIMENTAL PROGRAM

2.1 Details of Specimens

Six RC beams with a rectangular cross section of 150×300 mm and a testing span of 2400 mm were prepared in this study (Figure 3a). Each beam was reinforced with two tensile deformed bars of 16 mm in diameter, which had a concrete cover of 25 mm, two round bars 8 mm-diameter in the compressive zone, and steel stirrups of 8 mm in diameter and 100 mm in spacing (Figure 3a).



(a) Beam Geometry and Reinforcement Information

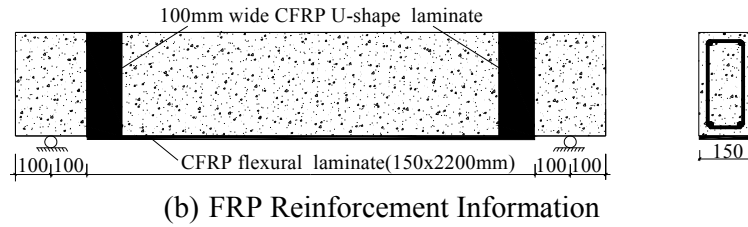


Figure 3. Details of Test Beams (unit: mm)

Among the six RC beams, four beams were externally strengthened in flexure with one layer of unidirectional CFRP sheet and two beams were un-strengthened as control specimens (see Table 1). As shown in Figure 3b, the CFRP sheet was 150 mm wide and 2200 mm long. Two U-shape anchorages were installed at the two ends of the CFRP sheet to prevent plate-end failure. Table 1 presents a summary of all the specimens. Beams BC0 and BC1 were un-strengthened. BC0 was loaded under monotonic static loading until failure while BC1 was cyclically overloaded before the monotonic static loading test. Beams BR0 and BR1 were all strengthened with 1 layer of CFRP sheet, and their loading schemes were the same as those of BC0 and BC1, respectively. Beams BD0 and BD1 are similar to beams BR0 and BR1 except that they had experienced initial overloading damage prior to CFRP strengthening. This initial damage caused the yielding of tensile steel reinforcement as shown in Figure 4. At the end of overloading, the width of the major crack (i.e. the one that had the maximum crack width) reached 1.0 mm.

Table 1. Summary of Test Specimens

Specimen code	Initial damage	Strengthening scheme	Loading type
BC0	None	None	Monotonic static loading
BC1	None	None	Cyclic overloading + Monotonic static loading
BR0	None	CFRP sheet	Monotonic static loading
BR1	None	CFRP sheet	Cyclic overloading + Monotonic static loading
BD0	Overloaded	CFRP sheet	Monotonic static loading
BD1	Overloaded	CFRP sheet	Cyclic overloading + Monotonic static loading

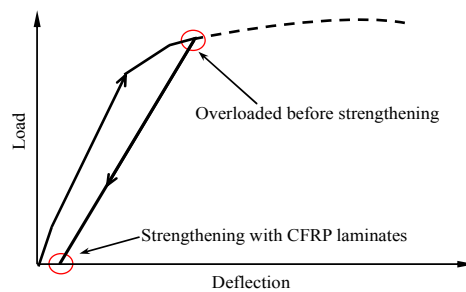


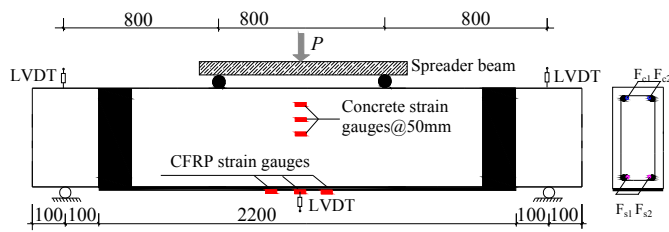
Figure 4. Introduction of Initial Overloading Damage Prior to FRP Strengthening

2.2 Materials Properties

The 16 mm deformed reinforcement in tension had a yield strength of 335 MPa and an elastic modulus of 200 GPa. The 8 mm round bar used as shear reinforcement exhibited a yield strength of 235 MPa and an elastic modulus of 210 GPa. The concrete was a ready-mixed type provided by a local plant and had a cube compressive strength of 30 MPa. The CFRP sheet used in the tests had a nominal thickness of 0.111 mm. Its ultimate tensile strength and elastic modulus were 3500 MPa and 230 GPa, respectively.

2.3 Loading Scheme and Testing Procedure

All the beams were subjected to four-point bending over a simply supported span of 2400 mm as shown in Figure 5a. An 800 mm long constant moment zone existed in the middle part of the beams. The monotonic and fatigue loads were applied onto the beams using an MTS machine, as illuminated in Figure 5b. During the production of the beams, optic fiber sensors were embedded in the beams to monitor the strains of concrete (see locations F_{c1} and F_{c2} in Figure 5a) and steel reinforcement (see locations F_{s1} and F_{s2} in Figure 5a). Prior to the tests, three gauges were also placed on the concrete surface at the heights of 250mm, 200mm and 150mm, respectively, from the top of the beam (Figure 5a). In addition, three gauges were attached on the surface of CFRP sheet within the constant moment zone (Figure 5a). Three linear voltage displacement transducers (LVDTs) were installed at the mid-span and support locations to obtain the mid-span deflection. During the tests, all the loads, displacement and strains were recorded using a data acquisition system.



(a) Four-point Loading Diagram



(b) MTS Machine in Test

Figure 5. Test Set-up (unit: mm)

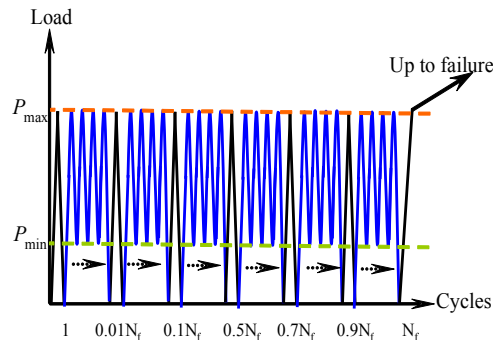


Figure 6. Loading Sequence of Fatigue Tests

As mentioned previously, there were two loading schemes: monotonic static loading and cyclic overloading. The un-strengthened control beam was loaded monotonically to failure to identify its ultimate load (P_u) firstly. Then the load sequence for fatigue tests was implemented as shown in

Figure 6. During the fatigue tests, the upper bound load (i.e., P_{max}) was set as $0.8P_u$ and the low bound load (i.e., P_{min}) was set as $0.35 P_u$ for both un-strengthened and CFRP-strengthened RC beams according to the in-situ survey carried out by Sun [3]. The fatigue loading was applied using a form of sinusoidal wave with a frequency of 2 Hz and the total number of fatigue cycles N_f was set as 10000 in the tests. Since it was difficult to record all the strain and deflection information during the whole fatigue loading period, the fatigue tests were stopped at certain numbers of fatigue cycles (i.e. 1st, $0.01 N_f$, $0.1 N_f$, $0.5 N_f$, $0.7 N_f$, $0.9 N_f$, and N_f). At these cycles, all the beams were unloaded and then reloaded to $0.8P_u$ and the structural responses including the sectional strains, deflections, crack patterns and the maximum crack widths were measured. At the end of the fatigue cycles, all the beams were loaded monotonically to failure.

3. RESULTS AND DISCUSSION

3.1 Static Responses

3.1.1 Failure modes

The control beam BC0 failed in a typical flexural mode by concrete crushing long after the yielding of steel reinforcement. The CFRP-strengthened RC beam BR0 failed due to the mid-span debonding of CFRP sheet (Figure 7a). However, the other CFRP-strengthened RC beam BD0, which experienced initial overloading damage, failed due to the fracture of CFRP sheets at the location of the maximum crack before the interfacial debonding (Figure 7b). It should be mentioned that the cracks in concrete due to overloading were sealed with epoxy resins prior to the strengthening of the beam BD0 and BD1. The CFRP-strengthened RC beam BR1, which experienced cyclic overloading, failed due to the mid-span debonding of CFRP sheet followed by its brittle rupture (Figure 7c). The CFRP-strengthened RC beam BD1, which experienced initial overloading damage and then cyclic overloading, exhibited the similar failure mode (Figure 7d) as beam BR1.



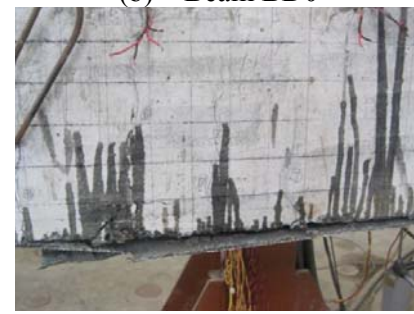
(a) Beam BR0



(b) Beam BD0



(c) Beam BR1



(d) Beam BD1

Figure 7. Failure Modes of CFRP-strengthened RC Beams under Monotonic Static Loading and Fatigue Loading

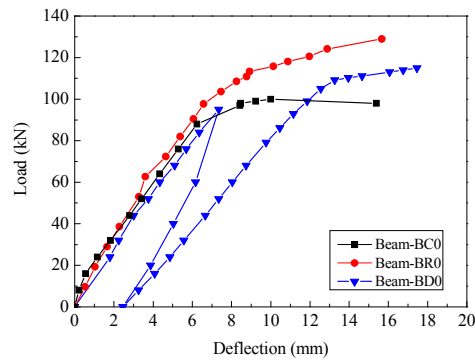


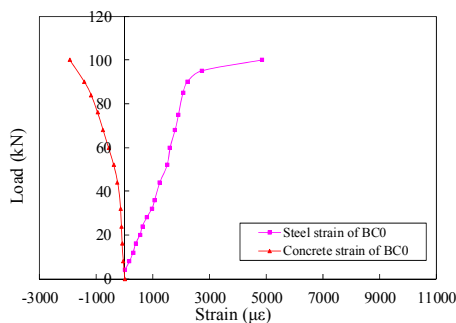
Figure 8. Load-deflection Responses of Beams Tested under Monotonic Loading

3.1.2 Load-deflection responses

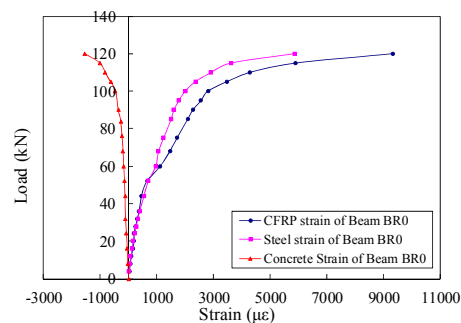
Figure 8 shows the load-deflection responses of beams BC0, BR0 and BD0 tested under monotonic static loading. It is shown that the beams BC0 and BR0 exhibited the similar load-deflection responses till the yielding of steel reinforcement while the latter had a slightly larger bending stiffness. Compared to BC0, BR0 achieved an increased ultimate strength by 29% due to the FRP strengthening effect. At all the loading stages, beam BD0 experienced larger mid-span deflections than BR0 due to the initial damage induced by the overloading prior to the FRP strengthening (Figure 8). Due to the presence of significant plastic deformation before the FRP strengthening, the ultimate load achieved by the beam BD0 was obviously less than that achieved by the beam BR0. Compared to the un-strengthened beam BC0, beam BD0 only achieved an increase in the ultimate strength by 15%.

3.1.3 Strain development

Figures 9a-9c shows the development of strains in CFRP, steel reinforcement and concrete with the load. It is shown that at the same load level, the strain in steel reinforcement was decreased in case of FRP-strengthened RC beams as expected. In beam BD0, there was a strain delay in FRP at the early loading stage due to the initial overloading damage. While later on, the strain development in FRP was more rapid than that in steel reinforcement in both BR0 and BD0 beams, which followed the plane sectional assumption. It is interesting to find that the strain development of FRP in beam BD0 was more rapid than that in beam BR0 at the latter loading stage (Figure 9d). This is probably because of the strain localization of FRP at the location of the major crack caused by the initial overloading damage. This also explains why the rupture of FRP occurred in beam BD0 rather than the debonding of FRP as observed in beam BR0 at the ultimate state.



(a) Beam BC0



(b) Beam BR0

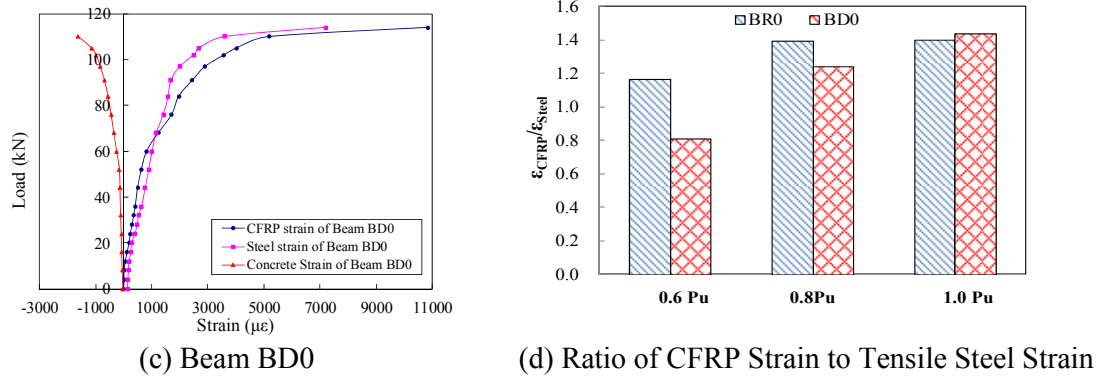


Figure 9. Strain Development in FRP, Concrete and Reinforcement under Monotonic Loading

3.2 Fatigue Responses

3.2.1 Crack propagation

The developments of cracks were monitored during the test. In the control beam, the cracks started from the bottom of the beam and propagated vertically toward the top of test beam. The number of cracks and the propagation depth depend on the number of fatigue cycles. In beam BR1, the cracking pattern was identical to that in the control beam under the first monotonic load. However, the number, the width, and the depth of cracks were all decreased due to the presence of CFRP laminates. Under cyclic overloading, the cracking depth and width evolved with fatigue cycles. As the increase of applied fatigue cycles, some new cracks developed between the original ones caused by the initial monotonic loading, as shown in Figure 10a. For the overloaded beam BD1, the cracks propagated differently from that of beam BR1 over the fatigue period, as illuminated in Figure 10b. All cracks developed along the original ones in beam BD1, and no new crack initiated during the fatigue loading period.

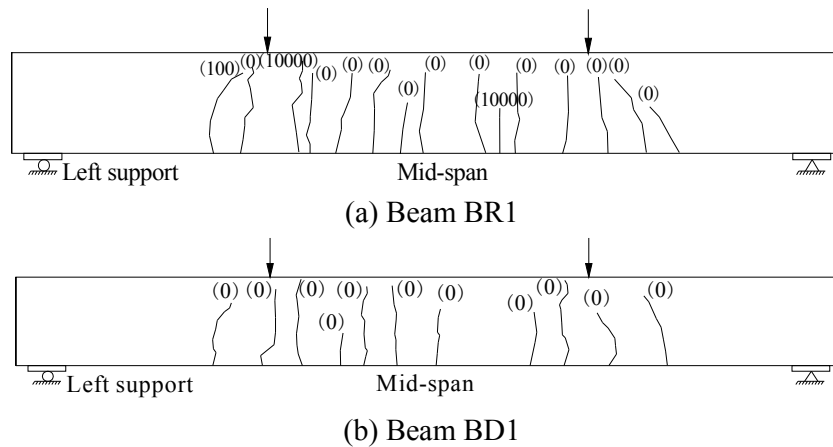


Figure 10. Crack Propagation in Beams under Fatigue Loading (Digits in Brackets Represent the Number of Fatigue Cycles)

3.2.2 Load-deflection responses during cyclic loading

Figure 11 shows the load-deflection hysteresis loops of all the beams, which were obtained after certain numbers of fatigue loading cycles. The seven hysteresis loops in Figures 11a to 11c

represent the structural responses of beams BC1, BR1 and BD1, respectively, after having experienced 0, 100, 1000, 5000, 7000, 9000 and 10000 cycles of fatigue overloading. It is seen that the mid-span deflections of both un-strengthened and FRP-strengthened beams exhibited remarkable increases and the stiffness exhibited remarkable degradation with the increase of the loading cycles, indicating there was a significantly negative impact of overloading on the fatigue life of the RC beams. However, the accumulation of fatigue damage with the number of cycles was found to be much slower when the maximum fatigue stress in steel reinforcement is below 65% of its yielding strength (Al-Rousan and Issa[17], Gheorghiu et al.[18]).

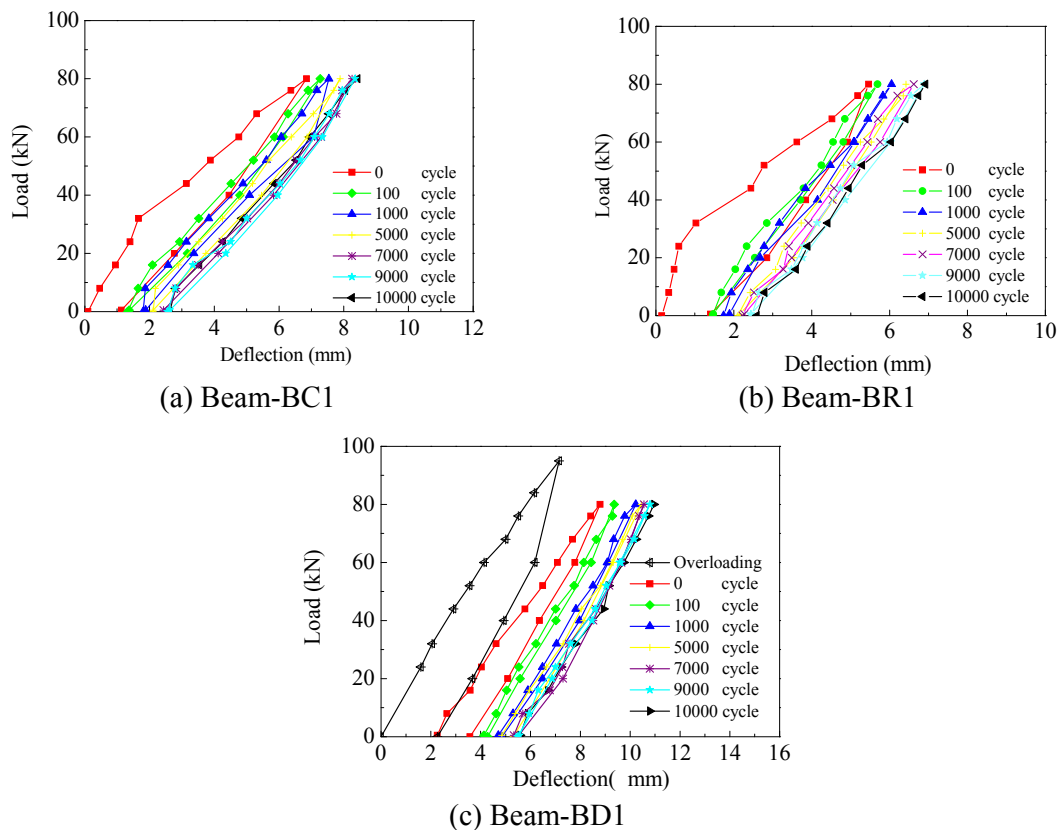


Figure 11. Load–deflection Responses of Beams under Fatigue Loading

The unrecoverable plastic deformation can be a useful index to assess the damage accumulation of RC beams under fatigue loading. Figures 12a to 12c present the evolution of the maximum mid-span deflection, and the residual mid-span deflection as well as their ratio with the number of fatigue cycles. It is shown that for both un-strengthened and strengthened beams, the maximum and residual deflections increased rapidly at the beginning and then increased stably with the number of fatigue cycles. Although the maximum deflection of beam BR1 was smaller than that of beam BC1, the residual deflections of two beams were the similar. This implies that the improvement of beam stiffness due to FRP strengthening under an overloading condition is more significant as compared to that under a normal service load. The initial overloading damage led to a largest ratio of the residual to maximum deflection as shown in Figure 12c.

Besides the deflection, the cracks in all the beams except beam BR1 were extended upwards and the crack widths were enlarged (Figures 13a and 13b) during the fatigue loading. The maximum crack width in beam BR1 was found to have no increase probably because of the occurrence of few new cracks due to the tension stiffening effects of FRP sheets, which absorbed the fatigue-induced

deflection increase. In beam BD1, however, no new cracks were detected due to the fatigue loading because the initial overloading prior to strengthening, which induced significant localized damage, so that the fatigue damage was concentrated at the major crack location.

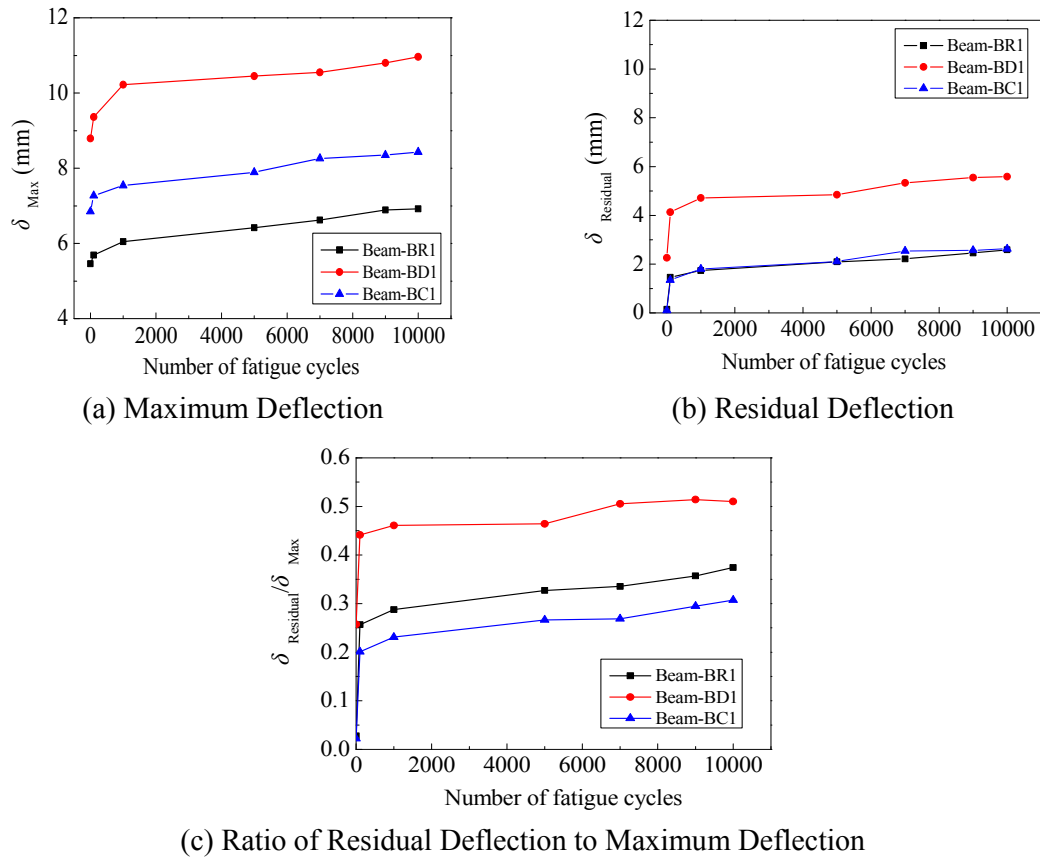


Figure 12. Maximum and Residual Mid-span Deflections Versus Fatigue Cycles

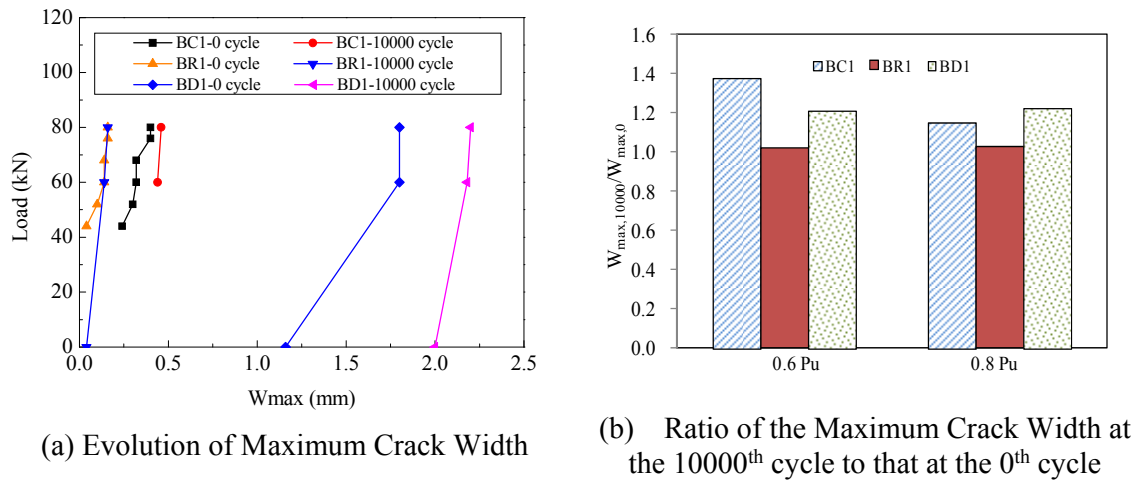


Figure 13. Maximum Crack Widths of Beams under Fatigue Loading

3.2.3 Strain development during fatigue overloading

Figure 14 shows the strains in the concrete, the steel, and the CFRP laminate monitored at the mid-span location during the monotonic tests after a certain number of fatigue cycles. The tendency of strain development in concrete and steel reinforcement with the number of fatigue cycles coincided with that of the deflection development in all the beams (Figures 14a and 14b). However, for the two CFRP-strengthened RC beams BR1 and BD1, the strain development in CFRP exhibited two different tendencies (Figure 14c). Although the initial strain in CFRP was much larger in beam BD1, its increase was insignificant, while in beam BR1, the initial strain in FRP was relatively lower, its increase was very significant with the increase of the fatigue cycles. The insignificant increase in CFRP strain in beam BD1 was probably due to the debonding of FRP during the fatigue loading, which was caused by the localized widening of the major crack (Figure 7d).

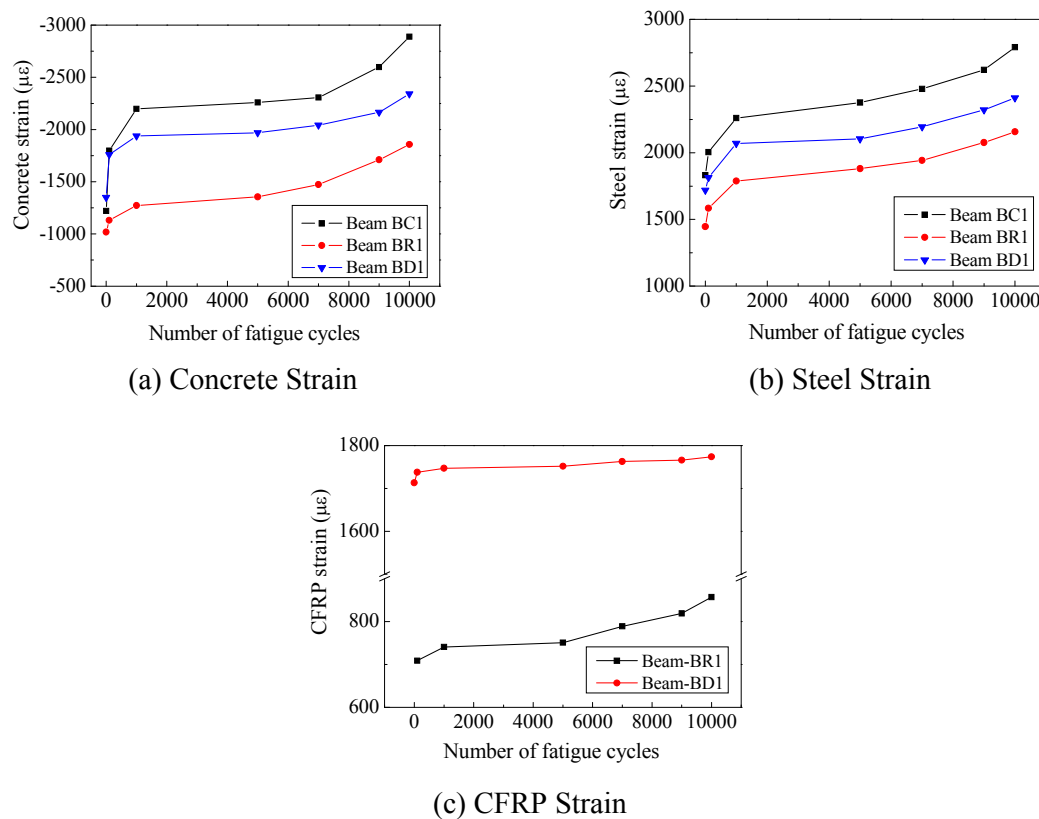


Figure 14. Strains Development Versus the Number of Fatigue Cycles

3.2.4 Post-fatigue monotonic static loading test results

At the end of 10000 fatigue cycles, all the beams were loaded monotonically to failure to reveal the influence of cyclic overloading history on the strength performance of the bridge girder. Figure 15 shows the load-deflection responses of all the cyclically loaded beams. The post-fatigue ultimate strength of un-strengthened beam BC1 was 95 kN, which was 5% lower than that of the control beam BC0 due to the initial cyclic overloading damage. Similarly, a 4% decrease in the post-fatigue strength was observed for the CFRP-strengthened beam BR1 in comparison with the static strength of the beam BR0. However, the post-fatigue ultimate strength of beam BD1 was 4.3% higher than the static strength of beam BD0. This is probably due to the strain hardening phenomenon of the internal steel reinforcement.

The post-fatigue ultimate strengths of CFRP-strengthened beam BR1 and FRP-strengthened initially overloaded beam BD1 were 124 kN and 120 kN, respectively, which were 30% and 26% higher than that of the un-strengthened beam BC1. It is evident that the CFRP strengthening was still efficient in terms of the strength even under cyclic overloading. However, the post-fatigue ultimate deflections of the beams BR1 and BD1 were increased by 2.44 mm and 9.75 mm, respectively, in comparison with that of their counterpart beams directly subjected to static loading (i.e., BR0 and BD0). However, under normal service loads, such a stiffness degradation mechanism is insignificant (Dong et al.[13], Ferrier et al.[14], Gheorghiu et al.[18]). Therefore the fatigue overloading caused much more damage to RC beams than normal fatigue loading due to the significant FRP debonding. As the member stiffness degradation and the widening of crack width may lead to severe serviceability problems, to keep the efficiency of the FRP strengthening during fatigue overloading, supplementary methods may be needed to suppress the debonding of FRP as well as to control the deflection and crack width of strengthened beams.

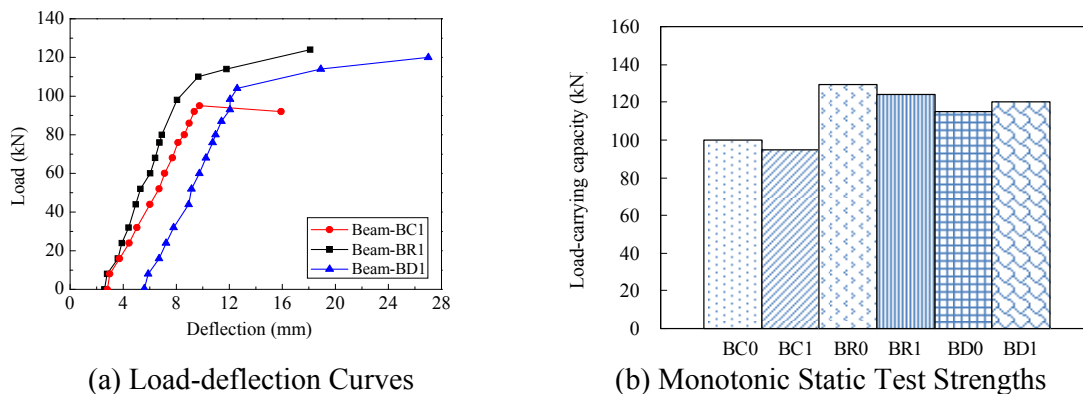


Figure 15. Static Responses of Cyclically Overloaded Beams

4. CONCLUSIONS

An experimental study was conducted to investigate the static and fatigue behaviours of CFRP-strengthened RC beams subjected to overloading. Some of the RC beams had initial overloading damage. On basis of the experimental observations, the following conclusions can be drawn:

- (1) FRP strengthening can improve the static load-carrying capacity of RC beams effectively. However, the overloading damage prior to the FRP strengthening may jeopardize the strengthening efficiency and change the failure mode of FRP-strengthened RC beams.
- (2) If there is initial overloading damage prior to the fatigue strengthening of RC beams using FRP, the fatigue strengthening efficiency decreases due to the easier debonding of FRP during the subsequently cyclic overloading, which is attributed to excessive local deformation.
- (3) The cyclic overloading also affects the post-fatigue static strength of both un-strengthened and FRP-strengthened RC beams. For un-strengthened and FRP-strengthened RC beams without initial overloading damage, the cyclic overloading history led to an about 5% decrease of the member strength compared to their static ones. However, if the RC beams were subjected to initial overloading damage, the post-fatigue static strength of FRP-strengthened RC beams even increased due to the strain hardening of internal steel reinforcement.

- (4) The cyclic overloading during the service of RC beams leads to significant member stiffness degradation and propagation of the crack widths. FRP strengthening could suppress effectively the maximum deflection since the stiffness contribution of FRP is more significant under an overloading condition and thus can improve the fatigue life of the strengthened beams. Under overloading condition, the fatigue life of RC bridge girders with or without FRP strengthening should be evaluated using the stiffness rather than the ultimate strength as a control index.

ACKNOWLEDGMENTS

The authors would like to thank the financial supports received from the National Natural Science Foundation of China (51378456), Qianjiang Talent Plan of Zhejiang Province (2012R10025), Natural Science Foundation of Zhejiang Province (LZ13E080001), the Key Science and Technology Innovation Team of Zhejiang Province (2010R50034), and the collaborative opportunity from The Hong Kong Polytechnic University through the research project G-YM26.

REFERENCES

- [1] AASHTO, "AASHTO LRFD Bridge Design Specifications-3rd Ed", Washington D.C., U.S.A., 2004.
- [2] Karabinis, A.I. and Kiouisis, P.D., "Plasticity Model for Reinforced Concrete Elements Subjected to Overloads", *Journal of Structural Engineering*, ASCE, 2001, Vol.127, No.11, pp.1251-1256.
- [3] Sun, X.Y., "Reliability-based Assessment of Reinforced Concrete Bridges in Commission and Strengthened Condition" (in Chinese), Dissertation Submitted to Dalian University of Technology in Conformity with the Requirements for the Degree of PhD, 2004.
- [4] Gu, M., Tong, L.W., Zhao X.L. and Zhang, Y.F., "Numerical Analysis of Fatigue Behavior of Welded CFCHST-Joints", *Advanced Steel Construction*, 2014, Vol. 10, No. 4, pp. 476-497.
- [5] Hersi, M.I., "Analysis of Bridge Failures in the United States", Graduate Program in Civil Engineering of Ohio State University. U.S.A., 2009.
- [6] Ji, B.H. and Fu, Z.Q., "Analysis of Chinese Bridge Collapse Accident Causes in Recent Years", *China Civil Engineering Journal*, 2010, Vol.43, No.s1, pp.495-499. (in Chinese)
- [7] Grace, N.F., Sayed, G.A., Soliman A.K. and Saleh., K.R., "Strengthening Reinforced Concrete Beams Using Fiber-reinforced Polymer (FRP) Laminates", *ACI Structural Journal*, 1999, Vol. 96, No. 5, pp. 865-875.
- [8] Pham, H. and Al-Mahaidi, R., "Experimental Investigation into Flexural Retrofitting of Reinforced Concrete Bridge Beams Using FRP Composites", *Composite Structures*, 2004, Vol. 66, No. 4, pp. 617-625.
- [9] Esfahania, M.R., Kianoushb, M.R. and Tajaria, A.R., "Flexural Behaviour of Reinforced Concrete Beams Strengthened by CFRP Sheets", *Engineering Structures*, 2007, Vol. 29, No. 10, pp. 2428-2444.
- [10] Wang, W.W., Dai, J.G. and Harries, K.A., "Performance Evaluation of RC Beams Strengthened with an Externally Bonded FRP System under Simulated Vehicles Loads", *Journal of Bridge Engineering*, ASCE, 2013, Vol. 18, No. 1, pp. 76-82.
- [11] Wang, W.W., Dai, J.G., Harries, K.A. and Bao, Q.H., "Prestress Losses and Flexural Behavior of Reinforced Concrete Beams Strengthened with Post-tensioned CFRP Sheets", *Journal of Composites for Construction*, ASCE, 2012, Vol. 16, No. 2, pp. 207-216.

- [12] Xie, J.H., Huang, P.Y. and Guo, Y.C., “Fatigue Behavior of Reinforced Concrete Beams Strengthened with Pre-stressed Fiber Reinforced Polymer”, *Construction and Building Materials*, 2012, Vol. 27, No. 1, pp.149-157.
- [13] Dong, J.F., Wang, Q.Y. and Guan, Z.W., “Structural Behaviour of RC Beams Externally Strengthened with FRP Sheets under Fatigue and Monotonic Loading”, *Engineering Structures*, 2012, Vol. 41, No. 8, pp. 24-33.
- [14] Ferrier, E., Bigaud, D., Clément, J.C. and Hamelin P., “Fatigue-loading Effect on RC Beams Strengthened with Externally Bonded FRP”. *Construction and Building Materials*, 2011, Vol. 25, No. 2, pp. 539-546.
- [15] Breña, S.F., Benouaich, M.A., Kreger, M.E. and Wood, S.L., “Fatigue Tests of Reinforced Concrete Beams Strengthened Using Carbon Fiber-reinforced Polymer Composites”. *ACI Structural Journal*, 2005, Vol. 102, No. 2, pp. 305-313.
- [16] Al-Hammoud, R., Soudki, K. and Topper, T.H., “Fatigue Flexural Behavior of Corroded Reinforced Concrete Beams Repaired with CFRP Sheets”. *Journal of composites for construction*, ASCE, 2011, Vol. 15, No. 1, pp. 42-51.
- [17] Al-Rousan, R. and Issa, M., “Fatigue Performance of Reinforced Concrete Beams Strengthened with CFRP Sheets”, *Construction and Building Materials*, 2011, Vol. 25, No. 8, pp. 3520-3529.
- [18] Gheorghiu, C., Labossiere, P. and Proulx, J., “Fatigue and Monotonic Strength of RC Beams Strengthened with CFRPs”, *Composite: Part A*, 2006, Vol. 37, No. 8, pp. 1111-1118.

RESIDUAL LIFE EVALUATION OF PRESTRESSED REINFORCED CONCRETE HIGHWAY BRIDGES UNDER COUPLED CORROSION-FATIGUE ACTIONS

Jin-song Zhu^{1,2,*}, Fa-min Huang¹, Tong Guo³ and Yun-he Song¹

¹ School of Civil Engineering, Tianjin University, Tianjin, China.

² Key Laboratory of Coast Civil Structure Safety (Tianjin University), Ministry of Education, Tianjin, China.

³ School of Civil Engineering, Southeast University, Nanjing, China

*(Corresponding author: E-mail: jszhu@tju.edu.cn)

ABSTRACT: To evaluate the residual life of prestressed reinforced concrete (PSC) highway bridges in coastal environment, the residual life analysis method of PSC highway bridges under coupled corrosion-fatigue effects is proposed. The multi-scale finite element model of the bridge is employed to perform the detailed stress analysis. The vehicle-bridge coupling vibration analysis is performed to obtain the stress impact coefficients and stress histories of key prestressing strands under the standard AASHTO fatigue truck model. A pit corrosion model is adopted to get stress concentration factors of prestressing strands induced by corrosion. A comprehensive analysis approach is proposed to determine stress amplitudes of key prestressing strands under coupled corrosion-fatigue actions. The S-N curve and the traffic conditions are integrated to determine the service life of the weakest prestressing strand, which is characterized as the service life of the bridge. The effectiveness of the methodology framework is demonstrated on a large-span continuous PSC box-girder bridge.

Keywords: Prestressed reinforced concrete bridges, Coupled corrosion-fatigue actions, Residual life, Multi-scale finite element model

DOI: 10.18057/IJASC.2015.11.3.10

1. INTRODUCTION

Prestressed reinforced concrete (PSC) bridges in coastal environment are exposed to the deterioration risk by fatigue loads as well as corrosion from the environmental medium. The formation and growth of pits in steel are influenced by both a corrosive environment and cyclic loads, which becomes a coupled damage mechanism of bridges and may cause load-carrying capacity decrease and sudden failure of bridges without any warnings [1].

In the last decades, large research efforts were made on predicting the fatigue reliability, the residual life or the performances of bridges due to the corrosion and/or fatigue loads. However, limited studies investigated the life-cycle performance of bridges under the coupled corrosion-fatigue deterioration processes. Emilio et al. [2] proposed a probabilistic lifetime assessment method of reinforced concrete (RC) structures, in which both corrosion and fatigue effects were combined. The method was validated on a simple supported RC bridge. Dong [3] investigated experimentally the fatigue and bonding performances of corroded RC members. Peng et al. [4] investigated the bonding performance between bars and concrete under fatigue loads. They selected the impressed current corrosion testing to study 13 steel bars with strain gauges which were placed in a machined axial cavity. From their study, the relationship between the cycle numbers of fatigue loads, the amount of corrosion and the bond-slip of bars and concrete were found. Ahn and Reddy [5] evaluated the durability of marine concrete structures subjected to fatigue loads. The accelerated fatigue tests were carried out on full- and half-size RC specimens with three different water cement ratios. Al-Hammoud et al. [6] investigated the fatigue bond

behavior of corroded steel RC beams by the tests of nine members. Shi et al. [7] investigated the bond degeneration at the bar-concrete interface under variable fatigue loads. Fang et al. [8] carried out tests for bond stress-slip response of corroded reinforcement and concrete under cyclic loads. Siebren et al. [9] presented the periodic overload and corrosion-fatigue resistance of machined specimens made of two corrosion resistant reinforcing steels, MMFX micro composite and 316LN stainless steel. Series of constant amplitude and periodic overload tests were performed in laboratory air and in an aqueous 3.5% by weight NaCl solution from which the fatigue resistance of these materials was compared with conventional reinforcing steel. However, reports describing how to directly and effectively evaluate the residual life for PSC bridges under the coupled corrosion-fatigue action are very rare.

This paper outlines a comprehensive method on evaluation of the residual life of PSC bridges under coupled corrosion-fatigue actions. Initially, a multi-scale finite element model of a bridge is created to perform detailed stress analysis. Stress impact coefficients and stress histories of key prestressing strands are obtained from the vehicle-bridge coupling vibration analysis in which the standard fatigue truck model specified in AASHTO are considered. A pit corrosion model is adopted to determine stress concentration factors of the prestressing strands due to corrosion. A comprehensive analysis method is proposed to compute stress amplitudes of key prestressing strands under coupled corrosion-fatigue effects. Consequently, the S-N curve and the traffic condition are integrated to find the service life of the weakest strand, which is characterized as the service life of the bridge. Finally, the effectiveness of the methodology framework is demonstrated on a large-span continuous PSC bridge, and several important observations are summarized.

2. VEHICLE-BRIDGE COUPLING VIBRATION ANALYSIS

2.1 Multi-scale Finite Element Model of the PSC Bridge

In general, structural analysis is usually carried out at different scale levels for different purposes. For a large structure, the size of the model beam element is usually at the level of meter for global structural analysis. Meanwhile, the beam element is also adopted at the centimeter level of component scale for nominal stress analysis. Furthermore, the scale of material points, usually modelled with shell or solid elements, is commonly less than the level of a millimeter for the local detailed hot-spot stress analysis. In order to achieve the magnitude of accuracy and efficiency between global finite element analysis and local refined stress analysis, a multi-scale finite element modelling technology is adopted in this study [10]. There are two key issues on establishing a multi-scale finite element model, the selection of key parts and the assembly of sub-models. Those parts of the structure which are vulnerable to damages are determined by the structural static analysis. In these key parts, solid elements are used to simulate the post-damaged performance, and other parts are designed from beam elements. In the interfaces between beam-element sub-models and solid-element sub-models, the master and slave nodes are defined to assemble the sub-models.

The general method of coupling elements of dissimilar dimensions via constraint equations has been proposed by McCune et al. [10], which is based on equating the work done on both sides of the interface of different elements. A basic requirement of the method is the knowledge of the stress distribution at the interface which can be obtained from the results of beam theory. Constraint equations are also adopted to connect the master and slave nodes herein, as shown in Figure 1.

The constraint equation method refers to a kind of linear equation connecting degrees of freedom (see Eq. (1)).

$$Const = \sum_{i=1}^N (C(i) \cdot U(i)) \quad (1)$$

where $U(i)$ is the variable of the i^{th} degree of freedom; $C(i)$ is the coefficient of $U(i)$; and N is the number of degrees of freedom.

If the constraint equations have been determined, they are successfully incorporated in the finite element formulation by standard methods such as Lagrange multiplier or penalty function methods. In the present study, constraint equations can be easily implemented in the general-purpose finite element software ANSYS [11] by *CERIG command.

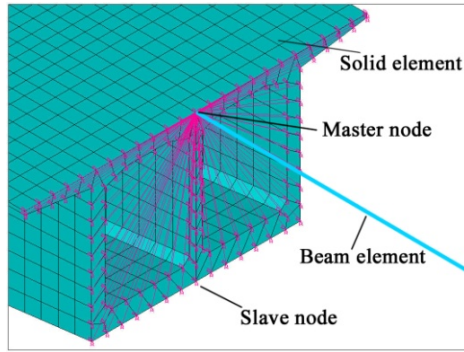


Figure 1. Details of Assembly Models

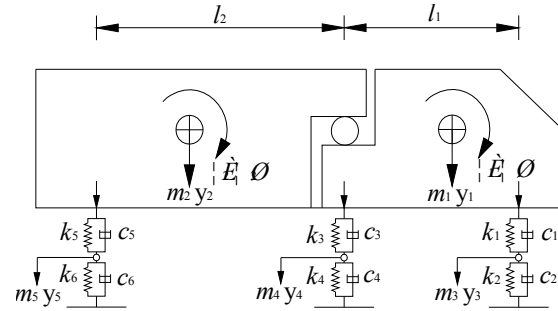


Figure 2. Model of AASHTO Fatigue Truck

2.2 Vehicle Model

The triaxial fatigue vehicle model of the American Association of State Highway and Transportation Officials (AASHTO) [12] is adopted in the present study. Taking the mass and rigidness of axles into consideration, it simplifies the head and body of the truck into two masses, respectively. There are seven independent degrees of freedom in total, as shown in Figure 2. The parameters of AASHTO fatigue truck are listed in Table 1.

Table 1. Parameters of AASHTO Fatigue Truck

Vehicle parameters	Value	Vehicle parameters	Value
vehicle head mass m_1	2612 kg	2 nd axle suspended mass m_4	808 kg
vehicle head pitching rotational inertia θ_1	2022 kg·m ²	2 nd axle upper spring stiffness k_3	1903172 N/m
vehicle head rolling rotational inertia ω_1	8544 kg·m ²	2 nd axle upper damping constants c_3	7882 N·s/m
vehicle body mass m_2	26113 kg	2 nd axle lower spring stiffness k_4	3503307 N/m
vehicle body pitching rotational inertia θ_2	33153 kg·m ²	2 nd axle lower damping constants c_4	2000 N·s/m
vehicle body rolling rotational inertia ω_2	181216 kg·m ²	3 rd axle suspended mass m_5	653 kg
1st axle suspended mass m_3	490 kg	3 rd axle upper spring stiffness k_5	1969034 N/m
1st axle upper spring stiffness k_1	242604 N/m	3 rd axle upper damping constants c_5	7182 N·s/m
1st axle upper damping constants c_1	2190 N·s/m	3 rd axle lower spring stiffness k_6	3507429 N/m

1st axle lower spring stiffness k_2	875082 N/m	3 rd axle lower damping constants c_6	2000 N·s/m
1st axle lower damping constants c_2	2000 N·s/m	vehicle length l_1+l_2	(4+4.5) m

Table 2. Road Surface Roughness Classifications

Road-roughness classifications	$\phi(n_0)$
Very good	$2 \times 10^{-6} \leq \phi(n_0) < 8 \times 10^{-6}$
Good	$8 \times 10^{-6} \leq \phi(n_0) < 32 \times 10^{-6}$
Average	$32 \times 10^{-6} \leq \phi(n_0) < 128 \times 10^{-6}$
Poor	$128 \times 10^{-6} \leq \phi(n_0) < 512 \times 10^{-6}$
Very poor	$512 \times 10^{-6} \leq \phi(n_0) < 2048 \times 10^{-6}$

2.3 Roadway Profile

The road surface condition is a very important factor that affects the dynamic responses of the bridge and vehicles. Deterioration of bridge road surfaces can occur at both the bridge deck and joints for numerous reasons, such as aging, varying environmental conditions, corrosion and the increased gross vehicle weight.

The road surface roughness is generally defined as an expression of irregularities of the road surface. The research conducted by Zhang and Cai [13] shows that the road surface roughness is usually assumed as a zero-mean stationary Gaussian random process and it could be generated through an inverse Fourier transformation as Eq.(2).

$$r(x) = \sum_{k=1}^N \sqrt{2\phi(n_k)\Delta n} \cos(2\pi n_k x + \theta_k) \quad (2)$$

where $r(x)$ is the roadway surface roughness; $\phi(\cdot)$ is the power spectral density function ($m^3/cycle/m$) for the road surface elevation; n_k is the wave number ($cycle/m$); Δn is the frequency increment and θ_k is the random phase angle uniformly distributed from 0 to 2π . The power spectral density function $\phi(\cdot)$ is defined as Eq. (3).

$$\phi(n) = \phi(n_0) \left(\frac{n}{n_0} \right)^{-2} \quad (3)$$

where n is the spatial frequency ($cycle/m$); n_0 is discontinuity frequency of $1/2\pi$ ($cycle/m$); $\phi(n_0)$ is roadway surface roughness coefficient ($m^3/cycle$), and its value is chosen depending on the road condition. According to the different value of roadway surface roughness coefficient, the roadway surface roughness could be divided into five levels combining Eq. (2) and Eq. (3), as listed in Table 2.

2.4 Stress Concentration Factor of Corroded Prestressing Strands

Under the corrosion environment of chloride salts in coastal areas, the passive films of embedded prestressing stands of PSC bridges are damaged, which induces corrosion uniformly and forms the pits. The stress concentrates around the corrosion pits of prestressing strands in service, which will reduce the load carrying capacity of the bridge sharply. Therefore, the stress concentration effects

of embedded prestressing strands due to corrosion must be considered for evaluating the residual life of the bridge more practically.

The stress concentration factor affects the fatigue life of the reinforcing steel bars and thus the fatigue life of the PSC bridge. Many factors affect the stress concentration factor and include the geometry of the notch, material type, and especially the pit depth of corrosion. When the geometry of the notch and the mechanical properties are uniform, differences due to corrosion of the reinforcing steel bars will cause different stress concentration factors in different service years.

Shi [14] investigated stress concentration properties of corroded prestressing strands by the meso-scale finite element method. The local stress states of embedded corroded prestressing strands are simulated by assumed corrosion pits on prestressing strands and cracks in the surrounding concrete. The relationships between the stress concentration factor and the corrosion period are formulized for round, oval and triangular corrosion pits, respectively. The stress concentration factors of prestressing strands induced by corrosion pits are defined as Eq. (4) [14].

$$\lambda = \begin{cases} 1.045 + 0.00335(t_1 - t_0) & \text{for the round pit} \\ 1.039 + 0.00313(t_1 - t_0) & \text{for the oval pit} \\ 1.095 + 0.00234(t_1 - t_0) & \text{for the triangular pit} \end{cases} \quad (4)$$

where t_0 is the reinforcement corrosion period (years) and t_1 is the service life of the bridge (years).

2.5 Impact Factor

To predict the dynamic responses of bridges resulting from a moving vehicle is a significant problem in bridge design. Most design codes assign an approximate quantity for the dynamic response for a normal design procedure, amplifying the static response with an impact factor μ . The impact factor is defined as Eq. (5).

$$\mu = \frac{R_{d \max} - R_{s \max}}{R_{s \max}} \quad (5)$$

where $R_{d \max}$ and $R_{s \max}$ are the maximum dynamic and static responses of the bridge, respectively.

In order to investigate the variability of impact factors of different parts in the bridge resulting from a moving vehicle, the vehicle-bridge coupling vibration analysis program developed by the same research group [15] is applied to calculate impact factors of the bridge under dynamic loads.

2.6 Stress Amplitude

The bridge suffers from the cyclic load and corrosion environment during service stage. As the damage of PSC bridges is usually caused by the failure of corrosion prestressing stands under the coupled corrosion-fatigue actions, the residual life of the weakest prestressing strand is used to characterize the residual life of the bridge. Combining the stress concentration of the prestressing strand and the dynamic impact, the stress amplitude of the prestressing strand S induced by one truck passage is expressed as Eq. (6).

$$S = \mu \cdot \lambda \cdot \Delta \sigma \quad (6)$$

where $\Delta \sigma$ is the original stress amplitude induced by one truck passage.

3. RESIDUAL LIFE EVALUATION OF PSC BRIDGES

3.1 Residual Life Analysis

It is extremely difficult to analyze a structure suffering from random loads since the weights, types and speeds of the vehicles on the bridge are different. In addition, the appearing time interval is also random. Thus, it needs to be simplified reasonably by the researcher to find the likely method for meeting the balance of the precision and the efficiency. The AASHTO fatigue vehicle mentioned above is selected as the standard loading model. The maximum stress amplitude of the stress cycle caused one fatigue truck passage is taken into consideration. The cumulated number of truck passages for the future year t can be estimated as Eq. (7) [16].

$$N_f(t) = 365 \times ADTT \times \int_0^t (1 + \alpha)^y dy = 365 \times ADTT \times \frac{(1 + \alpha)^t - 1}{\ln(1 + \alpha)} \quad (7)$$

Where t is the bridge life (years); $ADTT$ is the average daily truck traffic and α is the annual rate of traffic increase.

After stress amplitude $\Delta\sigma$ is obtained, the number of stress cycles N in the whole life cycle of the bridge can be calculated according to the S - N curve [17] of the prestressing strand (see Eq. (8)).

$$\lg N = 8.08 - 3.5 \lg S \quad (8)$$

If $N_f(t) = N$, the bridge life limit is reached, and then the theoretic service life of bridge could be predicted by Eq. (9).

$$t_T = \frac{\ln \left\{ \frac{10^{8.08} \cdot \ln(1 + \alpha)}{365 \cdot ADTT \cdot [\mu \cdot \lambda \cdot \Delta\sigma]^{3.5} + 1} \right\}}{\ln(1 + \alpha)} \quad (9)$$

Therefore, the residual life of the bridge is equal to $t_T - t$.

3.2 Procedure of Residual Life Evaluation of PSC Bridges

The proposed procedure for the residual life evaluation of PSC highway bridges (as shown in Figure 3) is summarized as following:

- Step 1:* establish the multi-scale finite element model of the bridge;
- Step 2:* obtain the hot spot stress history from the finite element analysis under one truck passage;
- Step 3:* obtain impact coefficients of prestressing strands by the vehicle-bridge coupling vibration analysis;
- Step 4:* obtain the stress concentration factor from the pit corrosion model of prestressing strands;
- Step 5:* obtain stress amplitudes of prestressing strands by combining *Step 2* to *Step 4*;
- Step 6:* determine the life of the weakest prestressing strand basing on the S - N curve and the traffic volume, which characterizes as the total service life of the bridge;
- Step 7:* calculate the residual life of the bridge according to its service time till now.

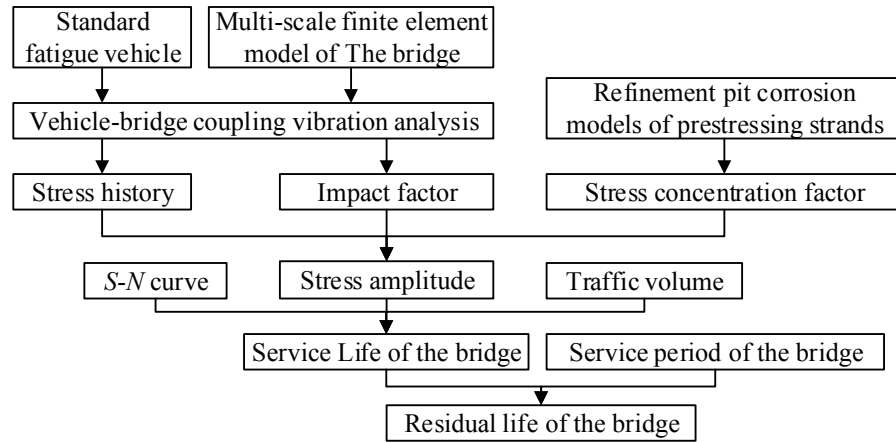


Figure 3. Flowchart of Residual Life Evaluation of PSC Bridges

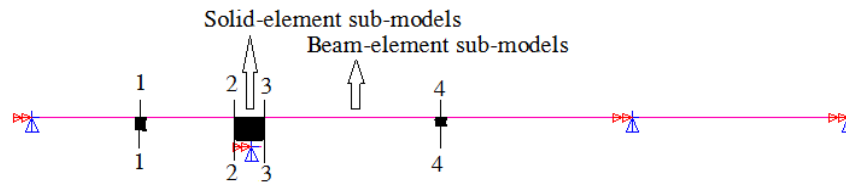
4. ILLUSTRATIVE EXAMPLE

4.1 Bridge Description

A three-span continuous trapezoidal box-girder bridge located at Binhai New Area of Tianjin, China, is used to illustrate the application of this proposed method. The span layout of the bridge is 90 m + 160 m + 90 m. The width of the bridge is 20.5 m. The maximum and minimum depths of the box-girder on the main span are 9.5 m and 3.5 m, respectively. The box-girder is the straight web single box with double chambers. The bottom and top widths of the box-girder are 12.5 m and 20.5m, respectively. The flange of the box-girder is 4.0 m at each side. The box-girder is a three-dimension PSC structure. The bridge was designed according to the China Code (JGJ D62-2004) for the Highway-I live load. The width of lanes was designed for meeting the demand of the vehicle speed 80 km/h. The designed service life of the bridge is 100 years, and it was open to the public in May 2008.

The multi-scale finite element model of the bridge is built as shown in Figure 4. Considering the mechanical characteristics of the bridge in service, the midspan and the negative moment region are the vulnerable areas. Therefore, refined finite element models with solid elements are built for them and beam element models are built for the rest parts. The middle section of side span (Section 1), two end sections of the negative moment region (Section 2 and 3), and middle section of mid-span (Section 4) are mainly analyzed herein as shown in Figure 4.

The midlines of the decks and bottom plates, webs and corners of the box-girder are vulnerable locations analyzed from the angle of the section [18]. The prestressing strands of these locations should be primarily focused in the present study. These critical prestressing strands are denoted in Figure 5.



Note: 1, 2, 3 and 4 denote locations of the concerned sections.

Figure 4. Multi-scale Finite Element Model of the Concerned Bridge

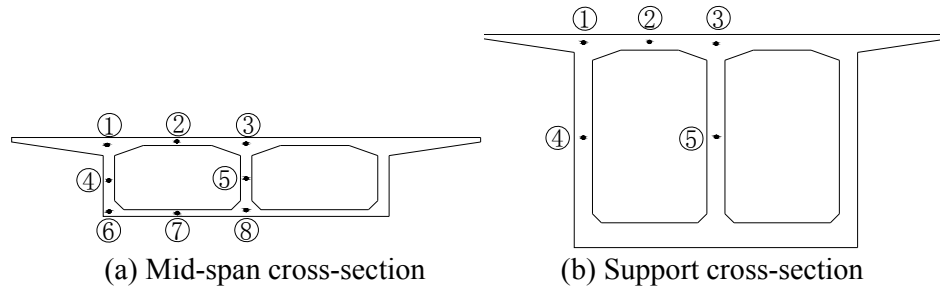


Figure 5. Typical Locations of the Vulnerable Prestressing Strands

4.2 Results and Discussions

4.2.1 Residual lives of the concerned prestressing strands in different sections

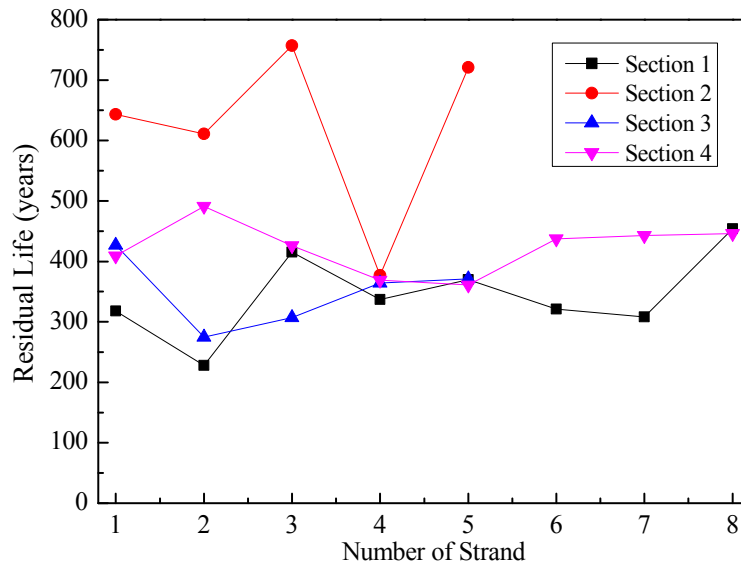


Figure 6. The Prestressing Strand lives on Different Sections

Residual lives of the prestressing strands at four different sections were predicted to characterize the residual life of the bridge as shown in Figure 6. The results were obtained at an 80 km/h vehicle speed and an ‘average’ road surface roughness condition. It can be seen that the predicted residual life of the bridge is longer than the design life, which proves that the bridge will not fail under the coupled corrosion-fatigue actions. It also can be seen from Figure 6 that the life of the prestressing strand at the center of the deck of the chamber is relatively shorter. One possible reason is that the deck bears vehicle loads directly and works in the repeated tension and compression stress state with large stress amplitude.

4.2.2 Effect of the roadway surface roughness on the residual life of the bridge

The deck surface suffers from the wheels of vehicle directly, which induces its deterioration during the service stage of the bridge. The deck surface roughness is a major factor in vehicle/bridge interaction [12]. To evaluate the effect of roadway surface roughness on the residual life of the bridge, five different road surface roughnesses are considered at an 80 km/h vehicle speed. As shown in Figure 7, the residual life of the bridge decreases as the road surface roughness increases. The residual life is 30% shorter when the ‘very poor’ road surface roughness in ‘very poor’

condition than that when the road surface roughness in ‘very good’ condition, which proves that road surface profile has a significant effect on the residual life of the bridge. When the road is rough, the vehicle cannot move steadily and bumps sharply, which results in the increase of the impact force on the bridge and the stress amplitude of the prestressing strand.

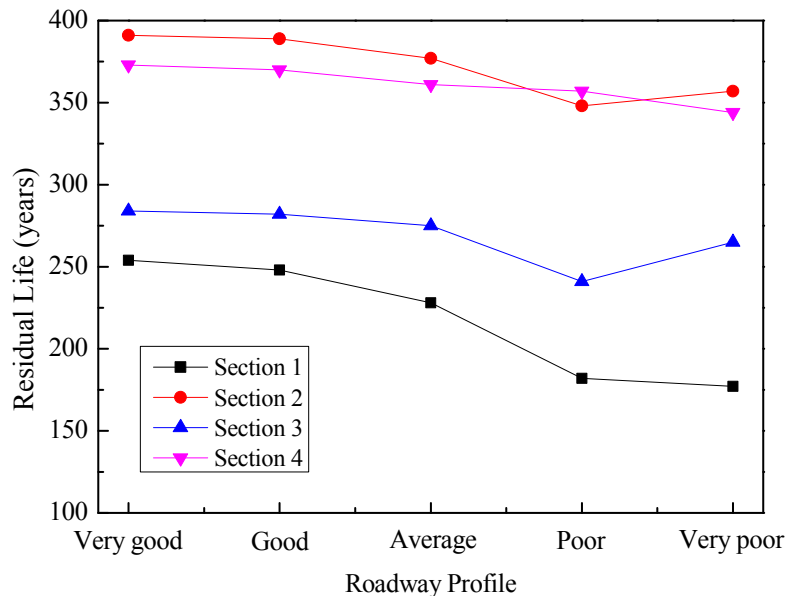


Figure 7. Effect of the Roadway Surface Roughness on the Residual Life

4.2.3 Effect of the vehicle speed on the residual life of the bridge

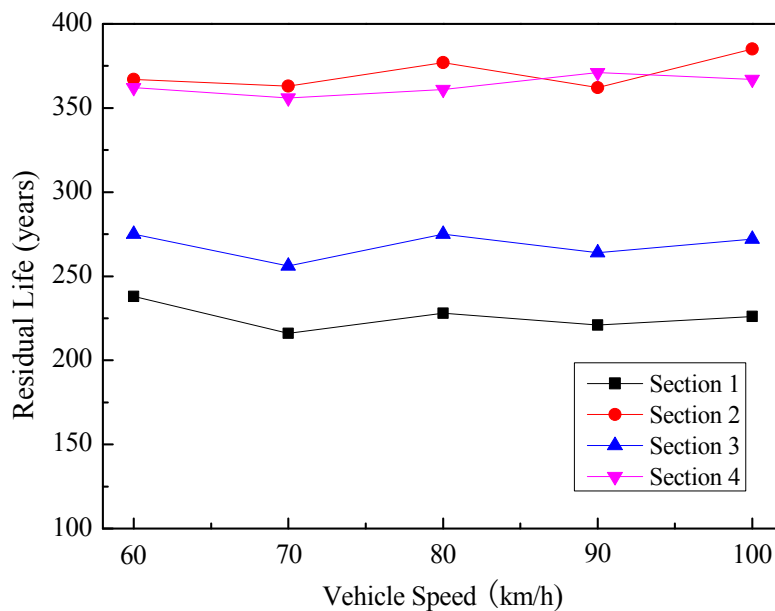


Figure 8. Effect of the Vehicle Speed on the Residual Life

As stated earlier by many researchers, the vehicle speed has an ambiguous effect on the impact factor of highway bridges, and the resonance will happen when the vehicle speed reaches a certain value [13, 19]. To evaluate the effect of the vehicle speed on the residual life of the bridge, five different vehicle speeds are considered at an “average” road surface roughness. There is not obvious discrepancy of residual lives of the bridge for the five different vehicle speeds at an “average” road surface roughness as shown in Figure 8. Similar results can also be observed for the fatigue life of a PSC multi-girder bridge in the previous study [19]. Attention should be paid to the middle of the bridge side spans because its life span is much shorter. It also can be seen that the life of the prestressing strand in the negative moment region prolongs with the increase of the vehicle speed, since with increase of the vehicle speed, the inertia of the vehicle will increase, which makes vehicle move steadier to bring less impact on the bridge.

5. CONCLUSIONS

This paper proposed a method to evaluate the residual life of PSC highway bridges under the coupled corrosion-fatigue actions. From the present study, the following conclusions are drawn:

- (1) The most vulnerable area is the deck of the chamber in the box-girder highway bridge.
- (2) The residual life of the prestressing reinforced concrete highway bridge is affected slightly by the vehicle speed.
- (3) The road surface roughness has more significant negative impact on the residual life of the bridge while the vehicle runs under relatively lower speed.
- (4) The present method to some extent is universal, and researchers can adopt different analysis softwares and identification principles according to the actual situation. Based on the complexity of the operational environment, such as overload or accidental damage, more refined analysis should be considered for the proposed method, and this remains to be investigated in future studies.

ACKNOWLEDGMENTS

The financial support from the National Science Fund of China (51178305), the Tianjin Research Program of Application Foundation and Advanced Technology (14JCYBJC21500), the Natural Science Foundation of Jiangsu (BK2011611) and the Fok Ying Tung Education Foundation (No.131074) are gratefully acknowledged.

REFERENCES

- [1] Lucia, T., and Chen, Liang., “ Numerical Simulation of Inelastic Cyclic Response of HSS Braces upon Fracture”, Advanced Steel Construction, 2014, Vol. 10, No. 4, pp. 442-462.
- [2] Emilio, B. A., Philippe, B., Alaa, C. and Mauricio S. S., “Probabilistic Lifetime Assessment of RC Structures under Coupled Corrosion-fatigue Deterioration Processes”, Structural Safety, 2009, Vol. 31, No. 1, pp. 84-96.
- [3] Dong, F.X., “Experimental Study on Fatigue Performance of Steel Corrosion Concrete Members”, Dissertation submitted to Nanjing University of Science and Technology in Conformity with the Requirements for the Degree of Master, 2007. (in Chinese)

- [4] Peng, X.N., Jin, L.Z., Xue, J.Y. and Wei, B.N., "Experimental Study on Bond Performance Deterioration between Corroded Bars and Concrete under Fatigue Loads", *Industrial Construction*, 2010, Vol. 40, No. 2, pp. 101-104. (in Chinese)
- [5] Ahn, W. and Reddy, D.V., "Galvanostatic Testing for the Durability of Marine Concrete under Fatigue Loading", *Cement and Concrete Research*, 2001, Vol. 31, No. 3, pp. 343-349.
- [6] Al-Hammoud, R., Soudki, K. and Timothy, H. T., "Bond Analysis of Corroded Reinforced Concrete Beams under Monotonic and Fatigue Loads", *Cement & Concrete Composites*, 2010, Vol. 32, No.3, pp. 194-203.
- [7] Shi, Z.F., Cui, C. and Zhou, L.M., "Bond Decay at Bar-concrete Interface under Variable Fatigue Loads", *European Journal of Mechanics A/Solids*, 2006, Vol. 25, No. 5, pp. 808-818.
- [8] Fang, C.Q., Kent, G., Karin, L. and Mario, P., "Effect of Corrosion on Bond in Reinforced Concrete under Cyclic Loading", *Cement and Concrete Research*, 2006, Vol. 36, No. 3, pp. 548-555.
- [9] Siebren, J. D., Trick, J. H. and Colin, M., "Periodic Overload Corrosion Fatigue of MMFX and Stainless Reinforcing Steels", *Journal of Materials in Civil Engineering*, 2009, Vol. 21, No. 1, pp.1-9.
- [10] McCune, R.W., Armstrong, C.G. and Robinson, D.J., "Mixed Dimensional Coupling in Finite Element Models", *International Journal for Numerical Methods in Engineering*, 2000, Vol. 49, No. 6, pp.725-750.
- [11] ANSYS Release 8.1, ANSYS Inc., 2004.
- [12] AASHTO. "AASHTO LRFD Bridge Design Specifications 4th Edition", American Association of State Highway and Transportation Officials, Washington, DC, 2007.
- [13] Zhang, W. and Cai, C.S., "Fatigue Reliability Assessment for Existing Bridges Considering Vehicle Speed and Road Surface Conditions", *Journal of Bridge Engineering*, 2012, Vol. 17, No. 3, pp. 443-453.
- [14] Shi, X.M., "Study on Life Prediction Method of RC Bridge under Coupled Corrosion-fatigue Effects"(in Chinese), Dissertation submitted to Tianjin University in Conformity with the Requirements for the Degree of Master, 2012.
- [15] Zhu, J.S. and Yi, Q., "Bridge-vehicle Coupled Vibration Response and Static Test Data based Damage Identification of Highway Bridges", *Structural Engineering and Mechanics*, 2013, Vol. 46. No. 1, pp. 75-90.
- [16] Kwon, K. and Frangopol, D.M., "Bridge Fatigue Reliability Assessment using Probability Density Functions of Equivalent Stress Range based on Field Monitoring Data", *International Journal of Fatigue*, 2010, Vol. 32, No.8, pp. 1221-1232.
- [17] Paulson, C., Frank, J. K. H. and Breen, J. E., "A Fatigue Study of Prestressing Strand", FHWA Research Report 300-1, Center for Transportation Research, The University of Texas at Austin, Austin, Texas, 1983.
- [18] Lee, S.Y. and Yhim, S.S., "Dynamic Behavior of Long-span Box Girder Bridges Subjected to Moving Loads", *Numerical Analysis and Experimental Verification*, 2005, Vol. 42, No. 18-19, pp. 5021-5035.
- [19] Zhu, J.S., Chen, C. and Han, Q.H., "Vehicle-bridge Coupling Vibration Analysis based Fatigue Reliability Prediction of Prestressed Concrete Highway Bridges", *Structural Engineering and Mechanics*, 2014, Vol. 49, No. 2, pp. 203-223.

FATIGUE LIFE EVALUATION FOR CRACKED LONG-SPAN CONTINUOUS PC BRIDGES

Xin Ruan¹, Hai-ying Ma^{2,*} and Xue-fei Shi¹

¹ *Department of Bridge Engineering, Email: ruanxin@tongji.edu.cn
Tongji University, Shanghai, China.*

² *ATLSS Center, Lehigh University, PA, USA*

**(Corresponding author: E-mail: ham208@lehigh.edu)*

ABSTRACT: Long span pre-stressed concrete box girder bridges are widely constructed in China. Some typical deficiencies, such as unacceptable deflections and cracks in the concrete, often occur in those bridges with increasing service time. The deficiencies change the distribution of internal forces in the girders, which induces new problems, such as fatigue of reinforcements in the girders. In this paper, a fatigue life evaluation for a cracked long-span continuous PC bridges was conducted, which integrated weigh-in-motion (WIM) data and non-destructive examination (NDE) techniques. WIM data was used to investigate properties of vehicle load. The FE models of the cracked structure were developed to analyse the behaviour due to cracks. Various fatigue truck loads were considered in the models. Fatigue life evaluation based on real WIM data was developed to obtain the fatigue stress ranges due to the presence of cracks. Based on the analysis, the service life of the bridge was assessed before and after cracking at critical locations. A pre-stressed concrete box girder bridge, with three spans: 65m+100m+65m, was taken as an example to introduce the method. The present study provides better understandings of the post-cracking behaviour of long span continuous PC bridges. The outcome of this research can be efficiently utilized to reduce the risk of failure and achieve better management of the bridges.

Keyword: Continuous PC Bridge, Crack, Vehicular load, Fatigue life evaluation, Weight-in-motion, Stress range

DOI: 10.18057/IJASC.2015.11.3.11

1. INTRODUCTION

Pre-stressed concrete box girder bridges are widely constructed in China. These kinds of bridges are usually designed with full pre-stresses, and cracks are prohibited in the girders. Fatigue is usually not necessary to consider in these bridges. However, with the service time increasing, some typical deficiencies occur in those bridges, such as cracks in the concrete and visible deflections in main spans. The deficiencies affect the durability and even influence the safety of structure. Previous and current research mainly focuses on the effect of cracks to the capacity of structures [1]. Reasons causing these deficiencies may be different from bridge to bridge, but changes of vehicle load and loss of pre-stressing are the most common and critical reasons. Usually these defected structures still hold a certain level of load carrying capacity, but a rapid improvement for durability and more attentions are still necessary [2]. It also should be noticed that the change of internal force distribution and structural behaviours may induce fatigue problems, which has not been studied before.

In the past, research was conducted to estimate and analyse the behaviour of concrete structures due to fatigue load [3-14]. Warner and Hulsbos [3] estimated the probable fatigue life of pre-stressed concrete beams. It was found that a steel fatigue failure could occur by successive fracture of the steel reinforcement in the beam. Lindorf and Curbach [4] found that the fatigue of bond between reinforcement and concrete were affected by transverse tension and it was important to separate verification of steel and concrete fatigue. Tilly [5] also studied the fatigue performance of high strength steel reinforcements. Reinforcement fatigue usually needs not to be checked according to AASHTO Specifications unless the pre-stressed tendons suffer a stress higher than the

constant-amplitude fatigue threshold, which is usually hard to reach by vehicular loadings [15]. However, for these kinds of defected pre-stress concrete box girder bridges, reinforcements at the cracked parts may have a very high stress range due to cracks of concrete and increase of vehicle load. To assess fatigue life, the fatigue load, reinforcement stress and stress amplitude needs to be determined accurately. Therefore, the identification of current structural condition and vehicle load are very important. In this paper, a fatigue life evaluation for cracked long-span continuous PC bridges was presented, integrating weigh-in-motion (WIM) data and NDE techniques.

2. A TYPICAL LONG SPAN CONTINUOUS PC BRIDGE

2.1 Prototype Bridge

In this paper, a typical pre-stressed concrete box girder bridge was taken as an example. The bridge, built in 1996, is located in the highway system in China, and it was constructed with cast on site. The elevation of the bridge is shown in Figure 1. It is a post-tensioned pre-stressed concrete continuous box girder bridge with three spans: 65m+100m+65m. The main girder has a single-cell box cross section, with the height varying from 5.6m (section over pier) to 2.2m (section at middle span). The girder carries two traffic lanes in the same direction. Some typical cross sections are shown in Figure 2.

2.2 Cracks Distribution

Several surveys were carried out to record the deflection changes from 1999 to 2008. It is found that the accumulative vertical deflection in the middle span came up to 70 mm due to the traffic in eight years. Some cracks, including transverse cracks on the top and bottom slabs of middle span, and diagonal cracks at the diaphragm of over pier section were observed in the first two years after the bridge was completed. In April 2000, cracks at the webs propagated to the bottom slabs in the middle section of mid span, and continued to propagate at least for four years. In 2007, a detailed survey was made to the bridge. The diagonal cracks occurred at the web in the side and middle span, and a lot of longitudinal cracks occurred at the top and bottom plates. Figure 3a shows the cracks distribution at the web of middle span, some of these cracks already extended to the junction points between web and top plate. Figure 3b shows longitudinal cracks distributed near middle span. Ruan and Shi [2] analysed the crack cause and assessed the cracked structure. The cracks in the web occurred due to the lack of vertical pre-stress tendons for shear resistance in the cracked region, and the cracks at bottom plate were caused by the local pre-stressed force and lower flexural rigidity.

3. LIVE LOAD INVESTIGATION BASED ON WEIGH-IN-MOTION STUDY

During the service life of bridges, truck loads are the main changeable loadings, which are of great randomness, high uncertainty and time variability. WIM system can record the truck load information, such as weight, axial load, speed and axial distance, which provides more accurate data resources for analysis. A WIM system was set up on the highway near the bridge location to investigate actual vehicle load. A set of data for two weeks vehicles was recorded and analysed as follow, which included the data of 577,882 axles and 237,899 trucks.

The statistical result of different vehicle types according to number of axles is shown in Table 1. Table 2 gives the average and maximum weight of each type of vehicle. Table 3 presents the proportion of vehicle weight. The axle weight proportion comparisons are provided in Table 4. From Table 1, although five-axle vehicles do not take a high proportion, around 2.39%, but the

proportion of six-axle vehicles is as high as up to 4.6%. Table 2 shows that the average weight of six-axle vehicles is up to 50t and the maximum weight exceeds 100t. As observed from Table 3, the proportion of recorded vehicles which have weights over the specified weight 55t, is near 7%. All the data above show that, the vehicles load on the bridge have changed a lot compared with the base data obtained in 1990s according to the design specification in China [16].



Figure 1. Elevation of the Prototype Bridge

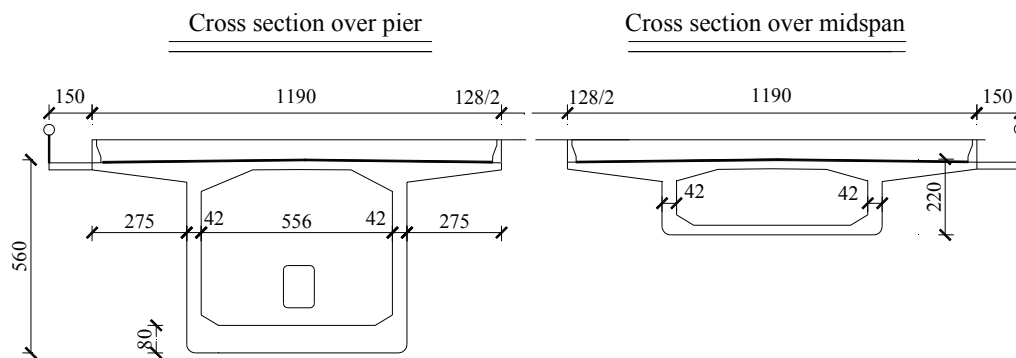


Figure 2. Two Typical Sections of the Prototype Bridge (in cm)

Table 1. Proportions of Different Vehicle Types in Gross Traffic on the Highway

Number of Axle	2	3	4	5	6	>6	Total
Number of Vehicles	191578	17932	11897	5686	9983	823	237899
Proportion	80.53%	7.54%	5.00%	2.39%	4.20%	0.4%	100%

Table 2. Comparison of Gross Vehicle Weight with Different Axial Types

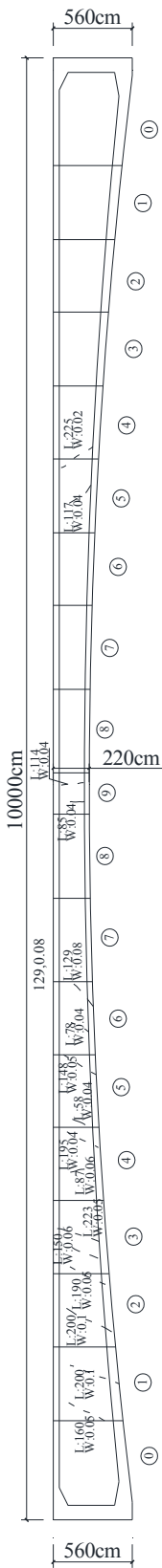
Number of Axle	2	3	4	5	≥6
Average (t)	4.50	9.20	33.00	39.10	50.00
Maximum	50.60	78.20	93.40	107.00	172.60

Table 3. Comparison of Gross Vehicle Weight with Different Classified Sections

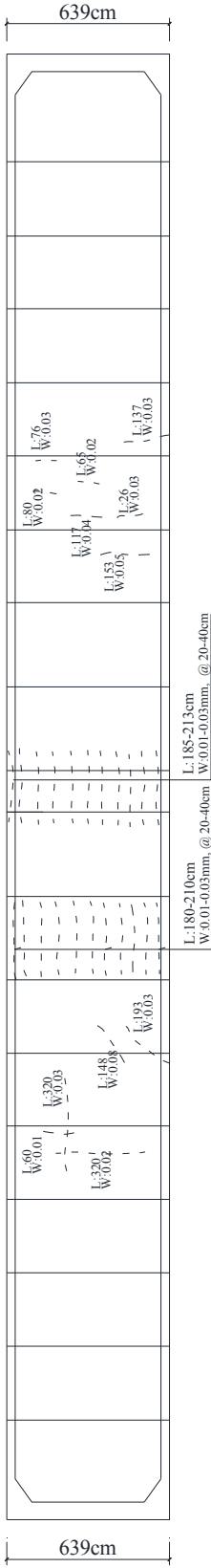
Vehicle Weight (t)	0~20	20~40	40~60	60~80	≥80	Total
Proportion	85.77%	7.61%	5.18%	1%	0.45%	100%

Table 4. Axial Weight Distribution in Different Classified Sections

Vehicle Weight (t)	0~5	5~10	10~15	15~20	20~25	25~30	30~35	Total
Proportion	72.71%	15.32%	7.97%	2.95%	0.83%	0.18%	0.03%	100%



(a) Cracks at Web Slab at Middle Span



(b) Cracks at Bottom Slab at Middle Span

Figure 3. Cracks Distribution at the Middle Span

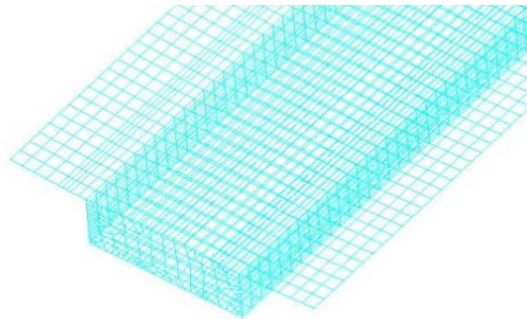
4. NUMERICAL SIMULATION

Comprehensive numerical simulations are carried out to understand the influence of cracking, the deflections, and also the changing of live load. The pavement surface properties obtained by site inspections, such as thickness, material strength, etc., have been considered in the analysis.

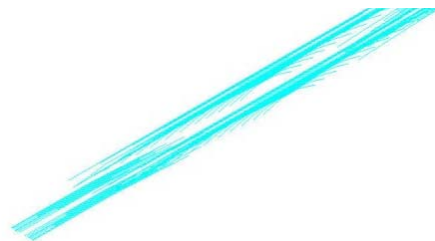
A detailed Finite Element Model (FEM) using software ANSYS 10.0 was developed to determine the stresses at various critical locations and to assess the fatigue life of bridges before and after cracking. Figure 4 gives detailed images of the model. The 8-node solid element (C3D8) was selected in the model to emulate the pre-stressed concrete. The 3-dimensional 2-node truss element (LINK8) was used for the pre-stressed tendons bonded in the concrete. The model has 50,495 nodes, and 145,768 elements. The stress-strain relationship of concrete is based on the stress-strain curves of CEB-FIP (1990).



(a) Web Slab and Its Cracks in the FEM



(b) Reinforcement Bars in the FEM



(c) Pre-stress Bar Model in the FEM

Figure 4. FEM of the Bridge Structure

The main cracks on the web slabs and bottom slabs were considered, and pre-stress bars and main reinforcements were considered as link element in the model to simulate the redistribution of force due to the crack. Figure 5 presents the comparison of FEM analysis results of design and cracked structure. It is found that there are obvious differences of the stresses distribution in the slabs before and after cracks occurred. The tension stresses were released because of the crack, and there are still enough compressive stresses in the girders after cracking. Figure 6 shows the stress variation of reinforcements at the bottom plate before and after cracking. The reinforcement stress changes are

large at the middle of middle span due to lots of cracks. The maximum change is up to 50 MPa. The cracks made the forces in concrete transferred to the reinforcements and pre-stressed tendon. In the cracked area, the tension forces carried by concrete transferred to reinforcements and tendons, which increased the stresses of reinforcements and tendons. In the area around the cracks, the tension stress of concrete also decreased while compression stresses increased. In the area between adjacent cracks, the stress of concrete was also increased due to the bonding with reinforcements. If the bond slip is small, the crack would be engendered. Therefore, cracks changed the stresses distribution in the sections, and caused larger deflections, which reduced the safety of the structure. Due to the cracks, the behavior of bridge changed a lot. This can be very important proof to assess the fatigue problem of the bridge.

5. FATIGUE LIFE ANALYSIS BASED ON WIM DATA

5.1 Fatigue Assessment Procedure using WIM Data

Fatigue loads are reconsidered based on WIM data, while not only based on the design specification since the vehicles loads changed compared to that in the specification. Classified trucks are simplified into four categories and the corresponding stress ranges are summarized based on two-week WIM data around the bridge area. The weight of each truck model would be scaled to the actual weight from WIM data. In this way it gives the derived equivalent stress range and the estimated fatigue life for comparison of the bridge models before and after cracking.

Fatigue stress-number of cycle (S-N) curves proposed by Warner and Hulsbos [3] for pre-stressed concrete bridges are used to estimate fatigue life by providing designers with an approximate relationship between stress ranges and the number of stress cycles to failure. The S-N curves were developed via experimental testing of typical strands with results from the tests being used to produce the curves within a certain confidence interval. Techniques are available to convert stress ranges at certain location to equivalent stress ranges that can be used with the S-N curves to more accurately estimate fatigue life cycles.

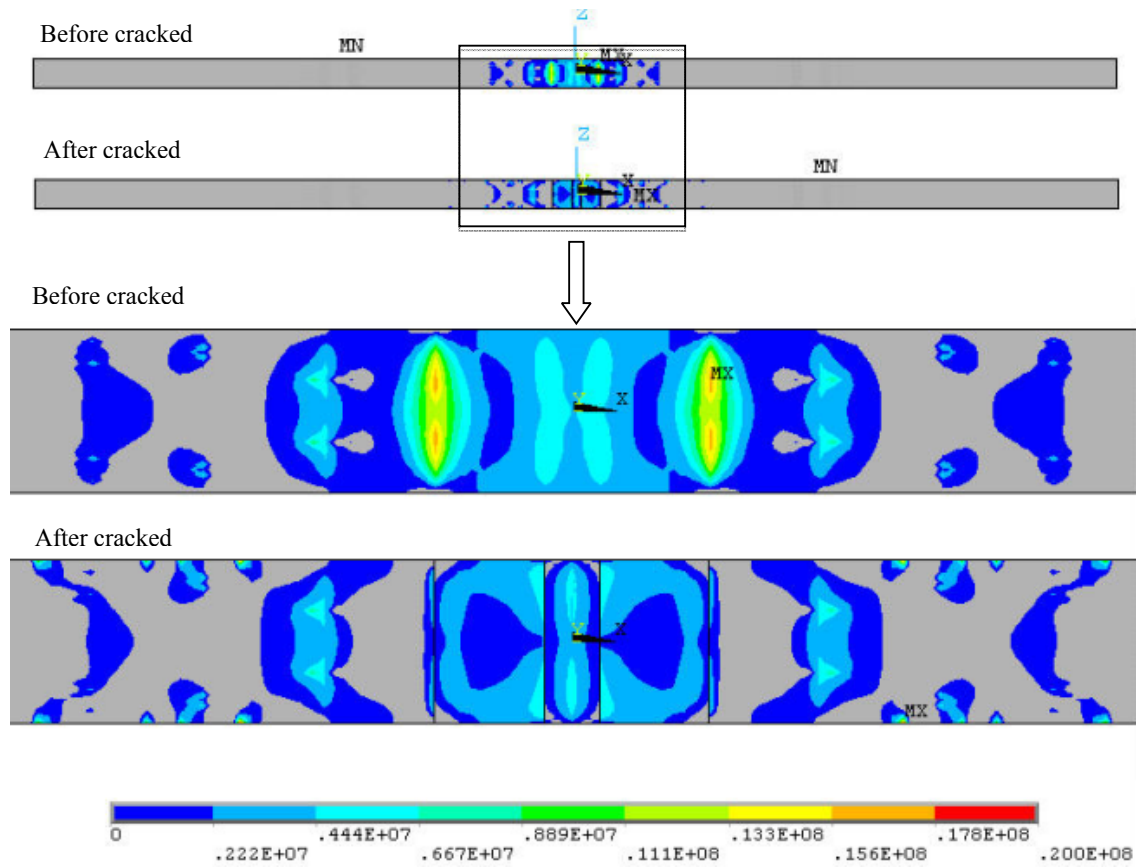
5.2 Formulations of Fatigue Accumulation

To account for different stress ranges due to various truck loads, a linear damage accumulation law is usually assumed in literatures [8]:

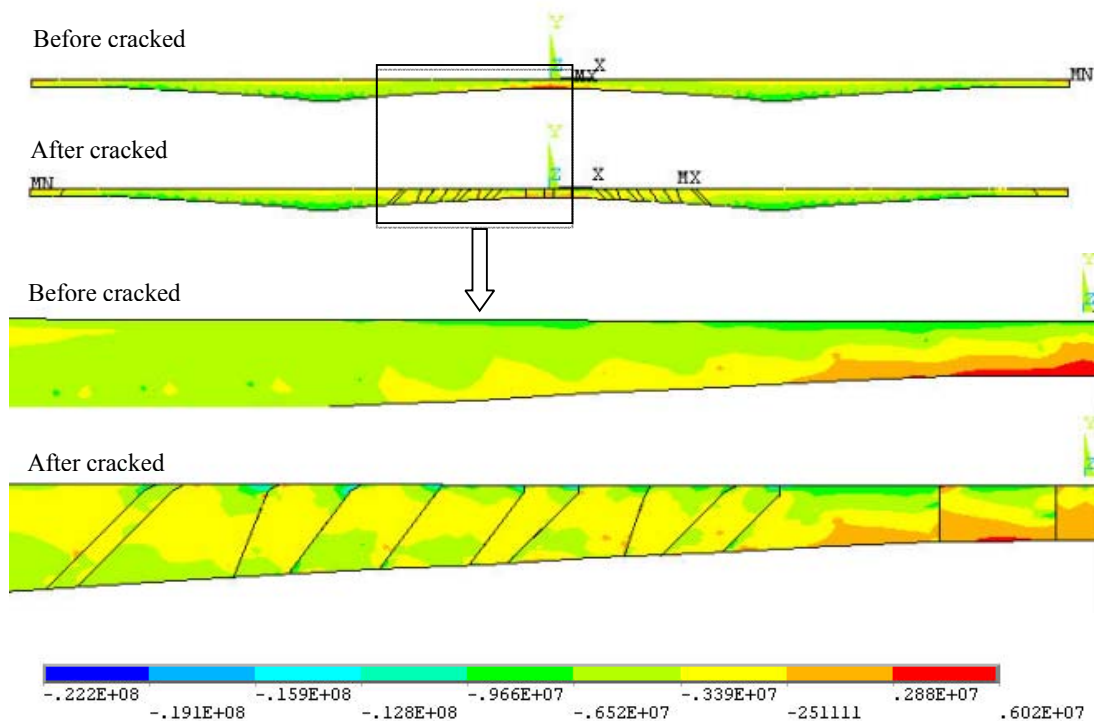
$$T = \sum_i \frac{n_i}{N_i} \quad (1)$$

where n_i is the number of applied load cycles at constant stress level S_i and N_i is the fatigue life at constant stress level S_i , obtained from the S-N curve; T is the fraction of life consumed by exposure to the cycles. For a linear S-N curve with a slope of -3 , as stipulated in AASHTO LRFD Bridge Design Specifications [AASHTO (2010)] [15], Schilling et al (1978) stipulated that:

$$\sum_i \frac{n_i}{N_i} = \frac{\sum_i n_i}{N_e} = C \quad (2)$$



(a) Comparison of Tension Stress of Bottom Slab with and without Cracks



(b) Comparison of Tension Stress of Web Slab with and without Cracks

Figure 5. Comparison of FEM Analysis Result of Design and Cracked Structure

where N_e is the computed fatigue life using the equivalent constant amplitude stress range S_{re} ; and $N_e = C_3 / S_{re}^3$. A log-log diagram combining the above equations and solving for S_{re} provides:

$$S_{re} = \left[\sum_i \gamma_i S_{ri}^3 \right]^{1/3} \quad (3)$$

where $\gamma_i = \frac{n_i}{N}$ is the percentage of occurrence of stress range S_{ri} in the histogram. The above equation is the equivalent stress range for fatigue life estimation under variable amplitude stress ranges as in AASHTO 2010[15]. Therefore, fatigue life can be accordingly calculated as [17]:

$$N_e = C_3 / S_{re}^3 \quad (4)$$

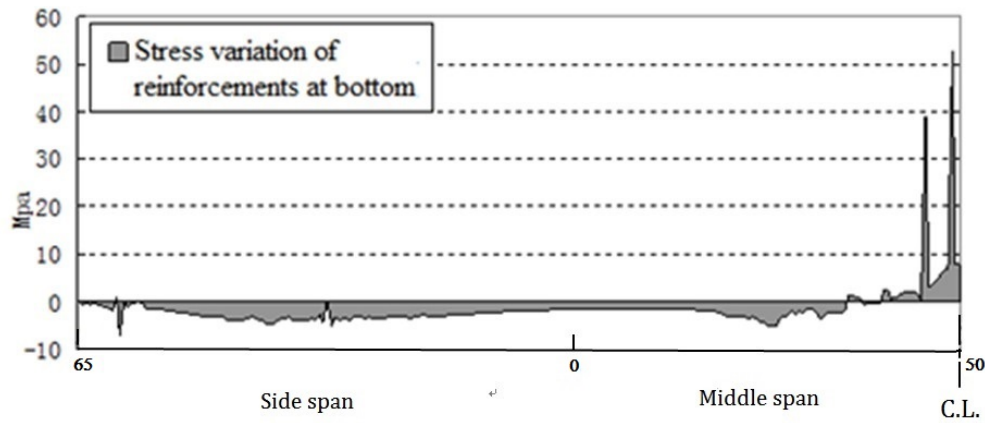


Figure 6. The Stress Variation of Reinforcement Due to the Cracking

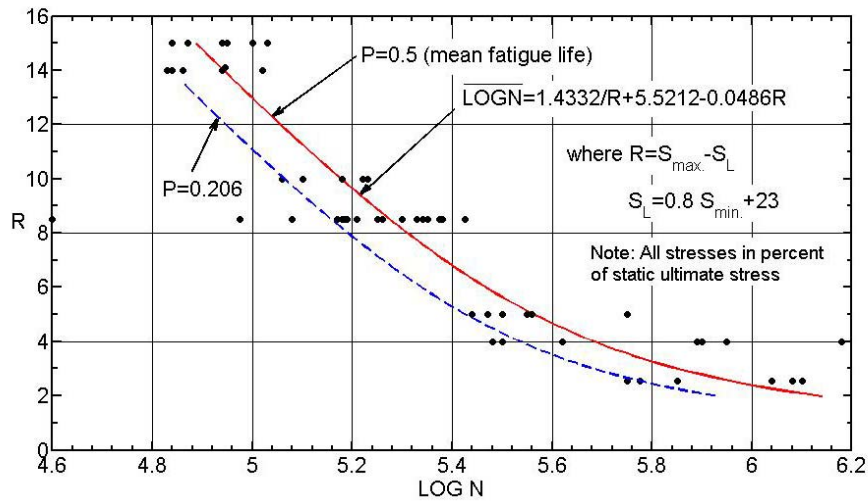


Figure 7. Fatigue Strength Curves for Direct Stress Ranges [3]

5.3 Determination of Equivalent Stress Range

Actual truckload data collected using a discrete bridge WIM system was used in the model. The data include axle loads, truck gross weight, axle configuration, and statistical data on multiple presence side by side or following. In order to determine the equivalent stress ranges induced by vehicular loadings, all the truck loading combinations are categorized into three cases: single, following, and side by side, as shown in Figures 8, 9 and 10, respectively. The statistical presence probability for each case has been roughly assumed according to Nassif et al 2003 [18]. Stress ranges of pre-stressed tendons at critical cross-sections of interest, e.g., middle span, quarter span, and piers, due to truck loadings are calculated and summarized using the verified FE model above. The vehicle weight was scaled to the measured data from WIM system.

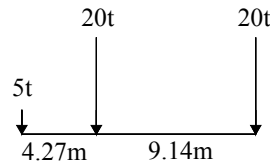


Figure 8. Truck Loading Combination: Single

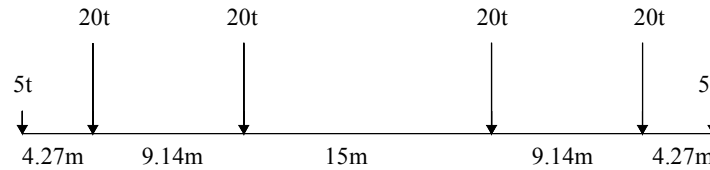


Figure 9. Truck Loading Combination: Following

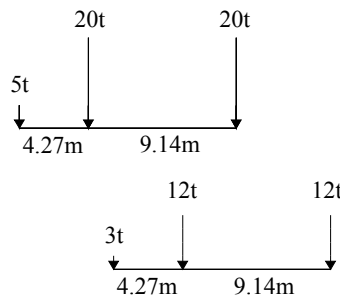


Figure 10. Truck Loading Combination: Side-by-Side

5.4 Fatigue Life Results Analysis

The fatigue strength comparison between pre-stressed concrete beams before and after cracking was shown in Table 5. The table presented the procedure of fatigue strength calculation, and as a result, the fatigue strength at middle spans controlled the fatigue service life over that at other cross-sections. In the table, trucks lighter than 20 tons were not accounted for and stress ranges lower than 4 MPa were considered as noise. As a summary, the effective stress range of pre-stressed concrete beams before cracking was 11.14 MPa while it increased to 20.61 MPa after

cracking. Accordingly, the fatigue service life reduced from infinity to 5.82E+07 cycles due to concrete beam cracking. The service year could be calculated based on the annual average daily traffic (AADT) given in Table 5 and with light trucks causing small stress ranges eliminated from the account.

Table 5. Fatigue Strength Calculation using WIM Data

Without Cracks				With Cracks			
S_{ri}	Cycles	Frequency (α)	$\alpha_i S_{ri}^3$	S_{ri}	Cycles	Frequency (α)	$\alpha_i S_{ri}^3$
4	6015	13.06%	8.36	4	811	1.76%	1.13
6	6346	13.78%	29.77	6	1253	2.72%	5.88
8	11488	24.95%	127.73	8	1147	2.49%	12.76
10	8467	18.39%	183.86	10	1518	3.30%	32.98
12	5312	11.53%	199.32	12	1583	3.44%	59.45
14	4002	8.69%	238.48	14	2824	6.14%	168.44
16	1657	3.60%	147.37	16	3712	8.07%	330.44
18	1278	2.78%	161.91	18	4561	9.91%	578.09
20	1118	2.43%	194.17	20	5843	12.70%	1015.88
22	292	0.63%	67.46	22	5103	11.09%	1180.98
24	36	0.08%	10.72	24	4271	9.28%	1283.25
28	28	0.06%	13.23	28	3523	7.66%	1680.59
32	5	0.01%	3.43	32	4076	8.86%	2902.60
34	4	0.01%	3.15	34	2695	5.86%	2302.00
36	1	0.00%	1.25	36	1253	2.72%	1270.75
40	1	0.00%	0.99	40	937	2.04%	1303.19
>4 0	1	0.00%	0.60	>4 0	902	1.96%	529.42
Effective Stress Range [$(\sum \alpha_i S_{ri}^3)^{1/3}$]			11.14MPa	Effective Stress Range [$(\sum \alpha_i S_{ri}^3)^{1/3}$]			20.61MPa
Fatigue Life in Cycles			Infinity	Fatigue Life in Cycles			5.71E+07

6. CONCLUSIONS

Finite element analysis was performed for a typical long span continuous pre-stressed concrete bridge before and after cracking. A general fatigue life estimation procedure was proposed to simplify the vehicular loading on a bridge and to develop fatigue life analysis using WIM data. The fatigue resistance of the target bridge due to vehicular loads was summarized. The study leads to better understanding and possible design modifications of long span continuous PC bridges. The main conclusions are summarized as follows:

- (1) The cracks in the bridge increase as the vertical deflection increases, and the cracks may increase the loss of pre-stress and more deflection.

- (2) Cracks released the concrete stresses intension, which increased the stress in compression. The cracks made the forces in concrete transfer to the reinforcements and pre-stressed tendon. The cracks caused large stress range of reinforcement, which may have fatigue problems during the service time.
- (3) The vehicle loads on the bridge have changed a lot compared with the base data obtained in 1990s according to the design specification in China, and the vehicles response should be reconsidered.
- (4) According to fatigue strength calculation using WIM data, the fatigue life of the bridge after cracking at the middle span was not infinite any more but possibly a limited value depending on various parameters such as traffic load, pre-stressed tendon configurations, etc.

REFERENCES

- [1] Patnaik, A., Shan, X., Adams, M., Srivatsan, T. S., Menzemer, C.C. and Payer, J., " Isolating Corrosion of Steel Plates Coupled with Titanium", *Advanced Steel Construction*, 2014, Vol. 10, No. 2, pp. 216-233.
- [2] Ruan, X. Shi, X.F. and Frangopol, D.M., "Extension Bridge Service Life based on Field Test and Condition Assessment" A Case Study of Long-span Continuous PC Bridge" *The 10th International Conference on Structural Safety and Reliability (ICOSSAR2009)*, 2009.
- [3] Warner, R.F. and Hulsbos, C.L., "Probable Fatigue Life of Prestressed Concrete Beams-Part IV: Estimation of Beam Fatigue Life" *Fritz Engineering Laboratory Report No. 223.24C4*, 1964.
- [4] Lindorf, A. and Curbach, M., "Fatigue of Bond between Reinforcement and Concrete under Transverse Tension" *Fib Symposium PRAGUE 2011, Session 5-5 Composites and Hybrids*, 2011.
- [5] Tilly, G.P., "Fatigue Testing and Performance of Steel Reinforcement Bars" *Materials and Structures*, 1984, Vol. 17, pp. 43-48.
- [6] Helgason, T., Hanson, J.M., Somes, N.F., Corle, G. and Hognestad, E., "Fatigue Strength of Hig-yield Reinforcing Bars" *Nchrp Report N.169*, *Transportation Research Board*, Washington, 1969.
- [7] Raithby, K.D., "Flexutural Fatigue Behavior of Plain Concrete", *Journal of Fatigue Engineering Materials and Structures*, 1979, Vol. 2.
- [8] Miner, M.A., "Cumulative Damage in Fatigue", *Journal of Applied Mechanics*, 1945, Vol. 12, pp. A159-A164.
- [9] Anon, "Good Detailing Extends Fatigue Life of Reinforcement", *New Civil Engineering*, 1978, No. 310. Sept.
- [10] Soretz, S., "Fatigue Behavior of High Yield Steel Reinforcement", *Concrete Construction Engineering*, 1965, Vol.60.
- [11] Tilly, G.P., "Fatigue of Steel Reinforcement Bars in Concrete: Review", *Fatigue and Fracture of Engineering Materials and Structures*, 1979, Vol. 2, No.3, pp. 251-268.
- [12] Menzies, J.B., "The Fatigue Strength of Steel Reinforcement in Concrete", *Building Research Station*, 1971.
- [13] Zeng, Z. and Li, Z., "Research on Fatigue S-N Curves of Reinforcements in Reinforced Concrete Beams", *China Civil Engineering Journal*, 1999, Vol.32, No.5, pp. 10-14. (in Chinese)
- [14] Nurnberger, U., "Fatigue Resistance of Reinforced Steel", *Proceeding Int. Ass. Bridge Structure Engineering, Lausanne, IABSE*. 1982, Vol. 37.

- [15] AASHTO, Load Resistance and Factor Design, Bridge Design Specifications, 5th Edition. America Association of State Highway and Transportation Official, Washington, D.C., 2010.
- [16] General Code for Design of Highway Bridges and Culverts (JTC D60—2004), People's Communication Press, Beijing. (in Chinese)
- [17] Xia, Y., Nassif, H., Hwang, E.S. and Linzell, D., "Optimization of Design Details in Orthotropic Steel Decks Subjected to Static and Fatigue Loads", Transportation Research Record, 2013, Vol. 2331, pp. 14-23.
- [18] Nassif, H., Liu, M. and Ertekin, O., "Model Validation for Bridge-Road-Vehicle Dynamic Interaction System", J. Bridge Eng., 2003, Vol. 8, No. 2, pp. 112-120.

LIFE-CYCLE COST BASED MAINTENANCE AND REHABILITATION STRATEGIES FOR CABLE SUPPORTED BRIDGES

Chun-sheng Wang^{1,*}, Mu-sai Zhai¹, Hai-ting Li¹, Yi-qing Ni² and Tong Guo³

¹ Engineering Research Center for Large Highway Structure Safety of Ministry of Education, College of Highways, Chang'an University, Xi'an, Shaanxi Province, China

² Department of Civil and Environmental Engineering, The Hong Kong Polytechnic University, Hong Kong, China

³ Key Laboratory of Concrete and Prestressed Concrete Structures of the Ministry of Education, Southeast University, Nanjing, China

*(Corresponding author: E-mail: wcs2000@chd.edu.cn)

ABSTRACT: Initial cost was mainly considered in constructing a bridge in the past, whereas future payments such as the cost of strengthening or rehabilitation were neglected. This situation has brought numerous economic as well as social problems due to the lack of rational maintenance and rehabilitation strategies. Thus, it is necessary and urgent to develop appropriate bridge maintenance and rehabilitation strategies that not only meet serviceability criteria but also consider the life-cycle cost (LCC) optimization. This paper discusses major hazards of in-service cable supported bridges, including fatigue cracking of orthotropic steel decks, deterioration of cables, damage of main cables, hangers and expansion joints et al. Advanced maintenance and rehabilitation tools are introduced to save the life-cycle cost, acoustic emission monitoring technique and cold retrofit technique are detailed studied. A framework is provided for the strategies of maintenance and rehabilitation based on life-cycle cost. The framework takes into account of the safety, serviceability and sustainability during the lifetime of cable supported bridges.

Keywords: Cable supported bridge, Fatigue and fracture, Durability, Life-cycle cost, Maintenance and rehabilitation, Cold retrofit technique, Sustainability

DOI: 10.18057/IJASC.2015.11.3.12

1. INTRODUCTION

Cable supported bridges, namely suspension bridges and cable-stayed bridges are important structures to the highway and railway infrastructures as they usually cross major rivers and act as critical links between highly habited zones [1]. In recent years, bridge engineering in China has progressed significantly and achieved marvellous success [2-3]. The design and construction of cable supported bridges has progressed considerably in China since 1980s. Main span lengths of the cable supported bridges were less than 300m in the 1980s and reached over 1000m in the 21st century. For example, Sutong cable-stayed bridge has a main span length of 1088m, and the Xihoumen suspension bridge has a main span length of 1650m. Tables 1 and 2 show the major suspension bridges and cable-stayed bridges constructed in China in the late 20th century, respectively. Cable supported bridges in China are relatively new and are still in an early stage of their expected service life. Some major hazards have been observed especially in those constructed in the 20th century. The maintenance and rehabilitation of these bridges are of great importance.

During a period of about 15 years, thirteen suspension bridges and twenty-two cable-stayed bridges with mains span over 400m were constructed across China [4]. The conditions of these bridges have begun to deteriorate and various damages continuously accumulate during their service life. Cable supported bridges may experience poor performance or even collapse much earlier than expected in their service life if no sound maintenance and rehabilitation strategies are taken place.

Problems mainly include fatigue failure of the orthotropic steel deck, fracture or deterioration of main cables and hangers, as well as wear and damage of expansion joints, due to wheel loading, harsh environments and natural hazards. Besides, as the traffic needs for them are very large in most cases, consequences of their closure or even traffic capacity reduction may lead to inconvenience for users and thus result in significant losses of society and economy. Therefore, sound maintenance and rehabilitation strategies for cable supported bridges are important for the purpose of providing an acceptable standard of safety and serviceability, as well as meeting the sustainability and low carbon energy requirements during their operation service time.

Table 1. Suspension Bridges Constructed in China in the Late 20th Century

No.	The Name of Bridge	Constructed Year	Main Span Length (m)
1	Sichuan Hanyuan Bridge	1982	208
2	Tibet Dazi Bridge	1984	500
3	Fujian Taining Bridge	1989	284
4	Sichuan Fengjie Bridge	1990	205
5	Shantou Bay Bridge	1995	452
6	Hubei Xiling Bridge	1996	900
7	Guangdong Humen Bridge	1997	888
8	Hongkong Tsingma Bridge	1997	1377
9	Sichuan Fengdu Bridge	1997	450
10	Xiamen Haicang Bridge	1999	648
11	Jiangsu Jiangyin Bridge	1999	1385

Table 2. Cable-stayed Bridges Constructed in China in the Late 20th century

No.	The Name of Bridge	Constructed Year	Main Span Length (m)
1	Guangzhou Haiyin Bridge	1988	175
2	Shanghai Nanpu Bridge	1991	423
3	Shanghai Yangpu Bridge	1993	602
4	Hubei Yunyan Bridge	1993	414
5	Wuhan Erqiao Bridge	1995	400
6	Anhui Tongling Bridge	1995	432
7	Chongqing Lijiatuo Bridge	1996	444
8	Hongkong Kap Shui Mun Bridge Bridge	1997	430
9	Shanghai Xupu Bridge	1997	590
10	Hongkong Tingkau Bridge	1998	475
11	Fujian Queshi Bridge	1999	518

During the past few decades, more and more engineers, researchers and managers have recognized that low tender prices usually may not lead to low lifetime costs and thereby the concept of life-cycle cost (LCC) of civil infrastructures have been widely adopted. Researchers and owners are more and more oriented to the promotion of sustainability as well as achieving the goal of life-cycle performance optimization with respect to the economic, environmental and social demands. As defined by the United States Department of Transportation that, life-cycle cost assessment (LCCA) is an evaluation technique which insists life-cycle cost optimization. It has been more and more widely used by the transportation agencies for new bridge construction projects as well as in-service bridge maintenance and rehabilitation.

In 1995, Mohammadi identified some key factors affecting the LCC of bridges [5]. They also proposed an optimized method for making rational decisions in scheduling the time and selecting candidate bridge components. Frangopol and his team [6-12] have discussed the past, present, and future of life-cycle design, inspection, assessment, rehabilitation and management of bridge structures. They also did research about optimum maintenance strategies and indicated that additional research works are required to develop a better life-cycle model. In addition, they also announced that tools to quantify risks, costs as well as benefits associated with bridges are needed. In order to ensure an adequate level of reliability at a minimal LCC, two maintenance models known as the Rijkswaterstaat's model and the Frangopol's model for deteriorating civil infrastructures were described and compared in 2006. Many studies were made about the life-cycle cost analysis, design, evaluation, rehabilitation, management, and maintenance of civil infrastructure system. However, the study of cable supported bridge maintenance and rehabilitation based on life-cycle cost is limited. It is necessary and urgent to develop appropriate maintenance and rehabilitation strategies that not only meet serviceability criteria but also consider the life-cycle cost optimization.

2. MAJOR HAZARDS OF CABLE SUPPORTED BRIDGES

2.1 Fatigue Cracking of Orthotropic Steel Decks

Orthotropic steel decks (OSDs) have been widely used in cable supported bridges for several decades in parts of the world for they are considerably lighter, thus allow longer spans to be efficiently designed [13]. Although the technology was developed in the 1970s, the use of OSDs in China began relatively late compared to US, Europe and Japan. Many long span cable supported bridges in China have adopted OSDs recently, such as Guangdong Humen Bridge, Xiamen Haicang Bridge, Nanjing Yangzi River Second Bridge, Jiangsu Jiangyin Yangzi River Bridge and Jiangsu Sutong Yangzi River Bridge. To date, there are about 30 cable supported bridges using orthotropic steel decks with main spans over 400m in China. The longest of these is the 1650-meter Zhoushan Xihoumen Suspension Bridge, which was opened to traffic in 2009 [2, 4]. The complex configurations and direct exposure to repeated vehicular loading lead to relatively high levels of stress concentration. Many details of OSDs are fatigue-sensitive. Recently, more and more engineers, researchers, as well as bridge owners pay more attention to the fatigue problem of the OSDs since a large number of fatigue cracks have been found [14]. As shown in Figure 1[15], hundreds of fatigue cracks have been detected in the steel decks of the 888-meter long box girder of Guangdong Humen Bridge just ten years after opening to traffic.



Figure 1. Cracking in Deck Plates and Along Fillet-welds Between Ribs and Deck Plates

In OSDs, details such as cut-outs in diaphragms, rib-to-diaphragm and rib-to-deck joints are susceptible to fatigue failure [16]. A complex combination of in-plane and out-of-plane stress may happen due to the distortion of diaphragm and web of rib under the action of repeated vehicular loading. Besides, as closed stiffening ribs can only be welded from the outside, the quality of such

welding is difficult to be guaranteed. As a result, fatigue damage is easy to be found in these zones. Presently, however, the number of full-scale fatigue test studies of OSDs in China is limited and it has restricted the application of OSD in cable supported bridges to some extent. Therefore, based on typical OSD for the long-span cable-stayed bridges, a full-scale orthotropic steel deck model was conducted at the bridge engineering laboratory of Chang'an University. Figure 2 shows the test setup and specimen dimensions.

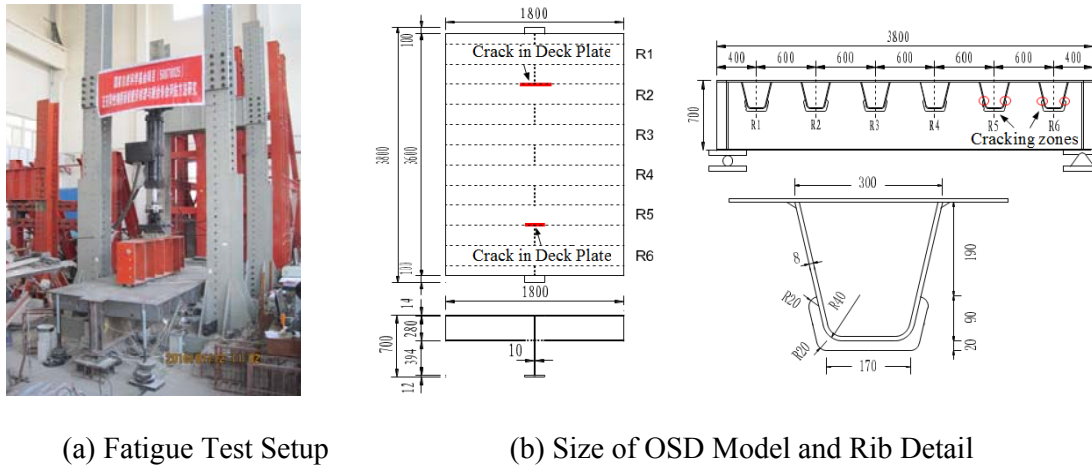


Figure 2. Full-scale Fatigue Test Model of OSD (Unit:mm)

Fatigue cracks were not found in rib-to-diaphragm joint (around Rib 5 and Rib 6) until 5.0 million loading cycles. The fatigue cracks initiated from the weld toe of rib-to-diaphragm joint and propagated into the rib web. The total length of fatigue cracks are 25mm for Rib 5 and 16mm for Rib 6 during the entire 10.2 million cumulative loading cycles, as shown in Figure 3(a). For rib-to-deck joint, fatigue cracks initiated from the weld root of rib-to-deck joints and extended through the deck plate were also found during the fatigue test, shown in Figure 3(b). The total length of fatigue crack around Rib 2 is 90mm, and fatigue crack around Rib 5 is 47mm at the end of the test. Besides, fatigue cracks in the diaphragm cut-outs are generally perpendicular to the free edges and propagate into the diaphragms. However, no visual fatigue cracks were found in the free edges of diaphragm cut-outs at the end of the test.

Compared with OSDs used in girder bridges, the OSDs used in cable supported bridges may expose to harsh environmental conditions for these bridges usually cross major rivers or bays and not only suffer from corrosion due to the presence of humidity and oxygen, but also may expose to chlorides accelerates chemically aggressive marine environments. Therefore, it may lead to corrosion fatigue problems, for the OSDs under joint action of both corrosion and repeated loading. Particularly, highly aggressive situations may occur when deicing salt is used on the bridge decks, melting ice and pouring brine into bridge structures. This phenomenon shouldn't be confused with stress-corrosion cracking in which corrosion would lead to a development of brittle fracture under sustained tension [17].

2.2 Deterioration of Stay Cables

Stay cables are important structural elements and their integrity directly affects the overall safety of cable-stayed bridges. Stay cables are made of high strength steel strands and are susceptible to corrosion with the presence of humidity and oxygen. Under the action of repeated vehicle load, stay cables may initiate fatigue cracks and in the meanwhile, the buffeting and fluttering vibrations caused by wind and rain would increase the stress in the stay cables and make the fatigue problem

worse. This may destroy the protection system of stay cables and accelerate the corrosion process as shown in Figure 4[18].

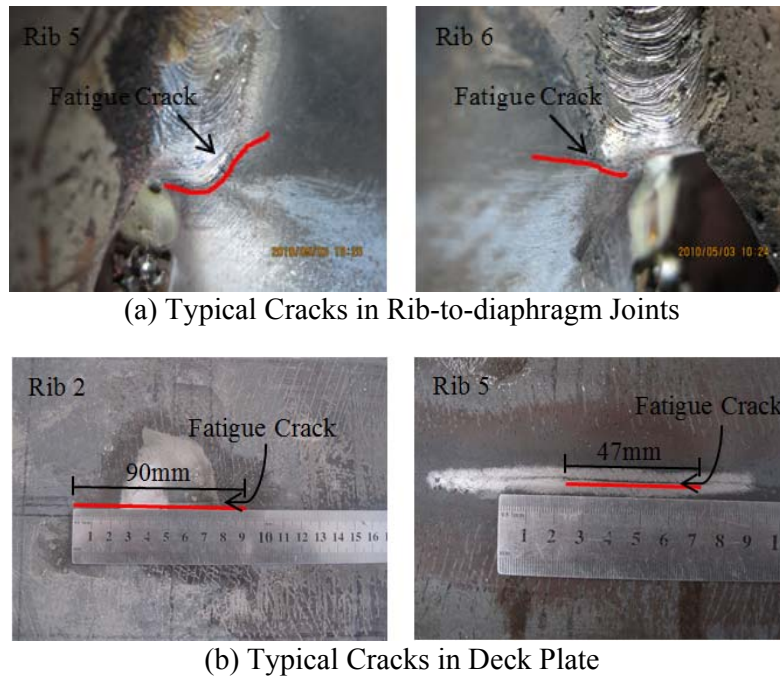


Figure 3. Typical Fatigue Cracks Observed During Orthotropic Steel Deck Test

Deterioration of stay cables mainly refers to damage in the cover, corrosion of steel wires, fatigue of cable and cable anchor systems, and other damages caused by excessive vibration. The corrosion of stay cables includes uniform corrosion, dent corrosion, crack corrosion, stress corrosion and corrosion fatigue. Anti-corrosion measures should be made on a case-by-case basis since each bridge is different in production, transportation, storage, erection and maintenance.

Commonly used PE protective cover of stay cables may deteriorate due to damages such as transverse cracks, longitudinal cracks, scratches, corrugations and indentations. After these, corrosion of the steel wire may accelerate. In addition, the actions of wind and rain, or the vibration of the bridge tower and deck, vibrations such as wake galloping, vortex-induced vibration, rain vibration, parametric-induced vibration as well as buffeting may occur. Some of these vibrations' amplitudes are not big, but the frequency is relatively larger while others amplitudes may be big, but the occurrence is relatively low. Such vibrations of the stay cables are the main cause of fatigue in the vicinity of the anchorages of cable-stayed bridges and may also damage the corrosion protection system of cables or even lead to the failure of stay cables.

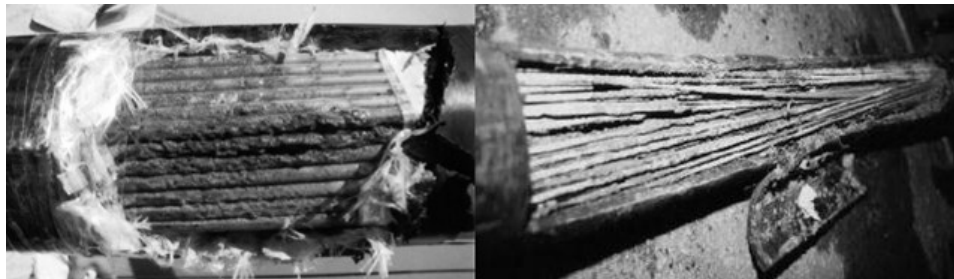


Figure 4. Corrosion of Stay Cables[18]

2.3 Damage of Main Cables and Hangers

The main cables and hangers are essential elements of a suspension bridge and in the meanwhile, they are also the most difficult components to maintain [19]. Thus, more attention should be paid to their maintenance and rehabilitation. Besides, a main cable's damage has always been associated with corrosion and the damage of hangers has always been associated with corrosion or vibrations such as buffeting, galloping and rain vibration or a combination of these [20].

Similarly to orthotropic steel decks and stay cables, the main cables and hangers of suspension bridges sometimes are exposed to harsh environmental conditions for the bridges located in chemically aggressive marine environments. Substances such as chlorides, oxygen and so on would eventually percolate into the gaps of the main cables and hangers through rain and water, which may lead to the corrosion of the steel strands. Figure 5 shows the details of corroded steel strands [21].

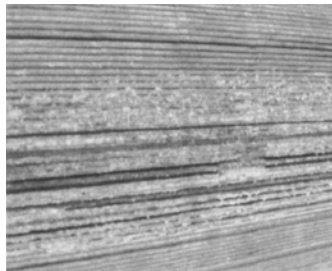


Figure 5. Details of Corroded Steel Strands [21]

2.4 Damage of Expansion Joints

As the temperature changes, the girder of cable supported bridges will experience expansion and contraction which may lead to longitudinal strain in the girder. In the meanwhile, the bridge deck will produce longitudinal displacements under vehicle loads. In order to meet the requirements of such strain and deformation, it is necessary to set expansion joints between the bridge girder and the abutment or between hinged joints.

As expansion joints are repeatedly subjected to vehicle loads, even a very small unevenness can cause a great impact. Expansion joints have been recognized as weak components in cable supported bridges for a long time. In addition, along with the rapid increase of traffic volume and the unavoidable phenomenon of overload, the impact of expansion joints increases. This may accelerate the wear and damage of expansion joints and cause both economic and social problems in maintenance and rehabilitation during the operation service time. Sørensen concluded that during the operation service life [20], compared with other maintenance, rehabilitation and replacement cost, the cost for movement elements such as expansion joints is usually a major expense.

3. ADVANCED TOOLS FOR MAINTAINENCE AND REHABILITATION

3.1 Acoustic Emission Technique

The acoustic emission (AE) technique is a non-destructive testing tool for real time monitoring of material damages. It has been widely used in aerospace, machine manufacturing pipelines, and many other fields. In bridge engineering, AE technique has been used to monitor concrete cracks

[22], pre-stressed concrete defects [23], and cable conditions [24]. It can also be used to monitor the fatigue damage process of cable supported bridges and become an important part of structural health monitoring. When cable supported bridges are under loads, the steel components such as orthotropic steel decks and stay cables will emit energy in the form of elastic waves due to various material-relevant damage mechanisms [25]. These waves can be detected by attached AE sensors [26-28] and further evaluation of the collected data can be used to assist decisions for bridge maintenance and rehabilitation.

The notable merits of AE technique for bridge fatigue damage monitoring of OSDs, stay cables and hangers etc. [29], including: (1) AE signals generated by fatigue crack growth are the result of the structural load history; (2) AE technique can be applied not only for local and short time monitoring, but also for overall and long term monitoring without interrupting the traffic; (3) Detection, location and analysis techniques have been improved greatly; (4) AE data are observable in real time through advanced data acquisition systems.

Locating the damage source (e.g. a cracking or a wire break activity) is an important characteristic of AE for structural health monitoring [30]. As shown in Figure 6, two sensors are set at a distance of L and when the crack propagates between the two sensors at a distance of l to the sensor 1, the reaching time to sensors $S1$ and $S2$ can be measured respectively as τ_1 and τ_2 . According to the different reaching time of the two sensors and the speed v in a particular material, the acoustic source can be located in the form of Eq. 1.

$$l = \frac{L - (\tau_2 - \tau_1) \cdot v}{2} \quad (1)$$

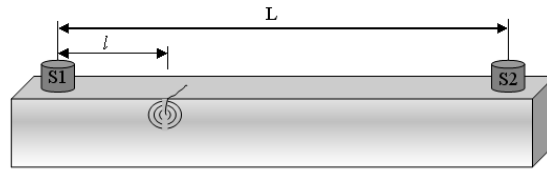


Figure 6. Model of AE Locating

In order to locate crack propagations of plane structures such as orthotropic steel decks, three sensors need to be used based on the same principle described above. However, as noises may occur during AE monitoring, which can lead to a side-effect on judging crack propagation signals, it is important to confirm the features of the crack propagation signals properly and correctly.

3.2 Application

A full-sized OSD specimen, which can be widely used in cable supported bridges, which is 6.1m×3.0m×0.53m, including 5 ribs with the spacing distance of 600mm. The thickness of top plate is 14mm, the diaphragm is 10mm, and the dimension of U-shape rib is 300mm×280mm×8mm, which were made by Q345qD. Piezoelectric paint sensors, commercial acoustic emission sensors as well as strain gauges were used to monitor and evaluate the fatigue cracks. Figure 7 shows the test setup and the locations of stress measurement at butt-weld joints where piezoelectric paint sensors and commercial acoustic emission sensors were attached.

In order to simulate real traffic load, fatigue load was applied to 2 loading area with 200mm long and 600mm wide, the spacing distance is 1800mm, and the fatigue load range is 300kN, shown in Figure 8. Strain measure points were arranged at the longitudinal connection to monitor the stress changes.



Figure 7. Laboratory Test Set-up and AE Sensor Placement

The circular shaped piezoelectric paint sensors, see Figure 7(b), have a diameter of 12 mm and a thickness of 0.5 mm as with a 42% volume fraction of PZT-5A. The stress monitoring results showed that the stress range at the bottom butt-welds of Rib 5 was around 70 MPa under fatigue load range of 300 kN before 2 million load cycles. From 2 to 3 million cycles, the stress range reduced from 70 MPa to 60 MPa, which indicated fatigue crack initiation and propagation. From 3 to 3.4 million cycles, the stress range decreased at a very fast rate and several long cracks were found at bottom butt-welds of Rib 5. In order to evaluate the performance of piezoelectric paint sensor in detecting AE events associated with fatigue crack initiation and propagation, the commercial AE sensors supplied by Physical Acoustics Company (PAC) and attached to the specimen with vacuum grease and held in place with plastic clamps were installed at the same zones after 3 million load cycles, as shown in Figure 7(c).

In this experimental fatigue research, the piezoelectric paint sensors were connected to a custom-designed signal conditioning circuit comprised of preamplifier with low pass and high pass filters. The amplifier voltage gain was set as 40 dB, while the bandwidth of band pass filter was from 5 to 600 kHz. AE data were processed and displayed through a DISP-16 outdoor acquisition work station manufactured by Physical Acoustics Company. To minimize extraneous noise while allowing for the record of genuine AE signals, the threshold of each AE channel was set as 45 dB. To assure the condition of each sensor and the locating capability of the sensors arrangement, pencil lead break (PLB) tests were conducted before testing.

Several types of AE signal waveforms were collected by the commercial AE sensors, as shown in Figure 8. The waveform shown in Figure 8(a) is a typical AE waveform for a fatigue crack activity, with shorter rise time, lower counts and higher peak amplitude. In Figure 8(b), the waveform reflects emissions during friction activities. Figure 8(c) is from a PLB test, where the signal rapidly attains the peak amplitude and then fades gradually. These representative waveforms can be used as references to distinguish noise data from the AE signals caused by crack growth.

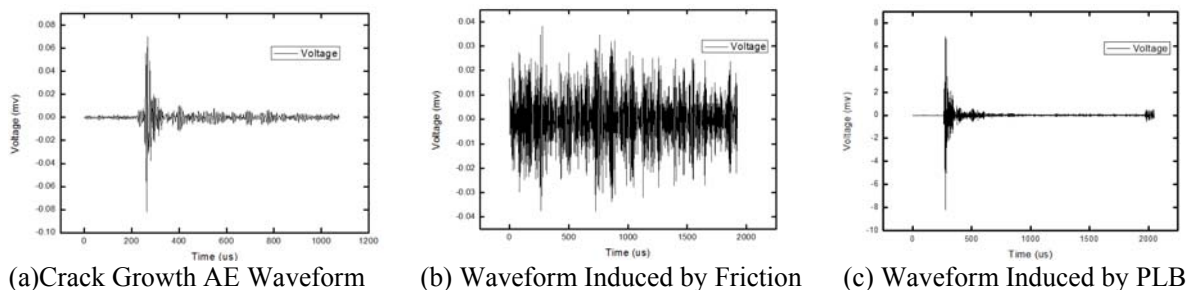


Figure 8. AE Waveforms Reference from Crack Growth, Friction and PLB Tests

Figure 9 shows that the AE signals are concentrated among three sensors one day after three long cracks were found at the bottom butt-welds of Rib 5. Comparing the locating graph with the AE sensors arrangement at the bottom butt-welds of Rib 5 as shown in Figure 7(c), two crack tips at the zone were found where AE signals were concentrated. Consequently, conclusion is drawn that AE signals are related to the existing crack growth activity.

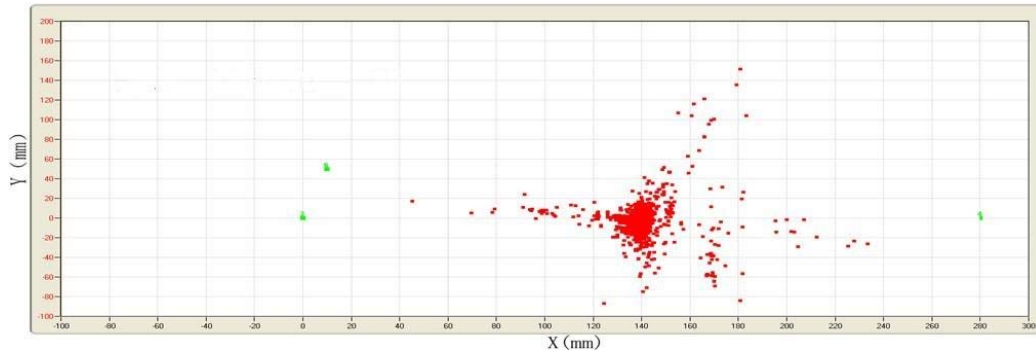


Figure 9. An AE Monitoring Locating Graph

3.3 Cold Retrofit techniques for OSDs

Fatigue cracking is a worldwide engineering problem of orthotropic steel deck (OSD), which affects the service safety and duration of the bridge structures. Since OSD is commonly used modern long span bridges, how to retrofit the fatigue cracks plays an important role in maintenance and rehabilitation for cable supported bridges. According to amount of in-site inspection results and experimental study results, stress levels of typical fatigue details in OSDs are relatively higher due to the thin deck plate, complex configuration and low construction quality. Researchers have tried a lot to find new ways to decrease the stress level, together with the goals to meet the durability and economy demands. Wang proposed concrete composite layer bonding to OSD system by stud welded on the deck system, which was applied to a real steel bridge [31]. Based on the loading test, the stress level of fatigue details is obviously lower compared to other similar bridge. Shao developed an innovative composite bridge deck system with thin reactive powder concrete (RPC) on orthotropic steel plate [32]. Static experiment result shows that tensile stresses in steel deck decrease obviously when the innovative steel-RPC composite deck system is adopted and the maximum reducing amplitude is over 70%.

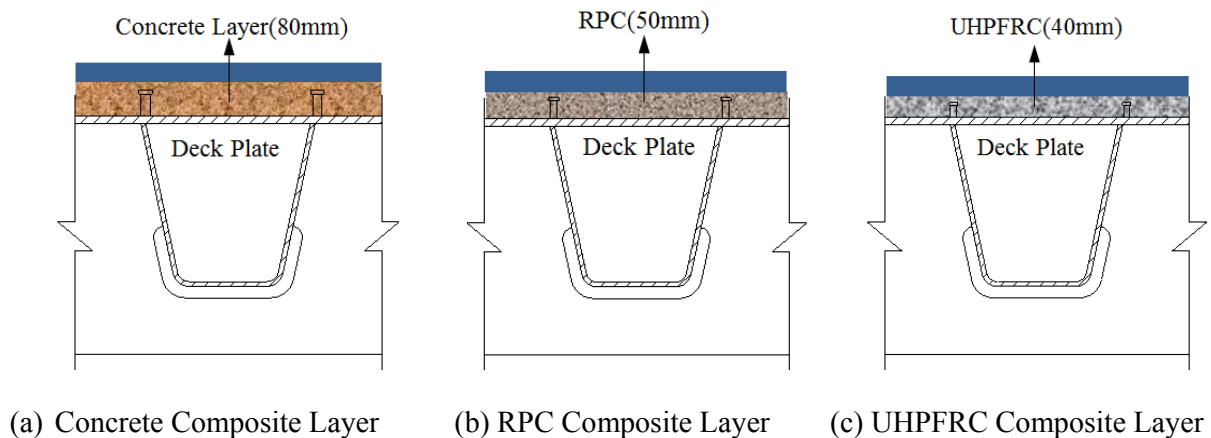


Figure 10. Different Composite Layer for OSDs

In recent years, Ultra high performance fibre reinforced concrete (UHPFRC) have caught engineers' eyes, which is made of silica fume, fly ash, steel fibre instead of coarse aggregates. Researchers have conducted a series of experiments to study the material performance, mechanical performance and the strengthening effect by UHPFRC. In this paper, UHPFRC composite layer is proposed to take place of traditional pavement, ordinary concrete composite layer and RPC composite layer. For the advantages of higher strength and better durability, the thickness of UHPFRC composite layer decreases to 40mm from the 80mm for ordinary concrete and 50mm for RPC (Figure 10). Since welding stud or steel bar as shear connector will bring new fatigue details, cold connecting techniques by high strength adhesive is introduced to connect the composite layer with OSD system.

Composite layer can be not only used in design stage, but also it can be used to maintenance stage. However, the traffic will be suspended when using composite layer to replace old pavement system, which will bring negative social influence and economy loss. Therefore, some researchers tried other means to strengthen the local areas according to the structural characteristic of OSDs. Kolstein installed stop hole on the fatigue crack hole, and bolted steel plate on the cracking region by the high tensile bolts [33]. Tabata developed an innovative method of retrofit OSD without the need for traffic restriction to eliminate fatigue cracks originating from the weld between the deck plate and U-shaped rib [34]. At present, retrofit method for orthotropic steel bridge deck mainly concentrate on mechanical repair or hot repair, the construction process is complex and is easy to bring new damage to the structure. In order to develop generally innovative retrofit method, cold maintenance concept is proposed, i.e. adopting cold connecting plate to strengthen the fatigue region. Compared with the traditional maintenance method, cold retrofit methods can enhance the local rigidity to prevent crack further propagation without any secondary damage. Cold connecting method includes high strength structural adhesive, bolting and self-tapping screw, plate can adopt steel plate, shape steel, sandwich plate system or carbon fibre plate. According to the characteristics of fatigue cracking region, different connecting method and different plate material can be used together for hybrid strengthening (Figure 11).

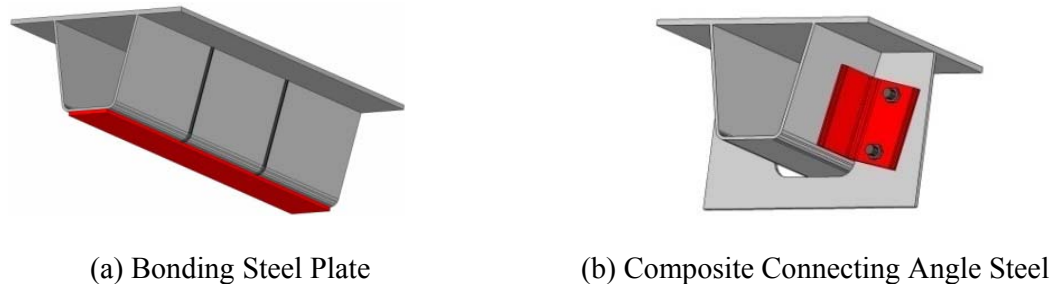


Figure 11. Cold Retrofit Method for OSDs

In order to study cold retrofit method feasibility, a full-scale orthotropic steel bridge deck fatigue test was conducted, the test setup shown in Figure 7. When the loading cycles accumulated to 3 million, the stress of measure point around rib 5 connection decreased, 3 cracks were observed after another 280 thousand cycles. Cold bonding steel plate method was applied to strengthen the fatigue cracking area, the dimension of steel plate is 3400mm×180mm×10mm based on the finite element analysis result (shown in Figure 12). After retrofit, strain gages were arranged on the steel plate corresponding to the gages on the ribs. With the loading cycles accumulating, stress level of longitudinal connection stayed a relatively low level, shown in Figure 13. When loading cycles reached 5.12 million, no crack propagation was observed, and the test was stopped. The test result shows that bonding steel plate can effectively prevent crack propagation, and the fatigue life can be prolonged for 75%.



Figure 12. Strengthened by Bonding Steel Plate

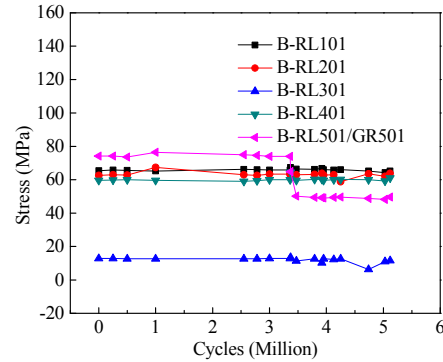


Figure 13. Stress Change Curves

A cable-stayed bridge with steel box girder was taken into study, the span layout is 100m+160m+318m. The steel box girder is comprised of top plate, U-shape stiffener, web, diaphragm and bottom plate, total width of the box girder is 37.1m, including 6 vehicle lanes with 2 hard shoulders. The thickness of top plate is 14mm, the bottom plate is 12mm, and the web and diaphragm are both 10mm. The dimension of U-shape rib is 300mm×280mm×8mm with the center distance is 600mm, and the diaphragm standard spacing is 3750mm, shown in Figure 14. Many fatigue cracks were detected on the orthotropic steel bridge deck after less than 10 years open to traffic, and the cracks are mainly initiated from the rib-to-diaphragm joint and free edges of cutout, shown in Figure 15. According to the characteristics of fatigue crack and cracking position, bonding equal angle steel of Q345 with high strength structural adhesive was adopted to retrofit the orthotropic steel bridge decks. The angle steel dimension was 140mm×140mm×14mm with the length of 220mm.

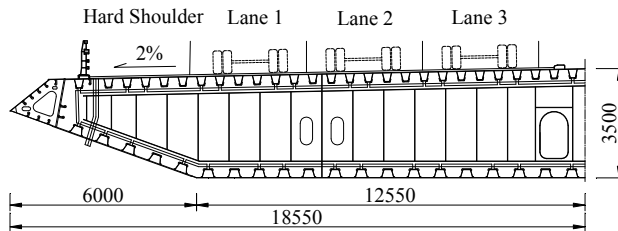


Figure 14. Cross Section of Steel Box Girder (Unit: mm)



Figure 15. Typical Fatigue Crack



Figure 16. Bonding Angle Steel Retrofit Method

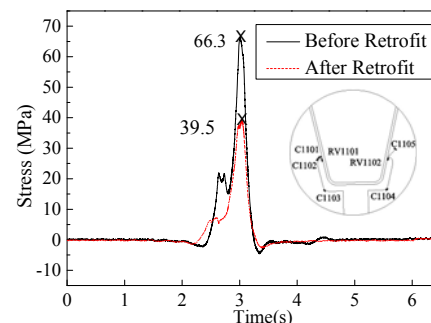


Figure 17. Stress Comparison

In order to determine the cold retrofit effect, several retrofit regions were selected to conduct loading test and dynamic monitoring before and after retrofit. Strain gages were arranged at the crack tip and other typical fatigue details. A 4-axle full truck was chosen to loading the test regions, shown in Figure 16. The axle distances are 1300 mm, 4500 mm and 1800 mm, the axle weights are

30kN, 80kN, 115kN and 115kN. Stress changes of measure point at crack tip were analyzed to assess the cold retrofit effect, shown in Figure 17. Take measure point C1105 as example, before cold retrofit the peak stress reached 66.3MPa, while the peak stress decreased to 39.5MPa after cold retrofit, the decrease rate was up to 40 percent.

3.4 Dehumidification System

Steel corrosion is a recognized cause for deterioration in bridge cables and girders. There were several cases worldwide where rehabilitation and replacement had to be done due to corrosion problems and these led to enormous costs of bridge maintenance [35]. Traditional anti-corrosion protection systems for components such as main cables and steel girder cannot totally prevent corrosion, but merely slow it down. The invention and application of dehumidification systems have proven to be able to totally prevent corrosion.

Generally, dehumidification systems can be designed and installed in components such as main cable, cables saddles and anchor houses of suspension bridges, stay cables of cable-stayed bridges and also steel girders. Moreover, some results of life-cycle cost analysis indicated that installing a dehumidification system may be much more economical than a traditional anti-corrosion system. This may inspire engineers in China when they are dealing with the maintenance of in-service cable supported bridges.

4. LIFE-CYCLE COST BASED MAINTAINENCE AND REHABILITATION STRATEGIES FOR CABLE SUPPORTED BRIDGES

4.1 Life-cycle Cost for Maintenance and Rehabilitation

As life-cycle costs depend on lots of quantitative data rather than some qualitative information, objective and quantitative data should be selected and collected. The life-cycle cost of cable supported bridges should include costs associated with design, construction, management, inspection, maintenance and rehabilitation during the entire service life. All the components and elements that comprise the structure should be taken into consideration when dealing with life-cycle cost optimization.

The cost of maintenance and rehabilitation depends on the reliability level for when the maintenance and rehabilitation work is to be applied. Thus, formulating a reasonable reliability level after maintenance and rehabilitation is important to provide an acceptable level of safety and serviceability during operation service over the entire life cycle. As maintenance and rehabilitation may lead to traffic controls or even closures, inconvenience for the users and the loss of bridge owners should also be concerned when optimizing the life-cycle cost. In addition, before starting rehabilitation, inspections and investigations should be carried out to determine the cause of the damages. The cost of inspections and investigations should also be included. During rehabilitation, it is important to focus on the prevention of traffic interruptions as LCC includes the costs of traffic delays and service time reductions. Besides, as some old cable supported bridges do not have sufficient maintenance access facilities, rehabilitation works are ideal opportunities to upgrade such facilities and in this way, future maintenance cost, which is a part of LCC, will decrease.

Refer to Kong & Frangopol's [10] analysis, the cost of maintenance for cable supported bridges during the service time is suggested to be computed as follows:

$$Cost_M = \sum_{i=1}^N \left\{ \int_0^T \frac{f_i[\alpha_i(t), \beta_i(t), \Delta\beta_i(t)]}{(1+v)^t} g_i(t) dt + \prod_{k=1}^{n-1} r_{ik} \sum_{j=1}^n \varphi_{ij} \right\} \quad (2)$$

Where $\alpha_i(t)$, $\beta_i(t)$, $\Delta\beta_i(t)$ are the deterioration rates of reliability depending on the type of the applied maintenance action, reliability index profile and reliability index change of element i , due to the applied maintenance action; $g_i(t)$ is the probability-density function of element i and T is the end service time; φ_{ij} is the factor concern about the cost caused by traffic control, inspections etc. and r_{ik} are the related coefficient factors; $f_i[\cdot]$ is the cost function and v is the discount rate of money; N is the number of all the elements which need to be maintained.

The cost for rehabilitation can also be computed similarly based on the same method and the rehabilitation strategies for cable supported bridges should also consider such factors.

4.2 Framework of Life-cycle Based Maintenance and Rehabilitation Strategy

A sound life-cycle based maintenance and rehabilitation strategy for cable supported bridges should concern not only the performance of all the components that comprise the whole structure, but also the life-cycle cost, which is made of economic cost (i.e. project design cost, construction cost, monitoring cost, assessment cost, inspection cost, material cost etc.), social cost (i.e. traffic interrupt cost, convenient cost, comfortable cost, user delay cost, reputation cost etc.) and environmental cost. In order to optimize the life-cycle costs during the whole service time as well as considering the safety, serviceability, reliability and sustainability of the cable supported bridges, a preliminary framework of life-cycle based maintenance and rehabilitation strategy is proposed in Figure 18.

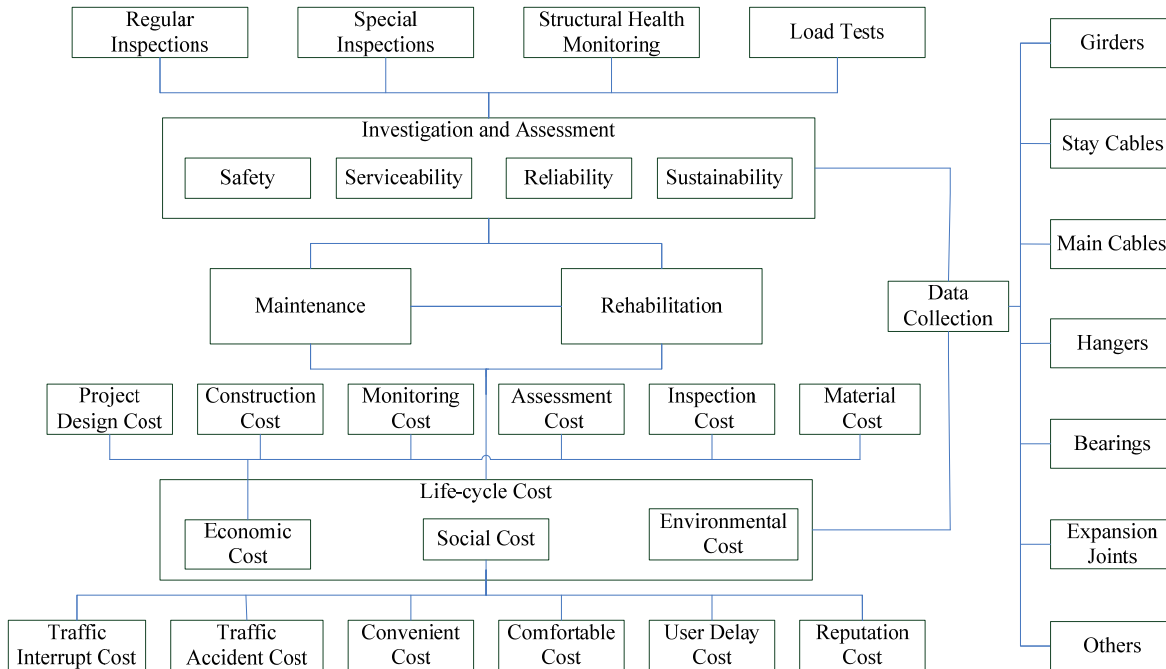


Figure 18. Preliminary Framework of Life-cycle Based Maintenance and Rehabilitation Strategy

5. SUMMARY

Recently, some cable supported bridges have experienced various performance problems or even collapse much earlier than expected in their service life. Maintenance and rehabilitation are necessary to maintain the safety, serviceability and sustainability of these bridge structures. In order to optimize maintenance and rehabilitation interventions and achieve a cost-effective life-cycle performance for in-service cable supported bridges, it is necessary and urgent to establish sound life-cycle based maintenance and rehabilitation strategies. Major hazards of in-service cable supported bridges, including fatigue cracking of orthotropic steel decks, deterioration of cables, damage of main cables, hangers and expansion joints, were analyzed in operation condition. Advanced maintenance and rehabilitation tools are introduced to save the life-cycle cost, acoustic emission monitoring technique and cold retrofit technique are detailed studied. Based on the above results, a preliminary framework of life-cycle based maintenance and rehabilitation strategy is proposed to inspire engineers to take into account of the safety, serviceability and sustainability as well as considering the life-cycle cost during maintenance and rehabilitation.

ACKNOWLEDGMENTS

The authors gratefully acknowledge the financial support provided by National Natural Science Foundation of China (Grant No.51078039), the Major State Basic Research Development program of China (973 Program) Sub-program (2015CB057706), the Special Fund for Basic Scientific Research of Central Colleges of the P.R. China, Chang'an University (10821153501, 310821153401, 310821153314), the Applied Basic Research Program of the Ministry of Transport of the P.R. China (2014319812080), the Jiangsu Transportation Department under grants (Grant No. 2011Y09-2) and the Doctoral Postgraduate Technical Project of Chang'an University (2014G5290008).

REFERENCES

- [1] Gimsing, N.J. and Georgakis, C.T., "Cable Supported Bridges: Concept and Design, Third Edition", John Wiley and Sons, Chichester, UK, 2011.
- [2] Xiang, H.F., Chen, A.R. and Ge, Y.J., "Major Bridges in China", China Communications Press, Beijing, China, 2003. (in Chinese)
- [3] Xiang, H.F. and Ge, Y.J., "State-of-the-art of Long-span Bridge Engineering in China", *Frontiers of Architecture and Civil Engineering in China*, 2007, Vol.1, No.4, pp. 379-388.
- [4] Ge, Y.J. and Xiang, H.F., "Concept and Requirements of Sustainable Development in Bridge Engineering", *Frontiers of Architecture and Civil Engineering in China*, 2011, Vol.5, No.4, pp. 432-450.
- [5] Mohammadi, J., Guralnick, S.A. and Yan, L., "Incorporating Life-Cycle Costs in Highway Bridge Planning and Design", *Journal of Transportation Engineering*, 1995, Vol.121, No.5, pp. 417-424.
- [6] Akgül, F. and Frangopol, D.M., "Lifetime Performance Analysis of Existing Steel Girder Bridge Superstructures", *Journal of Structural Engineering*, ASCE, 2004, Vol.130, No.12, pp. 1875-1888.
- [7] Frangopol, D.M. and Kong, J.S., "Expected Maintenance Cost of Deteriorating Civil Infrastructures", *Life-cycle Cost Analysis and Design of Civil Infrastructure Systems*, Virginia, USA, 2001, pp. 22-47.

- [8] Frangopol, D.M. and Liu, M., "Maintenance and Management of Civil Infrastructure Based on Condition, Safety, Optimization, and Life-cycle Cost", *Structure and Infrastructure Engineering*, 2007, Vol.3, No.1, pp. 29-41.
- [9] Kim, S. and Frangopol, D.M., "Cost-based Optimum Scheduling of Inspection and Monitoring for Fatigue-sensitive Structures under Uncertainty", *Journal of Structural Engineering*, ASCE, 2011, Vol.137, No.11, pp. 1319-1331.
- [10] Kong, J.S. and Frangopol, D.M., "Life-cycle Reliability-based Maintenance Cost Optimization of Deteriorating Structures with Emphasis on Bridges", *Journal of Structural Engineering*, ASCE, 2003, Vol.129, No.6, pp. 818-828.
- [11] Liu, M. and Frangopol, D.M., "Optimal Bridge Maintenance Planning Based on Probabilistic Performance Prediction", *Engineering Structures*, 2004, Vol.26, No.7, pp. 991-1002.
- [12] Okasha, N.M. and Frangopol, D.M., "Advanced Modeling for Efficient Computation of Life-cycle Performance Prediction and Service-life Estimation of Bridges", *Journal of Computing in Civil Engineering*, ASCE, 2010, Vol.24, No.6, pp. 548-556.
- [13] Partov, D. and Dinev, D., "Structure, Design and Construction of a Steel Orthotropic Bridge in Sofia ", *Advanced Steel Construction*, 2007, Vol. 3, No. 4, pp. 752-764.
- [14] Wang, C.S. and Feng, Y.C., "Review of the Fatigue Behaviors and Finite Element Analysis of Orthotropic Steel Bridge Decks", *Proceeding of the Second International Orthotropic Bridge Conference*, Sacramento, USA, 2008, pp. 290-304.
- [15] Xu, W. and Zhang, X.N., "Analysis Distress Characters and Design of Steel Orthotropic Bridge Decks Pavement in China", *Proceeding of the Second International Orthotropic Bridge Conference*, Sacramento, USA, 2008, pp. 184-192.
- [16] Wang, C.S., Fu, B.N., Zhang, Q. and Feng, Y.C., "Full-scale Fatigue Test of Orthotropic Steel Deck", *Proceedings of Seventh International Conference on Advanced in Steel Structures*, Nanjing, China, 2012a, Vol.1, pp. 710-716.
- [17] Barsom, J.M. and Rolfe, S.T., "Fracture and Fatigue Control in Structures: Applications of Fracture Mechanics, Third Edition", *American Society for Testing and Materials*, West Conshohocken, USA, 1999.
- [18] Bai, X.R., "Hazards and Causes Analysis of Cable-stayed Bridge", MS Thesis, Chongqing Jiaotong University, China, 2008. (in Chinese)
- [19] Jensen, J.S., "Cable Supported Bridges-design, Maintenance, Rehabilitation and Management", *Proceeding of the 5th International Association for Bridge Maintenance and Safety*, Philadelphia, USA, 2010, pp. 27-47.
- [20] Sørensen, O. Bloomstine, M. L., Bitsch, N. and Linneberg, P., "Design for Movements in Bridges", *Proceeding of IABSE Symposium Improving Infrastructure Worldwide*, Weimar, Germany, 2007, pp. 96-109.
- [21] Ye, J.M., Gong, Z.G., Li, R.Q. and Li, P., "Main Cable Protection by Using Dehumidification Systems", *World Bridges*, 2010, No.1, pp. 66-71. (in Chinese)
- [22] Suzuki, T., Ohtsu, M. and Shigeishi M., "Relative Damage Evaluation of Concrete in a Road Bridge by AE Rate-process Analysis", *Materials and Structures*, 2007, Vol.40, No.2, pp. 221-227.
- [23] Yuyama, S., Yokoyama, K., Niitani, K., Ohtsu, M. and Uomoto, T., "Detection and Evaluation of Failures in High-strength Tendon of Prestressed Concrete Bridges by Acoustic Emission", *Construction & Building Materials*, 2007, Vol.21, NO.3, pp. 491-500.
- [24] Sun, L.M. and Qian, J., "Experimental Study on Wire Breakage Detection by Acoustic Emission", *Frontiers of Architecture and Civil Engineering in China*, 2011, Vol.5, No.4, pp. 503-509.
- [25] Kova, J., Leban, M. and Legat, A., "Detection of SCC on Prestressing Steel Wire by the Simultaneous Use of Electrochemical Noise and Acoustic Emission Measurements", *Electrochim Acta*, 2007, Vol.52, pp. 7607-7616.

- [26] Bassim, M.N., Lawrence, S.S. and Liu, C.D., "Detection of the Onset of Fatigue Crack Growth in Rail Steels Using Acoustic Emission", *Engineering Fracture Mechanics*, 1994, Vol.47, No.2, pp. 207-214.
- [27] Holford, K.M., Davies, A.W., Pullin, R. and Carter, D.C., "Damage Location in Steel Bridges by Acoustic Emission", *Journal of Intelligent Material Systems and Structures*, 2001, Vol.12, No.8, pp. 567-576.
- [28] Li, D.S., Ou, L.P., Lan, C.M. and Li, H., "Monitoring and Failure Analysis of Corroded Bridge Cables under Fatigue Loading Using Acoustic Emission Sensors", *Sensors*, 2012, Vol.12, No.4, pp. 3901-3915.
- [29] Nair, A. and Cai, C.S., "Acoustic Emission Monitoring of Bridges: Review and Case Studies", *Engineering Structures*, 2010, Vol.32, No.6, pp. 1704-1714.
- [30] Wang, C.S., Tian, L. and Fu, B.N., "Fatigue Cracking Monitoring and Evaluation Using Smart Sensors for Steel Bridge Decks", *Proceeding of the 6th International Conference on Maintenance, Safety and Management*, Italy, 2012b, pp. 818-823.
- [31] Wang, C.S., Fu, B.N., and Xia, X.J., "Stress Test and Analysis of Steel Bridge Deck with Concrete Pavement", *Journal of Highway and Transportation Research and Development*, 2012, No.5, pp.147-150. (in Chinese)
- [32] Shao, X., Yi, D., Huang, Z., Zhao, H., Chen, B., and Liu, M., "Basic Performance of the Composite Deck System Composed of Orthotropic Steel Deck and Ultrathin RPC Layer." *J. Bridge Eng.*, 2013, Vol. 18, No.5, pp. 417-428.
- [33] Kolstein, M.H., Leendertz, J.S., and Wardenier, J., "Fatigue Performance of the Trough to Crossbeam Connection in Orthotropic Steel Bridge Decks. *Proceedings of Nordic Steel Conference*", Malmö, Sweden, 1995.
- [34] Tabata A., Aoki Y., and Takada Y., "Study on Improvement of the Fatigue Durability by Filling of Mortar in U-shaped Rib of Orthotropic Steel Deck", *Proceedings of the 5th International Conference on Bridge Maintenance, Safety and Management*. London: Taylor & Francis. 2010, pp. 2799-2805.
- [35] Bloomstine, M.L. and Sørensen, O., "Prevention of Main Cable Corrosion by Dehumidification", *Advances in Cable-Supported Bridges - Proceeding of the 5th International Cable-Supported Bridge Operators' Conference*, New York, USA, 2006, pp. 215-230.

11th International Conference

ASCCS 2015

**ADVANCES IN STEEL-CONCRETE
COMPOSITE STRUCTURES**

(First Announcement)



December 3-5, 2015

**Tsinghua University
Beijing, China**



KEY DATES

Abstract Submission Deadline: January 31, 2015

Author's Notification: March 1, 2015

Final Paper Submission: June 1, 2015

Final Paper Acceptance: August 15, 2015

End of Early-Bird Registration: October 1, 2015

Conference: December 3-5, 2015

ABSTRACT SUBMISSION

The conference covers topics on (but not limited to) any research area in steel-concrete composite structures. Submission of abstract is now opened, please submit your abstract of no more than 500 words to the conference e-mail address.

CONTACT

Address: Heshanheng Building, Tsinghua University, Beijing, 100084, China

E-mail: ASCCS2015@tsinghua.edu.cn

IMPORTANT MESSAGE

After the success of the 10th ASCCS conference held in Singapore in 2012, the upcoming 11th international conference on "Advances in Steel-Concrete Composite Structures" (ASCCS 2015) will be held in Tsinghua University, Beijing, China. The conference is intended to provide a forum to discuss the recent progress and advances in the research, design and practice of steel-concrete composite as well as hybrid structures.



Organized by

Department of Civil Engineering, Tsinghua University





The International Colloquium on Stability and Ductility of Steel Structures – SDSS 2016

30 May – 01 June 2016, Timisoara, Romania

www.ct.upt.ro/sdss2016.htm

First Announcement



*Main building of PU Timisoara
(the former Lloyd Palace)*

Organised by,

**Politehnica University of Timisoara
Department of Steel Structures and Structural Mechanics**



in cooperation with



Romanian Academy, Timisoara Branch



The steel bridge over the Oder River in Krosno Odrzańskie. The bridge was fabricated at Georg Beuchelt's works in Grünberg (presently Zielona Góra).

Conference language

English is the official language of the conference.

Conference sessions

All papers accepted by the Conference Scientific Committee will be presented orally during simultaneous thematic sessions. Keynote lectures given by eminent scholars are also planned.

Call for abstracts

Abstracts should be written in English in a Word file to be uploaded online. Authors are invited to submit the half page abstract (not more than 300 words) on the above topics. Guidelines for authors can be found on the conference web site: www.icms2016.uz.zgora.pl.

Proceedings

All accepted papers (6 page articles in English) will be published on a CD. 2 page extended abstracts will be printed in the hard-cover proceedings volume. The publisher will be CRC Press / Balkema, Taylor & Francis Group.

Key dates for participants

Abstract submission: 28.02.2015
 Abstract acceptance notification: 30.04.2015
 Second announcement: 30.06.2015
 Full Paper submission: 30.09.2015
 Full Paper final acceptance notification: 30.11.2015
 Fee payment: 31.12.2015
Conference: 15-17.06.2016

Venue

Zielona Góra has been selected as the venue of the Conference. The town with a population of 120,000 residents and 15,000 students is one of the most important educational centres in the western Poland.

Zielona Góra is located in the west of Poland quite near the western state border. Distances to the largest cities of this region are as follows: Poznań - 130 km, Wrocław - 160 km, Berlin - 190 km, Prague - 290 km, Warsaw - 410 km. There are very good, direct train connections from Berlin Hbf to Świebodzin or Żary (40 km away from Zielona Góra). A bus shuttle to these towns and to the main Berlin airports will be offered to participants by the organizers.



Zielona Góra - the historical town centre

The town does not lie on a river but it is very famous for steel bridges. More than 500 bridges were fabricated at this place at the beginning of XX-th century at Beuchelt & Co. steel structures works. Many of them still exist today.

The event is organized at the University of Zielona Góra by the Faculty of Civil and Environmental Engineering, Institute of Building Engineering. The conference will be held on Campus A of the University in Szafrana Street. The place is located near the town centre. More information about the University on the website: www.uz.zgora.pl.



University of Zielona Góra - the main building of the Faculty of Civil and Environmental Engineering.

XIII INTERNATIONAL CONFERENCE ON METAL STRUCTURES



15-17 June, 2016, Zielona Góra, POLAND

FIRST ANNOUNCEMENT AND CALL FOR ABSTRACTS

Organized by:

Section of Metal Structures of the Committee for Civil Engineering of the Polish Academy of Sciences (SMS CCE PAS)
 University of Zielona Góra, Faculty of Civil and Environmental Engineering, Institute of Building Engineering

Co-sponsored by:



Under the auspices of:

President of the Committee for Civil Engineering of Polish Academy of Sciences
 President of the Polish Chamber of Steelworks
 President of the Polish Chamber of Civil Engineers
 President of the Polish Association of Civil Engineers and Technicians
 Rector of the University of Zielona Góra
 Marshall of the Lubuskie Province
 Voivoda of the Lubuskie Voivodeship
 President of Zielona Góra

ICSAS 2016

The organizing committee is pleased to announce The Eighth International Conference on Steel and Aluminium Structures (ICSAS) 2016 to be held in Hong Kong, a dynamic metropolitan with thriving construction industry.

Introduction

Seven ICSAS Conferences have been successfully held in Cardiff, UK (1987), Singapore (1991), Istanbul, Turkey (1995), Helsinki, Finland (1999), Sydney, Australia (2003), Oxford, UK (2007) and Kuching, Malaysia (2011). The conference aims at bringing international experts and leaders together to disseminate recent research findings in the fields of steel and aluminium structures. It will also provide a forum for the discussion of the developments in the design and construction of steel and aluminium structures.

Who Should Attend

Steel and aluminium structure designers and manufacturers, trade associations, design engineers, steel fabricators, architects, owners or developers of steel and aluminium structures, researchers, academics and post-graduate students.

Key Dates

Abstract Submission	November 30, 2015
Acceptance of Abstract	January 15, 2016
Full Paper Submission	April 15, 2016
Acceptance of Full Paper	August 15, 2016
Conference	December 7–9, 2016

An aerial photograph of the Hong Kong skyline, showing a dense cluster of skyscrapers and buildings along the coast, with the Victoria Harbour in the background. The image is used as a background for the conference announcement.

**8TH INTERNATIONAL CONFERENCE ON STEEL AND ALUMINIUM STRUCTURES
DECEMBER 7 – 9, 2016 HONG KONG**

**ORDER
FORM**

ISSN 1816-112X

**Advanced Steel Construction,
an international journal**Indexed by the Science Citation Index Expanded,
Materials Science Citation Index and ISI Alerting Services**From:****To:** Secretariat, Advanced Steel Construction, an international journal
Fax: (852) 2334-6389

I/ We would like to enter a subscription to the *International Journal of Advanced Steel Construction (IJASC)* published by The Hong Kong Institute of Steel Construction.

Please complete the form and send to:

International Journal of Advanced Steel Construction
c/o Department of Civil and Environmental Engineering
The Hong Kong Polytechnic University
Hung Hom, Kowloon, Hong Kong

Fax: (852) 2334-6389 Email: ceslchan@polyu.edu.hkPublished by : The Hong Kong Institute of Steel Construction
Website: <http://www.hkisc.org/>**Please tick the appropriate box**

- ☐ Please enter my hard-copy subscription (**4 issues per year**).
☐ Please send me a complimentary copy of the *Advanced Steel Construction, an International Journal (IJASC)*.

Please tick the appropriate box(es)

	Print copy	ecopy is free to download at www.ascjournal.com in internet and mobile apps.
Personal	<input type="checkbox"/> US\$ 100	
Institutional	<input type="checkbox"/> US\$ 250	
Postage	<input type="checkbox"/> Surface mail (no charge) <input type="checkbox"/> Air mail (US\$ 30)	
Total Amount	US\$ _____	

Methods of payment ☐ Please invoice me
(please tick the appropriate box(es)) ☐ Cheque enclosed for US\$ _____ payable to
Hong Kong Institute of Steel Construction Limited
(No personal cheque accepted)

Ship to

Name (Prof./ Dr./ Mr./ Ms.) _____
Address _____

City/ State/ Postal Code _____
Country _____
Email _____ Fax _____